GAS PHASE ION - MOLECULE CHEMISTRY OF AN ANALOGOUS SERIES OF ARYL TRANSITION-METAL CARBONYL COMPOUNDS BY FOURIER TRANSFORM ION CYCLOTRON RESONANCE MASS SPECTROMETRY

by

SANDRA M. TAYLOR

B. A., University of British Columbia, 1956
M. Sc., University of British Columbia, 1958

A THESIS SUBMITTED IN PARTIAL FULFILMENT OF

THE REQUIREMENTS FOR THE DEGREE OF

DOCTOR OF PHILOSOPHY

in

THE FACULTY OF GRADUATE STUDIES

Department of Chemistry

We accept this thesis as conforming

to the required standard

THE UNIVERSITY OF BRITISH COLUMBIA
August, 1992

In presenting this thesis in partial fulfilment of the requirements for an advanced degree at the University of British Columbia, I agree that the Library shall make it freely available for reference and study. I further agree that permission for extensive copying of this thesis for scholarly purposes may be granted by the head of my department or by his or her representatives. It is understood that copying or publication of this thesis for financial gain shall not be allowed without my written permission.

Department of Chemistry

The University of British Columbia
Vancouver, Canada

Date August 31, 1992

Abstract

The gas phase ion-molecule chemistry of an analogous series of five aryl transition-metal carbonyl compounds has been examined using FT-ICR-MS techniques. Under 25 eV (positive ion) and 2.5 eV (negative ion) electron ionisation, ionic fragments of the following compounds were generated: $CpV(CO)_4$; $BzCr(CO)_3$; $CpMn(CO)_3$; $BuFe(CO)_3$; and $CpCo(CO)_2$; {where Cp = η^5-C_5H_5; Bz = η^6-C_6H_6; Bu = η^4-C_4H_6}. Ion-molecule reaction products were temporally monitored. Kinetic analyses showed that reaction pathways for each reactive cation fragment involved interaction with the neutral parent molecule, either by electron or ligand transfer, or by condensation with simultaneous carbonyl ejection. Condensations resulted in generation of higher molecular weight polynuclear ionic cluster fragments such as: $(CpV)_3(CO)_3^+$; $(BzCr)_2(CO)_3^+$; and $(BuFe)_2(CO)^+$.

In general, the reactivity of any cationic species varied directly with electron deficiency and coordination site availability of the central metal core. Some reactive cations exhibited unexpected reactivity patterns, despite their large formal electron deficiency, suggesting possession of unusual bonding configuration within cluster cores. Several reactive cations exhibited excited state behaviour, reacting more rapidly than their ground state counterparts. Reaction rate constants approximated those predicted by Langevin for unpolarised gas phase bimolecular processes.

Smaller, highly electron-deficient daughter cations, e.g. CpV^+ and $BzCrCO^+$, were reactive with respect to some small molecular addition reagents such as ammonia or dioxygen. Several important hydride adducts were also observed. On the other hand, anion-molecule chemistry was less complicated: anion daughter fragments reacted solely by formation of one or two stable clusters; and were relatively unreactive with respect to addition reagent molecules.

TABLE of CONTENTS

List of Figures

List of Tables

Acknowledgment

May I express my gratitude to my supervisor, Professor M. B. Comisarow, to committee members Professors E. Ogryzlo and A. Bree; to my colleagues Shu-Ping Chen, Ziyi Kan and Zamas Lam for helpful discussions and suggestions; to Eva Szende, Dave Steiner, Glenn Rouse, Ben Clifford and Irene Rodway for encouragement and support; to my patient and empathetic children, Norman, Renée, Angela, Colin, and Hillary; to my parents Kay and Ted Cardinall; to the knowledgeable and unstinting assistance of the staffs of the chemistry office, the mechanical and electronic shops; but mostly to my best friend, Jim Fitzsimmons. Thank-you everyone.

CHAPTER 1

A General Introduction to

Gas Phase

Aryl-Transition Metal-Carbonyl Chemistry

and

Experimental Procedures

I Introduction

1. Transition Metals

Since prehistoric time, transition metals have been esteemed for their great beauty and economic value. The very word 'metal' implies brilliant lustre and endurance, properties inherent in those elements arrayed along the central transition block of the modern periodic table. From earliest times, native gold, silver and mercury were accessible in pure form. With the discovery of fire and then ore extraction, other pure metals, such as copper, tin (Bronze Age) and later, iron (Iron Age), have enormously enhanced human survival and comfort. Tools made from such materials are sharp, hard and durable, lending themselves readily to the ingenuity of the user. Possession of such metals has acted as a cultural lever, enabling a people to achieve agricultural success, prevail over enemies, procure materials for clothing and shelter, etc. As small cultural enclaves developed into larger organised groups, highly-valued silver and gold also became the currency of commercial transaction. Early civilisations in China, India and pre-Columbian America developed sophisticated techniques for the procurement of these and other precious metals such as platinum, zinc, mercury and lead[118].

In classical Greece, intellectuals with time for speculative activity began laying the foundation for European theoretical science. During the early Medieval period, scholars in such intellectual outposts as Toledo, Cordova, Cairo and Baghdad examined closely some of the empirical properties of all known, economically valuable metals. Muslim scientists Jabir, Razi and Avicenna (721 - 1036 A.D.), the first true empiricists, carefully developed and documented procedures for metal separation and assaying[57,118]. These techniques, summarised much later by Agricola in De Re Metallica (1550 A.D.), are still used, largely unchanged, today. At the same time, in accordance with the spirit of the European

Renaissance, new ideas and practices began to be implemented in the study of all manner of natural phenomena, including the nature and behaviour of known transition metals and their compounds[17,57,118].

With the technological upheaval caused by the Industrial Revolution after 1700 A.D., new metallurgical procedures were devised in order to take advantage of global entrepreneurial opportunities. Heavy industrial processes such as the Bessemer process for steel production required high-melting, refractory metal construction materials[17,57]. The valuable properties which some transition metals bestowed upon their alloys became recognized. Many new transition metal elements were discovered; for example: cobalt (by Brandt, in 1735); nickel (Cronstedt, 1751); manganese (Gahn, 1774); titanium (Gregor, 1791); chromium (Vauquelin, 1797); vanadium (del Rio, 1801); and scandium (Nilson, 1876)[121]. These and other valuable metals grew in importance, in highly-refined form as well as in bulk.

In the late 1800's and early 1900's, commercial synthesis of strategic materials such as methane, sulfuric acid and ammonia became increasingly essential, and successful development of new and effective catalysts became mandatory. Most industrial processes required transition metal catalysts, their reactions proceeding heterogeneously on solid-support surfaces inside production chambers. For example, in the Deacon process, cupric chloride catalysed the oxidation of hydrogen chloride to produce chlorine (1883); finely-divided platinum was essential in the Contact oxidation of sulfur dioxide (1898)[17,57]. The Haber process (1913) utilized platinum or iron oxide catalysts for nitrogen hydrogenation[17]. Fischer and Tropsch (1925) engineered the use of catalytic nickel or iron for the production of methane from carbon monoxide[37]. Commercial hydrogenation of vegetable oils and ethylene became economically feasible through the action of 'Raney' nickel (1927) and cobalt (1933)[17]. Methanol became available by means of zinc oxide catalysed reduction of carbon monoxide in 1934[17,57].

As well as their catalytic function, large amounts of durable and refractory transition metal alloys in the form of materials and machinery were developed for use in construction and operation of factories producing new materials. Unique alloys were fabricated for specific tasks, such as for drilling, die-making, heat resistance, inertness to corrosion, electrical conductivity, etc. (e.g.; Monel metal, Nichrome, Prestal, Wood's alloy, 'stainless' steel, etc.)[121].

At the beginning of the twentieth century, almost all the stable transition metal elements had been isolated and characterised. During this century, transition metals and their compounds have become more important than ever for the industrial success of a modern economy. Understanding the mechanism of catalytic activity is crucial for developing new industrial materials with unique properties; and for creating innovative alloy compositions and semi-conductive materials for new electronic and structural technologies. In the last part of the twentieth century, the increase in production and expanded use of petroleum, fissile materials, plastics and pharmaceuticals as well as sophisticated research in such fields as computer and space technology, environmental monitoring, new industrial production and bio-engineering has made obligatory an understanding of transition metal chemistry.

2. Organo-Transition Metal Compounds

Historically, modern organo-transition metal chemistry began in 1827 with Zeise's discovery of an ethylene complex of platinum, $K[(C_2H_4)PtCl_3]$[131]. In 1919 Hein synthesised the first η^6-arene chromium complexes[53]. Expansion of the petroleum industry after 1898 and the need for high octane aircraft fuels during World War I led to the development of organometallic anti-knock agents such as tetraethyllead; organolead complexes were first synthesised by Pfeiffer in 1904[94]. Reihlen prepared butadienyl iron

tricarbonyl in 1930[100], and later its use as an anti-knock agent was patented by Veltman in 1947[119].

Some important recent developments in organo-transition metal chemistry were initiated with the discovery of ferrocene in 1951 by Kealy and Pauson[67] and by Miller[78]. The sandwich structure proposed for this complex by Wilkinson in 1952[124] led to radical new ideas concerning structure and the nature of chemical bonding, as well as to the synthesis of vast numbers of new and unique organo-transition metal compounds, such as the dicyclopentadienyl cobalt cation characterised by E. O. Fischer in 1952[38].

Investigation into the mechanism of transition-metal catalysed hydrogenation in solution was begun by Halpern in 1955[52]. In the same year, the existence of fluxionality in some organo-transition metal complexes was recognised by Cotton and Wilkinson[126]. The first covalent metal-metal bonds were proposed for the compound $[CpMo(CO)_3]_2$ in 1958[127] and the first dinitrogen organo-ruthenium complex identified by Allen and Senoff in 1965[1]. Commercially, other sophisticated organo-transition metal catalysts have been designed for non-destructive, low pressure and low temperature industrial processes, especially in fields such as new drug development and enzyme research.

3. Transition Metal Carbonyl Compounds

The first characterised transition-metal carbonyl complex, $PtCl_2(CO)_2$, was prepared in 1868 by Schützenberger[107]. In 1890 Mond identified nickel tetracarbonyl, $Ni(CO)_4$, in corrosion residues from nickel pipes[82] and in the next year (1891) prepared and characterised iron carbonyl, $Fe(CO)_5$[83]. Reihlen (1930) synthesised one of the first organo-transition metal carbonyl compounds possessing an unsaturated hydrocarbon ligand, butadienyl iron tricarbonyl, η^4-$C_4H_6Fe(CO)_3$[100]. During the decades after 1950, other transition metal carbonyl complexes derived from unsaturated precursors were prepared; for example, $CpMn(CO)_3$ in 1955[96]; $[CpMo(CO)_3]_2$ in 1958[127]; and

$Os_3(CO)_{11}C(CH_2)_2$ in 1982[62]. Hypotheses regarding such phenomena as d-π back-bonding[63,84,98]; metal-metal interactions in clusters[9-11,16,64]; multiple-decker sandwich structures[70-72,110]; fluxionality[8,120]; and agostic bonding[79-80] are continually being modified through ongoing study of the large assortment of these and other new and unusual complexes recently becoming available. Advances in spectroscopic techniques such as NMR, XRD and UV-vis-IR spectroscopy have enabled the characterisation of structural parameters of these materials, mainly in solid and liquid phases and in solution.

Over the past decade there has been increasing interest in the gas phase chemistry of transition metal carbonyl complexes[20,24,69,93,108,116]. In order to take advantage of the subtle and versatile capabilities of mass spectrometry, gas phase techniques have been developed for manipulating and examining transition metal complexes, utilizing guided ion-beam[4-6,51]; flowing afterglow[113,114]; or Fourier transform ion cyclotron resonance mass spectrometry [13,21,47,74,122]; coupled with EI[44,77,92,95]; CID[122,129] or laser ionisation[45,55,89]. Free of matrix and solvent interferences, transition metal carbonyl molecules and their ions in the gas phase can undergo a wealth of ion-molecular interactions within the ion source of the mass spectrometer and such studies can yield both structural and thermodynamic information regarding these materials and the mechanism of interaction with their ion fragments[3,18,43,65,75].

Using ICR in 1973, Dunbar[29] observed anion-molecule condensations in the metal carbonyl systems of $Cr(CO)_6$, $Ni(CO)_4$ and $Fe(CO)_5$, which resulted in formation of bimetallic cluster anions. Later, Beauchamp[40,41] examined fragment cations and cluster ion products in the $Fe(CO)_5$ system, observing cluster fragments containing up to four iron atoms. Ion-molecule clustering has been monitored in these and many other metal carbonyl systems, such as those of $Fe(CO)_5$[43], $Re_2(CO)_{10}$[75-77], $Ni(CO)_4$[44], $Cr(CO)_6$[12,43], $CoNO(CO)_3$[44], $Mn_2(CO)_{10}$[76] and $Os_3(CO)_{10}H_2$[85]. In the latter study, fragment ionic cluster cores containing up to 15 metal atoms were identified. The relationship between reactivity of fragment ions and ion clusters and the electron unsaturation of their central

metal atoms has been examined by Ridge[76] and Russell[43] and others. Multiple bonding between metal atoms has been invoked to explain some of the kinetic behaviour of these ions[102]. As well, efficiencies of reactions of certain metal-carbonyl ions with neutral molecules have been explained as depending upon electronic mobility within the complex itself[104].

Other ICR studies have concentrated on ion-molecule interactions between non-carbonyl ligated transition metal ions and their parent neutral molecules. For example, Schildcrout[104] has observed polynuclear clusters containing up to three metal atoms and five ligand moieties ($M_3L_5^+$) in the mass spectra of CrL_3, FeL_3, CoL_3 and CoL_2 where L=bidentate ligands bonded to the metal through oxygen atoms. Ligand binding energies have been determined by a number of techniques such as by CID[5,58,66,111], photodissociation[47,54,89], and thermochemical methods[23,112].

4. Aryl Transition Metal Compounds

The recognition of the unusual properties of tetraethyl lead encouraged preparation of other alkyl- and aryl- complexes of transition-metals. Methyl platinum compounds (1907)[97] and alkyl gold complexes (1934)[14] were discovered early in this century, as was Hein's peculiar benzene chromium compound[53]. Transition metal complexes with unsaturated, aryl-type hydrocarbon ligands have been a subject of intense interest since 1951, with the synthesis of ferrocene[67,78]. Characterisation of metallocenes containing vanadium, chromium, manganese, iron and cobalt by Wilkinson, Cotton and Birmingham in 1956[125] led to greater understanding of the unique Cp ligand and its mode of π-bonding to these metals.

Transition metal complexes and ions containing unsaturated, aryl-type hydrocarbon ligands have been studied more recently in the gas phase using ion cyclotron resonance mass spetrometry. Examining the ion-molecule chemistry of ferrocene (Cp_2Fe) and

nickelocene (Cp_2Ni), Beauchamp[25,41] found that the parent cation (i.e., Cp_2metal^+) was kinetically stable, whereas the daughter cations, therefore the ions $(metal)^+$ and $(Cp\text{-}metal)^+$ were reactive, and subsequently underwent charge exchange with the parent molecule to produce Cp_2metal^+, or else condensed with the parent neutral molecule to form larger cluster ions, $Cp_2metal_2^+$ and $Cp_3metal_2^+$ (the well-known "triple-decker sandwich" ion) which has been examined both experimentally[55,106,130] and theoretically[9,56,72]. In negative ion experiments, only the stable parent anion (i.e., Cp_2metal^-), generated by initial electron capture, was observed in the Cp_2Ni and Cp_2Fe systems[25,41].

5. Π-Alkenyl Transition Metal Carbonyl Complexes

Perhaps the earliest example of the "piano-stool", or "half-sandwich type" of compound (in which the transition metal center is linked both to carbonyl units, and in multi-hapto fashion, to unsaturated alkene ligands) was η^4-butadienyl iron tricarbonyl, first prepared by Reihlen in 1930[100]. Syntheses of new members of this class have continued to the present. Some examples are: $Cp_2Ti(CO)_2$ (by Murray in 1959)[86]; $[C_4H_6Co(CO)_2]_2$ (by E. Fischer, 1961)[39]; Cp allyl iron carbonyl (by Green and Nagy, 1963)[50]; benzene vanadium tetracarbonyl cation (by Calderazzo, 1964)[15]; $Cp_4Fe_4(CO)_4$ (by King, 1966)[68]. In these complexes the alkene-metal linkage consists of strong multiple π-bonding between the conjugated double bond system of the hydrocarbon ligand and the central metal atom. The bound alkyl group consequently modifies the electronic structure and electropositivity of the metal, and simultaneously acts as a partial steric barrier toward incoming reactive groups.

In one of the first gas phase studies of such complexes, Müller[87] noted that following ionisation, the ions and neutral molecules of η^5-cyclopentadienyl transition metal carbonyl complexes of chromium, manganese, cobalt and vanadium interacted to

produce secondary, bimetallic ion clusters consisting of various amounts of Cp and CO units, for example, $Cp_2V_2(CO)_3^+$.

In 1973, Müller and Goll[88] examined ion-molecule interactions of neutral CpNiNO and its fragment cations. Again, cluster cation products containing two nickel atoms were produced. Reactions of product cation $CpNiCO^+$ with small molecules apparently proceeded via simple addition combined with NO loss. In 1977, Corderman and Beauchamp[26] postulated that the marked non-reactivity of the cluster anion $Cp_2Co_2(CO)_2^-$ in the negative ion-molecule regime of $CpCo(CO)_2$ probably reflected partial double bonding between cobalt atoms within the cluster.

In a seminal positive ion study, Parisod (1980) showed that complex reaction pathways could be resolved by multiple resonance techniques, in which individual ions or groups of ions could be removed from the reaction cell, thus simplifying kinetic measurements on the remaining reactants. As a result of this technique, many fragment cations and their multi-metallic cluster products in each of the $CpMn(CO)_3$, $CpCr(CO)_2NO$ and $CpCr(CO)_2NS$ systems were shown to be relatively unreactive[92].

Other important features of these latter three systems were: firstly, that clusters were generated containing up to 3 Cp-metal moieties, and secondly, that most of the observed ionic cluster products in these systems retained the 1:1 ratio of Cp-metal stoichiometry, indicating that Cp-metal bonds were very stable, retaining their integrity throughout entire ion-molecule reaction regimes.

However, the high mobility of CO residues under the same experimental conditions demonstrated the relative lability of metal-carbonyl bonds in these ion clusters. Finally, in the latter two systems {$CpCr(CO)_2NO$ and $CpCr(CO)_2NS$}, unusual rupture of NO and NS ligands, with retention of metal-nitrogen linkages within the ion cluster, was seen in some cluster products, whereas comparable CO links appeared to remain undisturbed[92].

Comparing the CpCr and CpMn systems previously discussed, Chen[18] noted that in the cation-molecule cluster chemistry of $CpCr(NO)_2CH_3$, Cp-metal bonds also tended to

remain intact during the electron ionisation procedure, as well as throughout subsequent ion-molecule interactions, and retained 1 : 1 Cp-to-metal ratios in most product ions. Exceptions to this, where 1 : 1 Cp-to-metal stoichiometry was not maintained, were found only where bare metal cations underwent condensation with the parent neutral molecule, or in highly oxygenated ionic cluster products of chromium (e.g. $Cp_2Cr_3O_2^+$, $Cp_4Cr_5(NO)O_3^+$). These oxygenated clusters, containing more metal atoms than Cp ligands, were postulated to possess either chromium-oxygen multiple bonding, or lowered cyclopentadienyl hapticity[18].

Gas phase reactivities of a series of ion products of several substituted η^6-arene $Cr(CO)_3$ complexes were studied by Freiser in 1991[89]. In most cases, 1:1 arene-to-Cr stoichiometry was preserved throughout ion molecule interactions; principal reaction channels involved ion-molecule condensation, accompanied by CO loss.

Recently, Kan (1991) has found that reactivities of daughter cation products in the hexadienone iron (η^4 - $C_6H_6OFe(CO)_3$) system varied directly with electron deficiency of the central iron atom[65]. Kinetic trends in these and in other metal-carbonyl systems have been related earlier to coordination unsaturation and formal electron deficiency of the central metal atom. Anomalies in kinetic activity have been attributed to enhanced metal-metal bonding or to carbonyl ligand restructuring within the metal cluster cores[101,102].

Theoretical models of some of these metal-ligand clusters have been considered by Lauher[70-72] and Teo[117]. Closely-packed polyhedral metal cores with attendant cluster valence molecular orbitals (CVMO), have been invoked by Ridge and others[64,79-81,101] to explain observed kinetic stability patterns. Some fundamental aspects of ion reactivity in these systems, such as metal-ligand bond energies[44,47,55], ligand exchange[24,69,74,91,108], interaction with small molecules[12,49,114], and ability to activate carbon bonds[2,6,19,28,59-61,105] continue to be of great interest in the development of structural understanding of these important materials. With regard to cluster formation, fundamental comparisons have been drawn with respect to bonding reactivity and catalytic

behaviour of larger metal cluster ions, with bulk metal surfaces where the metal centres are extremely unsaturated with respect to their ligands[48,71,72,88,110,116]. Multiple or partial multiple bonding between metal atoms within clusters have long been invoked in order to explain spectroscopic and reactivity differences[27,127,128].

As well as coordination saturation, reactivity of bare metal ions depends upon their electronic state; bare metal cations in excited states may react in pathways or at rates which greatly differ from those of the corresponding ground-state cation[7,30-35,90,99,103,114].

6. An Analogous Series of "Aryl" Transition-Metal Carbonyls

An examination of "homologous series", wherein one chosen variable within a group of related substances differs in a consecutive, orderly manner, can be invaluable in determining trends, testing models of chemical behaviour, thus yielding insight into the fundamental mechanisms of interaction on the molecular scale[11]. Subtle chemical gradations between two members permit discrimination between the effects of that variable and of others, and enable exact parameters to be measured, and relationships to be determined. In the present study, organic compounds of five consecutive first row transition metals (vanadium to cobalt) are examined. These five metals are of vital economic importance, being catalytically active, and forming essential components of structural, electrical and tool alloys. Their chemical properties, both similarities and differences, arise from their electronic structure consisting of partly-filled 3d and 4s orbitals in the valence shell.

The present work comprises a study of quasi-homologous ('analogous') compounds consisting of complexes of this sequence of five early third-period, transition metals {vanadium (Z=23), chromium (Z=24), manganese (Z=25), iron (Z=26) and cobalt (Z=27)}. Each complex in the series contains both a conjugated hydrocarbon ('aryl type') ligand bonded in multi-π fashion, and several carbonyl ligands, all linked to the central transition metal. Each member of the series is ligand-saturated, containing an 18 - electron transition metal core, as follows: η^5-$C_5H_5V(CO)_4$ (**Chapter 2**); η^6-$C_6H_6Cr(CO)_3$ (**Chapter 3**); η^5-$C_5H_5Mn(CO)_3$ (**Chapter 4**); η^4-$C_4H_6Fe(CO)_3$ (**Chapter 5**); and η^5-$C_5H_5Co(CO)_2$ (**Chapter 6**). An attempt to correlate the results for all five systems is presented in **Chapter 7**. Since this series is not perfectly homologous (i.e., the complexes contain differing numbers of carbonyl ligands, and all arene ligands are not identical) it has been labelled an "analogous series". Obviously, chemical differences in this series arise

from differences in electronic constitution of the central metal atom, as well as arene type, and number of CO ligands present. Yet, their closely-related structures and similar overall composition make a comparative study of the ion-molecule chemistry of this "analogous" series of compounds potentially informative and interesting.

7. Structures of Compounds Examined

i) Tetracarbonyl (η^5 - cyclopentadienyl) vanadium

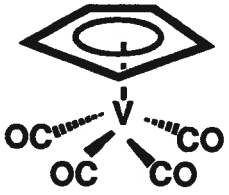

ii) Tricarbonyl (η^6 - benzene) chromium

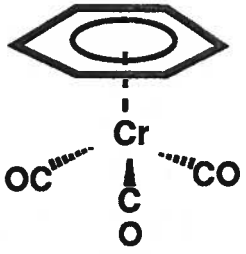

iii) Tricarbonyl (η^5 - cyclopentadienyl) manganese

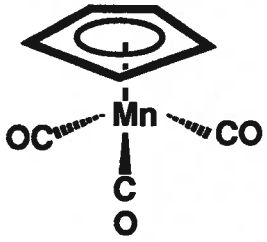

iv) Tricarbonyl (1-4-η^4 - butadienyl) iron

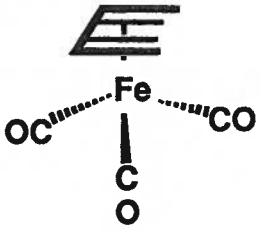

v) Bicarbonyl (η^5 - cyclopentadienyl) cobalt

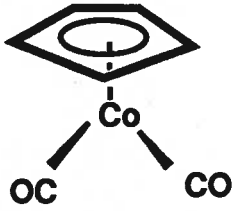

8. Gas Phase Techniques

Chemical interactions with the solvent often obscure and complicate the chemistry of metal complexes. Accordingly, gas phase techniques such as mass spectrometry can be extremely useful in the elucidation of solvent-free behaviour. However, most mass spectrometric methods require volatile sample materials or else some special volatilisation procedure in order to attain sufficient sample pressure for ion-molecule interactions to be observed and quantified. Moreover, some organometallics are involatile or thermally unstable. Fortunately, such compounds can be examined under the low pressure conditions of ICR-MS, at normal, non-destructive temperatures. Subject molecules can be introduced under high vacuum into the reaction cell of the ICR instrument, ionised with a burst of electrons, and the presence, appearance, and disappearance of daughter ions monitored at exact time intervals.

It was hoped that gas phase analysis of the kinetic behaviour and ion chemistry of the members of this analogous series of transition metal complexes would yield some insight into electronic trends among these important transition metals. Accordingly, attempts were made to conduct all parallel experiments, under experimental conditions which were as identical as possible .

II Experimental Procedure

1. Experimental Parameters

All experiments were performed using prototypic FT-ICR mass spectrometric instrumentation which had been assembled at the University of British Columbia in 1973, equipped with a 1.9 Tesla electromagnet, and later updated by the installation of a Nicolet FTMS 1000 computer-directed electronic console. A cubic cell (16.4 cm^3 volume) served

as the ion trap and reaction chamber, into which reagents were introduced through leak valves at ambient temperature. Typical operating parameters were as follows: electron beam energy ranges: 10-70 eV (positive EI); 1-5 eV (negative EI); trapping voltage ranges: ±1.0V; reagent pressure ranges: 10^{-6} - 10^{-9} torr; ion trapping time spans: 0 - 25 sec. Reagent pressures were monitored with a Varian model 971-0018 ionization gauge: constant system pumping speed and sample introduction rates were maintained during complete experimental sequences in order to maximise pressure equilibration between pressure gauges and reaction cell.

Corroborating structural and adduct composition data were obtained for $CpV(CO)_4$ with a Nermag R10-10C quadrupole mass spectrometer equipped with DCI capability. In these latter experiments parameters were as follows: collision gas pressure: 0.01 torr; electron beam energy: 70 eV (positive and negative EI); monitoring time: 0-10 seconds.

2. Chemical Compounds

Pure specimen compounds were obtained from Alfa Products. No impurities other than carbon monoxide, and benzene in the tricarbonyl benzene chromium study, from product decomposition, were observed in the mass spectra of any member of the series. Gaseous impurities were removed by freeze-pump-thaw cycles. Liquid samples were first purified by distillation under vacuum and stored cold under argon.

Sample materials of low volatility were introduced by means of a shortened, heated inlet system. Before admission into the reaction chamber, all sample materials were thoroughly degassed, and during admission were further degassed until no impurities appeared in their mass spectra. Highly volatile samples were held frozen in liquid nitrogen, carbon dioxide or ice during sample admission. Collision gases were introduced using a secondary inlet while maintaining constant pressure within the reaction chamber.

3. Principles of Ion Cyclotron Resonance

In a fixed magnetic field, charged particles (ions) are subject to a centripetal (Lorenz) force causing them to be constrained in a helical paths along the axis of the magnetic field. The frequency ϖ of this helical motion is given by $\varpi = qB/m$ where q is the charge on the ion, m is the ion mass and B is the magnetic field strength. To prevent ions from escaping the magnetic field region, similarly-charged plates are situated at the front and back of the helical pathways. The frequency of revolution of such a trapped ion is called its ion cyclotron frequency.

Identical ions thus electrically trapped can absorb energy from an externally applied alternating electric field, causing them to become excited as their velocity and orbital radius increase in a coherent spiral. If the applied frequency exactly matches that of the ion cyclotron frequency, the ions will move as packets in a larger coherent orbit and are said to be in resonance. When the ac electric field is terminated, the new expanded orbital radius of the ion collection remains constant. If the collection of ions passes close to a pair of sensing plates, an image current is established within the plates, whose frequency depends upon the mass-to-charge ratio (m/e) of the cycling ions, and whose intensity depends upon the numbers of ions within the ion packet in transit[21,22].

When an assortment of ions of differing masses is trapped, a range of radio frequencies, corresponding to the range of ion masses, can be used to energize all ions into resonance, and the sensed signal becomes a composite mixture of all their ion cyclotron frequencies. By computer-directed Fourier analysis, this signal can be sorted into the component ion frequencies and amplitudes, and this array then converted into masses and abundances of each type of ion, thus generating a mass spectrum of all the ions present ("single pulse resonance"). Many identical repetitions of this process will enhance the sensitivity of this mass spectrum[21,22].

If the collection of resonant ions is energised either by a strong single radio frequency ("double resonance"), or by a band of radio frequencies ("triple resonance"), the ions whose cyclotron resonances are in these ranges can be excited until they are ejected from the trapping zone[92]. Then the remaining ions can be detected as before (i.e., by "single resonance"). This procedure enables any specific ion mass to be expelled from the reaction cell in order to identify its ion products by difference; or, packages of ions to be eliminated from an ion mixture in order to quantify the disappearance of a single reactive ion and monitor its ion products[3,21,22,36,46,73,109,123]. A schematic diagram of the FT-ICR reaction cell is illustrated in Figure A.1. in Appendix II, page 257.

In practice, pressures of reactant molecules (Pm) in the ICR trapping zone were maintained at low, constant pressures, typically in the range 10^{-5} - 10^{-9} torr. Parameters such as ionising electron energies, electron flux, beam time, trapping voltage and ambient temperature were held as constant as possible. Each mass spectrum was generated and computer scanned 100-1000 times; and duplicate or triplicate series were performed for each set of timed experiments.

Calibration masses were chosen from available calibration compounds deuterium oxide, nitrogen and methyl bromide, and from three or four ions present in the mass spectra with as wide a mass range as possible. To simplify kinetic analyses, small molecule experiments were conducted at conveniently large pressure ratios; i.e.: pressure of small reactant gases was 10-100 times greater than pressure of each specimen compound. Kinetic behaviour was monitored for 0 - 25 seconds. Intensities of each reactant ion were normalised as proportions of total ions present, i.e.;

$$\text{Relative intensity of ion i} = [I_i^+] / \Sigma ([I_a^+] + [I_b^+] + \ldots + [I_n^+])$$

before kinetic analysis. Slopes of linear semilog plots were used to calculate pseudo-first order rate constants, typically with ±5% precision. Because of uncertainty in pressure calibration, second order rate constants were estimated to be accurate within ± 30% only.

III References

(1) Allen, A. D.; Senoff, C. V. *J. Chem. Soc. Chem. Commun.* **1965**, 621.

(2) Allison, J.; Freas, R. B.; Ridge, D. P. *J. Am. Chem. Soc.* **1979**, *101*, 1332.

(3) Allison, J. *Prog. Inorg. Chem.* **1986**, *34*, 627.

(4) Aristov, N.; Armentrout, P. B. *J. Am. Chem. Soc.* **1984**, *106*, 4065.

(5) Armentrout, P. B.; Halle, L. F.; Beauchamp, J. L. *J. Am. Chem. Soc.* **1981**, *103*, 6501.

(6) Armentrout, P. B.; Beauchamp, J. L. *J. Am. Chem. Soc.* **1981**, *103*, 784.

(7) Armentrout, P. B. in *Gas Phase Inorganic Chemistry*; Russell, D. H.; Plenum Press, New York, **1989**; pp 1 - 42.

(8) Benfield, R. E.; Johnson, B. F. G. *J. Chem. Soc., Dalton Trans.* **1980**, 1743.

(9) Bottomley, F.; Grein, F. *Inorg. Chem.* **1982**, *21*, 4170.

(10) Bottomley, F.; Paez, D. E.; White, P. S. *J. Am. Chem. Soc.* **1982**, *104*, 5651.

(11) Bottomley, F.; Sutin, L. *Adv. Organomet. Chem.* **1988**, *28*, 339.

(12) Bricker, D. L.; Russell, D. H. *J. Am. Chem. Soc.* **1987**, *109*, 3910.

(13) Buchanan, M. V. *Fourier Transform Mass Spectrometry*; Comstock, M. J.; American Chemical Society: Washington, D. C., **1987**.

(14) Burawoy, A.; Gibson, C. S. *J. Chem. Soc.* **1934**, 860.

(15) Calderazzo, F. *Inorg. Chem.* **1964**, *3*, 1207.

(16) Castleman Jr., A. W.; Keesee, R. G. *Chem. Rev.* **1986**, *86*, 589.

(17) Cavell, A. C. *An Introduction to Chemistry*; Macmillan and Co., Ltd.: London, **1957**.

(18) Chen, S.-P.; Comisarow, M. B. *Ann. Conf. ASMS All. Top.* **1989**, *37*, 323.

(19) Chen, H.; Lin, H.-Y.; Sohlberg, K.; Ridge, D. P. *Ann. Conf. ASMS All. Top.* **1991**, *39*, 1596.

(20) Chini, P. J. *Organomet. Chem.* **1980**, *200*, 37.

(21) Comisarow, M. B. *J. Chem. Phys.* **1978**, *69*, 409.

(22) Comisarow, M. B.; Buchanan, M. V. *ACS Symposium Series 359*, **1987**, 1 - 20.

(23) Connor, J. A. *Top. Curr. Chem.* **1977**, *71*, 71.

(24) Constable, E. C. *Metals and Ligand Reactivity*; Ellis Horwood Ltd.: Chichester, England, **1990**.

(25) Corderman, R. R.; Beauchamp, J. L. *Inorg. Chem.* **1976**, *15*, 665.

(26) Corderman, R. R.; Beauchamp, J. L. *Inorg. Chem.* **1977**, *16*, 313.

(27) Cotton, F. A.; Walton, R. A. *Struct. Bond.* **1985**, *62*, 1.

(28) Crabtree, R. H. *Chem. Rev.* **1985**, *85*, 245.

(29) Dunbar, R. C.; Ennever, J. F.; Fackler, J. P., Jr. *Inorg. Chem.* **1973**, *12*, 2734.

(30) Elkind, J. L.; Armentrout, P. B. *J. Phys. Chem.* **1984**, *88*, 5454.

(31) Elkind, J. L.; Armentrout, P. B. *J. Phys. Chem.* **1985**, *89*, 5626.

(32) Elkind, J. L.; Armentrout, P. B. *J. Chem. Phys.* **1986**, *84*, 4862.

(33) Elkind, J. L.; Armentrout, P. B. *J. Phys. Chem.* **1986**, *90*, 5736.

(34) Elkind, J. L.; Armentrout, P. B. *J. Phys. Chem.* **1986**, *90*, 6576.

(35) Elkind, J. L.; Armentrout, P. B. *J. Chem. Phys.* **1987**, *86*, 1868.

(36) Eller, K.; Schwarz, H. *Chem. Rev.* **1991**, *91*, 1121.

(37) Fischer, F.; Tropsch, H. *D.R.P.* **1922, 1925.**, # 411416; 484337.

(38) Fischer, E. O.; Pfab, W. *Z. Naturforsch.* **1952**, *7B*, 377.

(39) Fischer, E. O.; Kuzel, P.; Fritz, H. P. *Z. Naturforsch.* **1961**, *16B*, 138.

(40) Foster, M. S.; Beauchamp, J. L. *J. Am. Chem. Soc.* **1971**, *93*, 4924.

(41) Foster, M. S.; Beauchamp, J. L. *J. Am. Chem. Soc.* **1975**, *97*, 4808.

(42) Freas, R. B.; Dunlap, B. I.; Waite, B. A.; Campana, J. E. *J. Chem. Phys.* **1987**, *86*, 1276.

(43) Fredeen, D. J. A.; Russell, D. H. *J. Am. Chem. Soc.* **1985**, *107*, 3762.

(44) Fredeen, D. J. A.; Russell, D. H. *J. Am. Chem. Soc.* **1986**, *108*, 1860.

(45) Freiser, B. S. *Anal. Chim. Acta* **1985**, *178*, 137.

(46) Freiser, B. S. *Chemtracts-Anal. Phys. Chem.* **1989**, *1*, 65.

(47) Freiser, B. S. in *Bonding Energetics in Organometallic Compounds*; Marks, T.; American Chemical Society, Washington, D. C., **1990**; pp 55-69.

(48) Geusic, M. E.; Morse, M. D.; Smalley, R. E. *J. Chem. Phys.* **1985**, *82*, 590.

(49) Gord, J. R.; Freiser, B. S. *J. Am. Chem. Soc.* **1989**, *111*, 3.

(50) Green, M. L. H.; Nagy, P. L. I. *J. Chem. Soc.* **1963**, 189.

(51) Halle, L. F.; Armentrout, P. B.; Beauchamp, J. L. *Organometallics* **1982**, *1*, 963.

(52) Halpern, J. *Inorg. Chim. Acta* **1985**, *100*, 41.

(53) Hein, F. *Ber. D. Chem. Ges.* **1919**, *52*, 195 .

(54) Hettich, R. L.; Jackson, T. C.; Stanko, E. M.; Freiser, B. S. *J. Am. Chem. Soc.* **1986**, *108*, 508.

(55) Hettich, R. L.; Freiser, B. S. *J. Am. Chem. Soc.* **1987**, *109*, 3537.

(56) Hoffman, R. *Science* **1981**, *211*, 995.

(57) Holmyard, E. J. *Makers of Chemistry*; Clarendon Press: Oxford, **1931**.

(58) Houriet, R.; Halle, L. F.; Beauchamp, J. L. *Organometallics* **1983**, *2*, 181.

(59) Jacobson, D. B.; Freiser, B. S. *J. Am. Chem. Soc.* **1983**, *105*, 5197.

(60) Jacobson, D. B.; Freiser, B. S. *J. Am. Chem. Soc.* **1983**, *105*, 7485.

(61) Jacobson, D. B.; Freiser, B. S. *J. Am. Chem. Soc.* **1985**, *107*, 5870.

(62) Johnson, B. F. G.; Lewis, J.; Raithby, P. R.; Swankey, S. W. *J. Organomet. Chem.* **1982**, *231*, C65.

(63) Johnston, R. D. *Adv. Inorg. Chem. Radiochem.* **1970**, *13*, 471.

(64) Kaldor, A.; Cox, D. M.; Trevor, D. J.; Zakin, M. R. *Metal Clusters*; Trager, F. zu Putlitz, G.; Springer: Berlin, **1986**.

(65) Kan, Z.; Comisarow *Ann. Conf. ASMS All. Top.* **1991**, *39*, 461.

(66) Kappes, M. M.; Staley, R. H. *J. Phys. Chem.* **1981**, *85*, 942.

(67) Kealy, T. J.; Pauson, P. J. *Nature* **1951**, *168*, 1039.

(68) King, R. B. *Inorg. Chem.* **1966**, *5*, 2227.

(69) Lane, K. R.; Sallans, L.; Squires, R. R. *J. Amer. Chem. Soc.* **1986**, *108*, 4368.

(70) Lauher, J. W.; Elian, M.; Summerville, R. H.; Hoffman, R. *J. Am. Chem. Soc.* **1976**, *98*, 3219.

(71) Lauher, J. W. *J. Am. Chem. Soc.* **1979**, *101*, 2604.

(72) Lauher, J. W. *J. Organomet. Chem.* **1981**, *213*, 25.

(73) Marshall, A. G.; Grosshans, P. B. *Anal. Chem.* **1991**, *63*, 215A.

(74) McDonald, R. N.; Schell, P. L. *Organomet.* **1988**, *7*, 1806.

(75) Meckstroth, W. K.; Ridge, D. P. *Int. J. Mass Spectrom. Ion Proc.* **1984**, *61*, 149.

(76) Meckstroth, W. K.; Ridge, D. P.; Reents, W. D., Jr. *J. Phys. Chem.* **1985**, *89*, 612.

(77) Meckstroth, W. K.; Ridge, D. P. *J. Am. Chem. Soc.* **1985**, *107*, 2281.

(78) Miller, S. A.; Tebboth, J. A.; Tremaine, J. F. *J. Chem. Soc.* **1952**, 632.

(79) Mingos, D. M. P. *Acc. Chem. Res.* **1984**, *17*, 311.

(80) Mingos, D. M. P.; May, A. S. in *The Chemistry of Metal Cluster Complexes*; Shriver, D. F.; Kaesz, H. D. Adams, R. D.; VCH Publishers, New York, **1990**; pp 11 - 119.

(81) Mingos, D. M. P.; Slee, T.; Zhenyang, L. *Chem. Revs.* **1990**, *90*, 383.

(82) Mond, L.; Langler, C.; Quinche, F. *Trans. Chem. Soc.* **1890**, 749.

(83) Mond, L.; Langler, C. *Trans. Chem. Soc.* **1891**, *59*, 1090.

(84) Muetterties, E. L.; Rhodin, T. N.; Band, E.; Brucker, C. F.; Pretzer, W. R. *Chem. Rev.* **1979**, *79*, 91.

(85) Mullen, S. L.; Marshall, A. G. *J. Am. Chem. Soc.* **1988**, *110*, 1766.

(86) Murray, J. G. *J. Am. Chem. Soc.* **1959**, *81*, 752.

(87) Müller, J.; Fenderl, K. *Chem. Ber.* **1970**, *103*, 3128.

(88) Müller, J.; Goll, W. *Chem. Ber.* **1973**, *106*, 1129.

(89) Operti, L.; Vaglio, G. A.; Gord, J. R.; Freiser, B. S. *Organometallics* **1991**, *10*, 104.

(90) Oriedo, J. V.; Russell, D. H. *Ann. Conf. ASMS All. Topics* **1991**, *39*, 1610.

(91) Pan, Y. H.; Ridge, D. P. *J. Am. Chem. Soc.* **1989**, *111*, 1150.

(92) Parisod, G.; Comisarow, M. B. *Adv. Mass Spectrom.* **1980**, *8A*, 212.

(93) Pearson, R. G. *Inorg. Chem.* **1984**, *23*, 4675.

(94) Pfeiffer, P.; Truskier, P. *Ber. D. Chem. Ges.* **1904**, *37*, 1125.

(95) Pignataro, S.; Foffani, A.; Grasso, F.; Cantone, B. *Z. Physik. Chem. (Frankfurt)* **1965**, *47*, 106.

(96) Piper, T. S.; Cotton, F. A.; Wilkinson, G. *J. Inorg. Nucl. Chem.* **1955**, *1*, 165.

(97) Pope, W. J.; Peachey, S. J. *J. Chem. Soc. Transactions* **1909**, 571.

(98) Pruchnik, F. P. *Organometallic Chemistry of the Transition Elements*; Fackler Jr., J. P.; Plenum Press: New York, **1990**.

(99) Reents, J., W. D. ; Strobel, F.; Freas, R. B.; Wronka, J.; Ridge, D. P. *J. Phys. Chem.* **1985**, *89*, 5666.

(100) Reihlen, H.; Gruhl, A.; Hessling, G. v.; Pfrengle, O. *Liebig's Annalen Der Chemie* **1930**, *482*, 161.

(101) Ridge, D. P.; Meckstroth, W. K. in *Gas Phase Inorganic Chemistry*; Russell, D. H.; Plenum Press, New York, **1989**; pp 93-113.

(102) Russell, D. H.; Fredeen, D. A.; Tecklenburg, R. E. in *Gas Phase Inorganic Chemistry*; Russell, D. H.; Plenum Press, New York, **1989**; pp 115-135.

(103) Russell, D. H. *Ann. Conf. ASMS All. Top.* **1990**, *38*, 1261.

(104) Schildcrout, S. M. *Inorg. Chem.* **1980**, *19*, 224.

(105) Schultz, R. H.; Elkind, J. L.; Armentrout, P. B. *J. Am. Chem. Soc.* **1988**, *110*, 411.

(106) Schumacher, E.; Taubenest, R. *Helv. Chim. Acta* **1964**, *47*, 1525.

(107) Schützenberger, P. *Annalen* **1868**, *15*, 100.

(108) Sellers-Hahn, L.; Russell, D. H. *J. Am. Chem. Soc.* **1990**, *112*, 5953.

(109) Sharpe, P.; Richardson, D. E. *Coord. Chem. Revs.* **1989**, *93*, 59.

(110) Shriver, D. F.; Kaesz, H. D.; Adams, R. D. *The Chemistry of Metal Cluster Complexes*; VCH Publishers, Inc.: New York, **1990**.

(111) Simoes, J. A. M.; Beauchamp, J. L. *Chem. Revs.* **1990**, *90*, 629.

(112) Skinner, H. A.; Connor, J. A. *Pure Appl. Chem.* **1985**, *57*, 79.

(113) Squires, R. R. *Chem. Rev.* **1987**, *87*, 623.

(114) Squires, R. R.; Lane, K. R. in *Gas Phase Inorganic Chemistry*; Russell, D. H.; Plenum Press, New York, **1989**; pp 43-91.

(115) Strobel, F.; Ridge, D. P. *J. Am. Soc. Mass. Spectrom.* **1990**, *1*, 192.

(116) Sung, S.-S.; Hoffman, R. *J. Am. Chem. Soc.* **1985**, *107*, 578.

(117) Teo, B. K.; Longoni, G.; Chung, F. R. K. *Inorg. Chem.* **1984**, *23*, 1257.

(118) Thompson, C. J. S. *The Lure and Romance of Chemistry*; George C. Harrop and Co. Ltd.: London, **1932**.

(119) Veltman, P. L. *U.S.P.* **1946**, # 2409167.

(120) Wade, K. *Transition Metal Clusters*; Johnson, B. F. G.; J. Wiley and Sons: New York, **1980**.

(121) Weast, R. C. *Handbook of Chemistry and Physics* **1974**, *54*, B4 - 38.

(122) Weddle, G. H.; Allison, J.; Ridge, D. P. *J. Am. Chem. Soc.* **1977**, *99*, 105.

(123) Wilkins, C. L.; Chowdhury, A. K.; Nuwaysir, L. M.; Coates, M. L. *Mass Spectrometry Reviews* **1989**, *8*, 67.

(124) Wilkinson, G.; Rosenblum, M.; Whiting, M. L.; Woodward, R. B. *J. Am. Chem. Soc.* **1952**, *74*, 2125.

(125) Wilkinson, G.; Cotton, F. A.; Birmingham, J. M. *J. Inorg. Nucl. Chem.* **1956**, *2*, 95.

(126) Wilkinson, G.; Cotton, F. A. *Prog. Inorg. Chem.* **1959**, *1*, 1.

(127) Wilson, F. C.; Shoemaker, D. P. *J. Chem. Phys.* **1958**, *27*, 809.

(128) Wronka, J.; Ridge, D. P. *J. Am. Chem. Soc.* **1984**, *106*, 67.

(129) Wronka, J.; Forbes, R.; Laukien, F.; Ridge, D. P. *J. Phys. Chem.* **1987**, *91*, 6450.

(130) Zagorevskii, D. V.; Nekrasov, Y. S.; Nurgalieva, G. A. *J. Organomet. Chem.* **1980**, *194*, 77.

(131) Zeise, W. C. *Ann. Phys.* **1827**, *9*, 932.

CHAPTER 2

Ion Molecule Chemistry of

Tetracarbonyl (η^5 - Cyclopentadienyl) Vanadium

{ $CpV(CO)_4$ }

I Introduction

Tetracarbonyl (η^5-cyclopentadienyl) vanadium, $CpV(CO)_4$, is an orange-coloured crystalline, air-sensitive solid, melting at 139° C and subliming at 90° C (0.5 mm Hg). First prepared by Fischer and Hafner in 1954[10], its molecular geometry resembles a "four-legged piano stool", a square pyramidal $V(CO)_4$ unit capped by a pinacoid pentagonal η^5-Cp unit. The crystal structure was first elucidated in 1967[33].

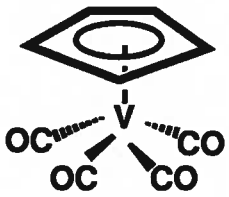

Vanadium carbonyls and organo-vanadium carbonyls have been of marked interest since the synthesis in 1956 of the vanadium homologue of ferrocene; i.e., Cp_2V, or vanadocene by Wilkinson[34]. Some related organo-vanadium species, first synthesised in solution, were $Cp_2V_2(CO)_5$ in 1970[24]; the $Cp_2V(CO)_2^+$ cation[7], and vanadium carbonyls, $V(CO)_4$ and $V(CO)_5$[21].

Gas phase reactions of bare, as well as complexed vanadium ions have been examined since the positive ion mass spectral analyses on $CpV(CO)_4$ by Winters[35] and Müller[23] from 1965 to 1970. In these studies, series of daughter cations showing successive losses of CO and Cp ligands were observed. Energetics of bonds involving vanadium atoms in the gas phase have been analysed and collated[1,5,6,30]. Bond order, bond strength and kinetics of gaseous V^+ when combined with hydrogen[9]; alkane, alkene and alkyne units[2-4,17]; and oxygen[18,26] have been examined.

Other mass spectral analyses have yielded evidence of gas phase cation-molecule condensations resulting in generation of bimetal clusters such as $Cp_2V_2(CO)_3^+$, first noted by Fischer and Schneider[11] and Müller[23] in 1970. In the latter study, $Cp_2V_2(CO)_{0\text{-}5}^+$

ions were seen in the mass spectra of $Cp_2V_2(CO)_5$. However, gas phase kinetic studies on these and related ions, and on other Cp-vanadium carbonyls have not yet been performed. The present study, involving $CpV(CO)_4$ positive and negative ion-molecule chemistry by FT-ICR-MS provides some useful information regarding the behaviour of bare and ligated organo-vanadium ions in the gas phase.

II Results and Discussion

1. Positive Ion Chemistry

Ionisation by a 25 eV electron beam on tetracarbonyl (η^5-cyclopentadienyl) vanadium, $CpV(CO)_4$, generates fragment ions in the following proportions: CpV^+ (42%), $CpVCO^+$ (10%), $CpV(CO)_2^+$ (14%), $CpV(CO)_3^+$ (4%), $CpV(CO)_4^+$ (12%), V^+ (7%) and minor amounts of $C_3H_3V^+$ (5%). This ion distribution compares with that of Winters[35], who found the following cation distributions using 70 eV electron ionisation: CpV^+ (41%), $CpVCO^+$ (2.5%), $CpV(CO)_2^+$ (4.3%), $CpV(CO)_3^+$ (1.5%), $CpV(CO)_4^+$ (3.3%), V^+ (24%), $C_3H_3V^+$ (13%). Typical examples of FT - ICR mass spectra measured at 6.0×10^{-8} torr pressure, exhibiting these ions immediately after electron ionisation, and subsequently, are as follows: Figure 2.1(a), initial cation fragments; Figure 2.1(b), after 300 msec had elapsed; Figure 2.1(c), after 600 msec; and Figure 2.1(d), after 25 seconds. A table of typical experimental data showing masses of ions and their intensities is shown in Table 2.1.

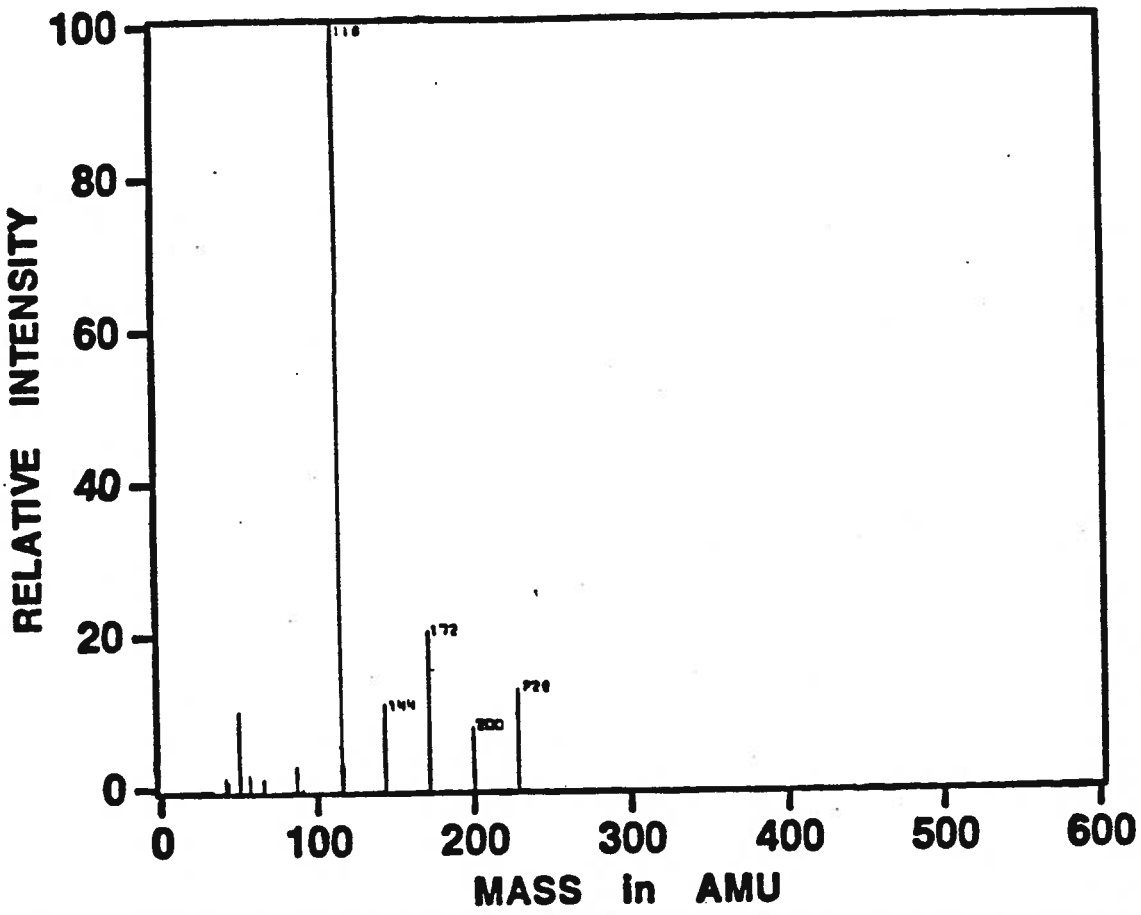

Figure 2.1(a). FT-ICR Positive Ion Mass Spectrum of $CpV(CO)_4$; 0 msec.; 25 eV; $p = 6.0 \times 10^{-8}$ torr

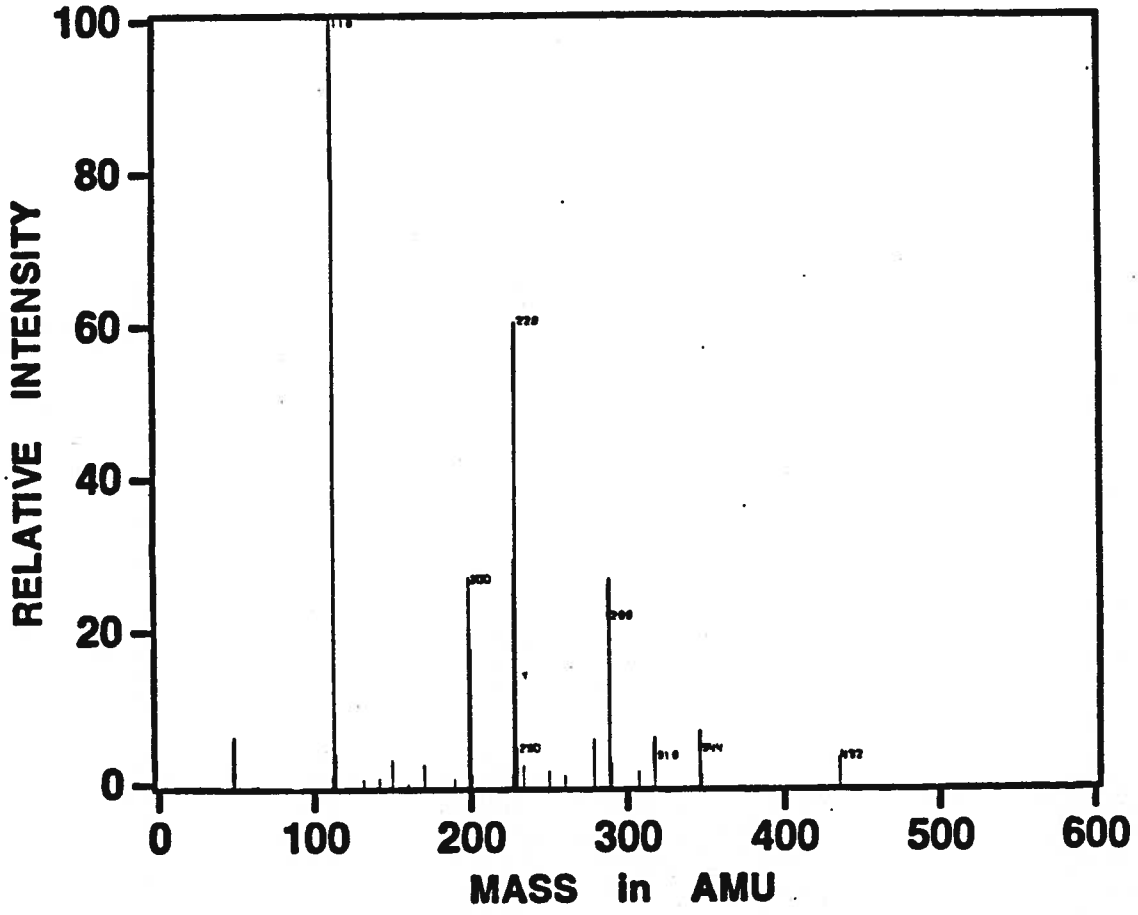

Figure 2.1(b). FT-ICR Positive Ion Mass Spectrum of $CpV(CO)_4$; 300 msec.; 25 eV; $p = 6.0 \times 10^{-8}$ torr

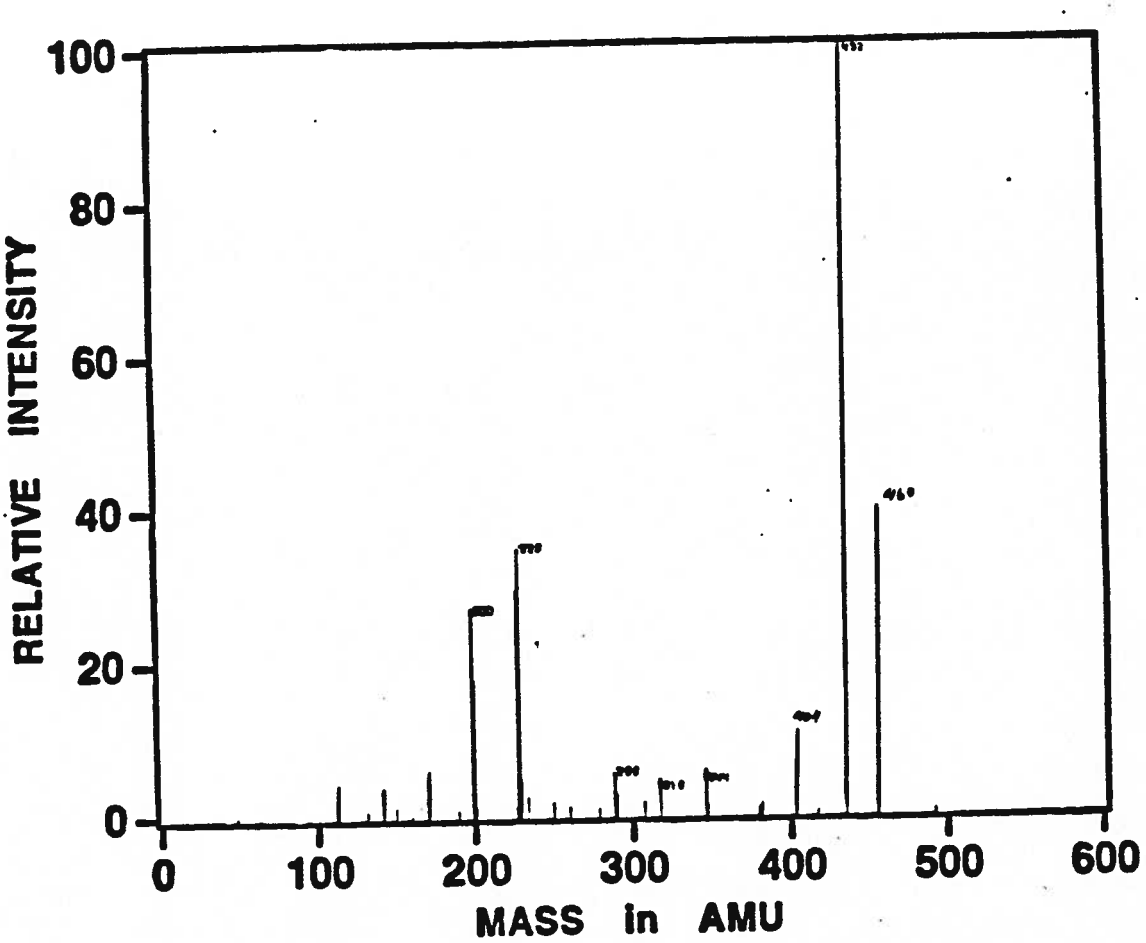

Figure 2.1(c). FT-ICR Positive Ion Mass Spectrum of $CpV(CO)_4$; 600 msec.; 25 eV; $p = 6.0 \times 10^{-8}$ torr

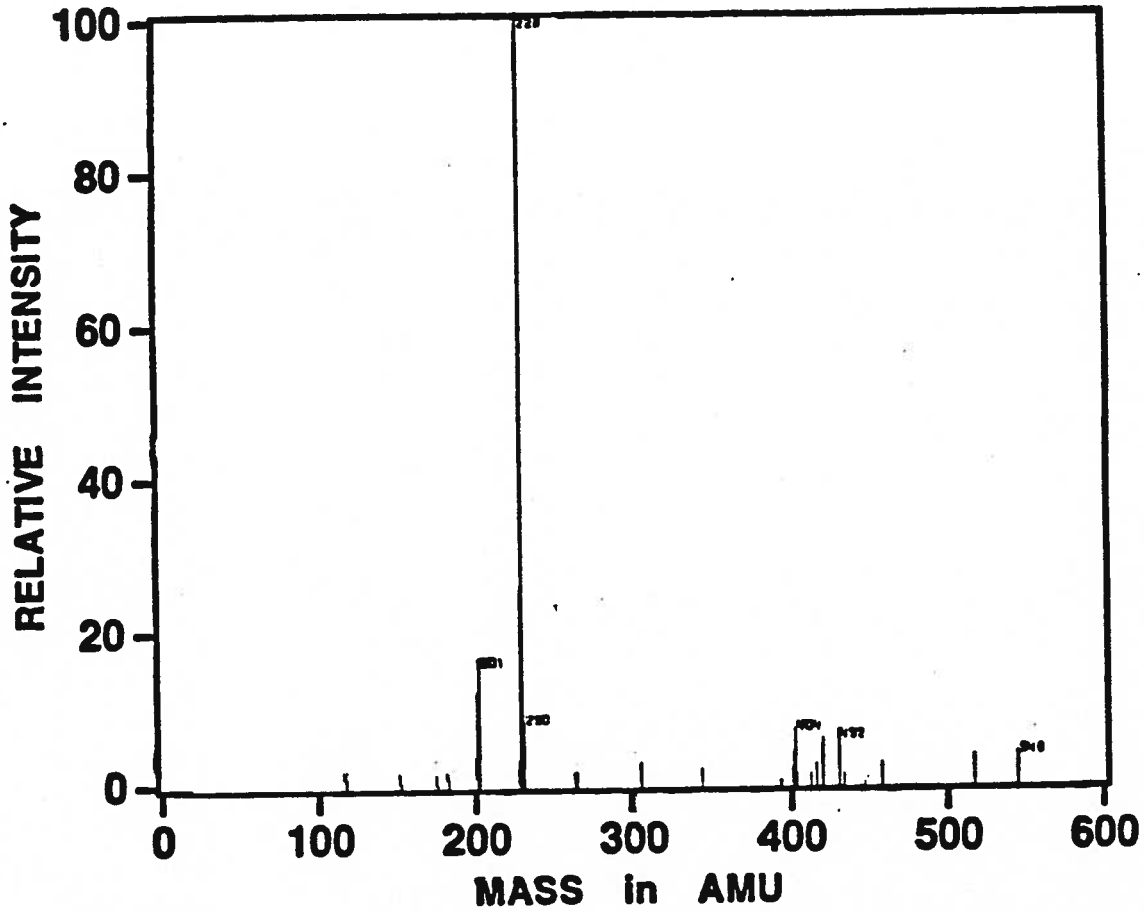

Figure 2.1(d). FT-ICR Positive Ion Mass Spectrum of $CpV(CO)_4$; 25 sec.; 25 eV; p = 6.0×10^{-8} torr

TABLE 2.1

Sample Mass Table for $CpV(CO)_4$ Cations (5000 msec)

Formula	Measured Mass[a]	Expected Mass[a]	Δ (ppm)	Rel. Int. (%)
^{51}V (99.76%)	50.9335	50.9435	10	2.6
C_3H_3V	89.8995	89.9670	68	2.0
C_5H_5V	115.9865	115.9826	4[b]	13.3
CpVCO	144.0002	143.9775	23	2.7
$CpV(CO)_2$	171.9898	171.9724	17	3.7
$CpV(CO)_3$	199.9358	199.9673	32	28.9
$CpV(CO)_4$	227.9626	227.9622	1[b]	100
$(CpV)_2$	231.8427	231.9657	123	2.0
$(CpV)_2CO$	259.8998	259.9606	61	5.1
$(CpV)_2(CO)_2$	287.9427	287.9555	13	7.0
$(CpV)_2(CO)_3$	315.9517	315.9504	2[b]	2.6
$(CpV)_2(CO)_4$	343.9555	343.9453	11	8.1
$(CpV)_3$	-----	347.9488	---	--
$(CpV)_3CO$	-----	375.9437	---	--
$(CpV)_3(CO)_2$	403.9750	403.9387	36	7.3
$(CpV)_3(CO)_3$	431.7990	431.9335	135	19.4
$(CpV)_3(CO)_4$	459.9129	459.9284	16(b)	13.5

[a] in daltons

[b] calibrant mass

General temporal behaviour patterns for each fragment ion were determined by the single resonance technique, in which the ions were generated by EI, allowed to react over measured time periods, then analyzed by FT-ICR. During reaction periods of up to 25 seconds, the following polynuclear ion cluster fragments were generated:

$Cp_2V_2(CO)_{0,1,2,3,4}^+$

$Cp_3V_3(CO)_{2,3,4}^+$

$Cp_4V_4(CO)_{3,4}^+$

Typical formation and disappearance behaviour of primary, $(CpV)_1(CO)_{0\text{-}4}^+$, fragment cations are illustrated in Figure 2.2. Figures 2.3 and 2.4 show analogous temporal behaviour patterns of some of the most prominent binuclear cluster cations, i.e., $(CpV)_2(CO)_{2\text{-}4}^+$, and trinuclear cluster cations, i.e., $(CpV)_3(CO)_{3,4}^+$.

Application of FT-ICR multiple resonance techniques developed earlier[25] permitted identification of reaction products of each daughter ion. Using multiple resonance, individual ion species were selected and products generated by that ion were temporally monitored. For example, Figure 2.5(a,b) shows two multiple resonance spectra of CpV^+ ion, initially and at 200 msec, after its ion products had been allowed to form. A plot of temporal behaviour of CpV^+ and its products is illustrated in Figure 2.6. Analogous spectra for the $CpV(CO)_3^+$ ion, taken at at the same time intervals, are shown in Figure 2.7(a,b), and temporal plots of this ion and its products are shown in Figure 2.8. An example of analogous spectra, measured initially and at 600 msec, and temporal behavioral plots for an important secondary cation cluster, $(CpV)_2(CO)^+$, and its reaction products, are shown in Figure 2.9(a,b) and Figure 2.10, respectively.

Kinetic data obtained from temporal ion monitoring were used to obtain initial relative rates of formation and decay of each ion product. Table 2.2 lists rate constants for the disappearance of the principal reactive ions over time. Monitoring the temporal history of each ion product revealed an interrelated series of reactive pathways which are summarized in the following paragraphs.

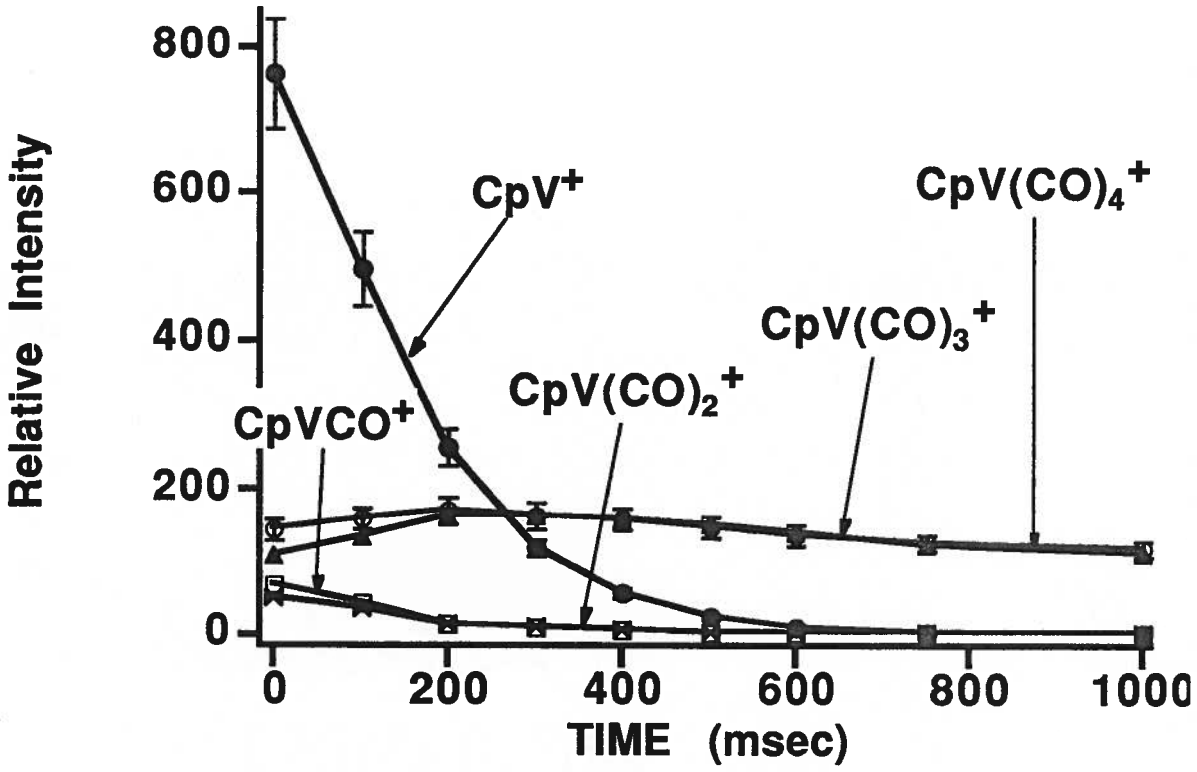

Figure 2.2. **Temporal Behaviour of Primary Fragment Cations of $CpV(CO)_4$**

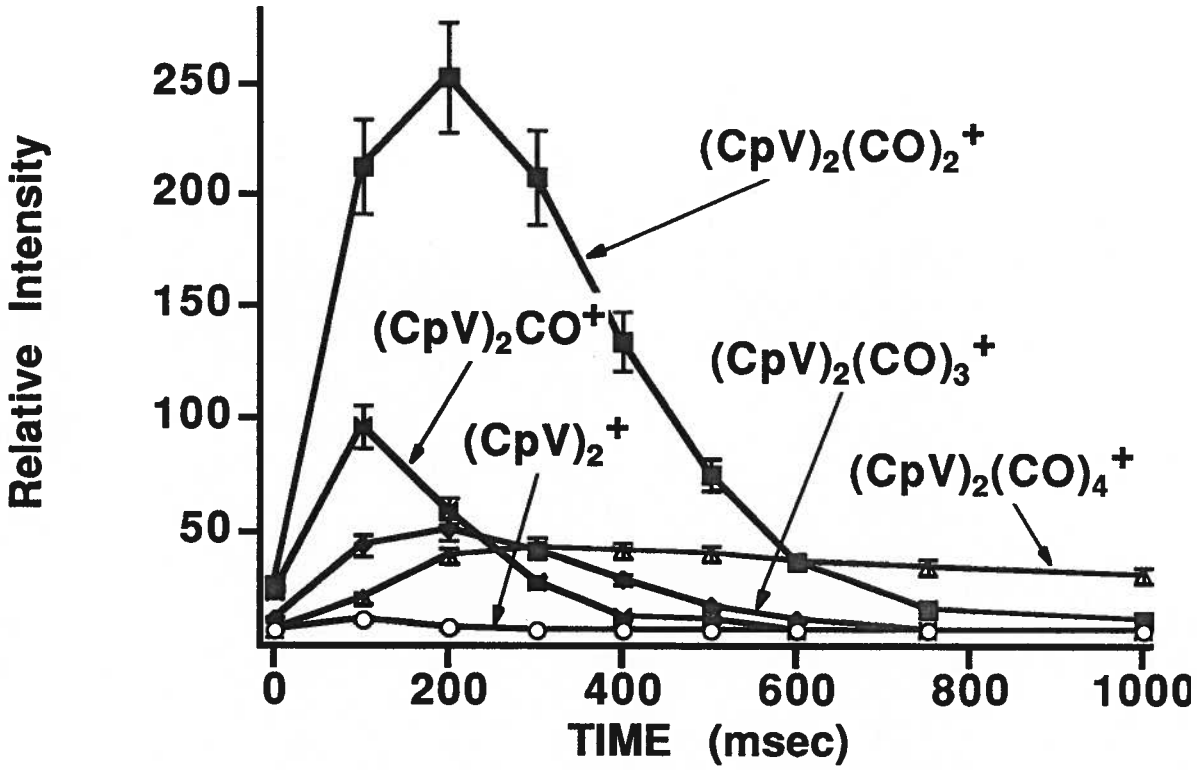

Figure 2.3. Temporal Behaviour of Binuclear Cluster Cations of $CpV(CO)_4$

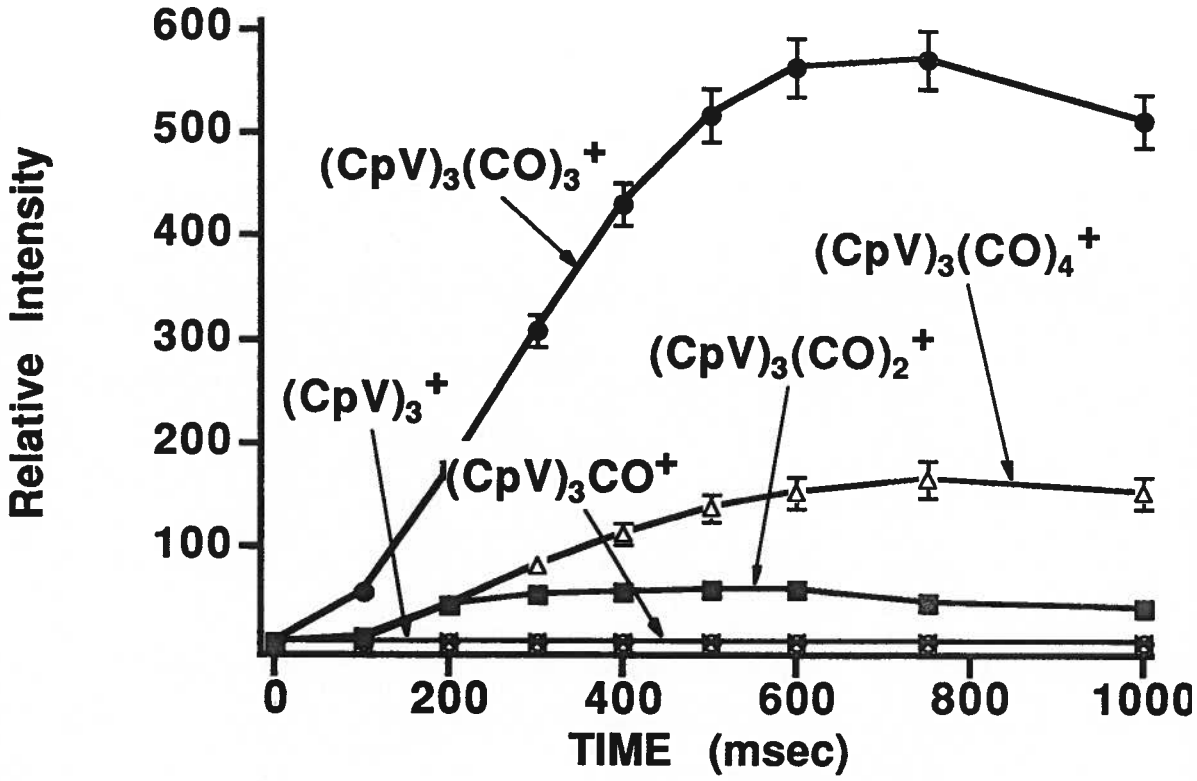

Figure 2.4. Temporal Behaviour of Trinuclear Cluster Cations of $CpV(CO)_4$

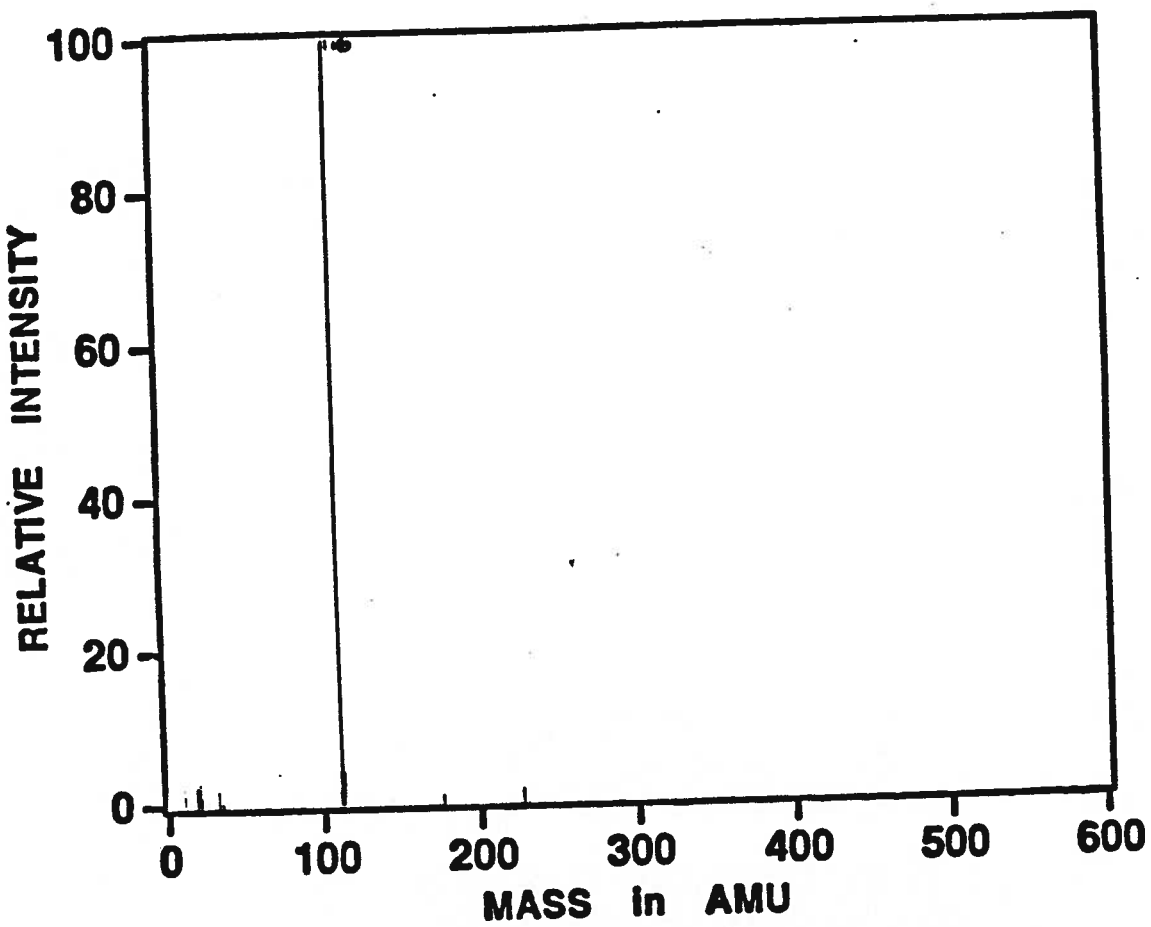

Figure 2.5(a). Multiple Resonance Mass Spectrum of CpV^+; 0 msec.; $p = 6.0 \times 10^{-8}$ torr

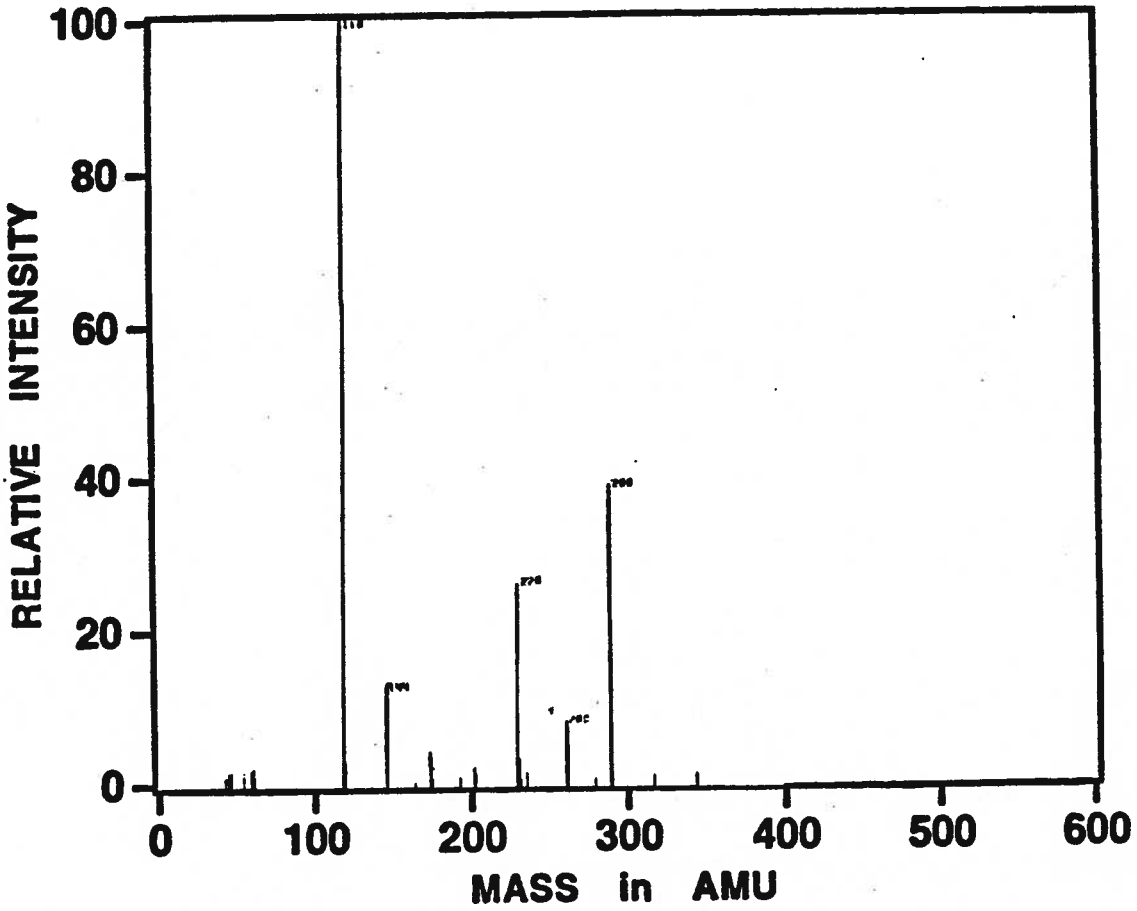

Figure 2.5(b). Multiple Resonance Mass Spectrum of CpV^+ and Cation Products; 200 msec; p = 6.0×10^{-8} torr

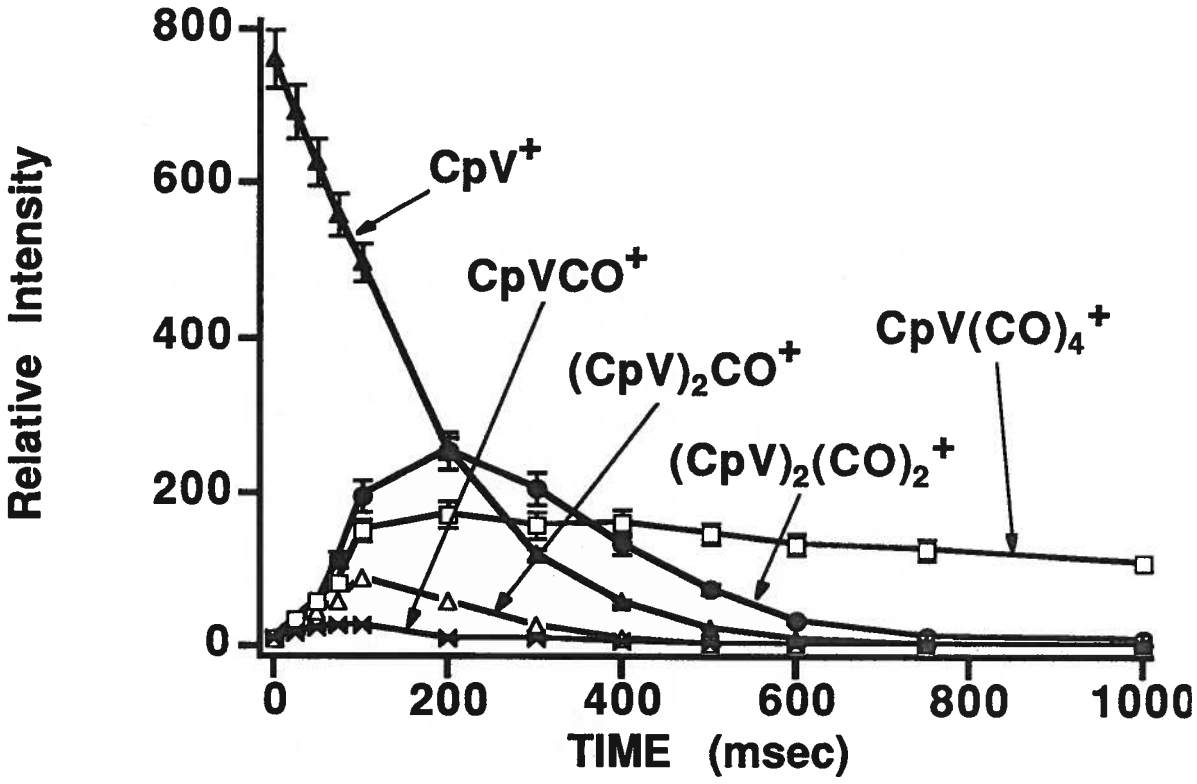

Figure 2.6. Temporal Behaviour of CpV^+ and Cation Products

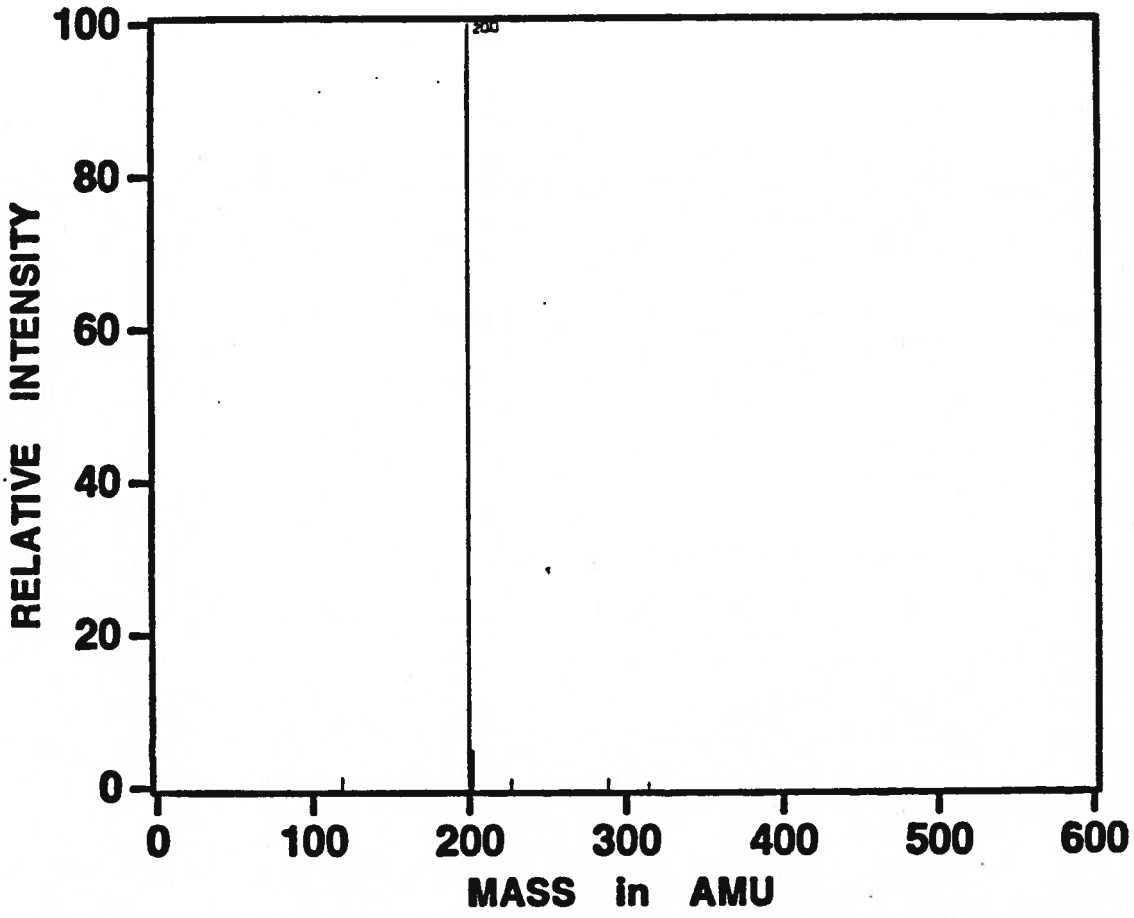

Figure 2.7(a). Multiple Resonance Mass Spectrum of $CpV(CO)_3^+$; 0 msec.; $p = 6.0 \times 10^{-8}$ torr

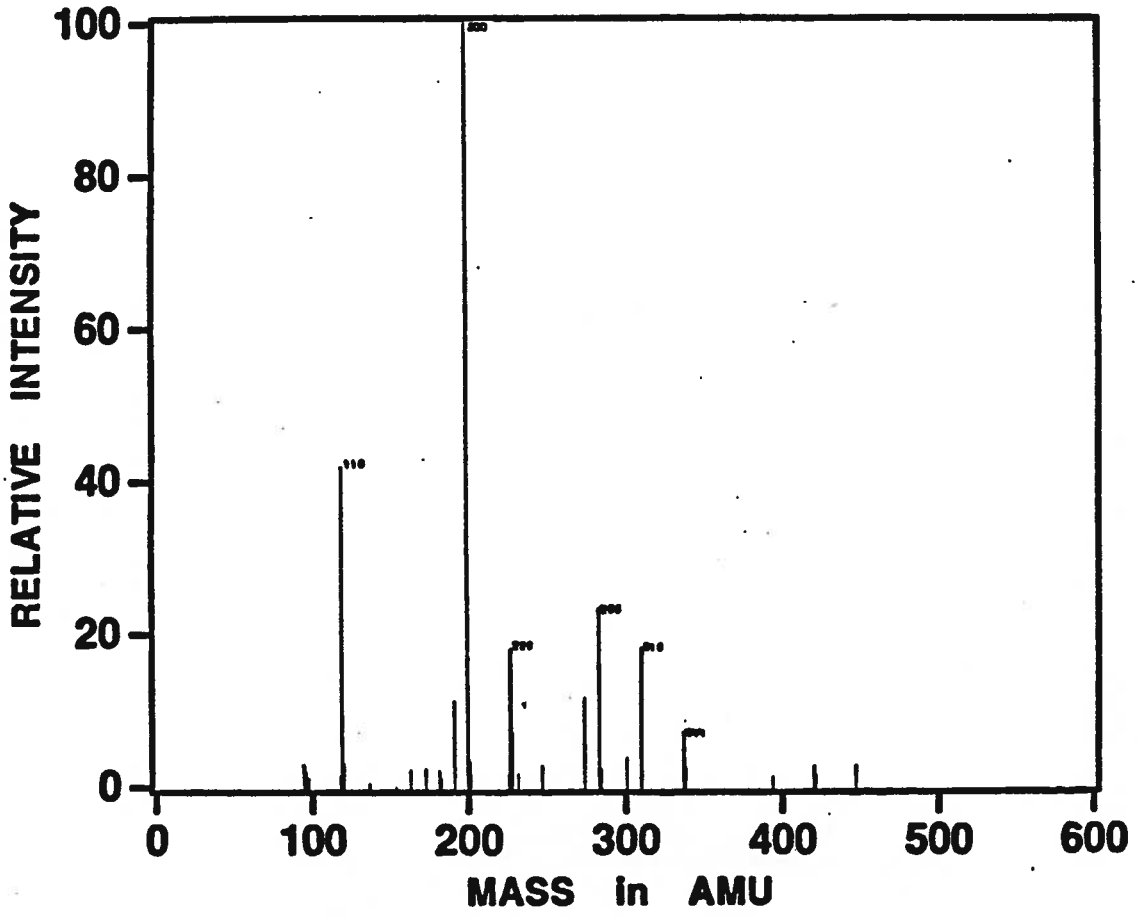

Figure 2.7(b). Multiple Resonance Mass Spectrum of $CpV(CO)_3^+$ and Cation Products; 200 msec; $p = 6.0 \times 10^{-8}$ torr

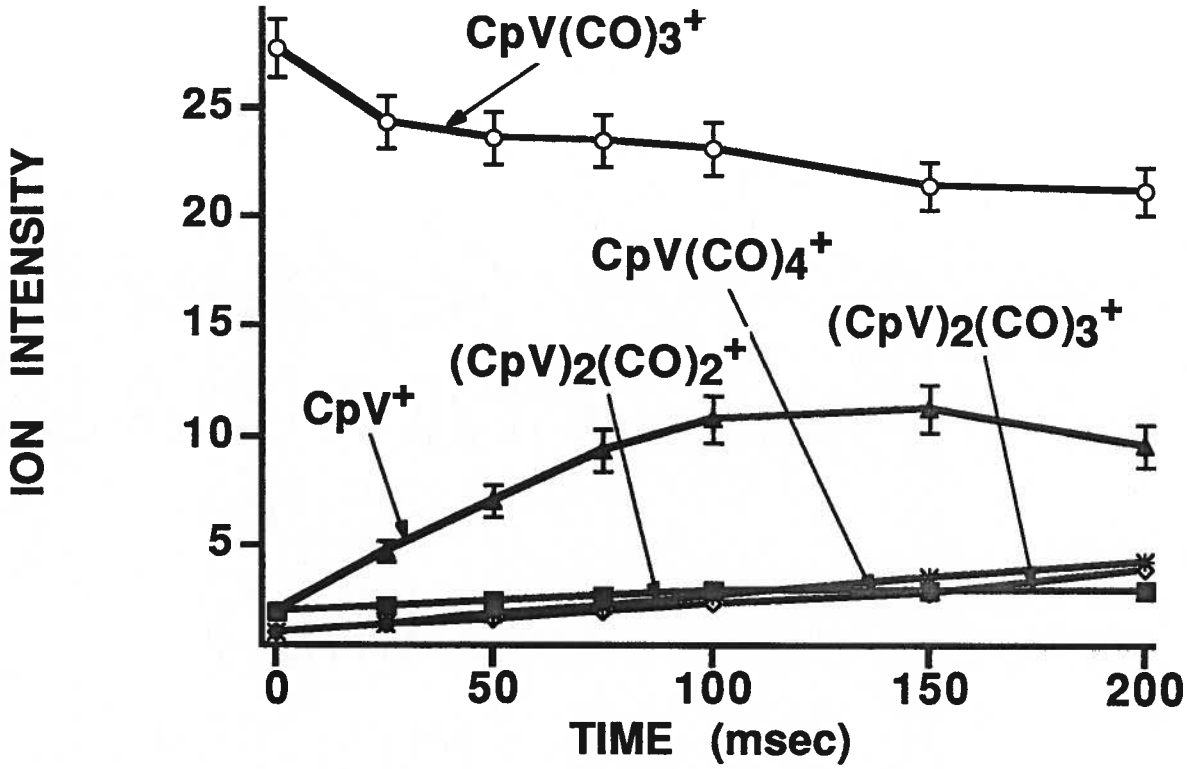

Figure 2.8. Temporal Behaviour of $CpV(CO)_3^+$ and Cation Products

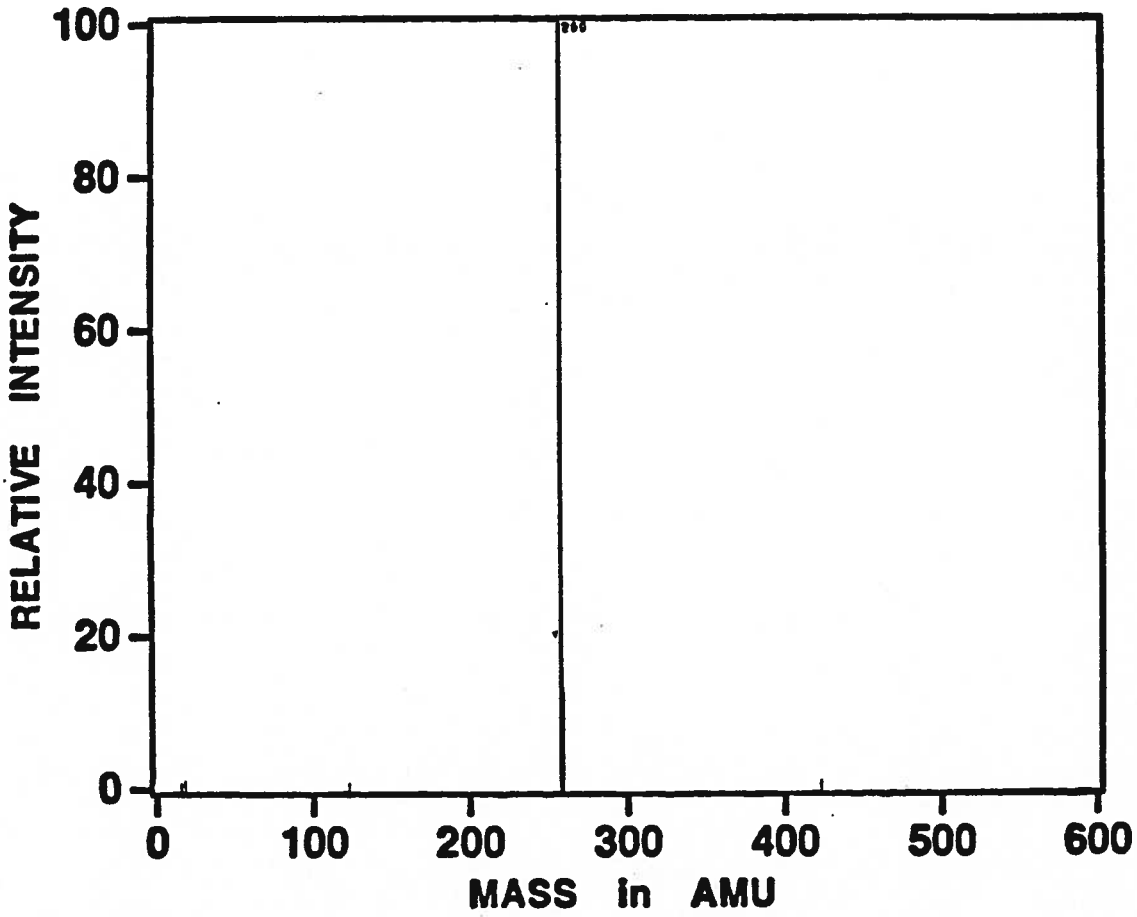

Figure 2.9(a). Multiple Resonance Mass Spectrum of $(CpV)_2CO^+$; 0 msec; p = 6.0×10^{-8} torr

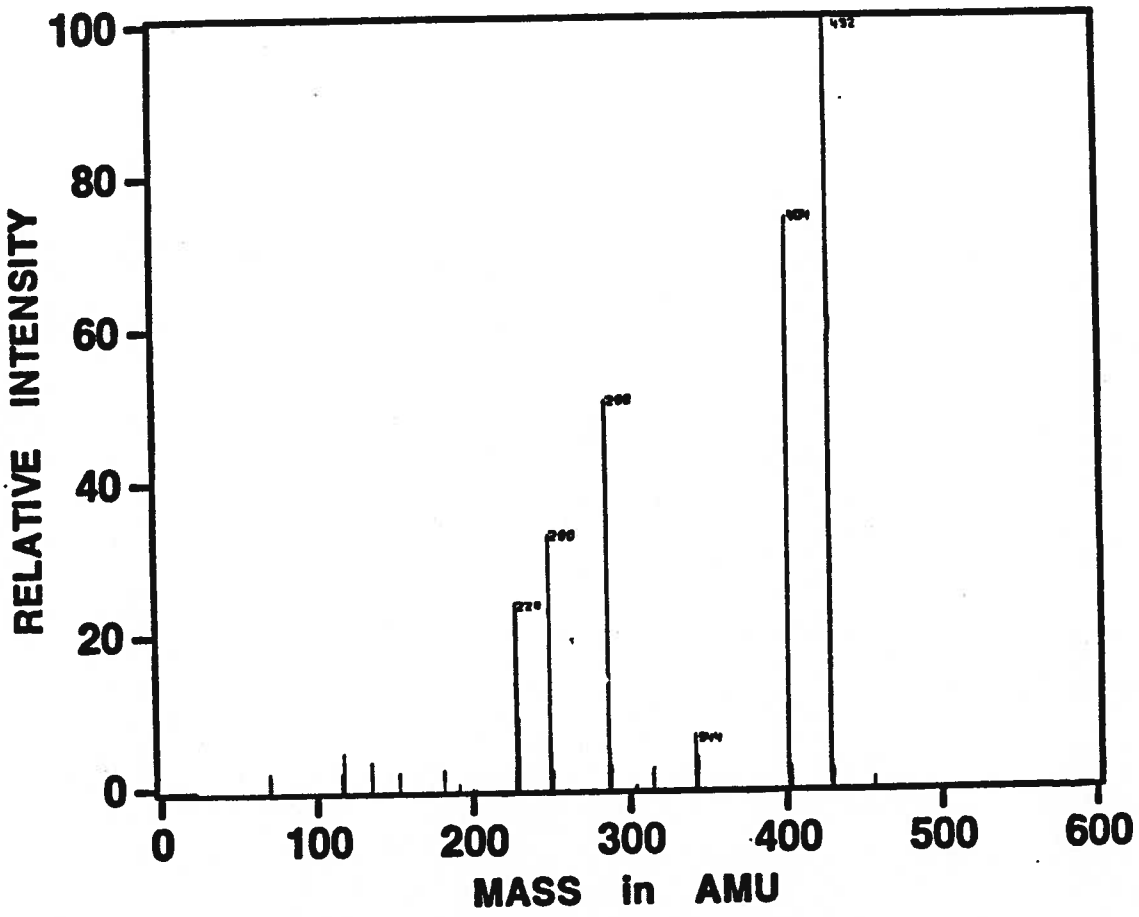

Figure 2.9(b). Multiple Resonance Mass Spectrum of $(CpV)_2CO^+$ and Cation Products; 600 msec; $p = 6.0 \times 10^{-8}$ torr

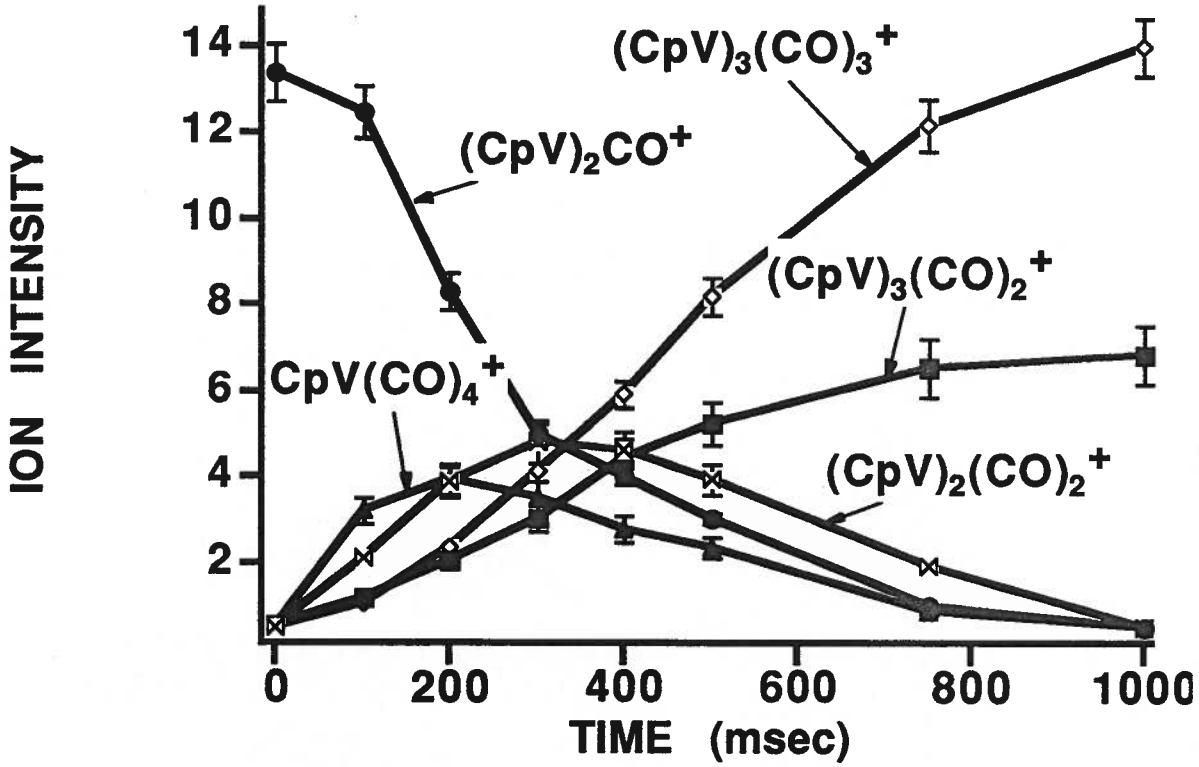

Figure 2.10. Temporal Behaviour of $(CpV)_2CO^+$ and Cation Products

TABLE 2.2

Disappearance Rates for Vanadium Cations

Ion	Rate Constant (k') (sec^{-1}) *	Rate Constant (k) ($x10^9$ $molec.^{-1}cm^3sec^{-1}$) #
V^+	0.604	2.61
CpV^+	0.382	1.65
$CpVCO^+$	0.227	0.98
$CpV(CO)_2^+$	0.120	0.52
$CpV(CO)_3^+$	0.0255	0.12
$CpV(CO)_4^+$	0.010	0.043
$(CpV)_2^+$	0.259	1.12
$(CpV)_2CO^+$	0.211	0.91
$(CpV)_2(CO)_2^+$	0.101	0.44
$(CpV)_2(CO)_3^+$	0.0394	0.17
$(CpV)_2(CO)_4^+$	<.005	<0.02
$(CpV)_3(CO)_2^+$	<.005	<0.02
$(CpV)_3(CO)_3^+$	0.0413	0.18
$(CpV)_3(CO)_4^+$	0.0749	0.32
$(CpV)_4(CO)_3^+$	<.005	<0.02

* Calculated from linear first-order rate plots; all data ± 10%

\# Calculated from experimental parameters:
pressure = $6.0x10^{-8}$ torr; temperature = 350°K; α = 22.36;
all data ± 30%

PRINCIPAL REACTIVE PATHWAYS IN THE $CpV(CO)_4$ SYSTEM

Primary (EI) fragmentation of the neutral parent $CpV(CO)_4$ molecule occurs as follows:

$$CpV(CO)_4 + e^- \rightarrow CpV(CO)_{0,1,2,3,4}^+ , V^+ \text{ (minor } C_3H_3V^+ \text{)}$$

Ion-Molecule Reactions **($Ion^+ + CpV(CO)_4 \rightarrow$ products)**

Class 1. Charge transfer from neutral parent molecule to ion-molecule product cation:

$(CpV)(CO)_{0,1,2,3}^+$	+	$CpV(CO)_4$	→	$CpV(CO)_4^+$	+ . . .
$(CpV)_2(CO)_{0,1,2,3,4}^+$	+	"	→	"	+ . . .
$(CpV)_3(CO)_{2,3,4}^+$	+	"	→	"	+ . . .
$(CpV)_4(CO)_{3,4}^+$	+	"	→	"	+ . . .
V^+	+	"	→	"	+ . . .

Relative rates of electron transfer for some of these processes are given in Table 2.3. The prevalence of electron transfer processes from the neutral $CpV(CO)_4$ molecule to each reactive cation in this system reflects the fact that electron affinities in all these CpV ionic cluster fragments exceed the ionization potential of the neutral $CpV(CO)_4$ molecule; an expected trend, since formal electron count per vanadium atom in each ion is lower than that in the neutral molecule. Ions with very large formal electron-deficient vanadium cores, such as in CpV^+ or $CpVCO^+$, should be expected to react rapidly in this mode, and this is observed; e.g., CpV^+ (with 9 electrons per vanadium atom) reacts approximately 2.3 times faster than $CpV(CO)_2^+$ (13 electrons per V atom), and $CpVCO^+$ (11 electrons per V atom) reacts 1.6 times faster in producing $CpV(CO)_4^+$. Again, $(CpV)_2^+$ reacts approximately 2.8 times faster, and $(CpV)_2CO^+$ reacts 2.0 times faster, than does $(CpV)_2(CO)_2^+$. [In some cases the assumption has been made that simple electron transfer from neutral molecule to the ion cluster fragment is occurring according to the equation

$$(CpV)_2(CO)_3^+ + CpV^*(CO)_4 \rightarrow CpV^*(CO)_4^+ + \ldots$$

rather than carbonyl transfer from the neutral combined with fracturing and loss of a CpV unit from $(CpV)_2(CO)_3^+$]

TABLE 2.3

Relative Electron Transfer Rates for Vanadium Cations Reacting with Neutral $CpV(CO)_4$ Molecules

Ion	Rate Constant (k) ($\times 10^9$ molec.$^{-1}$cm^{3}sec^{-1}) *	Relative Rate #
V^+	2.61	100
CpV^+	0.541	21
$CpVCO^+$	0.372	14
$CpV(CO)_2^+$	0.238	9
$CpV(CO)_3^+$	0.06[a]	2
$(CpV)_2^+$	0.368	14
$(CpV)_2CO^+$	0.273	10
$(CpV)_2(CO)_2^+$	0.134	5
$(CpV)_2(CO)_3^+$	0.02	1
$(CpV)_3(CO)_3^+$	0.043	2
$(CpV)_3(CO)_4^+$	<0.02	<1

* Calculated from total decay rate constant of reacting cation; all data ± 10%

Relative to V^+ rate taken as 100; all data ± 30%

[a] May be due to carbonyl addition contribution as well.

Apparently all ionic species present, including all polynuclear ionic cluster fragments such as $(CpV)_3(CO)_3^+$, $(CpV)_3(CO)_4^+$, and $(CpV)_4$ clusters eventually absorb an electron transferred from the parent molecule (which is ever-present in large excess). Consequently, $CpV(CO)_4^+$ becomes the predominant ionic species present after 25 sec.

Class 2. Ion-molecule condensation reactions with simultaneous ejection of up to 7 CO ligands. Principal reaction paths for each fragment ion are summarised in the following equations:

Primary fragment ion condensations:

$CpV^+ + CpV(CO)_4 \rightarrow (CpV)_2(CO)_{0,1,2}^+ + nCO$

$CpVCO^+ + " \rightarrow (CpV)_2(CO)_{0,1,2,3}^+ + "$

$CpV(CO)_2^+ + " \rightarrow CpV)_2(CO)_{0,1,2,3,(4*)}^+ + nCO$

$CpV(CO)_3^+ + " \rightarrow (CpV)_2(CO_{(0*),1,2,3,4}^+ + "$

$CpV(CO)_4^+ + " \rightarrow (CpV)_2(CO)_{1,2,3,4}^+ + "$

Binuclear ionic cluster condensations:

$(CpV)_2^+ + CpV(CO)_4 \rightarrow (CpV)_3(CO)_{(1*),2,3}^+ + nCO$

$(CpV)_2(CO)_{1,2,3}^+ + " \rightarrow (CpV)_3(CO)_{2,3,4}^+ + "$

$(CpV)_2(CO)_4^+ + " \rightarrow (CpV)_3(CO)_{3,4}^+ + "$

Trinuclear ionic cluster condensations:

$(CpV)_3(CO)_{2,3,4}^+ + CpV(CO)_4 \rightarrow (CpV)_4(CO)_{(2*),3,4}^+ + n\,CO$

[* ion intensities less than 5%]

Overall relative clustering rates for the more abundant cations are listed in Table 2.4. Rates decrease with cluster size, and numbers of carbonyl ligands present in the reacting cation.

Condensation with the parent neutral molecule, with simultaneous loss of one or more CO ligands, is a prominent reaction path in many other aryl transition-metal carbonyl

TABLE 2.4

Relative Clustering Rates for Vanadium Cations Reacting with Neutral $CpV(CO)_4$ Molecules

Ion	Rate Constant (k) ($\times 10^9$ molec.$^{-1}$cm^{3}sec^{-1}) *	Relative Rate #
CpV^+	1.02	100
$CpVCO^+$	.355	35
$CpV(CO)_2^+$	.199	20
$CpV(CO)_3^+$	.028	3
$CpV(CO)_4^+$	.017	2
$(CpV)_2^+$	.290	30
$(CpV)_2CO^+$	.411	40
$(CpV)_2(CO)_2^+$	.208	20
$(CpV)_2(CO)_3^+$	.100	10
$(CpV)_2(CO)_4^+$	<.02	<2
$(CpV)_3(CO)_2^+$	<.02	<2
$(CpV)_3(CO)_3^+$	.065	6
$(CpV)_3(CO)_4^+$	.260	26

* Calculated from total decay rate constant including all clustering pathways; all data ± 10%

Relative to CpV^+ rate taken as 100; all data ± 30%

systems recently investigated by many authors, including Fredeen[13,14]; Foster[12]; Meckstroth[19,20]; Parisod[25]; and Mullen[22]. In the present system, further condensation resulting in generation of larger cluster ions containing Cp_5V_5, Cp_6V_6 or larger cores may occur, but as yet has not been detected. If the process of condensation with the parent molecule must compete with electron transfer from the parent, then for the highly electron-deficient ions such as those in this system, a cluster can be generated during one collision with the parent neutral, but may gain an electron from the neutral molecule in a subsequent collision, losing its positive charge and becoming "invisible" to the detector. In each polynuclear series clustering rates apparently are largest for reactive ions with 2 or 3 CO ligands; rates dwindle when the number of CO units present in the ion is large (i.e. > 3).

Class 3. Carbonyl Transfer

(1) Loss of CO ligands by some reacting cations: (y = number of CO ligands lost subsequently by the following reacting ions):

$(CpV)(CO)_2^+$ (y = 1,2) $(CpV)(CO)_3^+$ (y = 1,2,3);

$(CpV)(CO)_4^+$ (y = 1,2,3,4); $(CpV)_2(CO)^+$ (y = 1);

$(CpV)_2(CO)_2^+$ (y = 1,2); $(CpV)_2(CO)_3^+$ (y = 1,2,3);

$(CpV)_2(CO)_4^+$ (y = 1);

$(CpV)_3(CO)_{3,4}^+$ (y = 1)

Table 2.5 lists relative rates of CO loss for some of these ions. Cations which are relatively rich in CO (e.g., $CpV(CO)_4^+$, $Cp_2V_2(CO)_4^+$, or $Cp_3V_3(CO)_4^+$) and which may be excited and possess excess kinetic energy after electron ionization or rebound from collisions with neutrals, react by ejecting one or more CO ligands. Measured CO loss rates reflect this to some degree: for instance relative rates of CO ejection by ions $CpV(CO)_3^+$; $CpV(CO)_2^+$; and $CpVCO^+$ are in the ratios 10 : 7 : <2, as shown in Table 2.5. on the following page.

TABLE 2.5

Relative CO Ligand Loss Rates for Vanadium Cations Reacting with Neutral $CpV(CO)_4$ Molecules

Ion	Rate Constant (k) ($\times 10^9$ molec.$^{-1}$cm^{3}sec^{-1})*	Relative Rate #
$CpVCO^+$	<.010	<.2
$CpV(CO)_2^+$	.043	.7
$CpV(CO)_3^+$	.061	1.0
$CpV(CO)_4^+$	.018	.3
$(CpV)_2CO^+$	.048	.8
$(CpV)_2(CO)_2^+$	.052	.9
$(CpV)_2(CO)_3^+$	.026	.45
$(CpV)_2(CO)_4^+$	<.010	<.2
$(CpV)_3(CO)_2^+$	<.010	<.2
$(CpV)_3(CO)_3^+$	.048	.8
$(CpV)_3(CO)_4^+$	<.010	<.2

* Calculated from total decay rate constant including all CO ligand loss pathways; all data ± 10%

Relative to $CpV(CO)_3^+$ rate taken as 1.0; all data ± 30%

(2) Addition of CO ligands by some reactive cations: (z = number of CO ligands abstracted from the neutral parent molecule by the following reacting ions) :

CpV^+ (z = 1,2,3);

$CpVCO^+$ (z = 1,2);

$CpV(CO)_2^+$ (z = 1);

$(CpV)_2^+$ (z = 1,2);

$(CpV)_2CO^+$ (z = 1,2);

$(CpV)_2(CO)_2^+$ (z = 1);

$(CpV)_2(CO)_3^+$ (z = 1);

$(CpV)_3(CO)_2^+$ (z = 1,2);

$(CpV)_3(CO)_3^+$ (z = 1).

Table 2.6 on the following page lists comparative CO absorption rates for some of these ions. The preceding ions, which are ligand unsaturated and "carbonyl - poor" (e.g. CpV^+, $Cp_2V_2CO^+$ or $Cp_3V_3(CO)_2^+$) abstract one or more CO ligands from the parent neutral $CpV(CO)_4$. During any specific ion-molecule interaction, the strong σ-basicity of CO ligands in the neutral $CpV(CO)_4$ molecule should favor their addition to cations of greater ligand unsaturation, (i. e. CO transfer to CpV^+, $Cp_2V_2^+$, $Cp_3V_3(CO)_2^+$) rather than their remaining attached to a neutral, electron-saturated, "CO - rich" $CpV(CO)_4$ parent molecule. Experimental rates of carbonyl abstraction generally exhibit this: for example, the relative rate of single CO absorption by $CpVCO^+$ and $CpV(CO)_2^+$ are in the approximate ratios 5: 1; and by $(CpV)_2(CO)^+$ and $(CpV)_2(CO)_2^+$ in the ratios 3: 1 , as shown in Table 2.6.

TABLE 2.6

Relative Rates of CO Ligand Addition for Vanadium Cations Reacting with Neutral $CpV(CO)_4$ Molecules

Ion	Rate Constant (k) ($\times 10^9$ molec.$^{-1}$cm^{3}sec^{-1})*	Relative Rate #
CpV^+	.100	1.0
$CpVCO^+$	.216	2.2
$CpV(CO)_2^+$	.043	.4
$CpV(CO)_3^+$	.013 **	.1
$(CpV)_2^+$	.494	5.0
$(CpV)_2CO^+$	.173	1.7
$(CpV)_2(CO)_2^+$	.048	.5
$(CpV)_2(CO)_3^+$	.026	.3
$(CpV)_2(CO)_4^+$	<.020	<.2
$(CpV)_3(CO)_2^+$	<.020	<.2
$(CpV)_3(CO)_3^+$	.048	.5
$(CpV)_3(CO)_4^+$	<.020	<.2

* Calculated from total decay rate constant including all CO ligand additions; all data ± 10%

Relative to CpV^+ rate taken as 1.0; all data ± 30%

** May be via electron transfer process only

Class 5. Hydrogen Exchange Reactions

The appearance of protonated ions, $CpV(CO)_{3,4}H^+$, implies that one of two processes occur: either the molecular cation donates a proton to a neutral molecule, i. e.:

$$C_5H_5V(CO)_4^+ + CpV'(CO)_4 \rightarrow CpV'(CO)_{3,4}(H)^+ + C_5H_4V(CO)_4 + ..$$

or else the neutral molecule donates a hydrogen atom to the molecular ion; i.e.:

$$CpV(CO)_4^+ + C_5H_5V'(CO)_4 \rightarrow CpV(CO)_{3,4}(H)^+ + C_5H_4V'(CO)_4 + ..$$

(Note: without discriminatory isotopic experiments, these processes are indistinguishable.) Initial rates of these reactions are similar to those of clustering and CO loss processes, but after 25 seconds the abundance of $CpV(CO)_4H^+$ (which possesses an 18-electron metal centre) slowly increases with respect to that of the molecular ion, $CpV(CO)_4^+$ (17 electron metal centre).

2. Reactions with Small Molecules

Some experiments were conducted using molecules H_2, O_2 and N_2 as collision gases with neutral $CpV(CO)_4$. Because of the experimental difficulties encountered (i.e.; in maintaining constant gas pressures, applying multiple resonance techniques to multiple, closely-spaced masses, and temporally monitoring a complex mixture of many adduct products), results were equivocal although many adduct product cations were observed, for example, $CpVO_2^+$, $CpV(CO)O^+$, $CpVH_2$+, $CpV(CO)_4H^+$.

In order to substantiate this adduct formation, high pressure, quadrupole mass analyses were performed. Reactivities of small molecules with neutral $CpV(CO)_4$ were studied in desorption chemical ionisation (DCI) experiments using available chemical ionization gases ammonia, methane and isobutane. Positive DCI spectra of $CpV(CO)_4$ using ammonia as a CI gas show many ammoniated adducts, for example, $CpVNH_3^+$. Analogous adduct ions containing CH_5^+ (i.e., CH_3+H_2) adducts were observed in positive DCI spectra using CH_4 and isobutane as chemical ionisation gases (e.g., $CpVCH_5^+$).

Addition products observed for each reagent gas molecule are summarised here and representative mass spectra (Figures 2.11-12) are shown on the following pages.

Cation Addition Products of $CpV(CO)_4$

1.Ammonia CI adduct formation

i. protonation: $CpV(CO)_4H^+$ (amu 229)

ii. ammonia adduct formation: $CpV(NH_3)_{1,2,3}^+$ (amu 133, 150, 167); bi- and trinuclear adduct formation: $(CpV)_2(CO)_{1,2}(NH_3)_2^+$ (amu 294, 322); $(CpV)_2(CO)_{2,3}NH_3^+$ (amu 306, 334); and $(CpV)_3(CO)_{2,3}NH_3^+$.(amu 421, 449). Figure 2.11 is a typical positive ion ammonia DCI spectrum of $CpV(CO)_4$, showing the presence of some of these protonated and ammoniated adducts.

2. Methane adducts

i. protonation: $CpV(CO)_4H^+$ (amu 229)

ii. methylated adduct formation:

$CpV(H)_{1,2}(CH_3)_{1,2}^+$ (amu 132, 133, 147, 148); $(CpV)_2(H)_{1,2}(CH_3)_{1,2}^+$ (amu 248, 249, 263, 264); $(CpV)_2CO(H)_{1,2}(CH_3)^+$ (amu 276, 277); and $(CpV)_2(CO)_{2,3}(H)_{1,2}(CH_3)_{1,2}^+$ (amu 304-348). Figure 2.12 is a representative methane positive ion DCI spectrum showing some of the adduct ions including several hydrogenated and methylated species.

3. Isobutane adducts

i. protonation: $CpV(CO)_4H^+$ (amu 229)

ii. methylated adduct formation: $CpV(H)_{1,2}(CH_3)_{1,2}^+$ (amu 132, 133, 147, 148). These adducts are similar to those produced by methane DCI in 2. above.

Protonation and adduct formation are the general processes occurring in each of the three cases. Most of the adduct cations contain from one to three addition ligands (NH_3, CH_5, CO or H) per CpV unit, depending upon ligand unsaturation of the fragment ion;

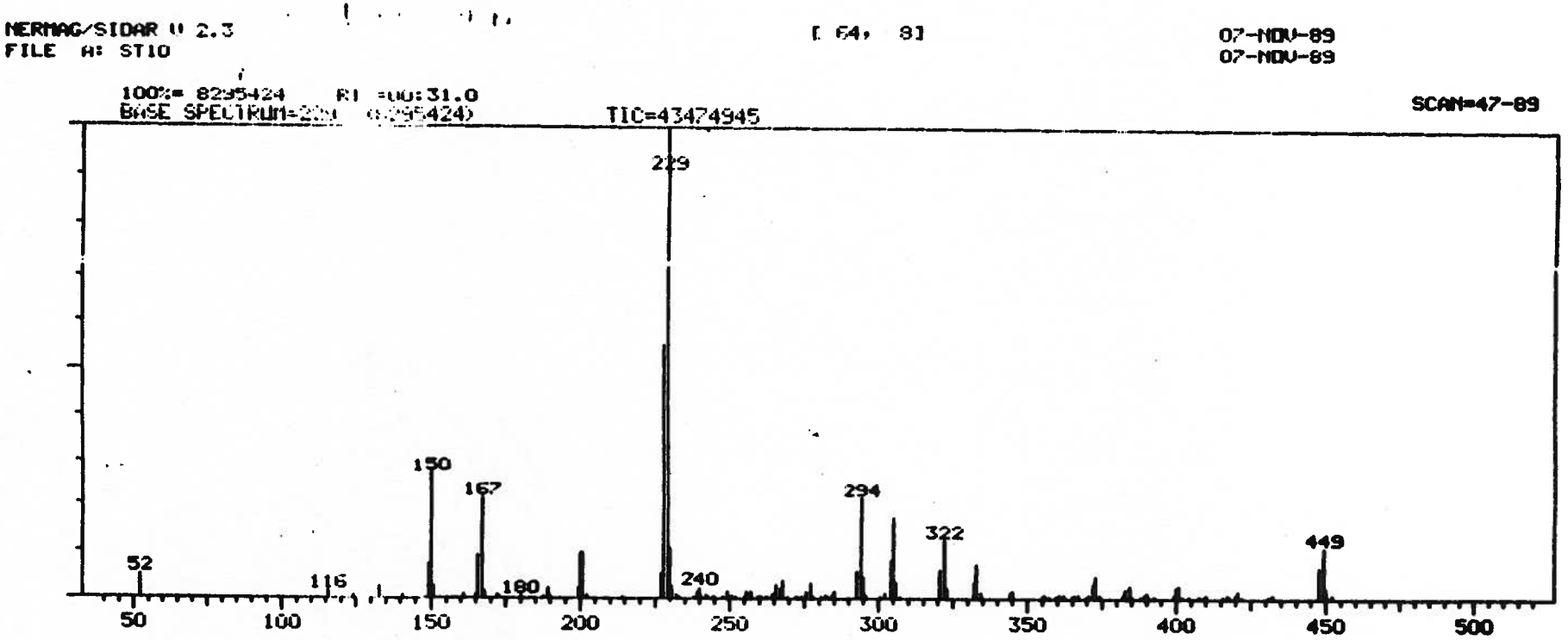

Figure 2.11. Positive Ion Mass Spectrum of $CpV(CO)_4$: Ammonia Chemical Ionization; 70 eV; p = .01 torr

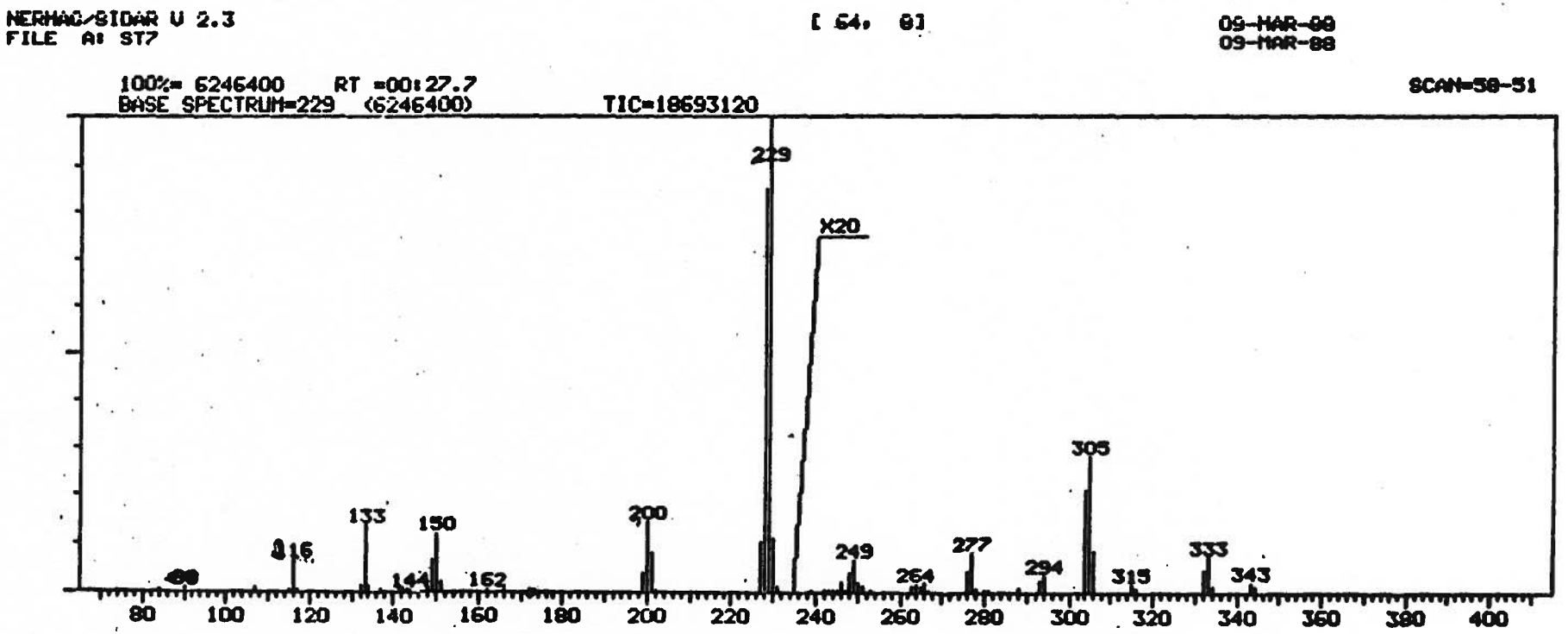

Figure 2.12. Positive Ion Mass Spectrum of $CpV(CO)_4$: Methane Chemical Ionization; 70 eV; p = .01 torr

e.g., addition of ligands such as NH_3, CH_4, and H atoms is strongly favored by ions such as CpV^+ because of the large coordination unsaturation and available space about their metal centres.

3. Negative Ion Chemistry

Electron impact (2.5 eV) on $CpV(CO)_4$ produces the following anions:

$$CpV(CO)_4 + e^- \rightarrow CpV(CO)_2^- (60\ \%),\ CpV(CO)_3^- (30\%)$$

This anion abundance distribution compares with that of Müller[23] using 70 eV EI: $CpV(CO)_2^-$ (33 %), $CpV(CO)_3^-$ (67%). Further reaction and clustering of these products was not observed for up to 1000 milliseconds. This unreactive behavior may reflect the fact that these anions are not highly electron deficient compared to their parent molecule, and consequently are relatively slow to interact with it. Figure 2.13 on the following page is a typical negative ion mass spectrum of $CpV(CO)_4$ showing the two unreactive negative ion products, $CpV(CO)_2^-$ and $CpV(CO)_3^-$.

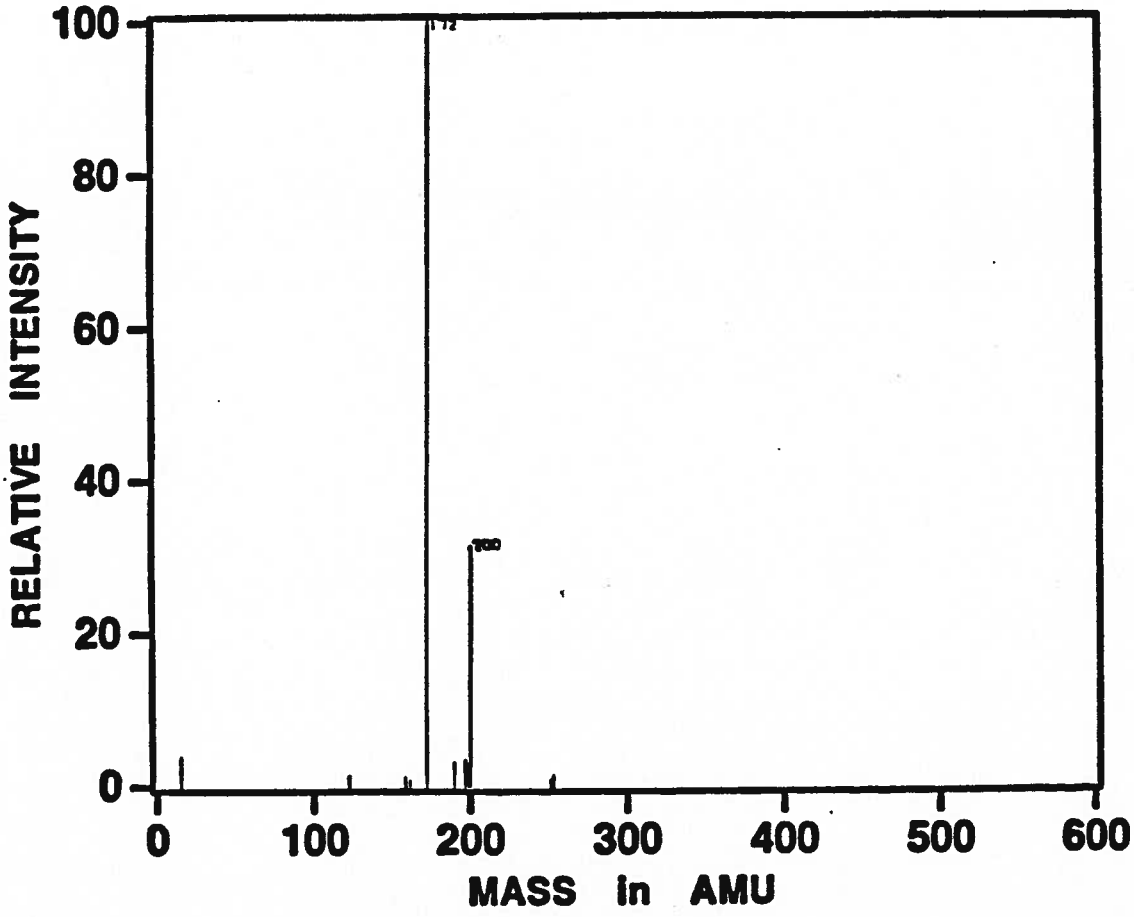

Figure 2.13. FT-ICR Negative Ion Mass Spectrum of $CpV(CO)_4$; 0 msec.; 2.5 eV; p = 6.0×10^{-8} torr

4. Reactions with Small Molecules

Using the same technique as for the generation of positive daughter ion adducts, $CpV(CO)_4$ molecules were reacted with ammonia, methane and isobutane DCI gases in negative ion mode. Mass spectra for these experiments (Figure 2.14-15) are shown on the following pages.

Anion Addition Products of $CpV(CO)_4$

1. Ammonia adducts

   i. deprotonation of the Cp ligand: $C_5H_4V(CO)_{3,4}^-$ (amu 199, 227)

   ii.aminated adduct formation: $CpVCO(NH_2)_{1,2}^-$ (amu 160, 176)

A typical spectrum showing some of these adduct peaks is shown in Figure 2.14.

2. Methane adducts

   i. deprotonation: $C_5H_4V(CO)_{3,4}^-$ (amu 199, 227)

   ii. methylated adduct formation: $CpVCO(CH_4)_{1,2}^-$ (amu 160, 176)

A typical spectrum showing these adduct peaks is shown in Figure 2.15.

3. Isobutane adducts

   i. deprotonation: $C_5H_4V(CO)_{3,4}^-$ (amu 199, 227)

   ii. methylated adduct formation: $CpV(H)_{1,2}(CH_3)_{1,2}^-$

   (amu 132-3, 147-8)

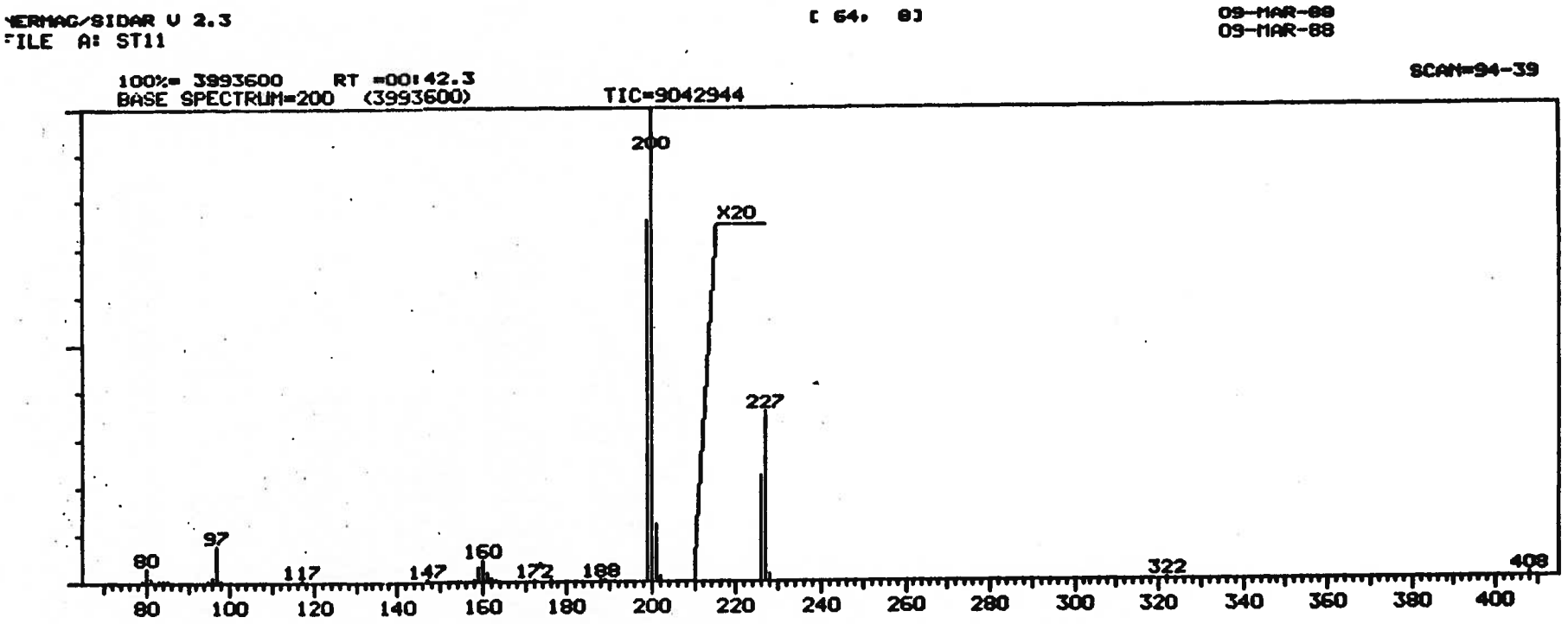

Figure 2.14. **Negative Ion Mass Spectrum of CpV(CO)4:**
Ammonia Chemical Ionization; 70 eV; p = .01 torr

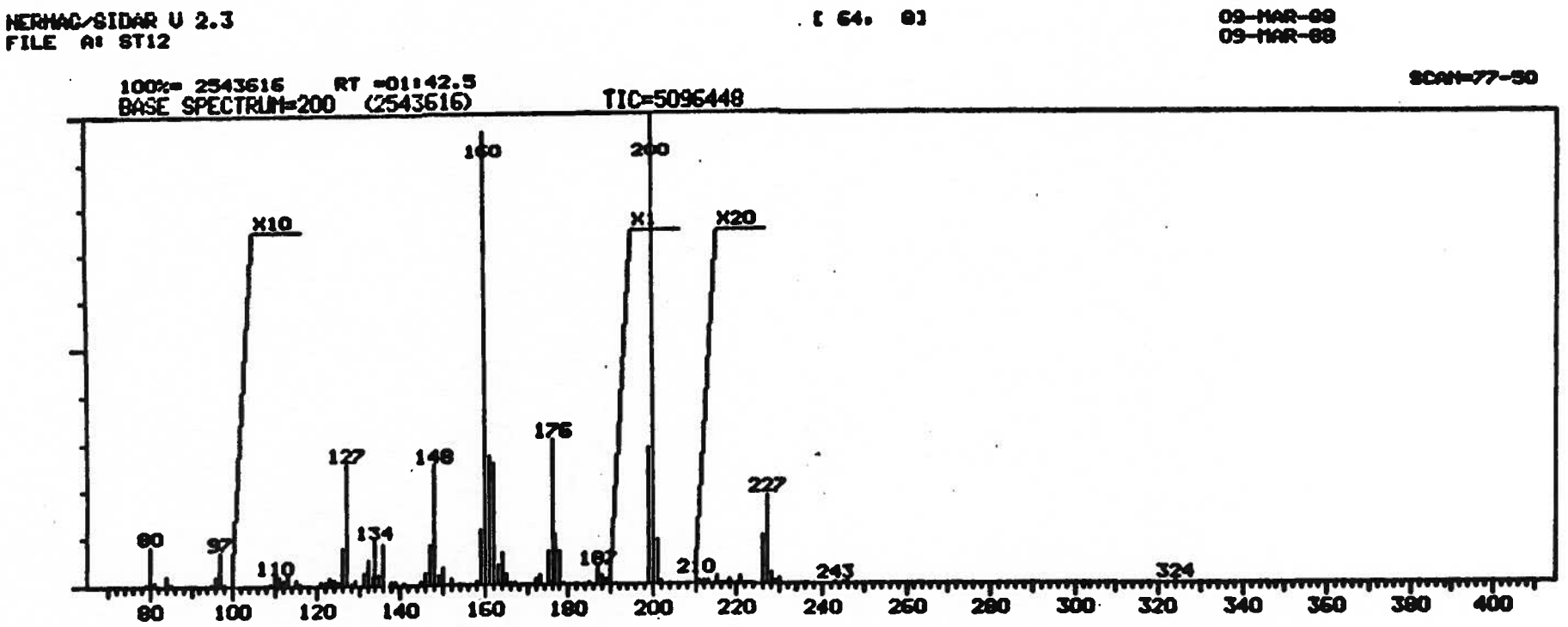

Figure 2.15. Negative Ion Mass Spectrum of CpV(CO)4:

Methane Chemical Ionization; 70 eV; p = .01 torr

Unlike positive ion DCI adduct spectra (Figure 2.11-2.12) but in accord with the present FT-ICR data (e.g. Figure 2.13), the negative ion DCI spectra showed no bi- or trinuclear fragment ion adducts, and very few mononuclear adduct ions, e.g., $CpVCONH_2^-$ (in ammonia); and $CpVCOCH_4^-$ and $CpVCO(CH_4)_2^-$ (in methane or isobutane). This unreactive behaviour may be a result of nonreactivity consistent with the anions $CpV(CO)_2^-$ and $CpV(CO)_3^-$, or may simply be due to kinetic effects, i.e., low anion reactant concentrations. Some ligated adducts were present, however, and like cation adducts, anion adducts contained from one to three ligands (i.e., NH_2, CH_4 or CO) per CpV moiety, depending on the degree of ligand unsaturation of the negative fragment ion cores. Deprotonation reactions occurred in all three cases because of the lower proton affinity of $CpV(CO)_4$ compared to NH_3, CH_4 and iso-butane.

III Conclusions

GENERAL FEATURES OF THE $CpV(CO)_4$ SYSTEM

1) All of the principal cations initially formed by electron impact on $CpV(CO)_4$, i.e., V^+, $CpV(CO)_{0-4}^+$, are chemically reactive with parent neutral, whereas both daughter anions, $CpV(CO)_{2,3}^-$, are unreactive.

2) Electron transfer, which is essentially a competition with the parent molecule for electrons, appears to be one of the most important reaction pathways for all the cationic species in this system. Rates of electron transfer were listed in Table 2.2. Indeed, for the bare metal cation V^+, electron transfer, rather than condensation, is the principal mode of interaction with the parent molecule. This behaviour of V^+ contrasts with that of the other bare metal cations of the $BzCr(CO)_3$ (Chapter 3), $CpMn(CO)_3$ (Chapter 4), $BuFe(CO)_3$ (Chapter 5), and $CpCo(CO)_2$ (Chapter 6) systems studied here, as well as of bare metal ions in earlier studies.

3) Cluster formation is a dominant reaction pathway for all the cations in this $CpV(CO)_4$ system except for that of the bare metal cation, V^+. Several new cations containing three and four vanadium atoms were seen here for the first time, i.e., $(CpV)_3(CO)_{1-4}^+$ and $(CpV)_4(CO)_{2-4}^+$ ions. Some evidence of even larger cations containing five vanadium atoms, for example, $(CpV)_5(CO)_4^+$ was also observed. The integrity of the Cp-V bond within these cluster cores tended to be maintained throughout successive condensation hierarchies; i.e., in $(CpV)_2$, $(CpV)_3$, $(CpV)_4$, etc., cationic cluster fragments. This behaviour was noted throughout all five metal systems of the analogous series in this study (i.e., in the $CpV(CO)_4$, $BzCr(CO)_3$, $CpMn(CO)_3$, $BuFe(CO)_3$ and $CpCo(CO)_2$ systems). Metal-aryl bond integrity seen here is a reflection of the powerful multiple d-π, metal-aryl electronic interactions that exist throughout this analogous series of complexes.

4) Clustering dwindles with formation of $(CpV)_3^+$, or larger cores at pressures presently used (10^{-6} - 10^{-9} torr); $(CpV)_4$ cation cluster fragments were observed in very low yields only in the higher pressure ranges or after long reaction times. Relative clustering rates as listed in Table 2.4, depend inversely upon cation size and carbonyl coordination number. Apparent cluster termination may be a consequence of ligand crowding around the central vanadium core of each ion-molecule cluster. Also, excess vibrational energies in the transition state complex formed by collisions between any specific cation and the neutral molecule may not favour formation of larger (i.e., $(CpV)_5$, etc.) cation clusters This may also explain the mobility of CO units seen in some of the primary cations.

5) The cations CpV^+, $CpV(CO)_4^+$, $(CpV)_2(CO)_2^+$, and $(CpV)_3(CO)_3^+$ appear kinetically stable compared to other ions in the same $(CpV)_n$ series. To illustrate this, Figures 2.16 and 2.17 show ion abundances at 500 msec and 1000 msec versus ionic mass. Relatively large intensities of ions $(CpV)_2(CO)_2^+$ and $(CpV)_3(CO)_3^+$ appear here as

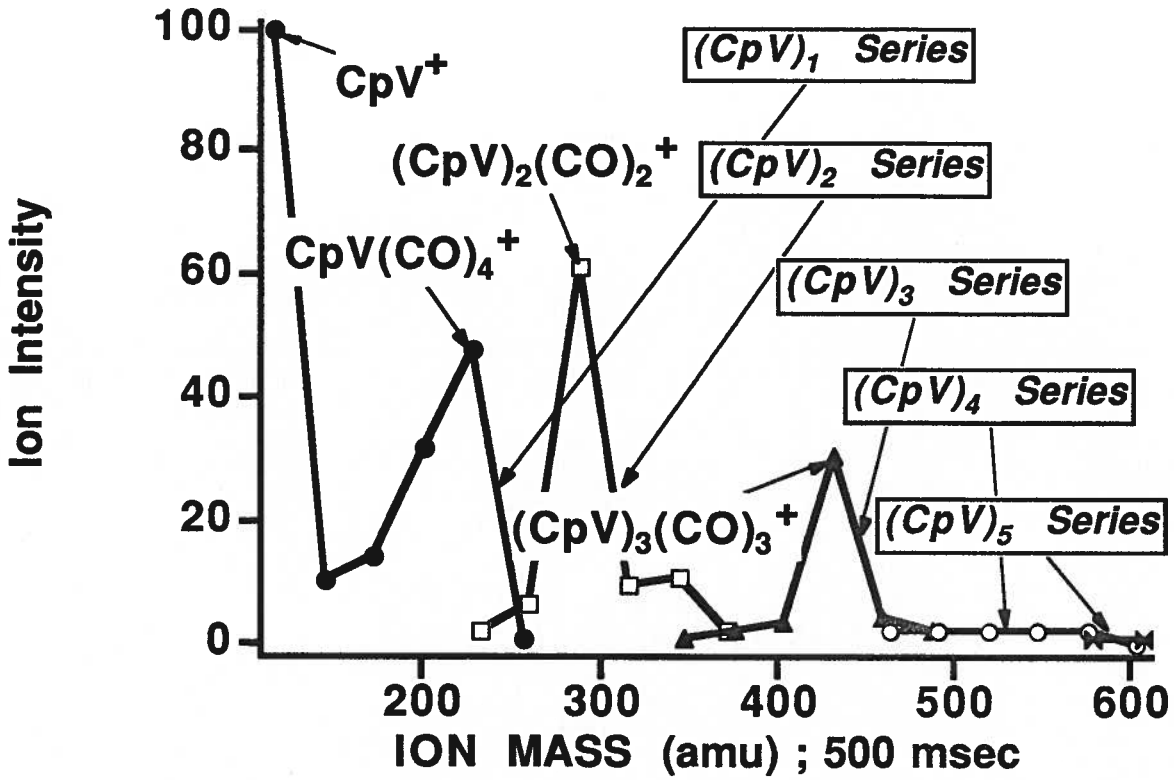

Figure 2.16. Relative Abundances of Cation Clusters of $CpV(CO)_4$ at 500 msec

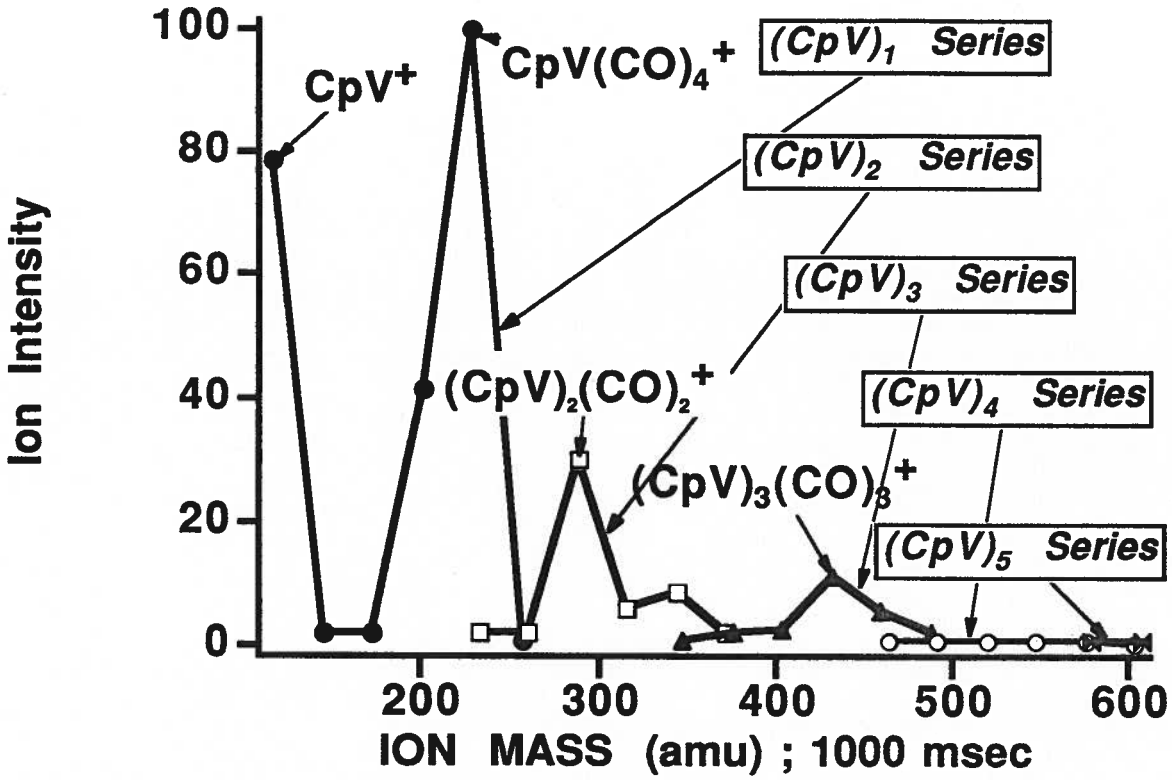

Figure 2.17. Relative Abundances of Cation Clusters of $CpV(CO)_4$ at 1000 msec

peaks on the intensity plots, whereas other ions in each series, such as $(CpV)_2CO^+$ and $(CpV)_3(CO)_2^+$, are of relatively low intensity. As suggested in earlier papers, the anomalously large numbers of certain ions such as these may be the consequence of increased metal-metal bond order, or of enhanced CO ligand hapticity[8,19,28,36].

The large intensity of $CpV(CO)_4^+$, illustrated in Figures 2.16 and 2.17, is not surprising, since it is the molecular ion and expectedly abundant immediately after 25 eV electron ionization. This ion dominates the entire reaction regime, because of its relative electronic stability and also because it is the principal product of all the electron transfer reactions.

However, large and persistent intensities of the ions CpV^+, $CpV(CO)_3^+$, $(CpV)_2(CO)_2^+$ and $(CpV)_3(CO)_3^+$ are unexpected, especially since all possess large formal electron deficiencies. Some degree of multiple metal-metal bonding within the latter two ions; $(CpV)_2(CO)_2^+$ and $(CpV)_3(CO)_3^+$, may contribute to their unusual lack of reactivity. This behaviour resembles that seen in some cationic Cr_2 complexes, as noted elsewhere[19,20,28,36].

CpV^+, possessing 9 electrons and a very strong Cp-vanadium linkage[30], may possess enhanced electronic (i.e, half-full metal orbital) stability. But apparent anomalies, as shown by CpV^+, $CpVCO^+$, and $CpV(CO)_4^+$, are possibly unrelated to bonding phenomena, but may be related to the presence of highly-reactive, excited states of some of these ion reactants.

6) Figure 2.18 on the following page illustrates the relationship between pseudo-first order decay rate constants for each reacting cation (summarised in Table 2.2) and formal electron deficiencies for several of the more abundant cations of this system. Such plots have proved useful for predicting unusual bonding patterns within ion clusters[20,28]. The relationship between rate and electron deficiency is fairly well-behaved here. The steep

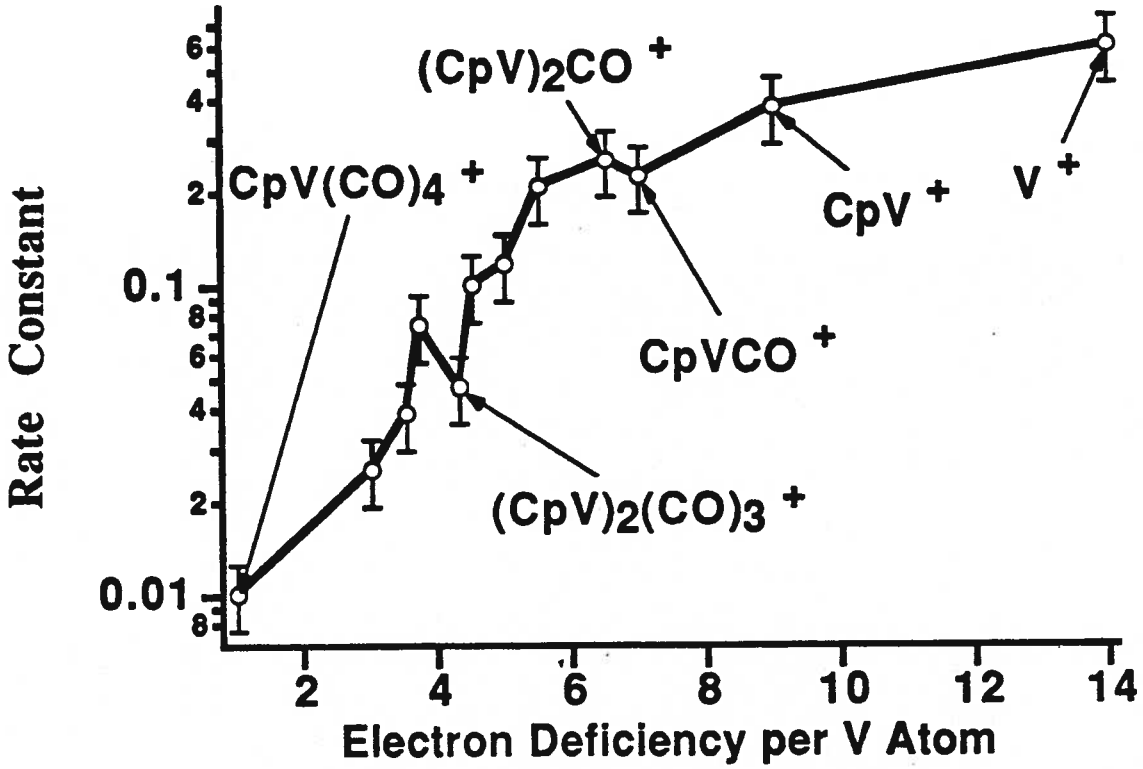

Figure 2.18. Relationship Between Reactivity and Electron Deficiency for Cations in the $CpV(CO)_4$ System

slope between electron deficiencies of one to four implies that ions falling in this region on the graph will predictably be highly reactive toward many nucleophilic reagents. The reactive centres in these ions are unprotected from nucleophilic attack, their central metal-metal cores having few shielding carbonyl ligands. As discussed later, the DCI experiments corroborate this conclusion. Other, more electron-rich ions such as $(CpV)_2(CO)_3^+$ may possess stabilising multiple- or partial multiple-bonded vanadium-vanadium cores, surrounded by a protective sheath of ligands.

7) In accounting for temporal behaviour of the vanadium cations, the participation of excited states among some or all of the primary cations in the $CpV(CO)_4$ system must be considered. The energy difference between ground and first excited state bare vanadium cations is only 0.33 eV[6], therefore it is not surprising that many smaller daughter ions possess excited electronic configurations after ionisation by 25 eV electrons. There are several lines of evidence for the existence of excited states in the $CpV(CO)_4$ system. These are: i) non-linear pseudo-first order (semi-log) decay behaviour shown by some of the smaller cation cluster fragments, e.g., V^+ and CpV^+, illustrated in Figure 2.19 on the following page; ii) marked mobility of CO ligands, especially in smaller cation cluster fragments; iii) lack of parallel anomalous behaviour in the anion regime (where reacting ions are generated at much lower energies); and iv) reappearance of the molecular ion $CpV(CO)_4^+$ after its initial disappearance (note Figure 2.19), suggesting that the initial species of $CpV(CO)_4^+$ may be excited and reactive, whereas the final species is in the ground state and kinetically more stable. From intercepts of the semilog rate plots, some estimation of the proportions of excited and ground state ions can be made. For the bare vanadium cation, V^+, the proportion of excited state ions was thus calculated to be approximately 45%; for CpV^+; 81%; and for the molecular cation, $CpV(CO)_4^+$; 30%. Since greater opportunity for relaxation should exist for larger cations (more vibrational modes) than for smaller ones such as monatomic V^+, residual energy would be expected to be retained longer in the smaller ion species; and in fact this was observed in most cases.

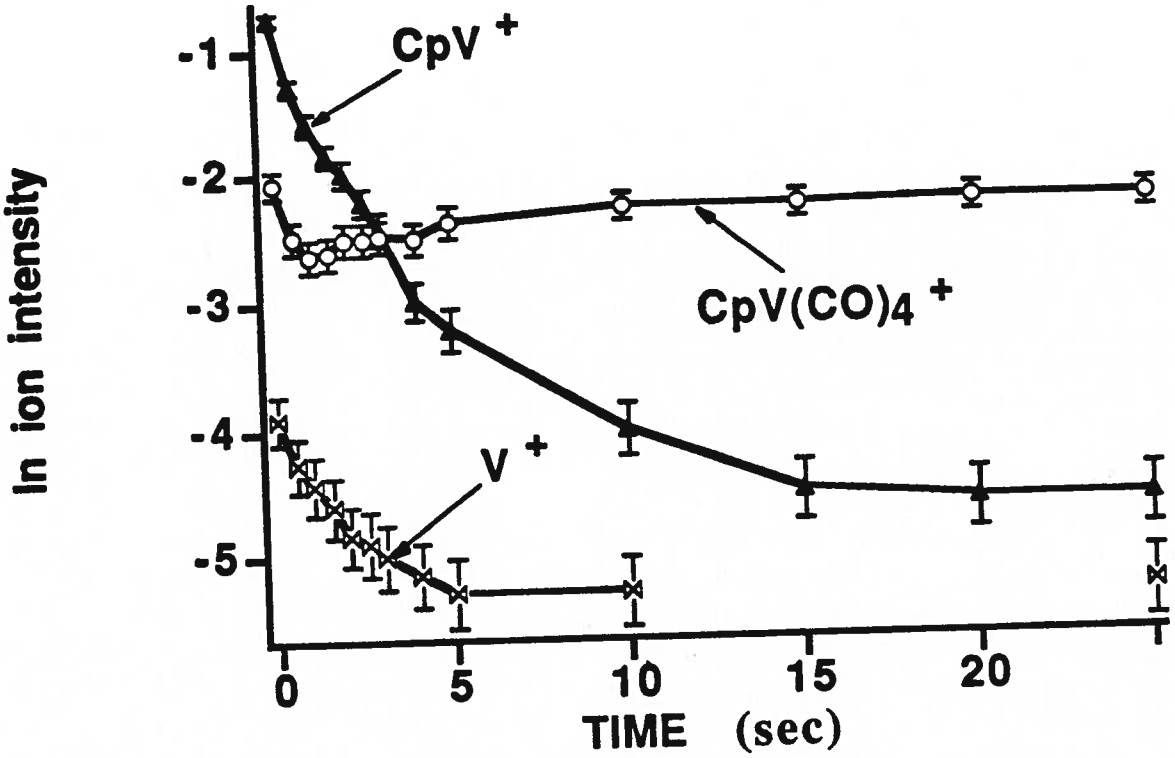

Figure 2.19. Deviations from Pseudo-First Order Decay Behaviour in the $CpV(CO)_4$ System

As Russell has noted[29], bare metal cations such as Fe^+ in the $Fe(CO)_5$ system, are apparently able to retain excess excitation energy even after many collisions; and the reactivity of such excited state ions may differ widely from that of the corresponding ground state ions. Excited state reactivity differences between ground and excited state metal ions have been measured for small cations in the $Cr(CO)_6$[27]; $Fe(CO)_5$[29]; Co_2NO^+[15]; and $Mn_2(CO)_{10}$[31,32] systems as well.

For the larger vanadium cations in this system, kinetic semi-log rate plots measured here are linear, suggesting ground state reactive behaviour.

8) As discussed in paragraph 6), most small, ligand-unsaturated vanadium ion fragments are very susceptible to addition by adduct molecules. FTMS experiments on daughter cations of $CpV(CO)_4$ using O_2, H_2 and N_2 produced many oxycations and hydrogenated cation adducts, although the spectra were very complex and difficult to interpret. However, in the higher pressure (0.01 torr) DCI experiments, multiple adducts were generated from the daughter cations of $CpV(CO)_4$, using ammonia, methane and isobutane as CI reagent gases. Depending upon the CI gas used, these adducts included a variety of ammoniated, methylated and protonated species, containing ligand groups such as NH_3 and CH_n (n=1-5). This rich assortment of addition products reflects the vulnerability of CpVCO fragment cations toward incoming nucleophilic groups.

9) Threshold energies for the appearance of positive ions and their abundance with varying electron energy of ionisation in the $CpV(CO)_4$ system are shown in the clastogram in Figure 2.20. The data shown in Figure 2.20 for appearance of cations with ionising voltage are generally in accord with earlier results obtained by other mass spectrometric methods.[23,35].

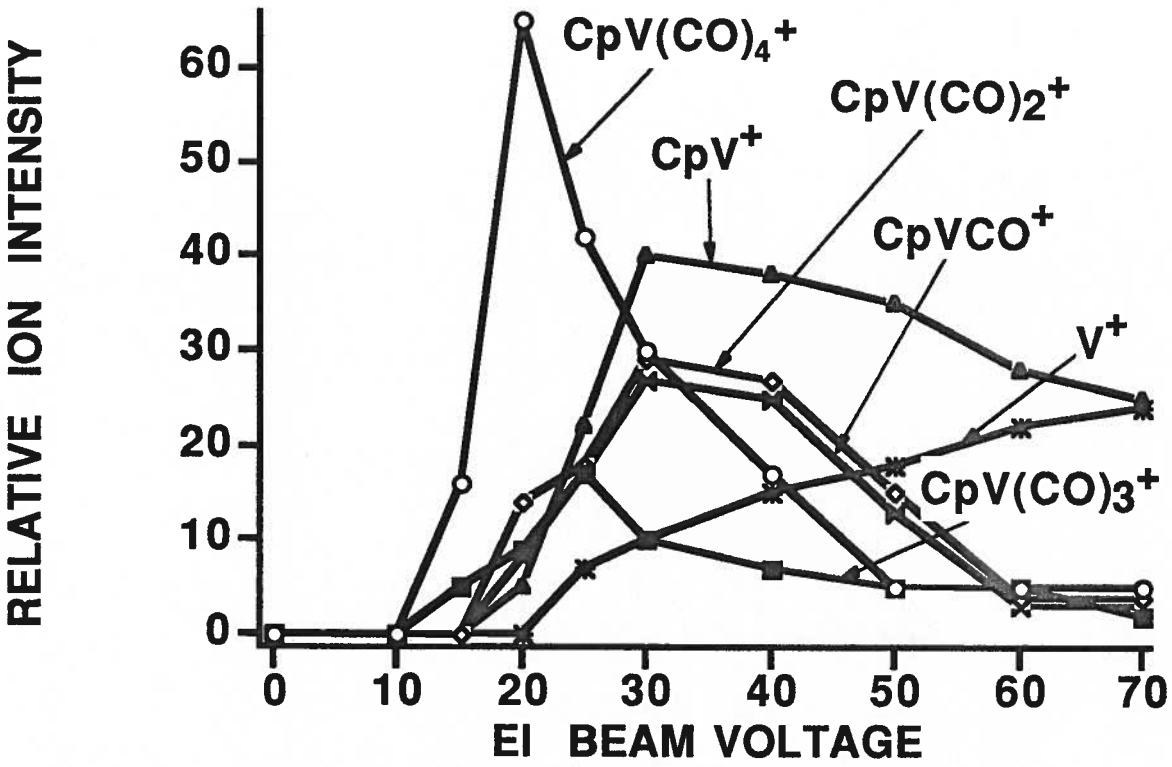

Figure 2.20. Clastogram for Cations of $CpV(CO)_4$

10) The structural geometries of the new binuclear and trinuclear cluster cations generated in this system are not well understood yet. Several possibilities for arrangement of multiple vanadium-Cp groups exist: either as intimately bound metal-metal cores; as Cp-metal-Cp-metal alternating chains; or as some combination of both models. Most probably, these multinuclear cluster ions resemble the V-V central single-bonded core structure in $(\eta^5\text{-CpV})_2\text{-}(\eta^1\text{-CO})_3\text{-}(\mu_2\text{-CO})_2$[24]. Only a few other multi-vanadium carbonyl clusters, prepared with difficulty in solution, such as $Cp_3V_3(CO)_9$ and $Cp_4V_4(CO)_4$[16] have been studied at the present time (1992).

Further detailed FT-ICR studies into long-term clustering processes of these and other vanadium complexes may provide information regarding these interesting complex ions. Multiple resonance MS-MS experiments with small molecular addition agents such as H_2, O_2, N_2; and laser photodissociation to induce rupture of secondary and tertiary polynuclear ion clusters, will help elucidate structural geometry and yield a clearer conformational picture. Moreover, dual-cell or drift cell collisional relaxation techniques with higher pressure inert gases may enable resolution of excited and ground state reactivities[29].

IV References

(1) Allison, J. *Prog. Inorg. Chem.* **1986**, *34*, 627.

(2) Aristov, N.; Armentrout, P. B. *J. Am. Chem. Soc.* **1984**, *106*, 4065.

(3) Aristov, N.; Armentrout, P. B. *J. Am. Chem. Soc* **1986**, *108*, 1806.

(4) Aristov, N.; Armentrout, P. B. *J. Phys. Chem.* **1987**, *91*, 6178.

(5) Armentrout, P. B.; Halle, L. F.; Beauchamp, J. L. *J. Amer. Chem. Soc.* **1981**, *103*, 6501.

(6) Armentrout, P. B. in *Gas Phase Inorganic Chemistry*; Russell, D. H.; Plenum Press, New York, **1989**; pp 1 - 42.

(7) Calderazzo, F.; Bacciarelli, S. *Inorg. Chem.* **1963**, *2*, 721.

(8) Cotton, F. A.; Walton, R. A. *Struct. Bond.* **1985**, *62*, 1.

(9) Elkind, J. L.; Armentrout, P. B. *J. Phys. Chem.* **1985**, *89*, 5626.

(10) Fischer, E. O.; Hafner, W. *Z. Naturforsch.* **1954**, *9B*, 503.

(11) Fischer, E. O.; Schneider, R. J. J. *Chem. Ber.* **1970**, *103*, 3584.

(12) Foster, M. S.; Beauchamp, J. L. *J. Am. Chem. Soc.* **1975**, *97*, 4808.

(13) Fredeen, D. J. A.; Russell, D. H. *J. Am. Chem. Soc.* **1985**, *107*, 3762.

(14) Fredeen, D. A.; Russell, D. H. *J. Am. Chem. Soc.* **1987**, *109*, 3903.

(15) Gord, J. R.; Freiser, B. S. *J. Am. Chem. Soc.* **1989**, *111*, 3754.

(16) Herrman, W. A.; Plank, J.; Reiter, B. *J. Organomet. Chem.* **1978**, *164*, C25.

(17) Jacobson, D. B.; Freiser, B. S. *J. Am. Chem. Soc.* **1985**, *107*, 5870.

(18) Kappes, M. M.; Staley, R. H. *J. Phys. Chem.* **1981**, *85*, 942.

(19) Meckstroth, W. K.; Ridge, D. P. *Int. J. Mass Spectrom. Ion Proc.* **1984**, *61*, 149.

(20) Meckstroth, W. K.; Freas, R. B.; Reents, W. D., Jr.; Ridge, D. P. *Inorg. Chem.* **1985**, *24*, 3139.

(21) Morton, J. R.; Preston, K. F. *Organometallics* **1984**, *3*, 1386.

(22) Mullen, S. L.; Marshall, A. G. *J. Amer. Chem. Soc.* **1988**, *110*, 1766.

(23) Müller, J.; Fenderl, K. *Chem. Ber.* **1970**, *103*, 3141.

(24) Otto, E.; Fischer, E. O.; Schneider, R. J. J. *Chem. Ber.* **1970**, *103*, 3884.

(25) Parisod, G.; Comisarow, M. B. *Adv. Mass Spectrom.* **1980**, *8A*, 212.

(26) Pope, R. M.; VanOrden, S. L.; Buckner, S. W. *Organometallics* **1991**, *10*, 1089.

(27) Reents, J., W. D. ; Strobel, F.; Freas, R. B.; Wronka, J.; Ridge, D. P. *J. Phys. Chem.* **1985**, *89*, 5666.

(28) Ridge, D. P.; Meckstroth, W. K. in *Gas Phase Inorganic Chemistry*; Russell, D. H.; Plenum Press, New York, **1989**; pp 93-113.

(29) Russell, D. H. *Ann. Conf. ASMS All. Top.* **1990**, *38*, 1261.

(30) Skinner, H. A.; Connor, J. A. *Pure Appl. Chem.* **1985**, *57*, 79.

(31) Strobel, F.; Ridge, D. P. *J. Phys. Chem.* **1989**, *93*, 3635.

(32) Strobel, F.; Ridge, D. P. *J. Am. Soc. Mass. Spectrom.* **1990**, *1*, 192.

(33) Wilford, J. B.; Whitla, A.; Powell, H. M. *J. Organomet. Chem.* **1967**, *8*, 495.

(34) Wilkinson, G.; Cotton, F. A.; Birmingham, J. M. *J. Inorg. Nucl. Chem.* **1956**, *2*, 95.

(35) Winters, R. E.; Kiser, R. W. *J. Organometal. Chem.* **1965**, *4*, 190.

(36) Wronka, J.; Ridge, D. P. *J. Am. Chem. Soc.* **1984**, *106*, 67.

CHAPTER 3

Ion Molecule Chemistry of

Tricarbonyl (η^6 - Benzene) Chromium

{ η^6 - C_6H_6 $Cr(CO)_3$ }

I Introduction

First prepared and characterised in 1957 by E. Fischer and Öfele[11], tricarbonyl (η^6-benzene) chromium is an involatile yellow, crystalline, air-sensitive solid, melting at 162° C and subliming at 130° C (2 mm Hg). Interatomic distances and conformation, measured by Bailey and Dahl in 1965[4] showed that in the solid state, the $Cr(CO)_3$ moiety has trigonal pyramidal shape with the CO ligands lying directly below alternate C-C bonds of the benzene ligand, with C_{3v} symmetry.

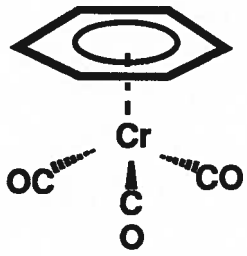

The energetics and reactivity of bare chromium ions in the gas phase have been analysed by several authors, e.g. Armentrout[3] and Connor[9]. Reactions of ground and excited state Cr^+ ions with hydrogen have been studied[10,14,26]. Trends in Cr-O, Cr-H and Cr-C bond strengths and electronic structure, compared with those of other transition metals have also been analysed[2,3,5,9]. Reactivity of transition metal carbene cations, such as $Cr{=}CH_2^+$, was studied[16]. Beauchamp[17] measured the reactivity of the CrO^+ cation with alkenes.

Chromium carbonyl complexes have been of mass spectrometric interest since 1965 when Winters studied $Cr(CO)_6$ and its ions by conventional methods[35,36]. The same year (1965), Pignataro also measured the anion fragments of $Cr(CO)_6$ produced by electron ionisation[24]. Chromium hexacarbonyl and its ions exhibit rich ion-molecule chemistry:

ion-molecule chemistry of $Cr(CO)_6$ was observed by Fredeen in 1985[12], who later compared the ion-molecule chemistry of carbonyl compounds of Cr, Mn, Fe, Co and Ni[12,27]. Bricker and Russell studied the interaction of the $Cr(CO)_5^-$ anion with dioxygen[6]. In 1990, Sellers-Hahn successfully reacted chromium carbonyl cations with various ligand exchange reagents[28]. Pan (1989) proposed that the reactive, 17-electron $Cr(CO)_5^-$ anions readily underwent ligand substitution via an electron transfer mechanism[22]. Aryl chromium compound chemistry was initiated by Wilkinson in 1956[34] with the synthesis of bis-(η^6-benzene) chromium, $(\eta^6\text{-}C_6H_6)_2Cr$. Its mass spectral behaviour was studied by Pignataro in 1967[25] and Müller in 1970[20].

Aryl chromium carbonyl compounds were also examined in Pignataro's work: primary daughter ions of benzene chromium tricarbonyl and some arene derivatives were examined as well[25]. In 1973, the appearance potentials and dissociation energies of η^6-$C_6H_6Cr(CO)_3$ and its various cation fragments were measured by Müller[19] and Gilbert[13]. Other aryl chromium carbonyl systems have been examined with mass spectral techniques. Using differential ion ejection techniques in 1980, Parisod and Comisarow[23] examined the positive ion-molecule reactions of dicarbonyl nitrosyl (η^5-cyclopentadienyl) chromium, $CpCr(CO)_2NO$ and dicarbonyl thionitrosyl (η^5-cyclopentadienyl) chromium, $CpCr(CO)_2NS$. Clustering with simultaneous expulsion of ligands was observed in both systems, and unusual nitrogen-oxygen and nitrogen-sulfur rupturing, along with simultaneous ejection of stable small molecules such as molecular N_2 and pyridine, occurred in both systems[23].

Arene ligand mobility in aryl chromium tricarbonyls in solution has been kinetically examined by Traylor[31,32]. Lability of the arene group apparently involves mobilisation of the $Cr(CO)_3$ unit along its substituent π systems, but benzene-chromium linkages remained unaffected in their studies.

In 1989, Chen observed extensive, complex clustering in the gas phase cation-molecule chemistry of $CpCr(NO)_2CH_3$ using FT-ICR-MS[8]. An assortment of

polynuclear cation clusters, some containing up to five Cr atoms, were generated. Resembling the NO and NS ligand systems examined by Parisod[23], some reaction channels showed NO ligand rupture (with molecular N_2 loss) and retention of oxygen atoms by the chromium cluster core. Like Cp-V linkages in the $CpV(CO)_4$ system examined here, Cp-Cr linkages were relatively stable compared to those of Cr-NO and Cr-CH_3.

In 1985, Cetini et. al. looked at CIMS interactions of several arene chromium tricarbonyl complexes with propene, benzene and toluene, noting that the predominant ion products were the molecular parent and hydrogenated adduct ions[7]. Recently (1991), ion-molecule studies of a selection of aryl-ligand chromium carbonyl complexes were conducted by Operti and Freiser using FTMS[21]. Aryl ligand groups included toluene, mesitylene and several oxygenated phenyl ligands. Each of the daughter cations in these systems was kinetically active except for the parent cation, $Cr(L)(CO)_3^+$; and in each case self-condensation processes followed a variety of reaction pathways depending somewhat upon the aryl ligand (L). Polynuclear cluster cations containing up to five chromium atoms and four aryls were detected.

The present study includes an examination of the kinetics of positive and negative ion-molecule reactions of η^5- $C_6H_6Cr(CO)_3$ [" $BzCr(CO)_3$"].

II Results and Discussion

1. Positive Ion Chemistry

Under 25 eV EI positive ionizing conditions, cation fragments of $BzCr(CO)_3$ were determined in the following proportions: Cr^+=29%; Bz^+=43%; $BzCr^+$=10%; $BzCrCO^+$=3%; $BzCr(CO)_2^+$=4%; $BzCr(CO)_3^+$=10%. These data compare with Pignataro and Lossing's 1967 data[25] using 70 eV EI: Cr^+=30%; Bz^+=20%; $CrCO^+$=10%; $BzCr^+$=35%; $BzCrCO^+$=5%; $BzCr(CO)_2^+$=<5%; $BzCr(CO)_3^+$=20%. Under similar

conditions Müller and Göser (1969) found Cr^+=63%; $CrCO^+$=2%; $BzCr^+$=20%; $BzCrCO^+$=2%; $BzCr(CO)_2^+$=<2%; $BzCr(CO)_3^+$=12% [19].

A typical FT-ICR positive ion mass spectrum of $BzCr(CO)_3$ showing all principal cation fragments is shown in Figure 3.1, and a sample of a mass table for product chromium cations is given in Table 3.1.

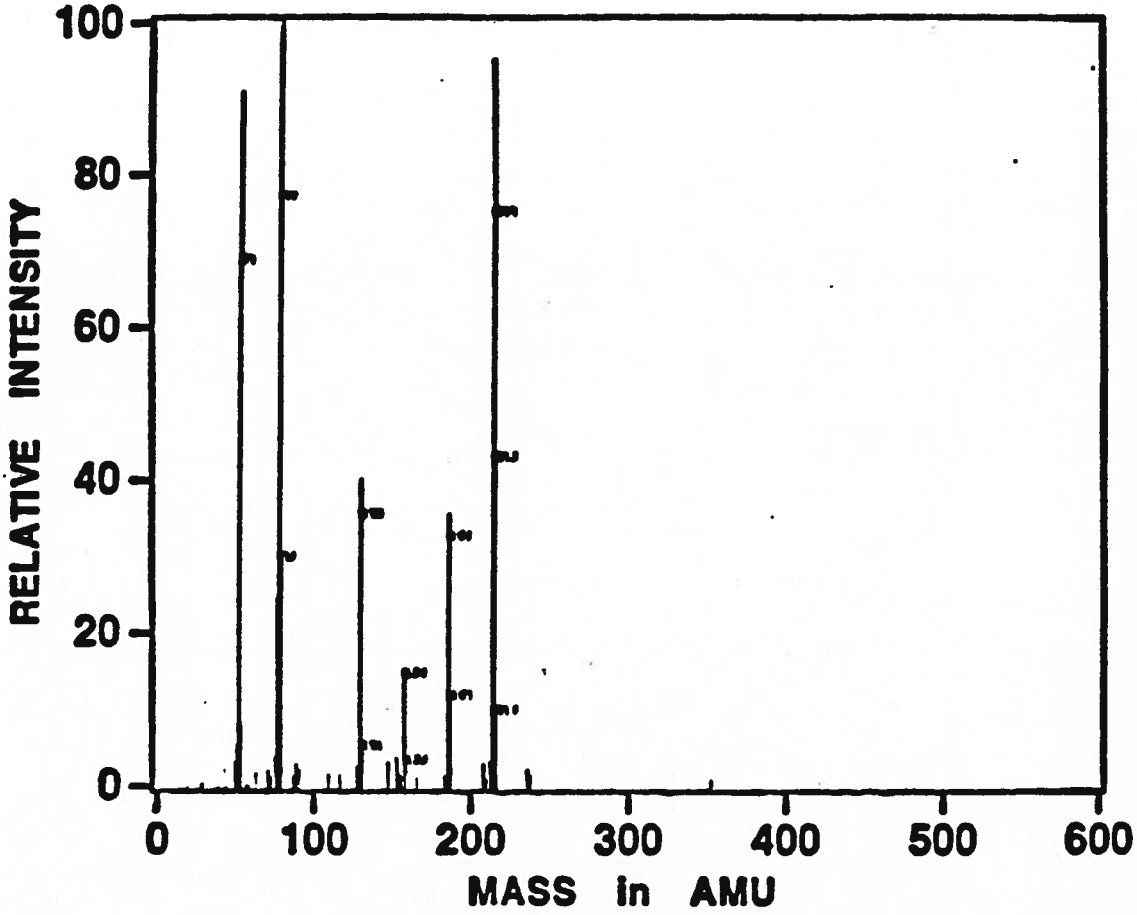

Figure 3.1. FT-ICR Positive Ion Mass Spectrum of $BzCr(CO)_3$; 0 msec.; 25 eV; p = 6.0×10^{-8} torr

TABLE 3.1

Sample Mass Table for $BzCr(CO)_3$ Cations (1000 msec)

Formula	Measured Mass[a]	Expected Mass[a]	Δ (ppm)	Rel. Int. (%)
^{50}Cr (4.31%)	49.9333	49.9455	12[b]	4.2
^{52}Cr.(83.76%)	52.0234	51.9400	83	81.2
^{53}Cr (9.55%)	53.0258	52.9401	86	8.6
^{54}Cr.(2.38%)	---	53.9384	--	<2
$^{52}CrCO$	79.9075	79.9349	27	6.8
$C_6H_6{}^{52}Cr$	129.9850	129.9870	2[b]	43.8
BzCrCO	157.9827	157.9819	8	14.7
$BzCr(CO)_2$	185.9971	185.9768	20	68.2
$BzCr(CO)_3$	213.9707	213.9717	1[b]	100
$(BzCr)_2$	259.9633	259.9744	11	8.4
(BzCr)2CO	---	287.9693	--	< 2
$(BzCr)_2(CO)_2$	315.9861	315.9643	23	4.4
$(BzCr)_2(CO)_3$	344.0511	343.9592	92	11.9
Bz_2Cr	208.1381	208.0339	104	17.6
$BzCr_2CO$	209.9848	209.9224	59	5.7
$BzCr_2(CO)_2$	237.9742	237.9173	57	5.3
$BzCr_2(CO)_3$	266.0608	265.9122	149	9.2

[a] in daltons

[b] calibrant mass

In this system, each primary cation fragment is reactive except for the parent $BzCr(CO)_3^+$ ion. At reaction times of up to 25 seconds, all the following polynuclear cluster cation fragments are generated:

Symmetric clusters (Bz=Cr)

$(BzCr)_2(CO)_{0,1,2,3}^+$

$(BzCr)_3(CO)_{2,3}^+$

Asymmetric clusters (Bz< or >Cr)

Bz_2Cr^+

$BzCr_2(CO)_{1,2,3}^+$

$Bz_2Cr_3(CO)_{2,3,4,6}^+$

Typical temporal behaviour of primary fragment ions at pressures of 6.0×10^{-8} torr is illustrated in Figure 3.2. Figure 3.3 shows analogous temporal behaviour of some of the principal binuclear and trinuclear ionic clusters. An example of a set of triple resonance spectra for the Cr^+ ion, taken initially and later at 5000 msec is given in Figure 3.4(a,b), illustrating the cation products of this single ion. An example of the temporal behaviour of this ion and its reaction products is shown in Figure 3.5. Analogous triple resonance spectra at 0 and 5000 msec are shown in Figure 3.6(a,b) for the $BzCr(CO)_2^+$ ion; temporal behaviour of this ion and its daughter ion products is illustrated in Figure 3.7. Ions containing chromium were identified by their chromium isotopic distribution: i.e., ^{50}Cr=4.31%; ^{52}Cr=83.76%; ^{53}Cr=9.55%; ^{54}Cr=2.38%. For each reactive ion, decay rate constants for reaction of each cation with the parent neutral molecule $BzCr(CO)_3$ were measured from the slopes of linear pseudo-first order plots; these values are listed in Table 3.2.

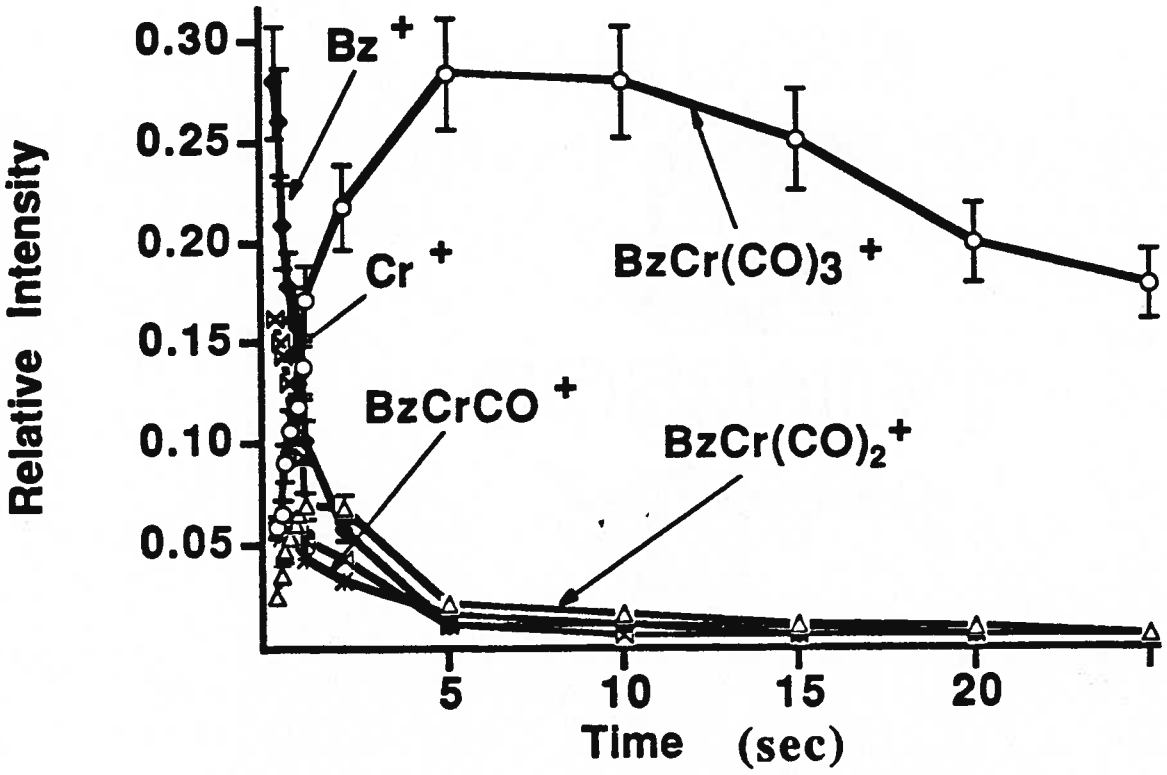

Figure 3.2. Temporal Behaviour of Primary Fragment Cations of $BzCr(CO)_3$

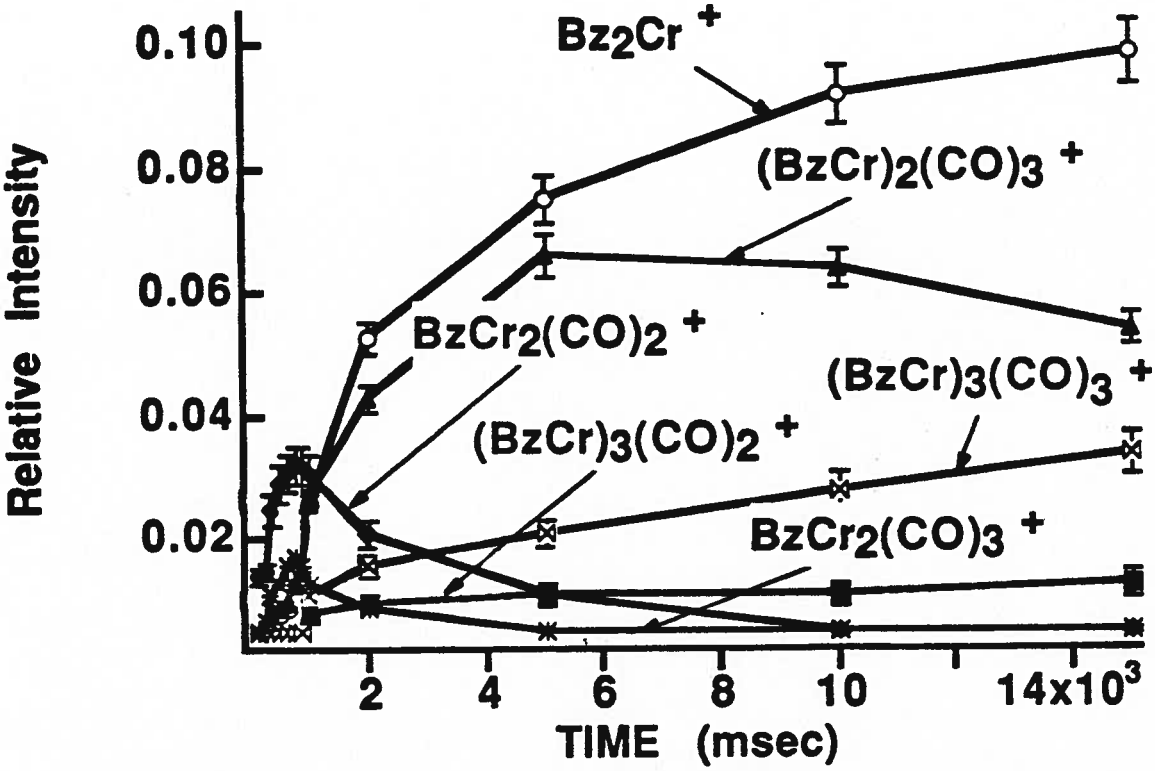

Figure 3.3. Temporal Behaviour of Binuclear and Trinuclear Cluster Cations of $BzCr(CO)_3$

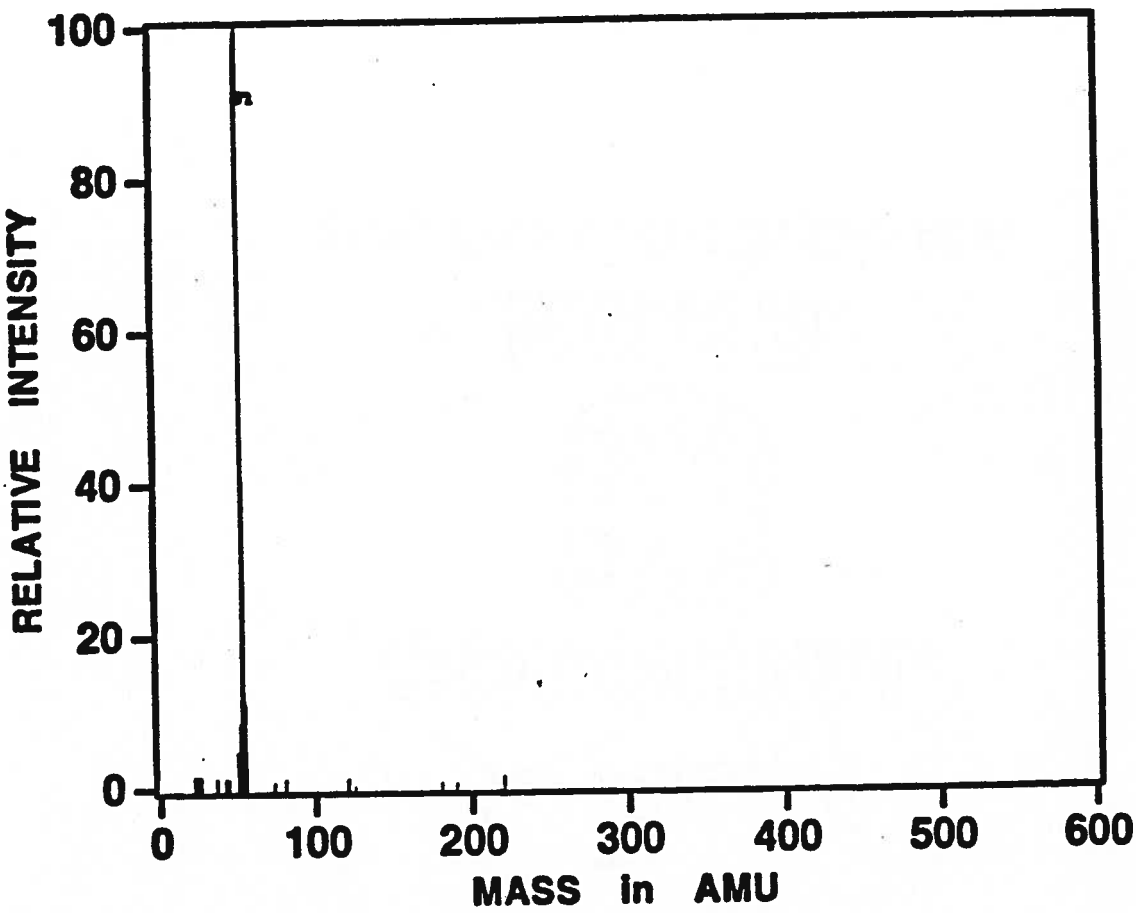

Figure 3.4(a). Multiple Resonance Mass Spectrum of Cr^+; 0 msec.; p = 6.0×10^{-8} torr

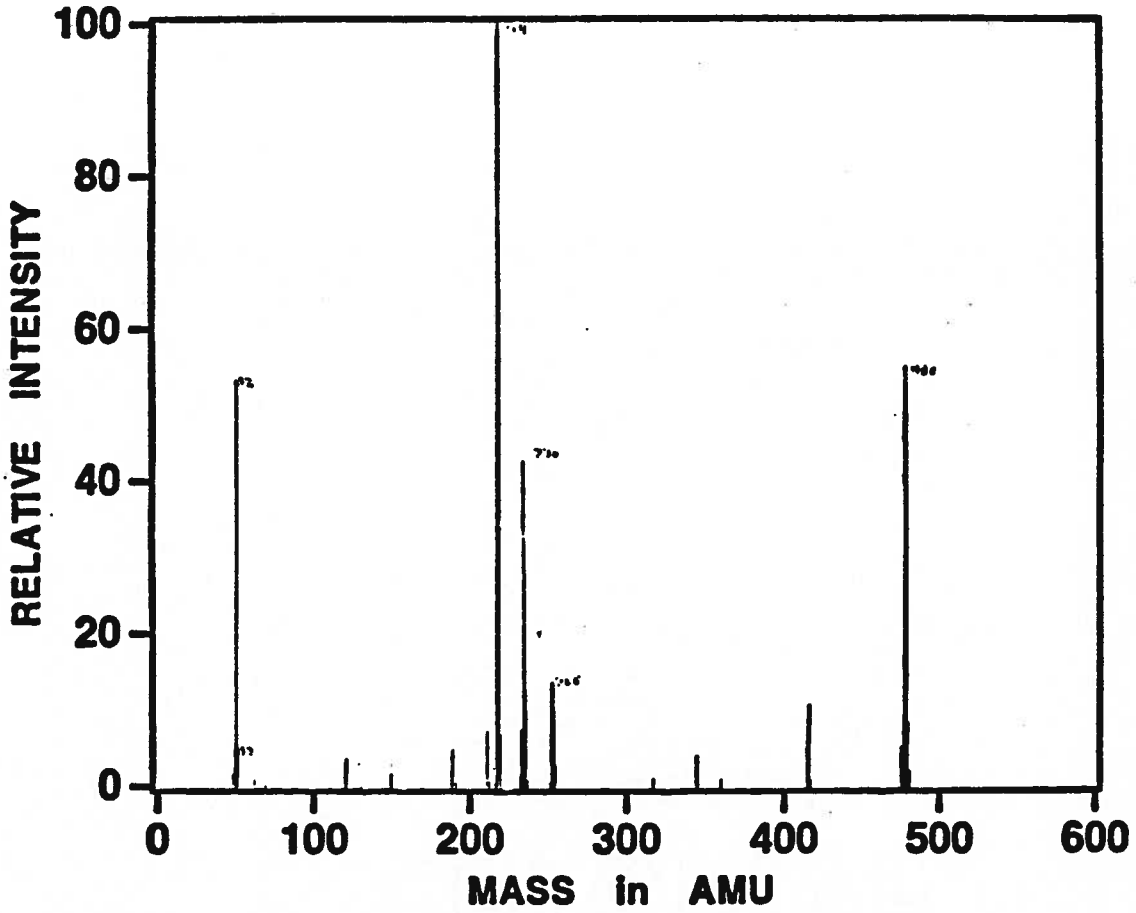

Figure 3.4(b). Multiple Resonance Mass Spectrum of Cr^+ and Cation Products; 5000 msec.; p = 6.0×10^{-8} torr

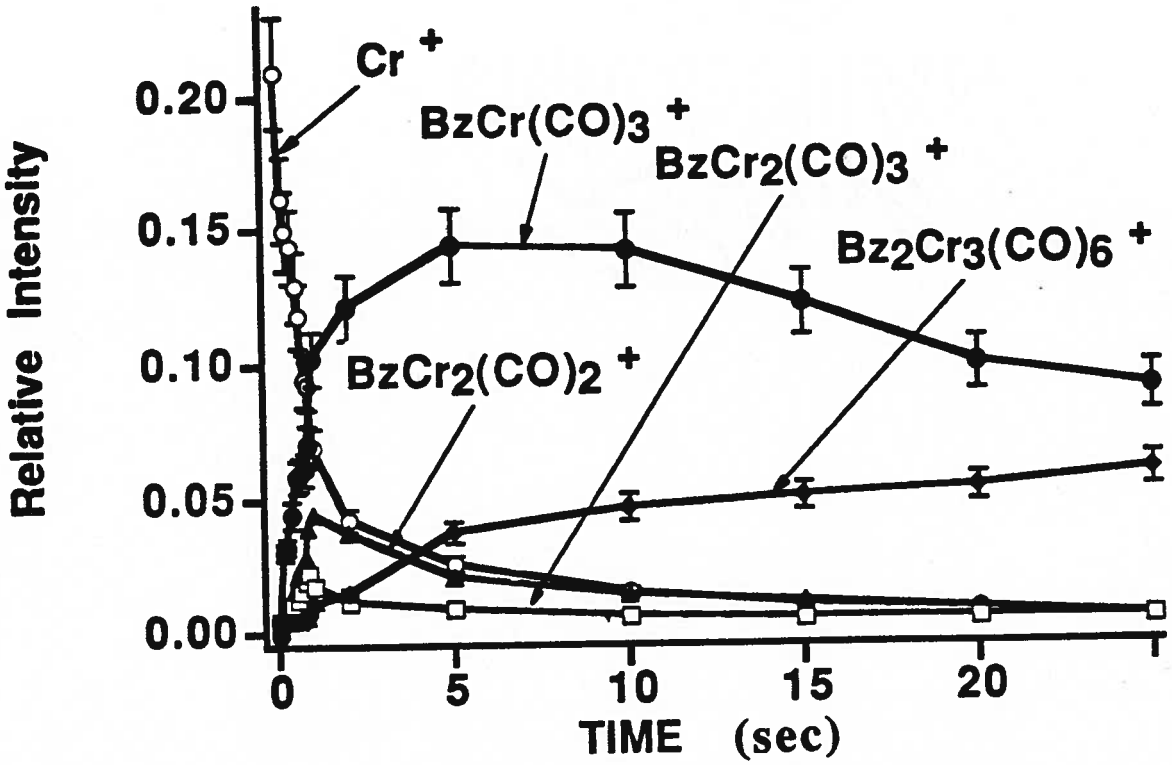

Figure 3.5 Temporal Behaviour of Cr^+ and Cation Products

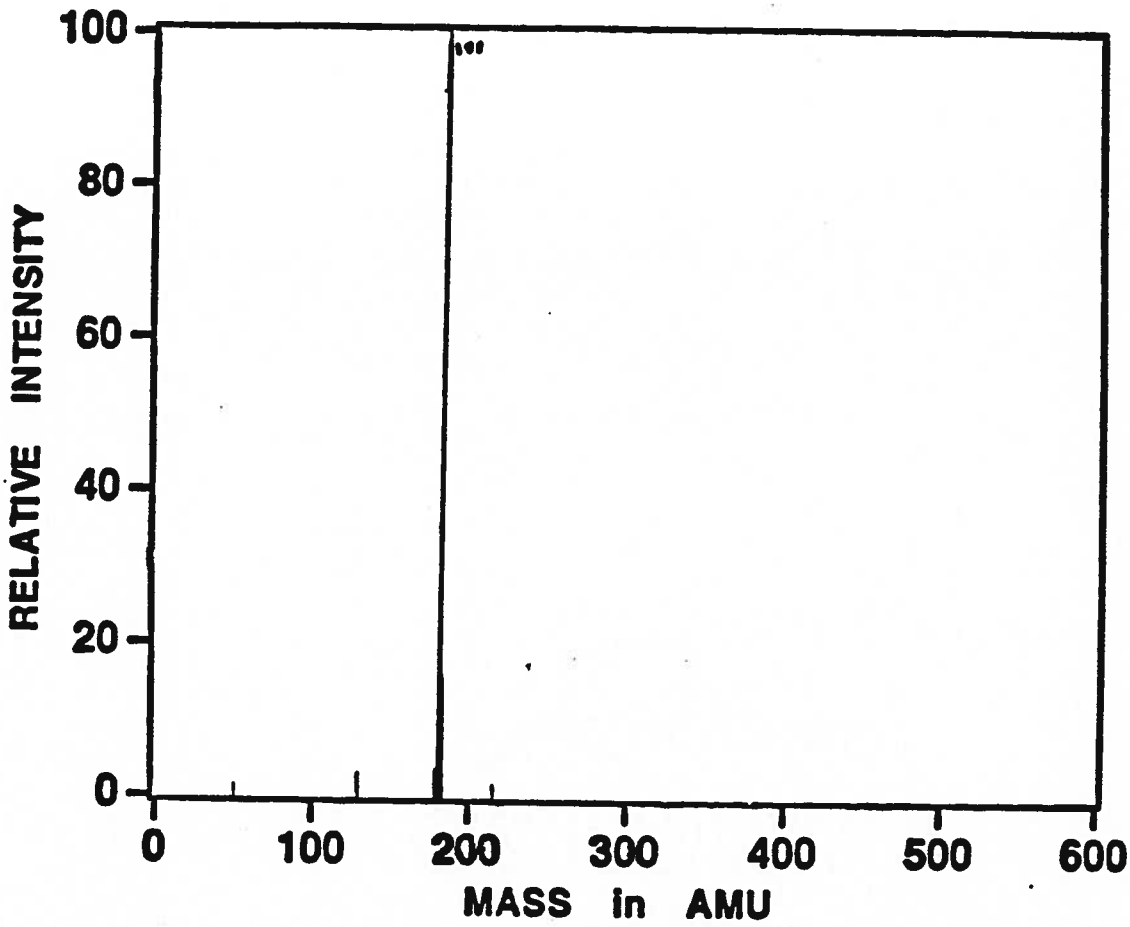

Figure 3.6(a). Multiple Resonance Mass Spectrum of $BzCr(CO)_2^+$; 0 msec.; p = 6.0×10^{-8} torr

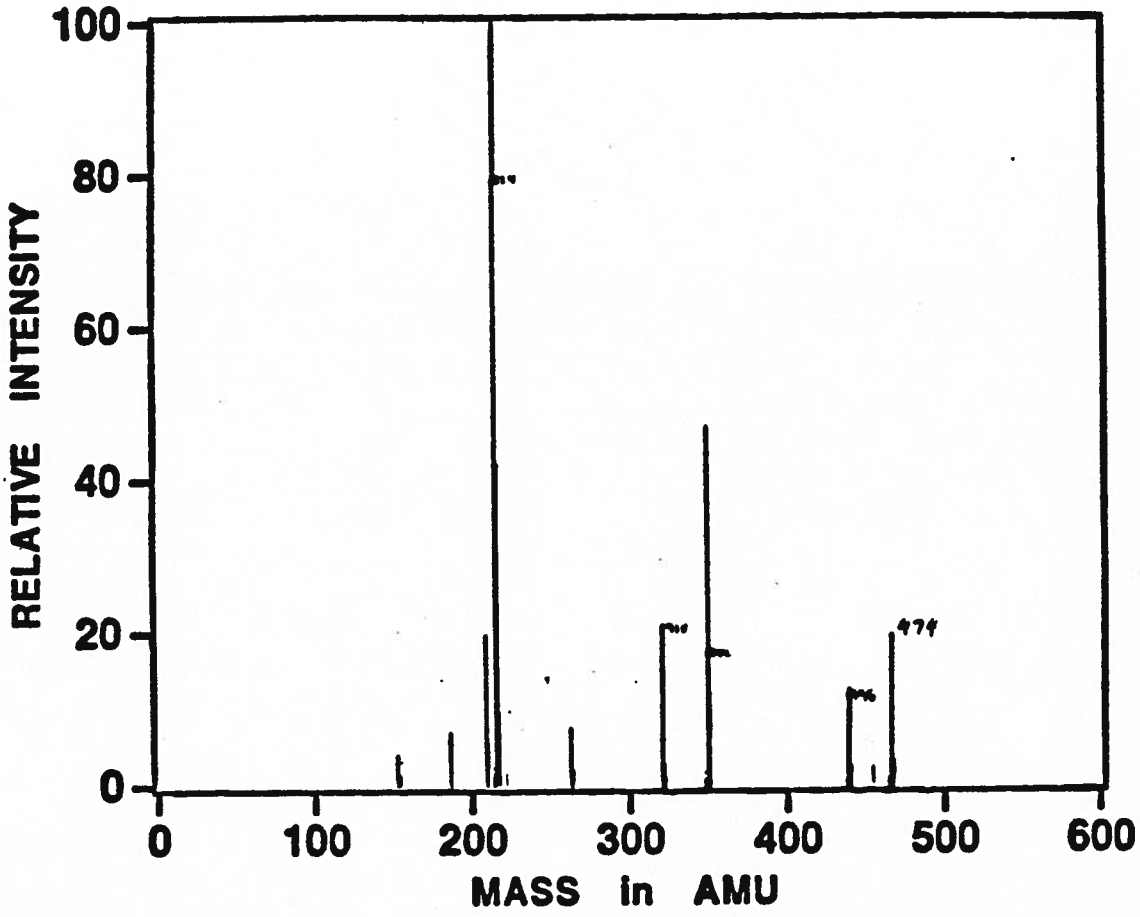

Figure 3.6(b). Multiple Resonance Mass Spectrum of $BzCr(CO)_2^+$ and Cation Products; 5000 msec; $p = 6.0 \times 10^{-8}$ torr

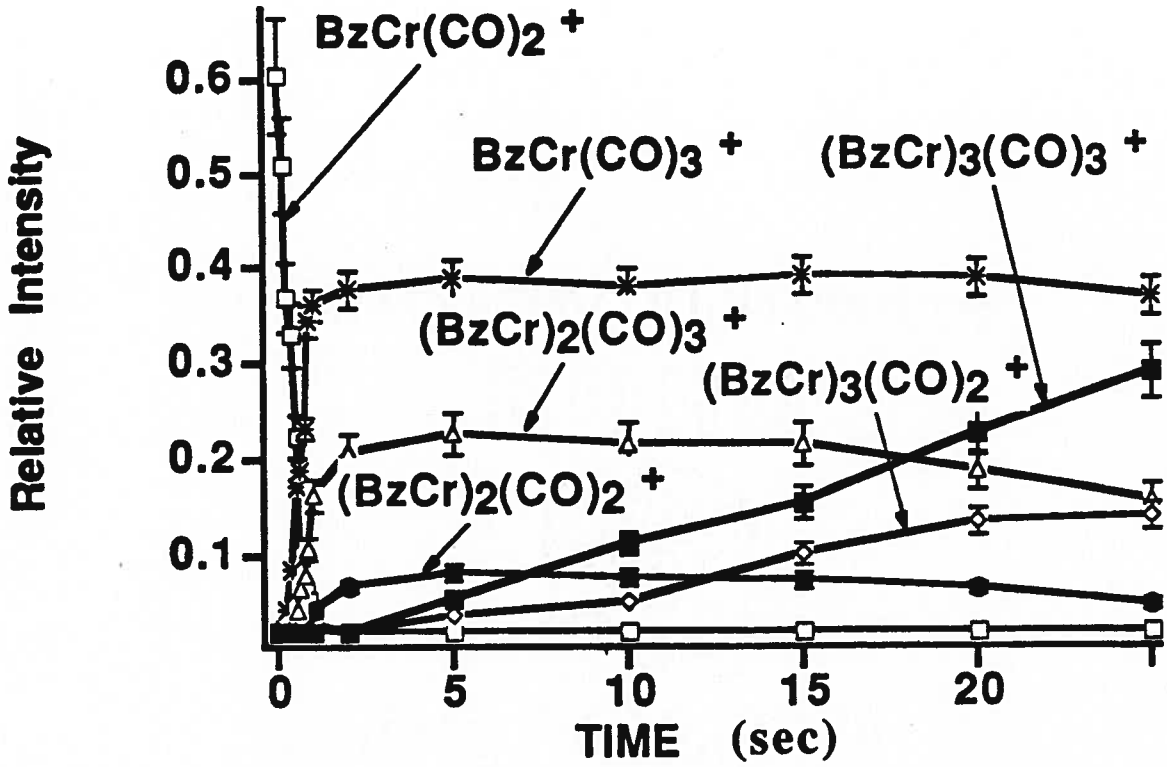

Figure 3.7. Temporal Behaviour of $BzCr(CO)_2^+$ and Cation Products

TABLE 3.2

Disappearance Rates for Chromium Cations Reacting with Neutral $BzCr(CO)_3$ Molecules

Ion	Rate Constant (k') (sec^{-1}) *	Rate Constant (k) $(x10^9\ molec.^{-1}cm^3sec^{-1})$ #
Cr^+	0.566	2.33
$BzCr^+$	0.374	1.54
$BzCrCO^+$	0.298	1.23
$BzCr(CO)_2^+$	0.227	0.93
$BzCr_2CO^+$	<0.005	<0.02
$BzCr_2(CO)_2^+$	0.480	1.98
$BzCr_2(CO)_3^+$	0.250	1.03
$(BzCr)_2^+$	<0.005	<0.02
$(BzCr)_2CO^+$	<0.005	<0.02
$(BzCr)_2(CO)_2^+$	0.057	0.24
$(BzCr)_2(CO)_3^+$	0.032	0.13
$(BzCr)_3(CO)_2^+$	0.025	0.10
$(BzCr)_3(CO)_3^+$	0.027	0.11

* Calculated from linear first-order rate plots; all data ± 10%

\# Calculated from experimental parameters:
pressure = $6.0x10^{-8}$ torr; temperature = 350°K; α = 21.25;
all data ± 30%

As revealed by the multiple resonance technique, interacting pathways of principal daughter cations in the $BzCr(CO)_3$ system are summarized in the following section. The predominant reaction type is that of condensation with the parent neutral molecule; however, electron transfer from the parent neutral molecule, which was prominent in the vanadium system also, is exhibited by several of the smaller daughter cations in this system.

PRINCIPAL REACTIVE PATHWAYS IN THE $BzCr(CO)_3$ SYSTEM

Primary (EI) fragmentation of the neutral parent $BzCr(CO)_3$ molecule occurs as follows:

$$BzCr(CO)_3 + e^- \rightarrow BzCr(CO)_{0,1,2,3}^+,\ Cr^+,\ C_6H_6^+ \ (+ \text{minor } C_3H_3Cr^+)$$

Ion-Molecule Reactions **(Cation + $BzCr(CO)_3$ → products)**

Class 1. Charge transfer from neutral parent molecule to fragment daughter cation:

Cr^+	+	$BzCr(CO)_3$	→	$BzCr(CO)_3^+$	+ . .
$BzCr_2(CO)_{1,2,3}^+$	+	"	→	" (*)	+
$BzCr(CO)_{0,1,2}^+$	+	"	→	"	+
$(BzCr)_2(CO)_{0,1,2,3}^+$	+	"	→	" (*)	+
$C_6H_6^+$	+	"	→	$BzCr(CO)_{1,2,3}^+$	+

(* low intensity)

Some relative rates of electron transfer are given in Table 3.3 on the following page. Like the vanadium system, rates of electron transfer from the neutral $BzCr(CO)_3$ molecule to reactant cations in this system are apparently governed by electron affinities of these BzCr cationic cluster fragments (in turn related to formal electron count per chromium atom in each ion cluster), compared to the ionization potential of the neutral $BzCr(CO)_3$ molecule.

TABLE 3.3

Relative Electron Transfer Rates for Chromium Cations Reacting with Neutral $BzCr(CO)_3$ Molecules

Ion	Rate Constant (k) ($\times 10^9$ molec.$^{-1}$cm^{3}sec^{-1}) *	Relative Rate #
Cr^+	1.44	100
$BzCr^+$	0.848	59
$BzCrCO^+$	0.761	53
$BzCr(CO)_2^+$	0.597	41
$BzCr_2CO^+$	---	--
$BzCr_2(CO)_2^+$	0.535	37
$BzCr_2(CO)_3^+$	0.239	17
$(BzCr)_2^+$	---	--
$(BzCr)_2CO^+$	---	--
$(BzCr)_2(CO)_2^+$	0.119	<1
$(BzCr)_2(CO)_3^+$	0.041	<1

* Calculated from total decay rate constant of reacting cation; all data ± 30%

Relative to Cr^+ rate taken as 100; all data ± 10%

Ions with very large formal electron-deficient chromium cores, such as Cr^+, $BzCr^+$, $BzCrCO^+$, etc., should predictably react rapidly in this mode, and indeed this is observed: for example, $BzCr^+$ (11 electrons per chromium) reacts approximately 1.1 times as fast as $BzCrCO^+$ (13 electrons per chromium), and 1.4 times as fast as $BzCr(CO)_2^+$ (15 electrons per Cr) in generating $BzCr(CO)_3^+$ by electron transfer (see Table 3.3). As was done for the vanadium system, the assumption has been made that the process involves simple electron transfer from neutral molecule to ion cluster fragment, e.g.;

$$(BzCr)_2(CO)_3^+ + BzCr^*(CO)_3 \rightarrow BzCr^*(CO)_3^+ + \ldots$$

rather than complex fracturing with BzCr loss by $(BzCr)_2(CO)_3^+$.

Reactant cations which undergo electron transfer with the parent molecule include Cr^+ and the mononuclear and polynuclear ionic cluster fragments $BzCr(CO)_{0,1,2}^+$ and $(BzCr)_2(CO)_{2,3}^+$. Asymmetric cluster cores such as $BzCr_2(CO)_{2,3}^+$ are also reactive with respect to electron transfer.

Class 2. Ion-molecule condensation reactions with simultaneous ejection of up to 4 CO ligands. Principal reaction paths for each fragment ion are as follows:

Primary fragment ion condensations:

Asymmetric cluster formation

$$Cr^+ + BzCr(CO)_3 \rightarrow BzCr_2(CO)_{1,2,3}^+ + n\,CO$$

$$C_6H_6^+ + BzCr(CO)_3 \rightarrow (Bz)_2Cr^+ + n\,CO$$

Symmetric cluster formation

$$BzCr^+ + BzCr(CO)_3 \rightarrow (BzCr)_2(CO)_{(0^*,1^*),2,3}^+ + nCO$$

$$BzCr(CO)_{1,2}^+ + \text{"} \rightarrow (BzCr)_2(CO)_{2,3}^+ + \text{"}$$

The parent molecular ion, $BzCr(CO)_3^+$, and the dibenzenechromium ion, Bz_2Cr^+ were unreactive for the 25-second duration test period.

Binuclear ionic cluster condensations:

Asymmetric cluster formation

$$BzCr_2(CO)_{1,2,3}^+ + BzCr(CO)_3 \rightarrow Bz_2Cr_3(CO)_{2,3,(4,6^*)}^+ + n\,CO$$

Symmetric cluster formation

$$(BzCr)_2(CO)_{2,3}^+ + BzCr(CO)_3 \rightarrow (BzCr)_3(CO)_{2,3}^+ + n\,CO$$

The preceding reaction schemes illustrate the wide variety of binuclear and trinuclear clusters generated. Relative overall clustering rates for chromium ions are listed in Table 3.4 on the following page. As was the case for the cations of $CpV(CO)_4$, clustering of these cations depends inversely upon carbonyl number and cluster size.

Except for the lack of CO ligand exchange pathways, in most cases reaction channels in this chromium system mirror those observed in the $CpV(CO)_4$ system. However, many of these ions also condense by extraction of one benzene from a neutral molecule to produce the extremely stable, 17-electron dibenzenechromium ion, Bz_2Cr^+.

TABLE 3.4

Relative Clustering Rates for Chromium Cations Reacting with Neutral $BzCr(CO)_3$ Molecules

Ion	Rate Constant (k) ($\times 10^9$ molec.$^{-1}$cm^{3}sec^{-1}) *	Relative Rate #
Cr^+	0.885	100
$BzCr^+$	0.691	78
$BzCrCO^+$	0.465	53
$BzCr(CO)_2^+$	0.337	38
$BzCr_2CO^+$	<0.020	<2
$BzCr_2(CO)_2^+$	1.44	160
$BzCr_2(CO)_3^+$	0.794	90
$(BzCr)_2^+$	<0.020	<2
$(BzCr)_2CO^+$	<0.020	<2
$(BzCr)_2(CO)_2^+$	0.115	13
$(BzCr)_2(CO)_3^+$	0.091	10
$(BzCr)_3(CO)_2^+$	<0.020	<2
$(BzCr)_3(CO)_3^+$	<0.020	<2

* Calculated from total decay rate constant including all clustering pathways; all data ± 30%

Relative to Cr^+ rate taken as 100; all data ± 10%

Symmetric clusters are produced (in which Bz = Cr, as for example, in $(BzCr)_2(CO)_2^+$) which resemble those seen in the vanadium system (Chapter 1), whereas asymmetric clusters (where Bz < or > Cr as in $BzCr_2(CO)_3^+$ or Bz_2Cr^+) are similar to those generated in the manganese system (Chapter 3). In most cases clustering rates appear to dwindle with cluster size, as occurs in the $CpV(CO)_4$ system. Small clusters may possess sandwich structures with alternating benzene-chromium-benzene arrangements (analogous to ferrocene) or, more plausibly, with some central multi-chromium cluster core into which further metal addition is still spatially possible. The marked parallel between these reactions and those of the vanadium system (Chapter 2) probably reflects the similarity in reactivity and structure of the two transition metals, Vanadium and Chromium, and their complexes. The marked CO ligand mobility in the vanadium system, not seen for this chromium analogue, may be a result of excess energy injected by the ionisation procedure, rather than from any fundamental structural or energetic differences between the two systems.

Class 3. Reactions with Benzene and CO cations

As noted in the preceding section, at reagent gas pressures of $6x10^{-7}$ torr (neutral $BzCr(CO)_3$ pressure = $6x10^{-9}$) the following reactions occur:

Bz^+	+ M	→	$BzCr(CO)_{1,2,3}^+$	+	nCO	Charge transfer
Bz^+	+ M	→	Bz_2Cr^+	+	3CO	Clustering
CO^+	+ M	→	HCO^+	+ ...		H atom transfer
HCO^+	+ M	→	MH^+	+ ...		Proton transfer

Two triple resonance spectra showing benzene cation initially and its cation product ions at 500 msec are shown in Figure 3.8(a,b); temporal behaviour of benzene cation and its product cations is shown in Figure 3.9 on the following pages. Benzene cation (Bz^+) reacts principally by electron transfer from neutral $BzCr(CO)_3$ molecule to Bz^+, thus making the latter species charge neutral and invisible to the detector.

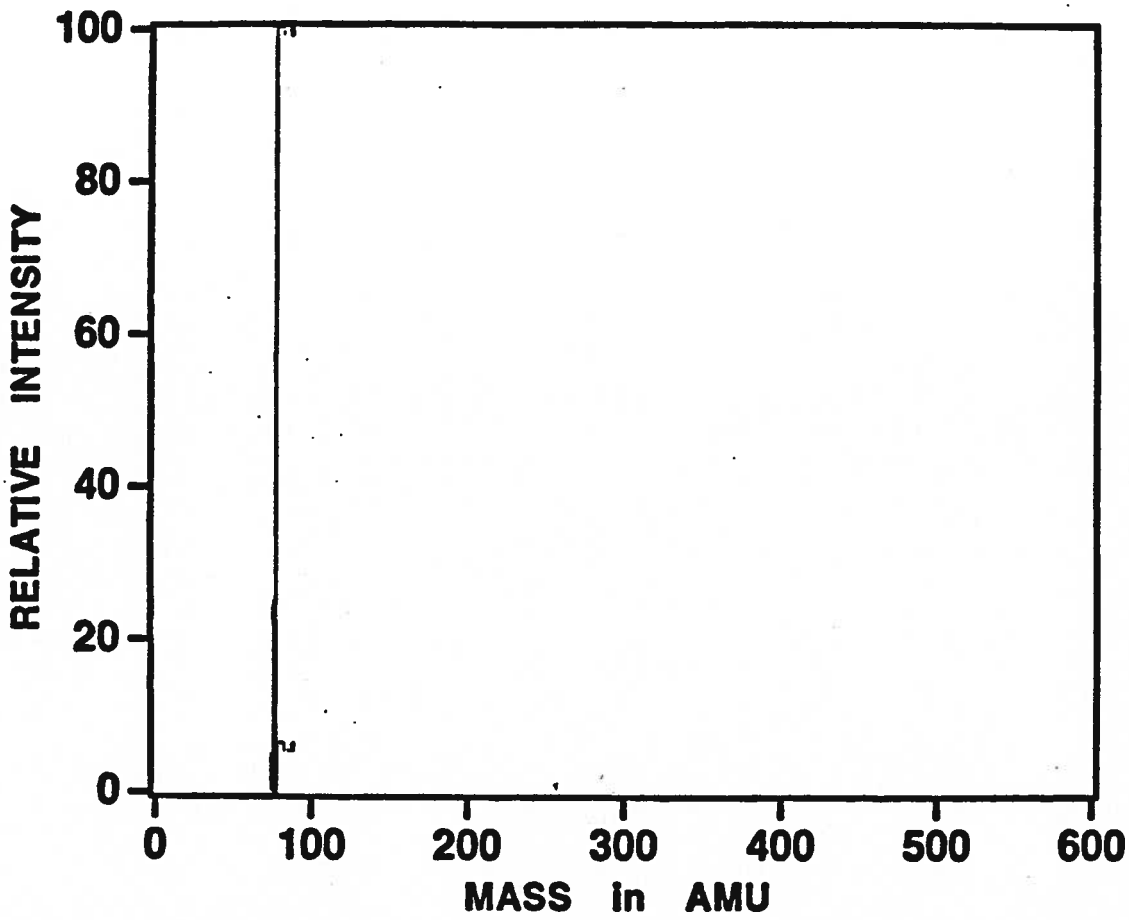

Figure 3.8(a). Multiple Resonance Mass Spectrum of $C_6H_6^+$; 0 msec.; p = 6.0×10^{-8} torr

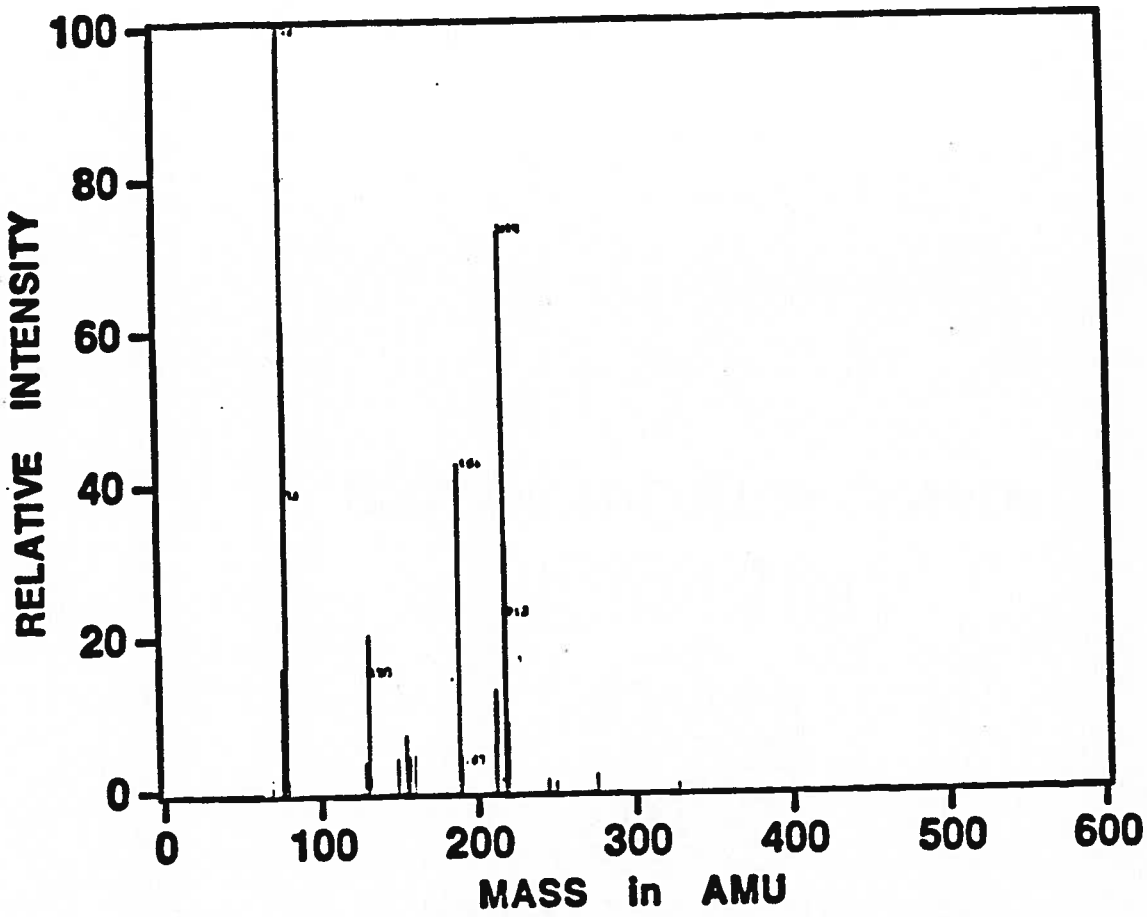

Figure 3.8(b). Multiple Resonance Mass Spectrum of $C_6H_6^+$ and Cation Products; 500 msec; $p = 6.0 \times 10^{-8}$ torr

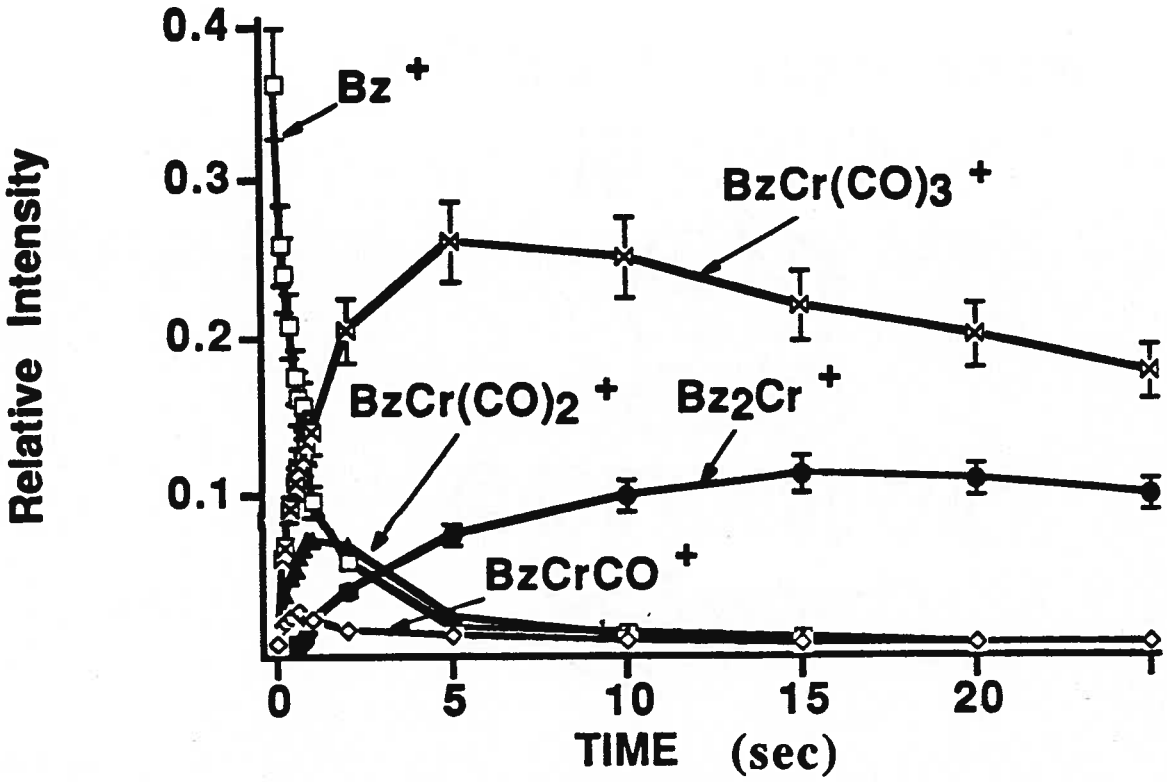

Figure 3.9. Temporal Behaviour of $C_6H_6^+$ and Cation Products

Electron transfer from a neutral molecule to a benzene cation is thermodynamically favored whenever the ionization potential of benzene (9.25 eV) exceeds that of the neutral reactant, in this case, 7.3 eV for $BzCr(CO)_3$. As Munson notes recently[1], this makes benzene attractive as a selective reagent gas in CIMS for characterising aromatic mixtures containing components of differing ionisation potential. Loss of CO by the neutral $BzCr(CO)_3$ molecule during this transfer process is seen in some of the products; i.e. in $BzCr(CO)_{1,2}^+$, suggesting that some collisional energy, effecting CO ligand loss, is transferred as well during reaction.

As well, benzene cation undergoes condensation with neutral $BzCr(CO)_3$ to produce dibenzene chromium cation, Bz_2Cr^+. After formation, this stable cation, having 17 valence electrons, is apparently inert to further ion-molecule interaction.

The other small cation reactant, CO^+, reacts first by hydrogen atom extraction from the neutral $BzCr(CO)_3$ molecule, followed by proton donation to a second neutral to produce the hydrido-form of the molecular cation, $BzCr(CO)_3H^+$.

Reactions of CO^+ and HCO^+ ions have been reviewed elsewhere[15]. Identical behaviour is seen in the present $CpCo(CO)_2$ system (Chapter 6) where hydrogen is first extracted from the neutral molecule by gaseous molecular ions N_2^+, CO^+ and CO_2^+, producing reactive HN_2^+, HCO^+, and HCO_2^+, respectively. Subsequently these reactive cations then donate a proton to a second neutral molecule to produce the hydride ion, $CpCo(CO)_2H^+$. In this chromium system, HCO^+ reacts by proton donation to generate the hydride ion $BzCr(CO)_3H^+$. Other hydrogenated chromium carbonyl ions have been characterised, such as $HCr(CO)_5^-$, formed by hydride ion addition to $Cr(CO)_6$[18].

2. Negative Ion Chemistry

In 1987 Bricker and Russell studied the ion-molecule reaction of the $Cr(CO)_5^-$ anion with molecular oxygen[6]. They noticed that anion products generated using thermal

ionisation methods were different from those products formed after electron ionisation (i.e., thermal ionisation of $Cr(CO)_6$ molecules gave oxygenated ion products while EI did not), suggesting that electronically-excited $Cr(CO)_5^-$ anion, formed by thermal decomposition of $Cr(CO)_6$, plays an important part in reactions with O_2. In this system, no products containing multi-chromium cluster cores were observed.

In the present study, under 1-5 volt EI negative ion monitoring, neutral $BzCr(CO)_3$ undergoes electron capture to produce daughter anions $Cr(CO)_3^-$, $Cr(CO)_4^-$, and $Cr(CO)_5^-$, completely rupturing the benzene-chromium linkage even using EI voltages as low as 1 eV (i.e., benzene-chromium linkages are not retained in anionic products). Figure 3.10 on the following page is a typical negative ion mass spectrum of $BzCr(CO)_3$ showing peaks corresponding to $Cr(CO)_3^-$, $Cr(CO)_4^-$, and $Cr(CO)_5^-$.

Temporal monitoring of $Cr(CO)_{3,4,5}^-$ daughter ion fragments for 25 seconds at pressures of 6.0×10^{-8} torr showed slow accumulation of CO ligands by both $Cr(CO)_3^-$ (13-electron) and $Cr(CO)_4^-$ (15-electron) reactant ions, eventually resulting in the final, unreactive (17-electron) product ion, $Cr(CO)_5^-$. Unequivocal evidence of excited state reactants such as non-linear semilog kinetics was not seen. Probable reaction paths are as follows:

$$Cr(CO)_3^- + M \rightarrow Cr(CO)_4^- + ..$$

$$Cr(CO)_4^- + M \rightarrow Cr(CO)_5^- + ..$$

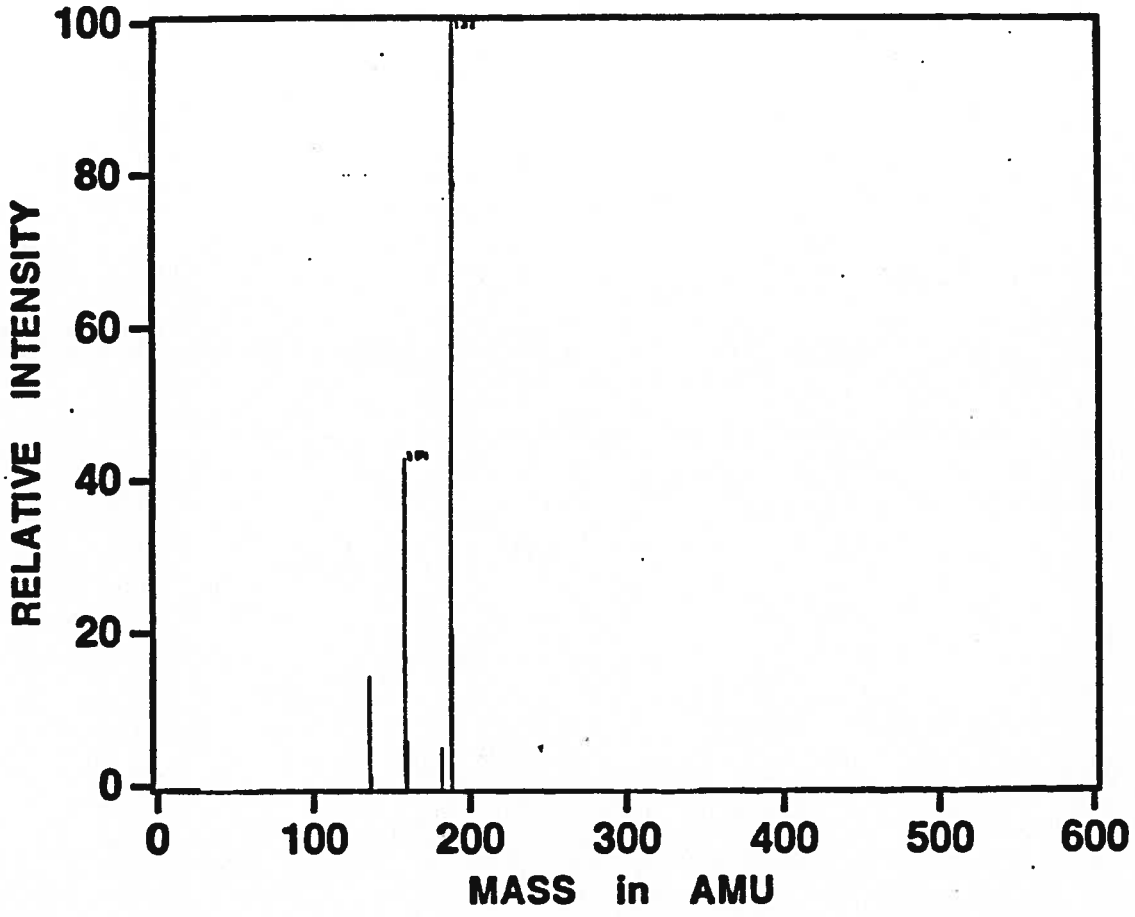

Figure 3.10. FT-ICR Negative Ion Mass Spectrum of $BzCr(CO)_3$; 0 msec.; 2.5 eV; $p = 6.0 \times 10^{-8}$ torr

III Conclusions

GENERAL FEATURES OF THE $BzCr(CO)_3$ SYSTEM

1) Except for the unreactive parent molecular ion, $BzCr(CO)_3^+$, all of the cations initially formed by electron impact on $BzCr(CO)_3$ are chemically reactive with the parent neutral; whereas the principal daughter anion, $Cr(CO)_5^-$ is unreactive. Only carbonylated chromium anions were detected; the aryl-chromium linkage did not survive the ionisation process.

2) As seen in the vanadium case, most cations in the $BzCr(CO)_3$ system underwent electron transfer with their parent neutral molecule, generating $BzCr(CO)_3^+$. Rates of electron transfer are listed in Table 3.1. Like V^+, Cr^+ also reacts by charge exchange with the neutral, but unlike V^+, Cr^+ reacts as well by unsymmetrical clustering with the parent neutral molecule.

3) As in the vanadium system, the integrity of the aryl-Cr bond within cluster cores tends to be retained in the cationic system throughout successive reaction hierarchies; i.e., in $(BzCr)_2$ and $(BzCr)_3$ cluster cores. Condensation rates as listed in Table 3.4 reveal that this reactive pathway is strongly correlated with carbonyl coordination number and cluster size, as was the case for vanadium ions. However, in contrast with the vanadium anion system, where Cp-V linkages remained intact, Bz-Cr linkages are labile in the negative ion regime; only oxy-chromium anions, $Cr(CO)_{3,4,5}^-$ were observed.

4) Clustering dwindles after formation of trinuclear cluster ions, i.e., $(BzCr)_3$ cores, at pressures used (10^{-6}-10^{-9} torr); $(BzCr)_4$ cation cluster fragments were observed in low yields, only at higher pressure ranges or after long reaction times. As in the vanadium system, these clustering processes are in competition with electron transfer pathways.

5) Stability of cationic clusters is directly related to formal electron deficiency of the central chromium core. Figure 3.11 on the following page shows electron deficiencies plotted against pseudo-first order rate constants for principal cation clusters in the $BzCr(CO)_3$ system. In Figure 3.11, single metal fragment ions are plotted as open squares; while cluster products are plotted as circles.

Since metal-metal bond order in each cluster is not known, each cluster point was plotted more than once, corresponding to bond orders of one, two or three, respectively. (The exact placement of cluster points on this diagram depends upon the electron count arbitrarily considered to contribute to chromium-chromium bonds (i.e., 2, 4 or 6 electrons per Cr-Cr bond.) Points for most clusters fall closest to the curve with triple metal-metal bonding; this is strong evidence for multiple bond order in these ions. As is apparent, the unreactive, stable cations Bz_2Cr^+ and $BzCr(CO)_3^+$, each possessing 17 valence electrons, predictably disappear slowly.

Formal electron counts in the asymmetric clusters, (e. g. $BzCr_2(CO)_{0,1}^+$) depend upon whether Cr-Cr linkages are considered to be present or absent. The rapid rate of decay of these ions suggests that metal-metal linkages in these unsymmetric product ions possess low coordination, and are unprotected by ligand spheres, hence vulnerable to attack during further collisions. On the other hand, the slower decay rates of the symmetric clusters, (e. g., $(BzCr)_2(CO)_{2,3}^+$) again give support to the multiple-bonded central Cr core models. The steep slope on the left side in Figure 3.11 indicates that ions with electron deficiencies above 2 are highly reactive, with probable strong reactivity toward one- or two- electron donor reagents such as ammonia and carbon monoxide.

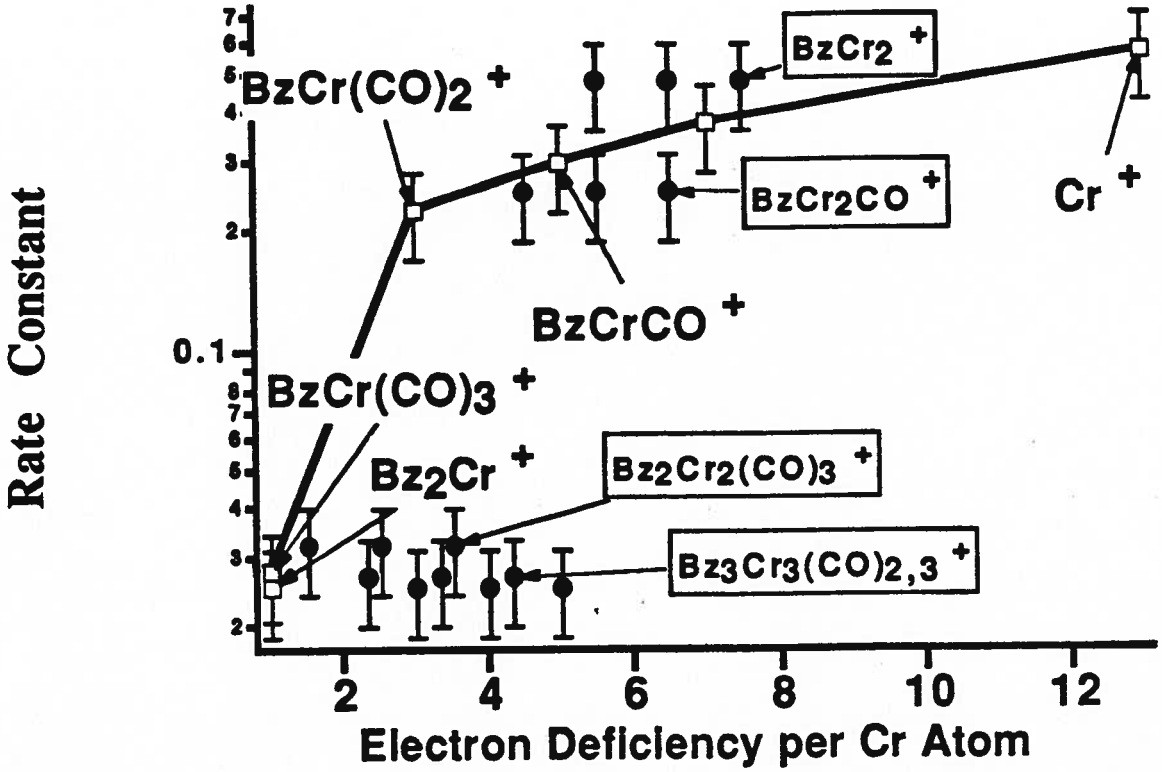

Figure 3.11. Relationship Between Reactivity and Electron Deficiency for Cations in the $BzCr(CO)_3$ System

6) Like the smaller, highly electron-deficient cations of vanadium, those of chromium are also extremely susceptible to adduct formation, rapidly accepting new ligands such as O_2, O, H_2 , H. Precise measurements of these adduct products was not possible because of low product ion concentrations. Interestingly, in reactions with carbon monoxide at elevated CO pressures (pressure of CO=6.0×10^{-7} torr), protonation of the neutral molecule was the overall result. The final product of this pathway was the hydrido cation, $BzCr(CO)_3H^+$. Other hydrogenated chromium ions formed in the gas phase such as $HCr(CO)_5^-$ are known to exist in the gas phase[18].

7) As in the vanadium system, excited state ion participation by the bare metal cation, in this case Cr^+, probably occurs in this $BzCr(CO)_3$ regime as well. To illustrate this, curved kinetic pseudo-first order semi-log plots for Cr^+, $BzCr^+$ and $BzCrCO^+$, are shown together in Figure 3.12 on the following page.

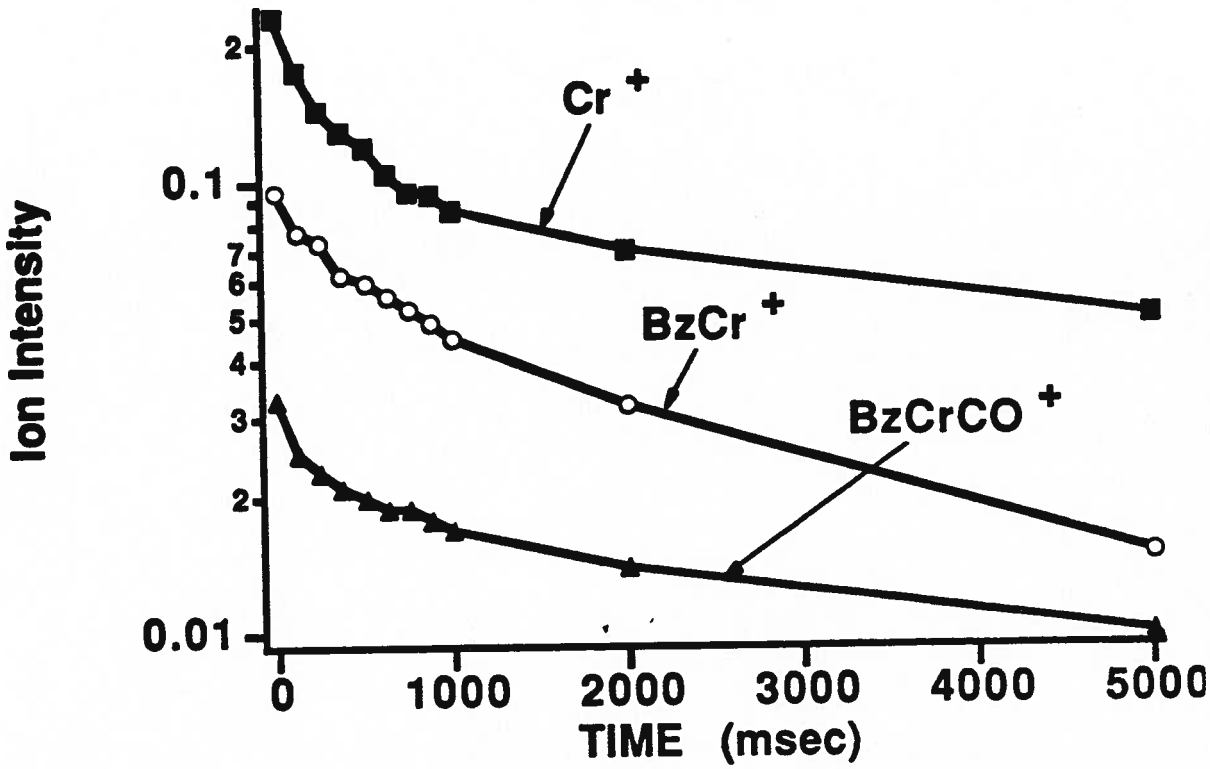

Figure 3.12. **Pseudo-First Order Decay Behaviour and Deviations for Cations in the $BzCr(CO)_3$ System**

Since the energy difference between the electronic ground state and the first excited state is much larger for Cr^+ than for V^+ (i.e., 1.52 eV compared to 0.33 eV)[3], a small but still significant portion of chromium cations (comparable to that of V^+) would be expected to exist in excited states during ionisation, and hence would make a contribution to alternate kinetic pathways. Assuming that reaction rates or pathways differ for excited and ground state ions, the approximate proportion of excited state Cr, $BzCr^+$ and $BzCrCO^+$ obtained from extrapolation of the semi-log plots are 63%, 42% and 45% respectively. These data are summarised in Figure 7.5; Chapter 7. This phenomenon of altered reactivity in excited state chromium ions has been considered earlier by several authors including Kiser[30], Armentrout[10] and Reents[26]. Reactions of several excited state transition metal cations with benzene have resulted in formation of metal-benzene- or benzyne- cations such as C_6H_6-metal$^+$ and C_6H_4-metal$^+$ ions[33], not seen for ground state ions. Similarly, the cations $BzCr^+$ and Bz_2Cr^+ are produced in the present system, and may possibly be a product of excited state Cr^+.

Pseudo-first order semi-log plots for the larger daughter cation fragments in this system (i.e., $BzCrCO^+$, etc.) are linear, indicating that ground state ions predominate for the larger cation fragments.

8) A representative clastogram illustrating the appearance and abundances of positive ions of the $BzCr(CO)_3$ system with respect to ionisation energy is shown in Figure 3.13 on the following page. Results are in general accord with those measured by earlier workers using sector instruments[19,25].

9) Structures of the multi-chromium cluster ions observed here are still unknown. Probably these clusters consist of chromium atoms in multiple-bonded central chromium cores, surrounded externally by protective ligands, such as exist in the trichromium dianion, $Cr_3(CO)_{12}S^{2-}$[29]. Few multi-chromium clusters are known, however, apparently requiring stabilisation through multiple chromium-oxygen or chromium-sulfur linkages within the central core[8,29].

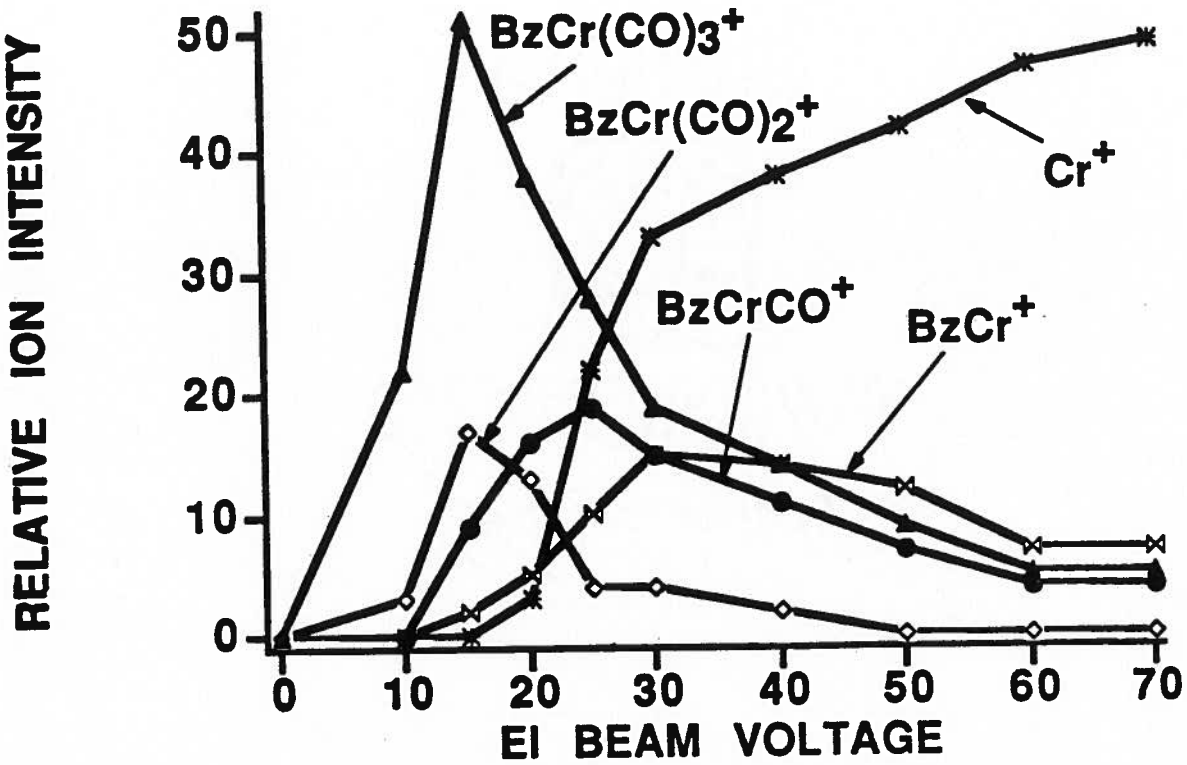

Figure 3.13. Clastogram for Cations of $BzCr(CO)_3$

IV References

(1) Allgood, C.; Yee, C. M.; Munson, B. *Anal. Chem.* **1991**, *63*, 721.

(2) Armentrout, P. B.; Halle, L. F.; Beauchamp, J. L. *J. Amer. Chem. Soc.* **1981**, *103*, 6501.

(3) Armentrout, P. B. in *Gas Phase Inorganic Chemistry*; Russell, D. H.; Plenum Press, New York, **1989**; pp 1 - 42.

(4) Bailey, M. F.; Dahl, L. F. *Inorg. Chem.* **1965**, *4*, 1314.

(5) Bottomley, F.; Sutin, L. *Adv. Organomet. Chem.* **1988**, *28*, 339.

(6) Bricker, D. L.; Russell, D. H. *J. Am. Chem. Soc.* **1987**, *109*, 3910.

(7) Cetini, G.; Gambino, O.; Lausarot, P. M.; Operti, L.; Vaglio, G. A.; Valle, M.; Volpe, P. *Inorg. Chim. Acta* **1985**, *104*, 69.

(8) Chen, S.-P.; Comisarow, M. B. *Ann. Conf. ASMS All. Top.* **1989**, *37*, 323.

(9) Connor, J. A. *Top. Curr. Chem.* **1977**, *71*, 71.

(10) Elkind, J. L.; Armentrout, P. B. *J. Chem. Phys.* **1987**, *86*, 1868.

(11) Fischer, E. O.; Ofele, K. *Chem. Ber.* **1957**, *90*, 2532.

(12) Fredeen, D. J. A.; Russell, D. H. *J. Am. Chem. Soc.* **1985**, *107*, 3762.

(13) Gilbert, J. R.; Leach, W. P.; Miller, J. R. *J. Organomet. Chem.* **1973**, *49*, 219.

(14) Halle, L. F.; Armentrout, P. B.; Beauchamp, J. L. *J. Am. Chem. Soc.* **1981**, *103*, 962.

(15) Harrison, A. G. *Chemical Ionization*; Wiley - Interscience: New York, **1984**.

(16) Jacobson, D. B.; Freiser, B. S. *J. Am. Chem. Soc.* **1985**, *107*, 5870.

(17) Kang, H.; Beauchamp, J. L. *J. Am. Chem. Soc.* **1986**, *108*, 5663.

(18) Lane, K. R.; Squires, R. R. *J. Am. Chem. Soc.* **1985**, *107*, 6403.

(19) Müller, J.; Göser, P. *Chem. Ber.* **1969**, *102*, 3314.

(20) Müller, J.; Fenderl, K. *Chem. Ber.* **1970**, *103*, 3128.

(21) Operti, L.; Vaglio, G. A.; Gord, J. R.; Freiser, B. S. *Organometallics* **1991**, *10*, 104.

(22) Pan, Y. H.; Ridge, D. P. *J. Am. Chem. Soc.* **1989**, *111*, 1150.

(23) Parisod, G.; Comisarow, M. B. *Adv. Mass Spectrom.* **1980**, *8A*, 212.

(24) Pignataro, S.; Foffani, A.; Grasso, F.; Cantone, B. *Z. Physik. Chem. (Frankfurt)* **1965**, *47*, 106.

(25) Pignataro, S.; Lossing, F. P. *J. Organometal. Chem.* **1967**, *10*, 531.

(26) Reents, J., W. D. ; Strobel, F.; Freas, R. B.; Wronka, J.; Ridge, D. P. *J. Phys. Chem.* **1985**, *89*, 5666.

(27) Russell, D. H.; Fredeen, D. A.; Tecklenburg, R. E. in *Gas Phase Inorganic Chemistry*; Russell, D. H.; Plenum Press, New York, **1989**; pp 115-135.

(28) Sellers-Hahn, L.; Russell, D. H. *J. Am. Chem. Soc.* **1990**, *112*, 5953.

(29) Shriver, D. F.; Kaesz, H. D.; Adams, R. D. *The Chemistry of Metal Cluster Complexes*; VCH Publishers, Inc.: New York, **1990**.

(30) Sullivan, R. E.; Kiser, R. W. *J. Chem. Phys.* **1968**, *49*, 1978.

(31) Traylor, T. G.; Stewart, K. J.; Goldberg, M. J. *J. Am. Chem. Soc.* **1984**, *106*, 4444.

(32) Traylor, T. G.; Stewart, K. J. *J. Am. Chem. Soc.* **1986**, *108*, 6977 .

(33) VanOrden, S. L.; Cooper, B. T.; Pope, R. M.; Buckner, S. W. *Ann. Conf. ASMS All. Topics* **1991**, *39*, 1614.

(34) Wilkinson, G.; Cotton, F. A.; Birmingham, J. M. *J. Inorg. Nucl. Chem.* **1956**, *2*, 95.

(35) Winters, R. E.; Kiser, R. W. *Inorg. Chem.* **1965**, *4*, 157.

(36) Winters, R. E.; Kiser, R. W. *J. Chem. Phys.* **1966**, *44*, 1964.

CHAPTER 4

Ion Molecule Chemistry of

Tricarbonyl (η^5 - Cyclopentadienyl) Manganese

{ $CpMn(CO)_3$ }

I Introduction

Tricarbonyl (η^5-cyclopentadienyl) manganese, $CpMn(CO)_3$, is a pale yellow, crystalline solid subliming at 60° C (1 atm) and melting at 77° C. First prepared and characterised by Piper, Cotton and Wilkinson in 1955[21], this complex is reactive with oxygen, water and polar solvents, readily undergoing electrophilic substitution, its spatial geometry resembling that of a "three-legged piano stool".

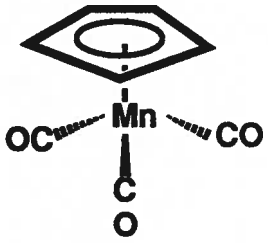

Ion-molecule chemistry of ligated manganese ions has been the subject of several studies over the past few years[1,2,23,30]. Anion reactions of mono- and dimanganese decacarbonyl complexes have been monitored and interpreted by Junk[12,27] and Meckstroth[15,16]. The reactivity of the dimanganese cation Mn_2^+ with dioxygen[3], and bases[13] has been analysed, and its photodissociative properties by Jarrold[11]. Bond energies of manganese-hydrogen[2,22], Mn-CO[2,8,20], M-CH_2[10], Mn-Cp[8,23], and Mn-O[2] linkages have been determined.

The first dicyclopentadienyl complex of manganese, manganocene (Cp_2Mn), was first prepared by Wilkinson in 1956[28], and this complex was later mass analysed by Winters in 1965[29]. A comparison of aryl-manganese and other aryl transition metals has been theoretically treated by Burdett[7] and others[8,30].

Müller (1968-70) was first to examine $CpMn(CO)_3$ and some of its derivatives mass spectrometrically[17,18]. Some of the cation fragments were observed to condense, producing bimanganese clusters such as $Cp_2Mn_2(CO)_3^+$. In 1976 Lichtenberger measured photoelectronic spectra of $CpMn(CO)_3$ and some derivatives, including those of the dioxygen and ammoniated complexes[14]. Positive ion-molecule kinetics of the $CpMn(CO)_3$ system was first studied by FT-ICR-MS in 1980[19]. In this work, cation daughter products were observed to undergo a wide variety of condensation reactions with the parent neutral molecule $CpMn(CO)_3$, generating cluster ions containing up to at least three Mn atoms. The following work involves a detailed study of ion-molecule interactions and products of $CpMn(CO)_3$ under a variety of experimental conditions.

II Results and Discussion

1. Positive Ion Chemistry

In most experiments, cation-molecule chemistry was monitored for a 25 second time span. Under 25 ev EI and pressures of 6.0×10^{-8} torr, the following assembly of daughter ions was obtained: Mn^+ (5%), $CpMn^+$ (41%), $CpMnCO^+$ (11%), $CpMn(CO)_2^+$ (5%), $CpMn(CO)_3^+$ (22%), these products identical and in similar proportions to those measured by Parisod[19] (Mn^+ (8%), $CpMn^+$ (28%), $CpMnCO^+$ (15%), $CpMn(CO)_2^+$ (8%), $CpMn(CO)_3^+$ (30%)). A typical mass spectrum showing principal daughter cations is shown in Figure 4.1, and a sample mass table given in Table 4.1.

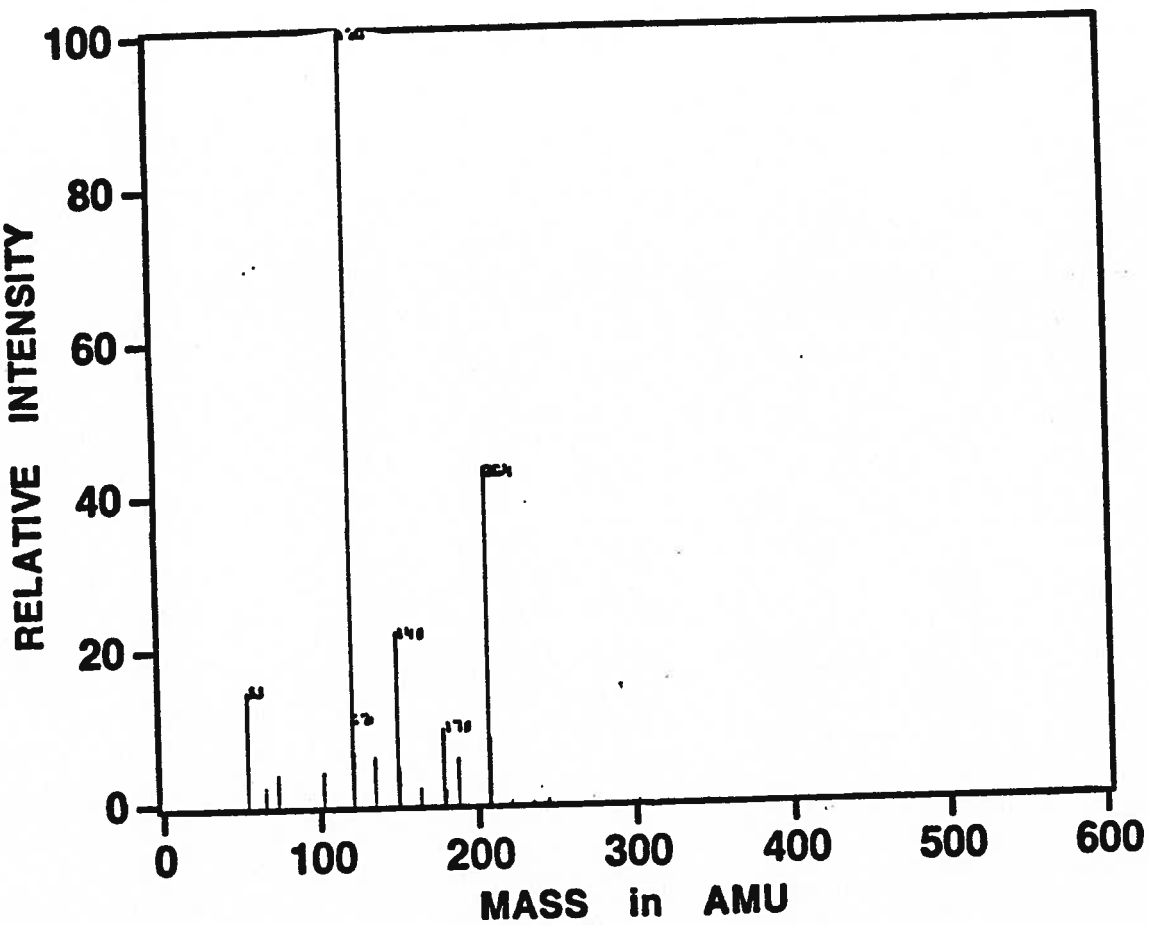

Figure 4.1. FT-ICR Positive Ion Mass Spectrum of $CpMn(CO)_3$; 0 msec.; 25 eV; $p = 6.0 \times 10^{-8}$ torr

TABLE 4.1

Sample Mass Table for $CpMn(CO)_3$ Cations (500 msec)

Formula	Expected Mass[a]	Measured Mass[a]	Δ (ppm)	Rel. Int. (%)
^{55}Mn (100%)	54.9375	54.9721	35[b]	25.5
C_5H_5Mn	119.9767	120.0616	90	100
CpMnCO	147.9716	147.9853	14	18.7
$CpMn(CO)_2$	175.9665	175.9847	18	8.2
$CpMn(CO)_3$	203.9614	203.9614	0[b]	43.0
$(CpMn)_2$	239.9538	240.1052	151	9.4
$(CpMn)_2CO$	267.9488	267.9875	39	8.3
$(CpMn)_2(CO)_2$	295.9437	295.9995	56	2.3
$(CpMn)_2(CO)_3$	323.9386	323.9772	39[b]	2.5
$(CpMn)_3(CO)_2$	415.9208	415.8127	108	2.2

[a] in daltons
[b] calibrant mass

All the primary fragment cations except for the molecular ion, $CpMn(CO)_3^+$, react further with the $CpMn(CO)_3$ neutral molecule. Subsequent ion-molecule interactions produce symmetrical (Cp = Mn) polynuclear cluster ions, including binuclear clusters such as $(CpMn)_2(CO)_2^+$, trinuclear clusters such as $(CpMn)_3(CO)_2^+$, and several asymmetrical (Cp < Mn) clusters, e.g.: $CpMn_2(CO)_2^+$, $Cp_2Mn_3(CO)_5^+$. Cation clusters generated are as follows:

Symmetric clusters (Cp=Mn)

$(CpMn)_2(CO)_{0,1,2,3}$ +

$(CpMn)_3(CO)_{(1*),2,3}$ +

Asymmetric clusters (Cp< or >Mn)

$CpMn_2(CO)_{(0,1*),2,(3)}$ +

$Cp_2Mn_3(CO)_{(4*),5}$ +

Cp_2Mn^+

(* low intensity)

Typical formation and disappearance of primary fragment ions is illustrated in Figure 4.2. Temporal behaviour of binuclear and of trinuclear ionic clusters is shown in Figures 4.3 and Figure 4.4.

Figure 4.5(a,b) displays two triple resonance spectra of $CpMn^+$ ion, initially and at 5000 msec, after its ion products had been allowed to form. Temporal behaviour of this ion and its daughter ion products is illustrated in Figure 4.6; analogous spectra for the $(CpMn)_2(CO)_3^+$ cation cluster, measured at identical time intervals, are shown in Figure 4.7(a,b) and temporal plots of these product ions are shown in Figure 4.8. For each reactive ion, decay rate constants for reaction of each cation with the parent neutral molecule $CpMn(CO)_3$ were measured from the slopes of linear pseudo-first order semi-log plots; these values are listed in Table 4.2.

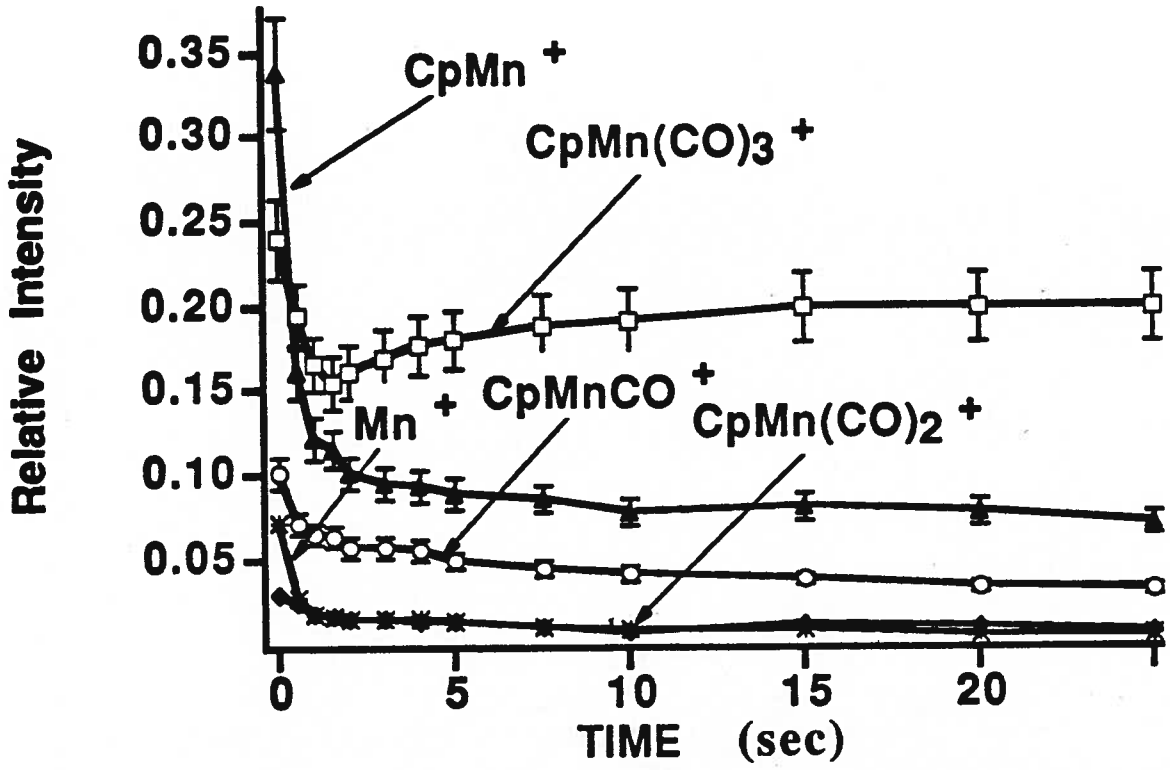

Figure 4.2. Temporal Behaviour of Primary Fragment Cations of $CpMn(CO)_3$

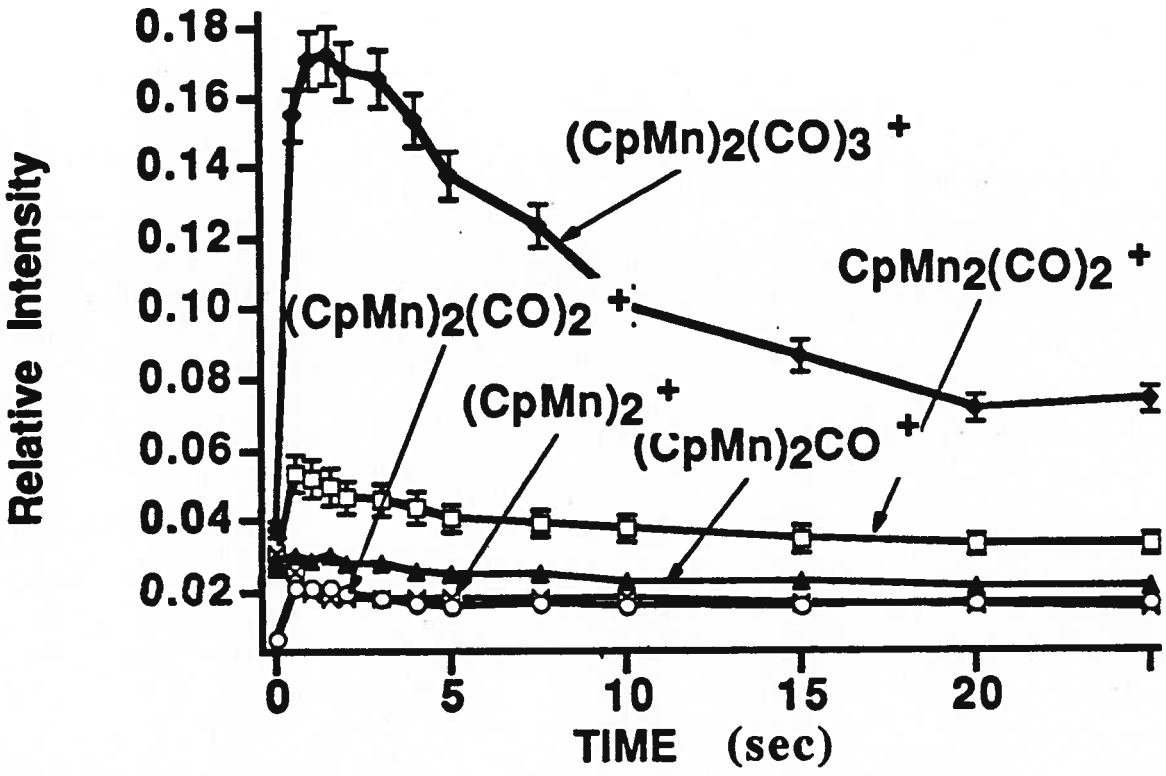

Figure 4.3. Temporal Behaviour of Binuclear Cluster Cations of $CpMn(CO)_3$

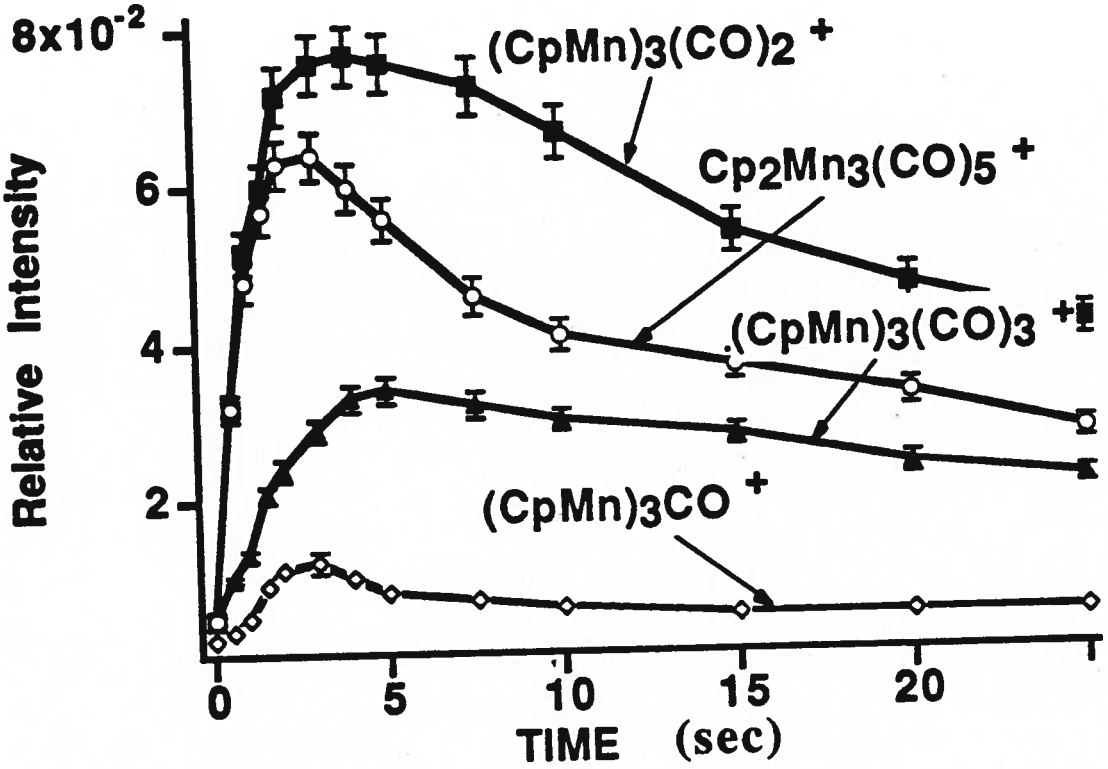

Figure 4.4. Temporal Behaviour of Trinuclear Cluster Cations of $CpMn(CO)_3$

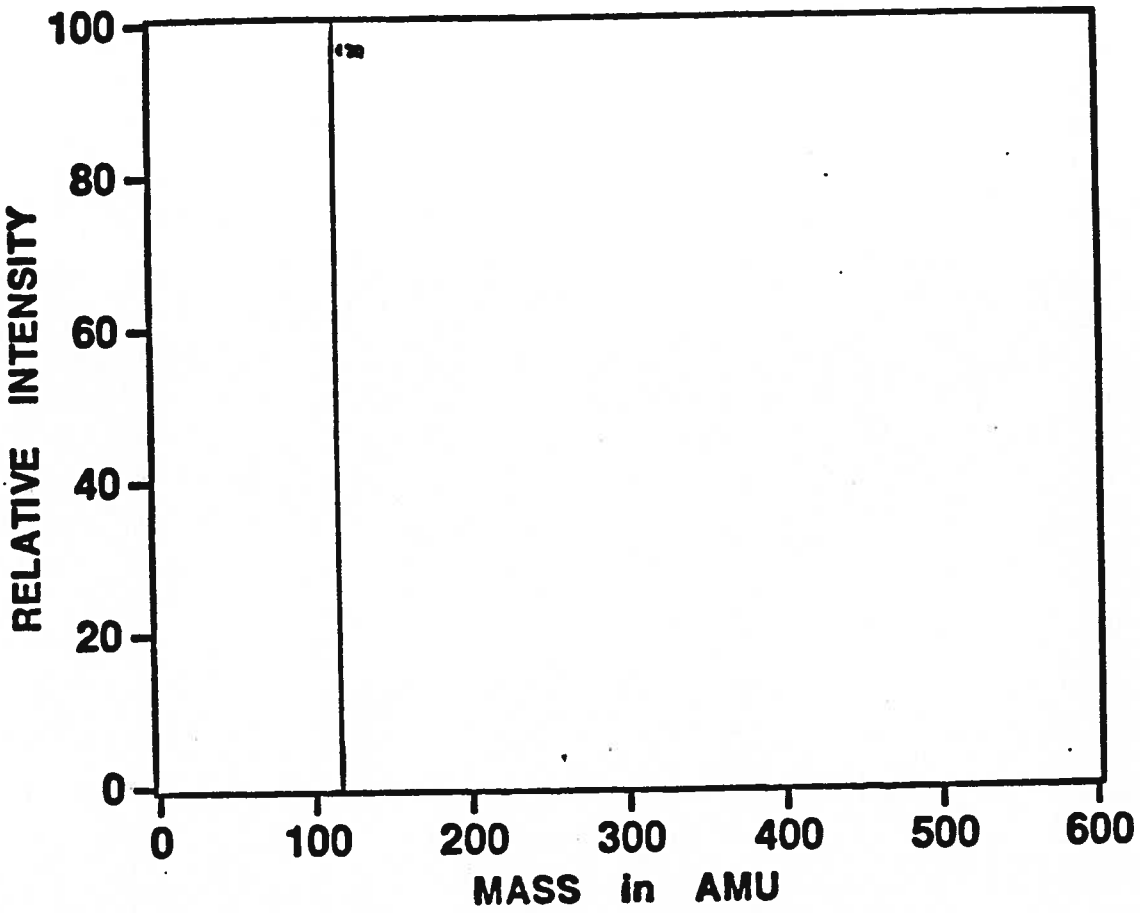

Figure 4.5(a). Multiple Resonance Mass Spectrum of $CpMn^+$;

0 msec.; p = 6.0×10^{-8} torr

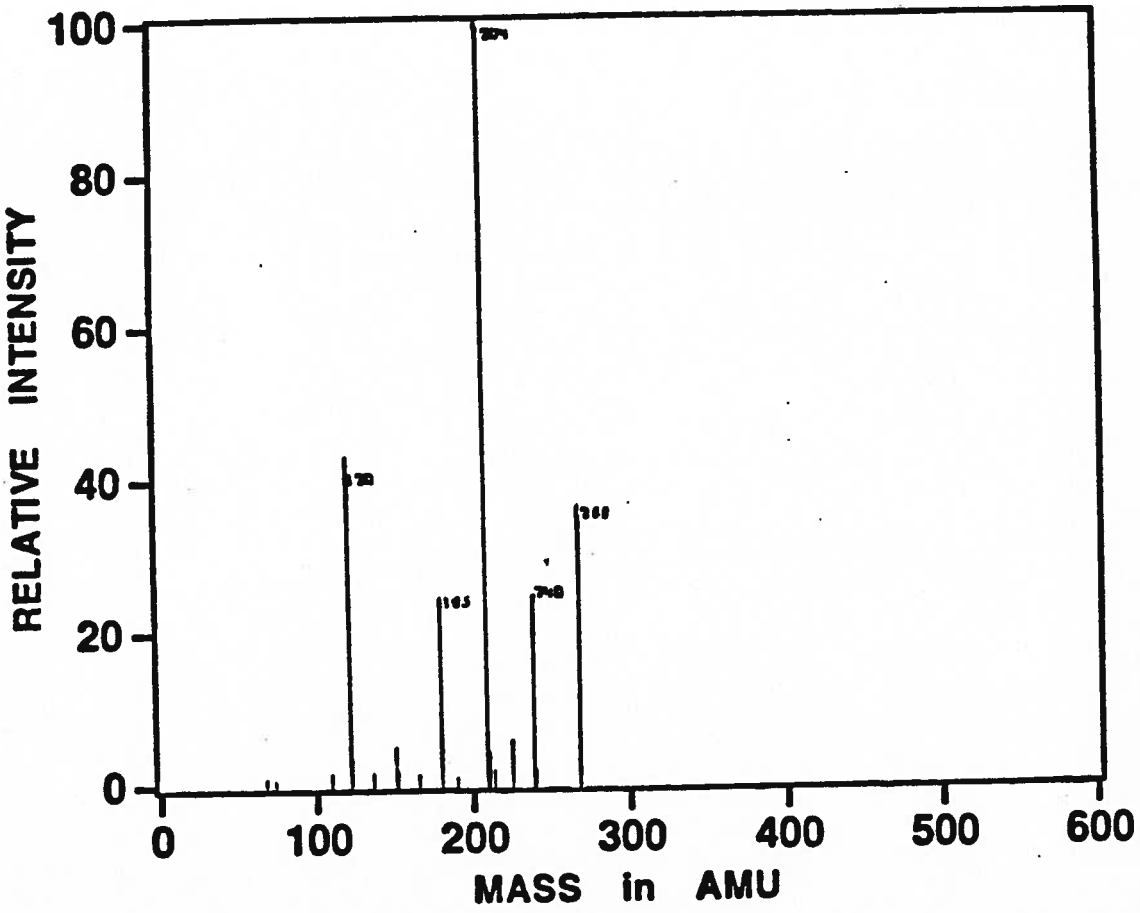

Figure 4.5(b). Multiple Resonance Mass Spectrum of $CpMn^+$ and Cation Products; 5000 msec.; $p = 6.0 \times 10^{-8}$ torr

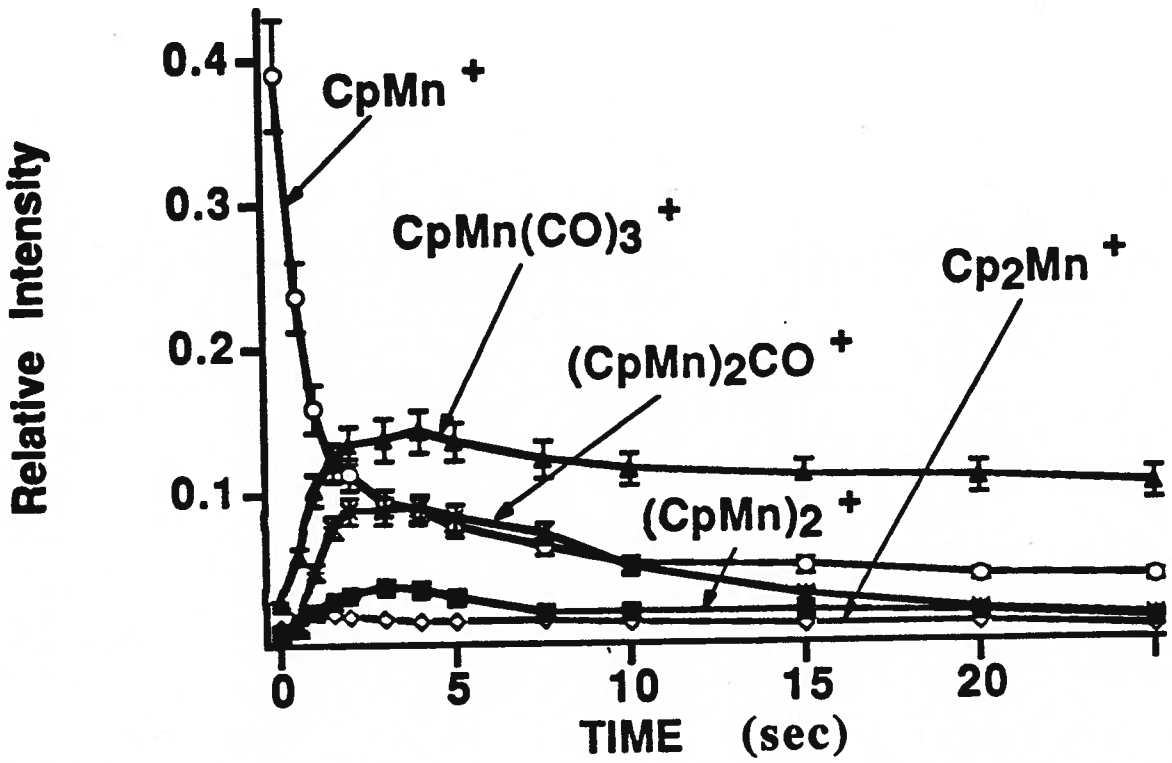

Figure 4.6. Temporal Behaviour of CpMn+ and Cation Products

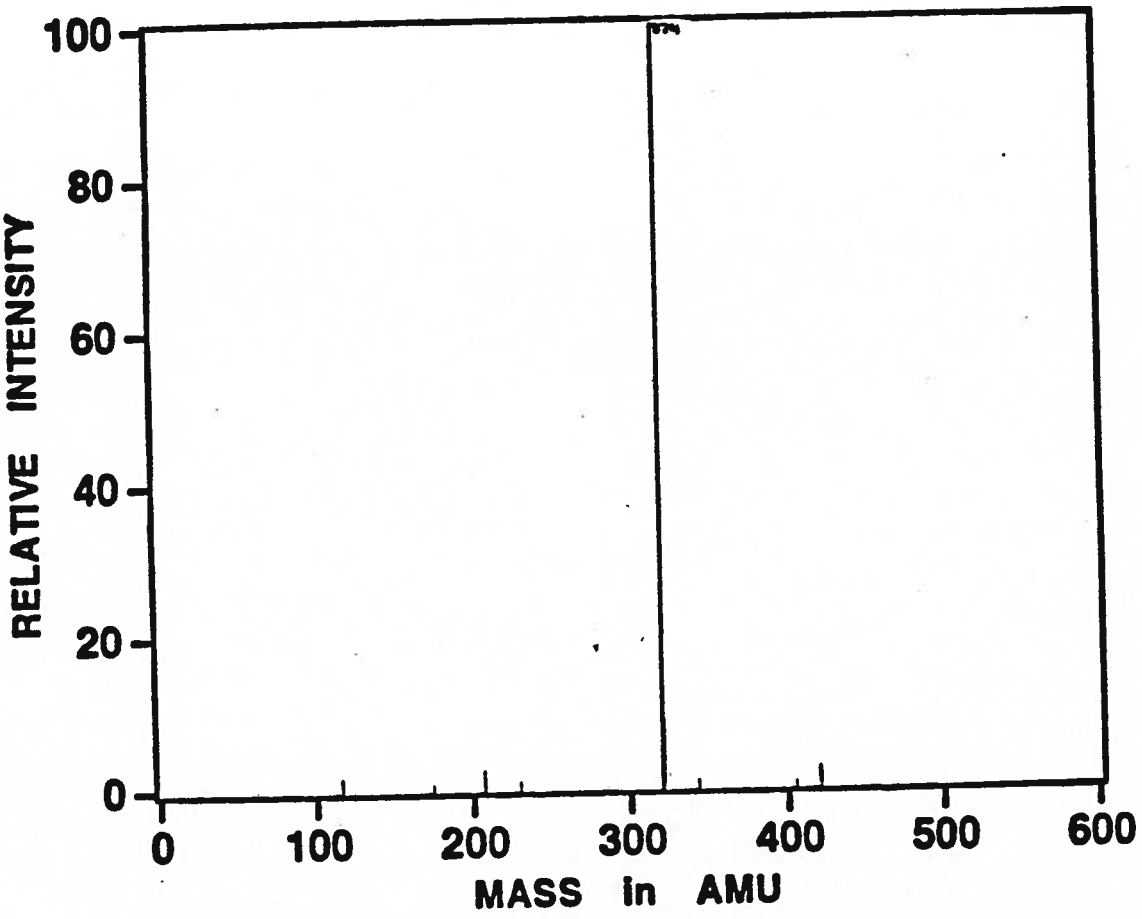

Figure 4.7(a). Multiple Resonance Mass Spectrum of $(CpMn)_2(CO)_3^+$; 0 msec.; p = 6.0×10^{-8} torr

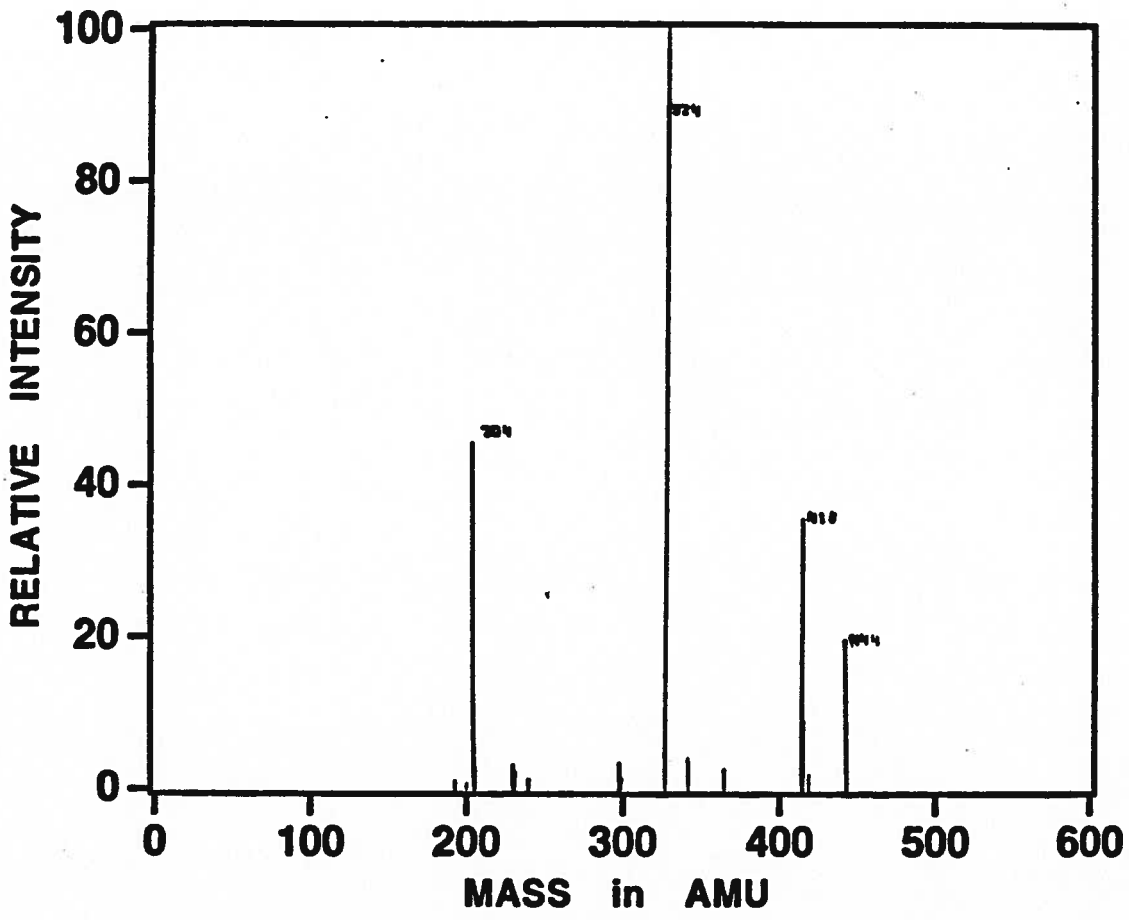

Figure 4.7(b). Multiple Resonance Mass Spectrum of $(CpMn)_2(CO)_3^+$ and Cation Products; 5000 msec; $p = 6.0 \times 10^{-8}$ torr

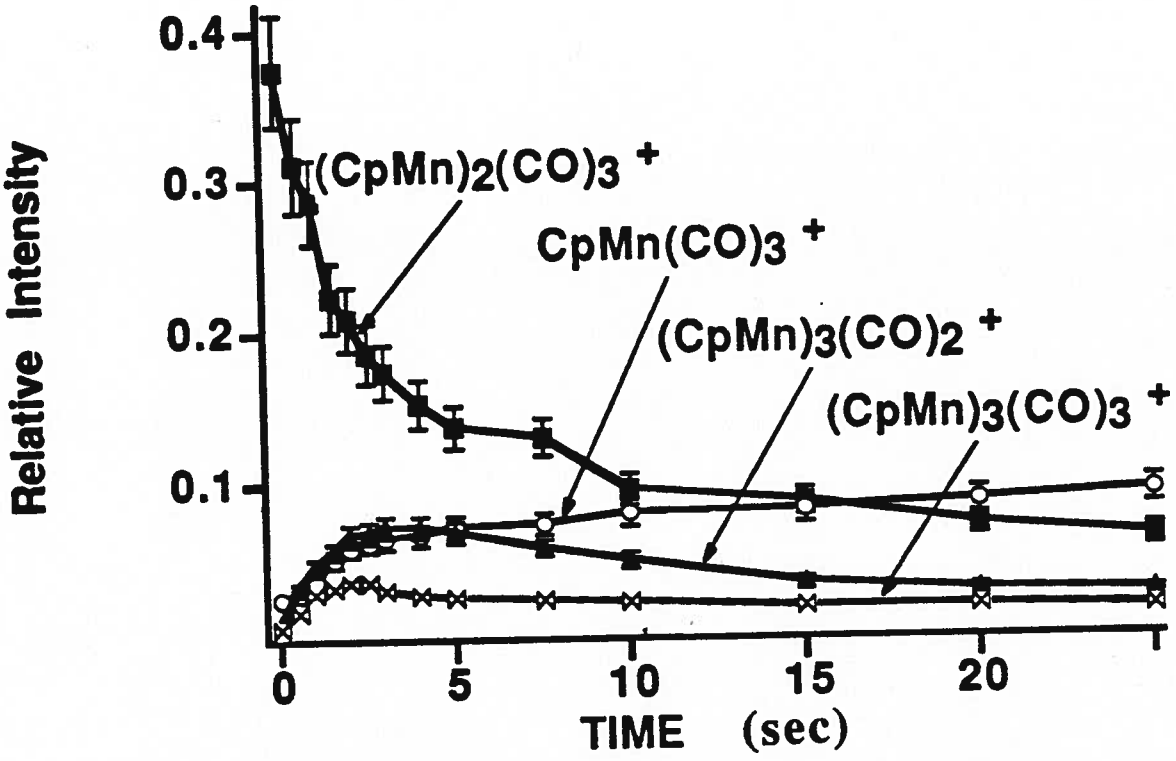

Figure 4.8. Temporal Behaviour of $(CpMn)_2(CO)_3^+$ and Cation Products

TABLE 4.2

Disappearance Rates for Manganese Cations Reacting with Neutral $CpMn(CO)_3$ Molecules

Ion	Rate Constant (k') (sec^{-1}) *	Rate Constant (k) ($x10^9$ molec.$^{-1}cm^3sec^{-1}$) #
Mn^+	0.532	2.02
$CpMn^+$	0.393	1.49
$CpMnCO^+$	0.211	0.80
$CpMn(CO)_2^+$	0.183	0.70
$(CpMn)_2^+$	0.094	0.36
$(CpMn)_2CO^+$	0.080	0.30
$(CpMn)_2(CO)_2^+$	0.060	0.23
$(CpMn)_2(CO)_3^+$	0.044	0.17
$(CpMn)_3CO^+$	<0.01	<0.04
$(CpMn)_3(CO)_2^+$	0.017	0.07
$(CpMn)_3(CO)_3^+$	0.01	0.04

* Calculated from linear first-order rate plots; all data ± 10%

Calculated from experimental parameters as follows: pressure = $6.0x10^{-8}$ torr; temperature = 350°K; α = 19.53; all data ± 30%

Interacting pathways are summarized in the following section. The predominant reaction pathway is condensation with the parent neutral molecule; however, electron transfer from the parent neutral molecule, which was prominent in the vanadium system also, is exhibited by several of the smaller daughter cations in this system.

Reactive pathways determined by temporal monitoring of individual ions are summarized in the following section.

PRINCIPAL REACTIVE PATHWAYS IN THE $CpMn(CO)_3$ SYSTEM:

Primary (EI) fragmentation of the neutral parent $CpMn(CO)_3$ molecule occurs as follows:

$$CpMn(CO)_3 + e^- \rightarrow CpMn(CO)_{0,1,2,3}^+, Mn^+ (+ \text{minor } C_3H_3Mn^+)$$

Ion-Molecule Reactions ($Ion^+ + CpMn(CO)_3 \rightarrow$ products)

Class 1. Charge transfer from neutral parent molecule to reacting cation:

$$(CpMn)(CO)_{0,1,2}^+ + CpMn(CO)_3 \rightarrow CpMn(CO)_3^+ + \ldots$$

$$(CpMn)_2(CO)_{0,1,2,3}^+ + \text{"} \rightarrow \text{"} + \ldots$$

$$(CpMn)_3(CO)_{(1*),2,3}^+ + \text{"} \rightarrow \text{"} + \ldots$$

$$Mn^+ + \text{"} \rightarrow \text{"} + \ldots$$

Some relative rates of electron transfer are given in Table 4.3. Electron affinities in all these Cp-Mn ionic cluster fragments are expected to exceed the ionization potential of the neutral $CpMn(CO)_3$ molecule, since formal electron count per manganese atom in each ion is lower than that in the neutral molecule. Ions with very large formal electron-deficient manganese cores, such as Mn^+, $CpMn^+$, $CpMnCO^+$, etc., should react rapidly in this mode and in fact $CpMn^+$ (11 electrons per Manganese atom) does react approximately twice as fast as the cation $CpMnCO^+$ (13 electrons per Mn atom), and three times as fast

TABLE 4.3

Relative Electron Transfer Rates for Manganese Cations Reacting with Neutral $CpMn(CO)_3$ Molecules

Ion	Rate Constant (k) ($\times 10^9$ molec.$^{-1}$cm^{3}sec^{-1}) *	Relative Rate #
Mn^+	1.35	100
$CpMn^+$	0.753	56
$CpMnCO^+$	0.361	27
$CpMn(CO)_2^+$	0.224	17
$(CpMn)_2^+$	0.076	5.6
$(CpMn)_2CO^+$	0.061	4.5
$(CpMn)_2(CO)_2^+$	0.034	2.5
$(CpMn)_2(CO)_3^+$	0.072	5.3
$(CpMn)_3CO^+$	<0.04	< 1
$(CpMn)_3(CO)_2^+$	0.065	4.8
$(CpMn)_3(CO)_3^+$	<0.04	<1

* Calculated from total decay rate constant of reacting cation; all data ± 30%

Relative to Mn^+ rate taken as 100; all data ± 10%

as $CpMn(CO)_2^+$ (15 electrons per Mn atom), in producing $CpMn(CO)_3^+$, as is shown in Table 4.3. (Again, it is assumed that these processes simply involve electron transfer from neutral molecule to ion cluster fragment, e.g.;

$$(CpMn)_2(CO)_3^+ + CpMn^*(CO)_3 \rightarrow CpMn^*(CO)_3^+ + \ldots$$

rather than complex fracturing of $(CpMn)_2(CO)_3^+$ followed by loss of one CpMn unit.)

As in the vanadium system, all fragment ionic species, including all polynuclear ionic cluster fragments such as $(CpMn)_2(CO)_3^+$ and $(CpMn)_3(CO)_2^+$ undergo electron transfer from the parent molecule $CpMn(CO)_3$ (Table 4.3). As a consequence, the molecular ion $CpMn(CO)_3^+$ becomes the predominant ionic species after 10-25 seconds.

Class 2. Ion-molecule condensation reactions with simultaneous ejection of up to five CO ligands. Principal reaction paths for each fragment ion are as follows:

Primary fragment ions:

Symmetric cluster formation (Cp=Mn)

$CpMn^+ + CpMn(CO)_3 \rightarrow (CpMn)_2(CO)_{0,1,2}^+ + n\,CO$

$CpMn(CO)_{1,2}^+ + \text{"} \rightarrow (CpMn)_2(CO)_{0,1,2,3}^+ + \text{"}$

Asymmetric cluster formation (Cp< or >Mn)

$Mn^+ + \text{"} \rightarrow CpMn_2(CO)_2^+ + \text{"}$

$CpMn^+ + \text{"} \rightarrow Cp_2Mn^+ + \text{"}$

The molecular parent ion, $CpMn(CO)_3^+$ and the manganocene ion, Cp_2Mn^+, were kinetically unreactive for 25 seconds.

Binuclear ionic cluster fragment condensations:

Symmetric cluster formation (Cp=Mn)

$(CpMn)_2^+ + CpMn(CO)_3 \rightarrow (CpMn)_3(CO)_{(1^*,)2,3}^+ + n\,CO$

$(CpMn)_2(CO)_{1,2,3}^+ + \text{"} \rightarrow (CpMn)_3(CO)_{2,3(,4^*)}^+ + \text{"}$

Asymmetric cluster formation (Cp<Mn)

$$CpMn_2(CO)_2^+ + CpMn(CO)_3 \rightarrow Cp_2Mn_3(CO)_{(4*,)5}^+ + \text{"}$$

Because of low intensities of products, further polymerization forming clusters containing more than three manganese atoms was not measured.

Overall relative clustering rates for the more abundant cations are listed in Table 4.4. In general, rates decrease with cluster size, and numbers of carbonyl ligands present in the reacting cation, like the clustering rates in the vanadium and chromium systems.

TABLE 4.4

Relative Clustering Rates for Manganese Cations Reacting with Neutral $CpMn(CO)_3$ Molecules

Ion	Rate Constant (k) ($x10^9$ molec.$^{-1}$cm^{3}sec^{-1})*	Relative Rate #
Mn^+	0.669	100
$CpMn^+$	0.741	110
$CpMnCO^+$	0.441	66
$CpMn(CO)_2^+$	0.471	70
$(CpMn)_2^+$	0.281	42
$(CpMn)_2CO^+$	0.243	36
$(CpMn)_2(CO)_2^+$	0.190	28
$(CpMn)_2(CO)_3^+$	0.152	25
$(CpMn)_3CO^+$	<0.04	<10
$(CpMn)_3(CO)_2^+$	<0.04	<10
$(CpMn)_3(CO)_3^+$	<0.04	<10

* Calculated from total decay rate constant including all clustering pathways; all data ± 30%

Relative to Mn^+ rate taken as 100; all data ± 10%

2. Negative Ion Chemistry

Using 2.5 eV negative ionisation and pressure of 6.0×10^{-8} torr, $CpMn(CO)_3$ produces the product anions $CpMn^-$, $CpMnCO^-$ and $CpMn(CO)_2^-$. Daughter anions $CpMn^-$ and $CpMnCO^-$ subsequently reacted with the parent neutral to generate the dimeric product ion $Cp_2Mn_2(CO)_2^-$ according to the following scheme:

$$CpMn(CO)_{0,1}^- + M \rightarrow Cp_2Mn_2(CO)_2^- + \ldots$$

$CpMn(CO)_2^-$ was kinetically unreactive.

A typical negative ion mass spectrum of $CpMn(CO)_3$ is shown in Figure 4.9, showing $CpMn(CO)_2^-$ (17 electrons) and $Cp_2Mn_2(CO)_2^-$ (29 electrons). Some $Cp_2Mn_2(CO)_2^-$ forms already during beam time. A temporal plot showing anion behaviour is given in Figure 4.10. Both anion products $CpMn(CO)_2^-$ and $(CpMn)_2(CO)_2^-$ are long-lived and unreactive in the gas phase. The $CpMn(CO)_2$ fragment is known to be weakly coordinated to solvent THF in solution, and is a strong coupling agent[24] , so that the dimeric ion $Cp_2Mn_2(CO)_2^-$ may be isolable in solution.

Not surprisingly, the negative ion-molecule chemistry of $CpMn(CO)_3$ strongly resembles that of $CpV(CO)_4$, in that Cp-metal linkages are retained, chemistry is simple, and only a few anion products were detected.

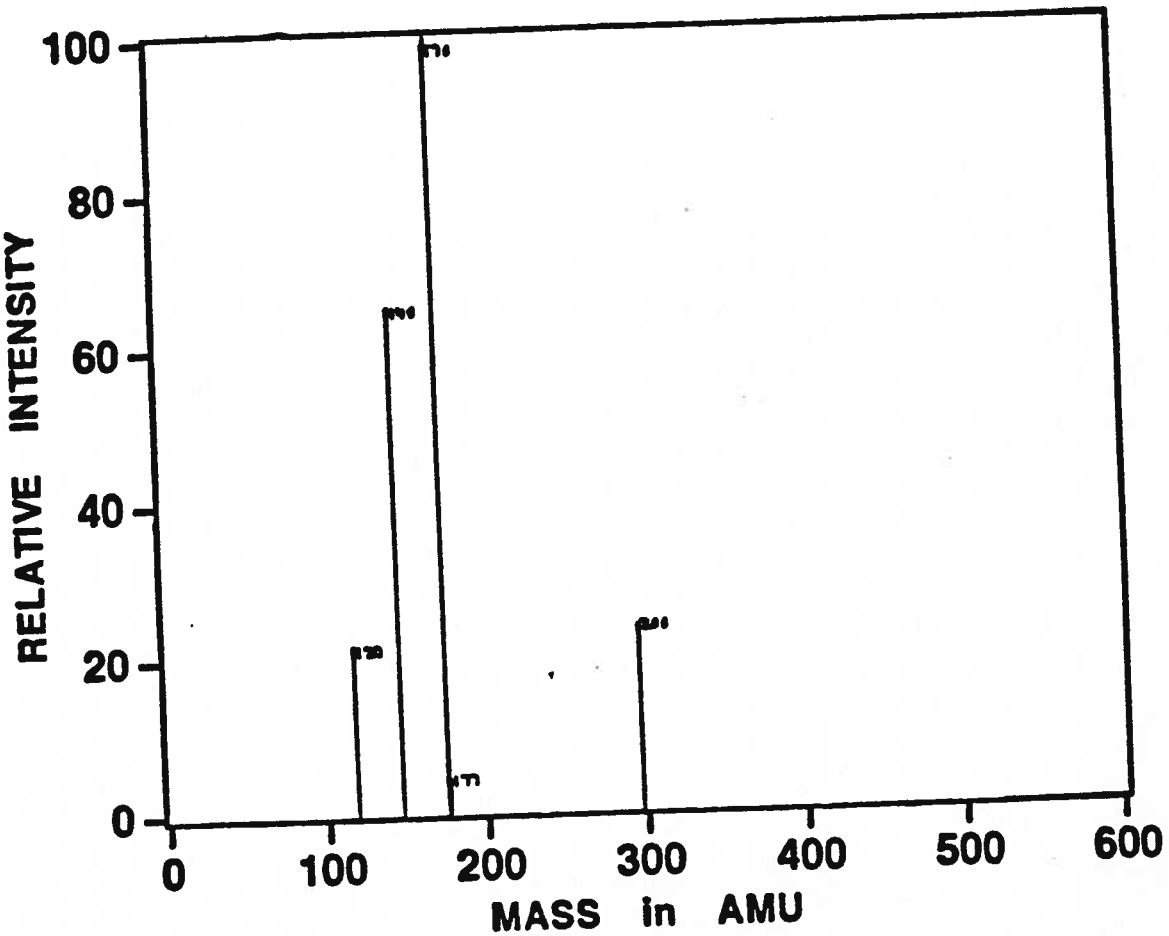

Figure 4.9. FT-ICR Negative Ion Mass Spectrum of $CpMn(CO)_3$; 0 msec.; 2.5 eV; $p = 6.0 \times 10^{-8}$ torr

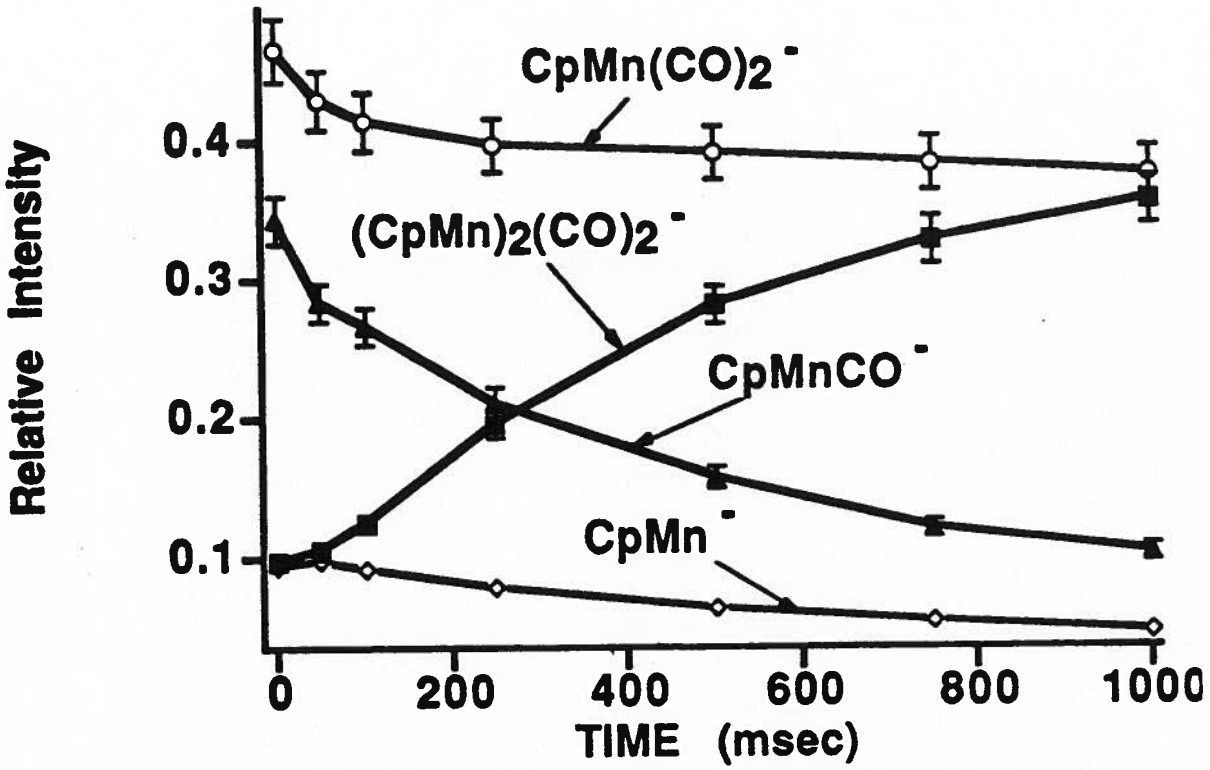

Figure 4.10. Temporal Behaviour of Primary Fragment Anions of $CpMn(CO)_3$

III Conclusions

GENERAL FEATURES OF THE $CpMn(CO)_3$ SYSTEM

1) Except for the molecular ion, $CpMn(CO)_3^+$, all of the cations initially formed by electron impact on $CpMn(CO)_3$ are chemically reactive with parent neutral, whereas only two daughter anions, $CpMn(CO)_{0,1}^-$, are reactive. $CpMn(CO)_2^-$ (17 electrons) and $Cp_2Mn_2(CO)_2^-$ (29 electrons per ion) are unreactive. Including the Mn-Mn bonding electrons, possibly of partially or completely multiple character, electron density on each Mn atom will range from 15.5 (Mn-Mn single bond) to 17.5 (Mn-Mn triple bond).

2) Electron transfer, as seen in the vanadium (Chapter 2) and chromium (Ch. 3) systems, is a prominent pathway for most cations in this manganese system. Relative rates of electron transfer for manganese ions were listed in Table 4.1. Like Cr^+, the bare metal cation Mn^+ reacts either by accepting an electron from the neutral, or condensing with the neutral to produce asymmetric, manganese-rich clusters.

3) As was observed in the vanadium (Chapter 2) and chromium (Chapter 3) systems, here the integrity of aryl-metal bonds within cluster cores is usually retained throughout successive reaction hierarchies; i.e., cluster products containing increasingly large $(CpMn)_2$, $(CpMn)_3$ and $(CpMn)_4$ cores retain 1:1 stoichiometry. However, in one reaction product of $CpMn^+$, the Cp-Mn bond was fractured, producing Cp_2Mn^+ (manganocene cation) in low intensity, a very stable 16-electron ion product. This pathway parallels that of the reaction between Bz^+ and $BzCr(CO)_3$, which generates Bz_2Cr^+ (17 electrons) in the $BzCr(CO)_3$ system; and between Co^+ and $CpCo(CO)_2$ in the cobalt system, which yields Cp_2Co^+ (18 electrons).

4) Clustering dwindles after the formation of $(CpMn)_3^+$ cores at current pressures (ranging from 10^{-6} - 10^{-9} torr); $(CpMn)_4$ cation cluster fragments were observed in very low yields only in the higher pressure ranges, or after long reaction times. Overall clustering rates were listed in Table 4.4. This cluster termination was also observed in both

the vanadium and chromium systems; and is apparently a consequence of ligand crowding around the metal core as well as coordination saturation of the metal.

5) The cations $CpMn^+$, $CpMn(CO)_3^+$, $(CpMn)_2(CO)_3^+$, and $(CpMn)_3(CO)_2^+$ appear relatively unreactive compared to other ions in the same $(CpMn)_n$ series. The prominent daughter cation $CpMn^+$, with 11 electrons and a strong Cp-manganese linkage[23], may possess enhanced electronic stability, as CpV^+ may do. Similarly, the abundant molecular cation $CpMn(CO)_3^+$, like $CpV(CO)_4^+$ in the vanadium system (Ch. 2), dominates the entire reaction regime because of its relative electronic stability (17 electrons) and because it is the sole product of all electron transfer reactions. Some of the other unreactive cations may possess altered hapticities or increased metal-metal bonding order.

6) Disappearance rates for reactive cations in this manganese system are directly related to formal electron deficiency. Figure 4.11 illustrates rate decay data for primary $(CpMn)_1$ cations (upper curve) and secondary-tertiary, $(CpMn)_{2,3}$ cations (lower curve) compared with formal electron deficiencies for several of the more abundant cations of this system. The upper curve is drawn for ions containing one manganese atom; the lower curve assumes multiple (double or triple) metal-metal bonding in bi- and trinuclear cation clusters. In both upper and lower curves, rate constants vary in a fairly direct manner with electron deficiency of the central metal. These electron-deficient ions are expected to be relatively more reactive with respect to one- or two-electron donor agents. The data point for initial decay of $CpMn(CO)_3^+$ (which species later becomes unreactive) is included for comparison.

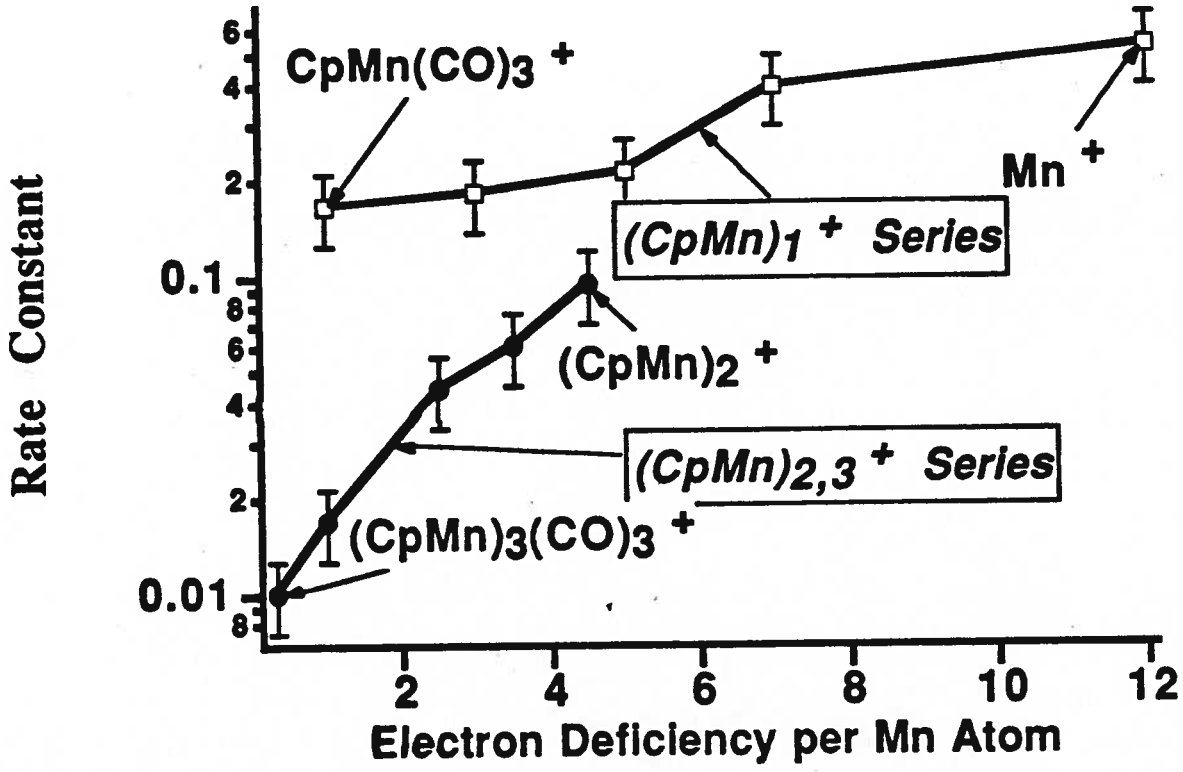

Figure 4.11. Relationship Between Reactivity and Electron Deficiency for Cations in the $CpMn(CO)_3$ System

7) The participation of excited states of some of the smaller cation fragments of the $CpMn(CO)_3$ system, as seen in both vanadium and chromium systems, must be considered, as they have been in earlier studies [4,9,25,26]. Non-linear pseudo-first order decay rate behaviour of ions Mn^+, $CpMn^+$ and $CpMn(CO)_3^+$ is illustrated in semi-log kinetic plots in Figure 4.12, these cations perhaps exhibiting such behaviour. The energy difference between ground state and first excited state Mn^+ is 1.17 eV[4]; therefore during the ionisation procedure, large numbers of excited ions may be formed. As shown in Figure 4.12, the initial downward curvature in the semilog decay rate plot for $CpMn(CO)_3^+$ suggests initial, excited-state reactivity which is collisionally quenched after a few milliseconds, leaving unreactive, stable $CpMn(CO)_3^+$ only. Using extrapolated values of initial concentrations of ground and excited state ions from the semi-log plots, and assuming that excited state ions are more reactive than the corresponding ground state, the proportions of excited state ions were estimated to be as follows: Mn^+, 77%; $CpMn^+$, 83%; $CpMn(CO)_3^+$, 48%. The other fragment cations in this system showed linear semi-log behaviour, and so were assumed to be thermalised.

8) The $CpMn(CO)_3$ molecule appears to be less reactive than the vanadium or chromium analogues with respect to small molecular adduct reagents H_2, N_2 and O_2 although quantitative data have not yet been obtained. Some evidence of addition of atomic O or H (appearance of $CpMn(CO)_3O^+$ (amu 220) and $CpMn(CO)_3H^+$ (amu 205)) were observed in the product spectra. A sample mass spectrum showing several mono- and di-hydrogenated ions, for example the hydrido-molecular ion, $CpMn(CO)_3H^+$ (amu 205) is illustrated in Figure 4.13. As shown by Lichtenberger[14], the ionisation potentials of $CpMn(CO)_2N_2$ and $CpMn(CO)_2NH_3$ are similar to that of $CpMn(CO)_3$, so that substitution of N_2 or NH_3 for one CO ligand in $CpMn(CO)_3$ should occur at high reactant pressures.

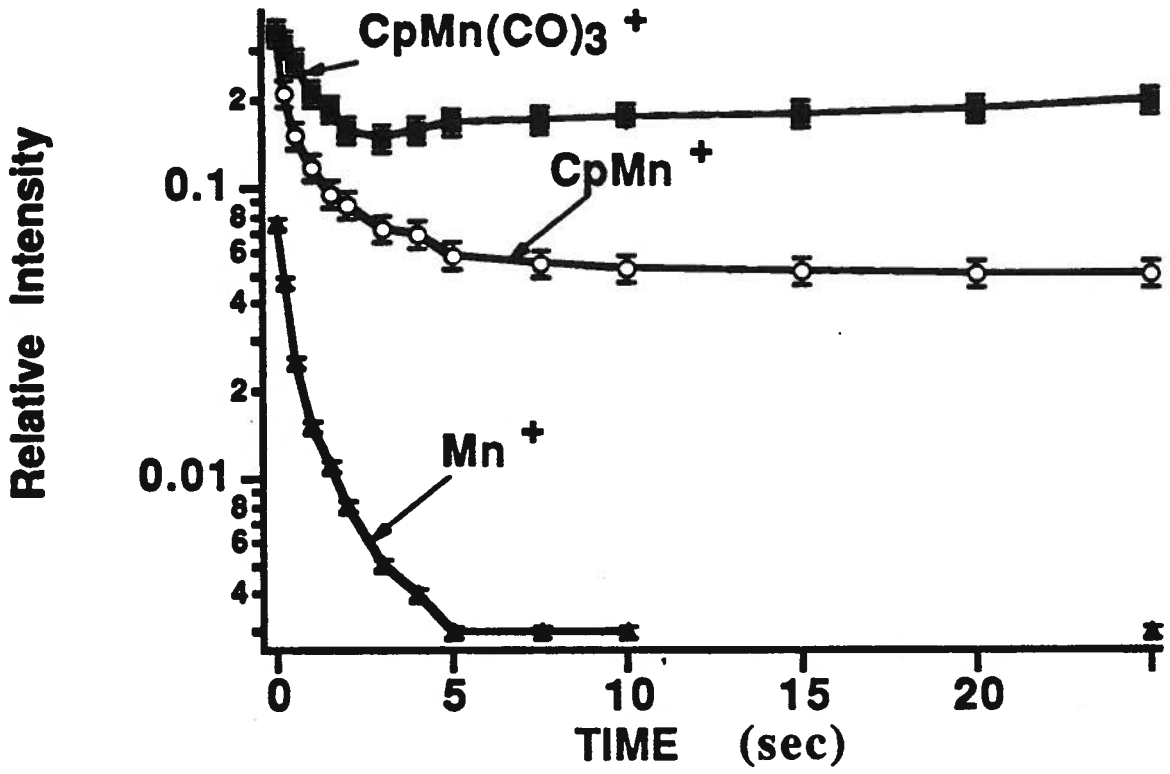

Figure 4.12. Deviations from Pseudo-First Order Decay Behaviour in the $CpMn(CO)_3$ System

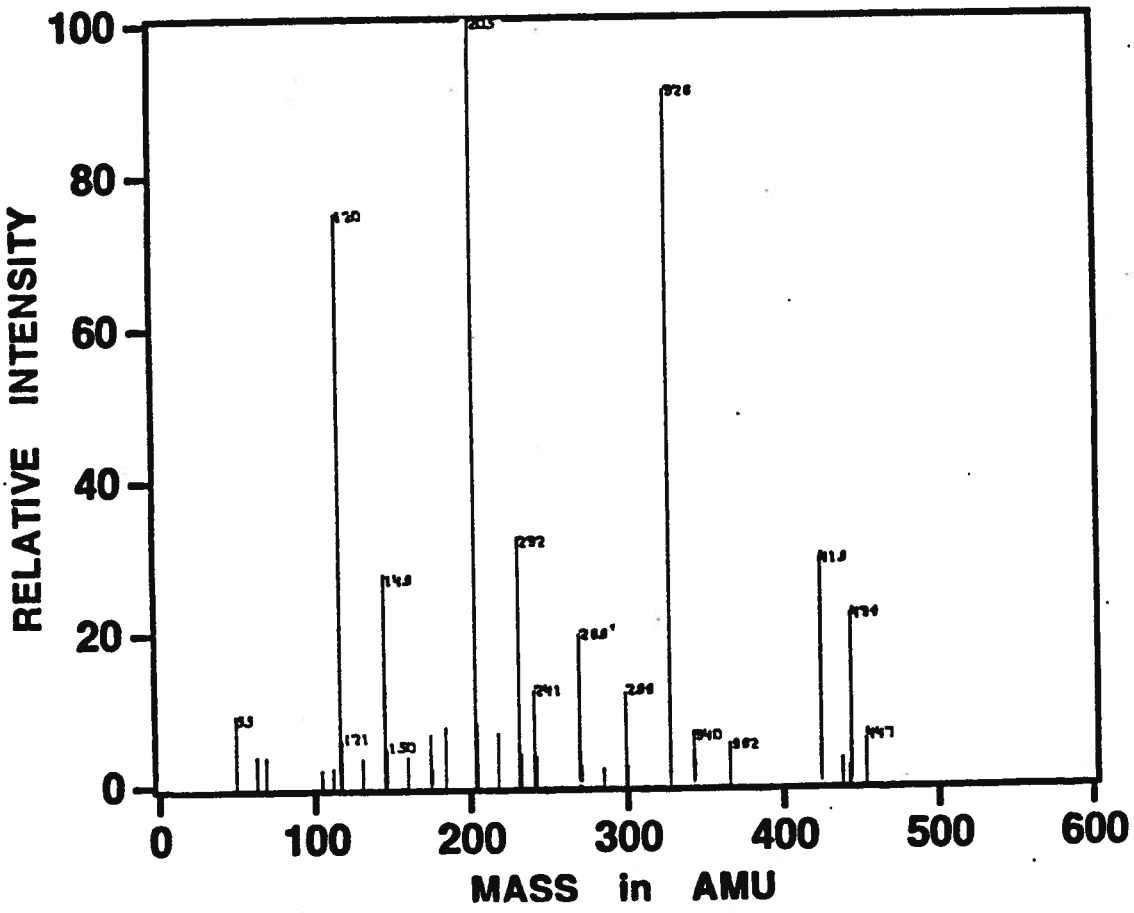

Figure 4.13. FT-ICR Positive Ion Mass Spectrum of $CpMn(CO)_3$; 0 msec.; 25 eV; $p = 6.0 \times 10^{-8}$ torr; $p(H_2) = 6.0 \times 10^{-7}$ torr

9) A clastogram for appearance of positive fragment ions in this $CpMn(CO)_3$ system with ionising energies is shown in Figure 4.14. In general, ion distributions are in agreement with appearance energies of the ion fragments as determined by Müller[17,18].

10) Like the vanadium and chromium cluster ions observed (Chapters 2,3), the geometries of the binuclear and trinuclear ionic cluster manganese fragments are not yet well understood, although the results here strongly suggest that in at least some of the cluster products, multiple-bonded, metal-metal cores exist, surrounded on their perimeters by carbonyls, each metal bonded to one Cp ligand. Increased central metal stabilisation by oxygen, hydrogen or other atomic ligands may be experimentally feasible; and should be examined in future work.

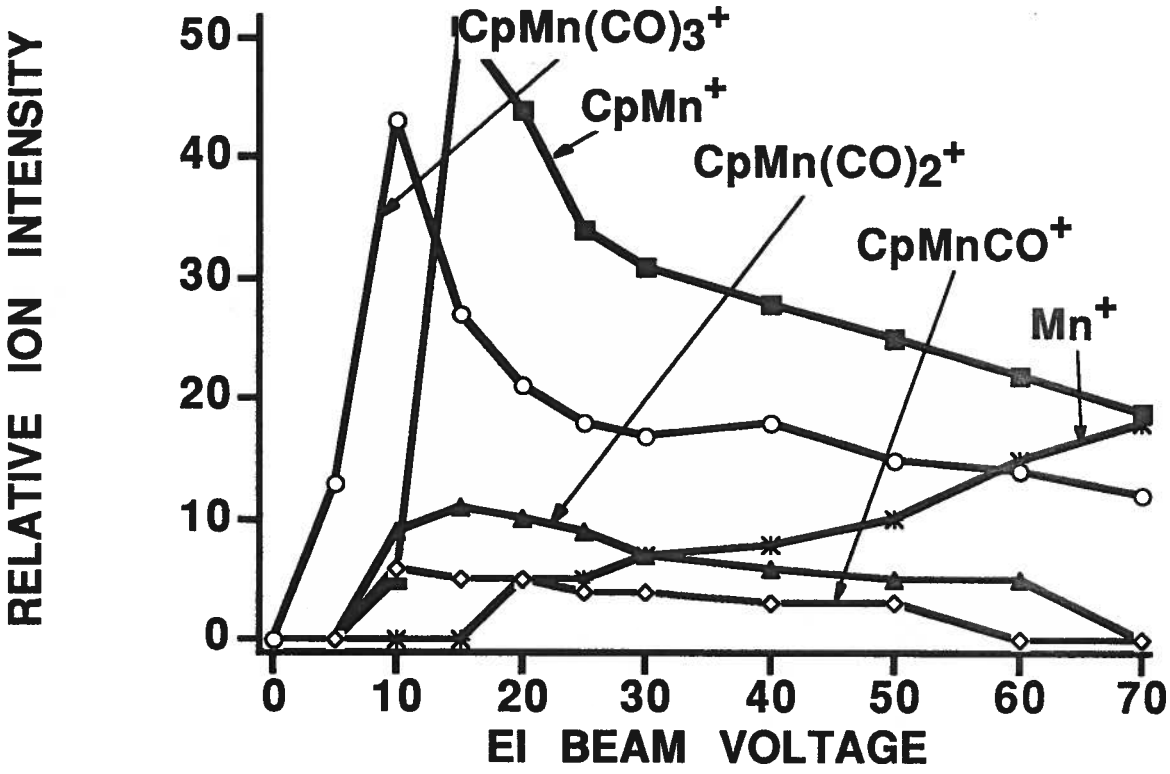

Figure 4.14. Clastogram for Cations of $CpMn(CO)_3$

IV References

(1) Allison, J. *Prog. Inorg. Chem.* **1986**, *34*, 627.

(2) Armentrout, P. B.; Halle, L. F.; Beauchamp, J. L. *J. Am. Chem. Soc.* **1981**, *103*, 6501.

(3) Armentrout, P. B.; Loh, S. K.; Ervin, K. M. *J. Am. Chem. Soc.* **1984**, *106*, 1161.

(4) Armentrout, P. B. in *Gas Phase Inorganic Chemistry*; Russell, D. H.; Plenum Press, New York, **1989**; pp 1 - 42.

(5) Bjarnason, A. *Organomet.* **1991**, *10*, 1244.

(6) Bjarnason, A. *Anal. Chem.* **1991**, *61*, 1889.

(7) Burdett, J. K.; Canadell, E. *Organometallics* **1985**, *4*, 805.

(8) Connor, J. A. *Top. Curr. Chem.* **1977**, *71*, 71.

(9) Elkind, J. L.; Armentrout, P. B. *J. Chem. Phys.* **1986**, *84*, 4862.

(10) Jacobson, D. B.; Freiser, B. S. *J. Am. Chem. Soc.* **1985**, *107*, 5870.

(11) Jarrold, M. F.; Illies, A. J.; Bowers, M. T. *J. Am. Chem. Soc.* **1985**, *107*, 7339.

(12) Junk, G. A.; Svec, H. J. *J. Chem. Soc. A* **1970**, 2102.

(13) Larsen, B. S.; Freas, R. B. I.; Ridge, D. P. *J. Phys. Chem.* **1984**, *88*, 6014.

(14) Lichtenberger, D. L.; Sellmann, D.; Fenske, R. F. *J. Organomet. Chem.* **1976**, *117*, 253.

(15) Meckstroth, W. K.; Freas, R. B.; Reents, W. D., Jr.; Ridge, D. P. *Inorg. Chem.* **1985**, *24*, 3139.

(16) Meckstroth, W. K.; Ridge, D. P. *J. Am. Chem. Soc.* **1985**, *107*, 2281.

(17) Müller, J.; Heberhold, M. *J. Organomet. Chem.* **1968**, *13*, 399.

(18) Müller, J.; Fenderl, K. *Chem. Ber.* **1970**, *103*, 3141.

(19) Parisod, G.; Comisarow, M. B. *Adv. Mass Spectrom.* **1980**, *8A*, 212.

(20) Pearson, R. G. *Inorg. Chem.* **1984**, *23*, 4675.

(21) Piper, T. S.; Cotton, F. A.; Wilkinson, G. *J. Inorg. Nucl. Chem.* **1955**, *1*, 165 .

(22) Schilling, J. B.; Goddard III, W. A.; Beauchamp, J. L. *J. Am. Chem. Soc.* **1986**, *108*, 582.

(23) Skinner, H. A.; Connor, J. A. *Pure Appl. Chem.* **1985**, *57*, 79.

(24) Stone, F. G. A. *Phil. Trans. R. Soc. Lond.* **1982**, *A308*, 87.

(25) Strobel, F.; Ridge, D. P. *J. Phys. Chem.* **1989**, *93*, 3635.

(26) Strobel, F.; Ridge, D. P. *J. Am. Soc. Mass. Spectrom.* **1990**, *1*, 192.

(27) Svec, H. J.; Junk, G. A. *J. Am. Chem. Soc.* **1967**, *89*, 2836.

(28) Wilkinson, G.; Cotton, F. A.; Birmingham, J. M. *J. Inorg. Nucl. Chem.* **1956**, *2*, 95.

(29) Winters, R. E.; Kiser, R. W. *J. Organometal. Chem.* **1965**, *4*, 190.

(30) Ziegler, T.; Tschinke, V. in *Periodic Trends in the Bond Energies of Transition Metal Complexes*; Marks, T.; American Chemical Society, Washington, D. C., **1990**; pp 279-292.

CHAPTER 5

Ion Molecule Chemistry of

Tricarbonyl (1-4 η^4 - Butadienyl) Iron

{ $C_4H_6Fe(CO)_3$ }

I Introduction

Tricarbonyl (1-4 η^4-butadienyl) iron compound, $C_4H_6Fe(CO)_3$, (hereafter called $BuFe(CO)_3$ for convenience), is a pale orange, soft solid at room temperature, melting at 19° C and boiling at 64° C (13 mm Hg). First synthesised by Rheilen, Grühl, Hessling and Pfrengle in 1930[53], it became the subject of a patent in 1947 taken by Veltman[61]. Later, Hallam and Pauson ascertained its π-bonded structure (1956 - 1958)[24,25].

Crystallographic measurements on tricarbonyl (1-4 η^4-butadienyl) iron, an 18 valence-electron, single-iron compound, were first made by Mills and Robinson in 1963[47]; and its ionization potential measured photoelectronically by Dewar and Worley in 1969-70[14,66], and by Connor in 1974[11]. Davis used electron diffraction methods to determine its gas phase structure in 1970[13]. The solid state structures of tricarbonyl (1-4-η^4-butadienyl) iron complexes were studied by NMR in 1969[44,68] and by ESR in 1981[40,41].

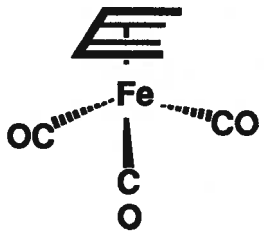

Kinetics of reactions involving bare iron ions in the gas phase have been determined with hydrogen[15]; chlorobenzene[3]; alkanes[7,22,31]; alkenes[32]; and thiols[57].

Bond energies of iron-carbon, iron-iron and other iron linkages have been subjects of study for several years. For example, Freiser looked at the Fe-O bond in 1984. Energies of Fe-Cobalt$^+$ links in mono- and clustered iron carbonyls and reactions of this heteronuclear core cation were measured by Jacobson[35,36] in 1984-5.

Iron carbonyl compounds have been examined since the inception of organometallic chemistry, with such work as that of Mond on the characterisation of $Fe(CO)_5$ in 1891[48]. In the gas phase, iron carbonyl ions have been examined by Foster and Beauchamp in 1971-5[19,20]; and by Russell[23] and Ridge[52] in 1985.

Reactive mechanisms of iron alkyl ions such as $FeCH_3^+$ have been considered by Jacobson and Freiser[33,34], and the Fe-benzyne$^+$ cation by Huang and Freiser[26-30].

Aryl iron compounds have been in the forefront in transition metal organometallic chemistry since Miller, Pauson and Wilkinson discovered and characterised ferrocene in 1951-2[38,46,64]. "Sandwich" and later "triple-decker sandwich" structures have been important in the development of new structural and bonding concepts ever since that time[6,42]. In 1964, Schumaker and Taubenest observed the "triple-decker sandwich" cations $Cp_3Fe_2^+$ and $Cp_3Ni_2^+$ in mass spectra of gas phase ferrocene and nickelocene[58]. ICR was used by Beauchamp[12,21], Dunbar and Faulk[18], and Lin[43] in order to examine the reactive behavior of ferrocene ions. The reaction of $CpFe^+$ with ethane was studied by Chen and Ridge[10]. Aryl iron carbonyl complexes have been studied both structurally and mechanistically[45]. Negative ion gas phase studies of some aryl iron carbonyls revealed that after electron capture by the parent neutral molecule, further reaction pathways

involved aryl restructuring within the iron complex ion, followed by consecutive decarbonylations[4,5,60]. A tetra-iron complex in solution, $Cp_4Fe_4(CO)_4$, was synthesized and characterised by King in 1966[39]. Von Gustorf (1971)[62] and Williams-Smith (1972)[65] synthesized and characterised a closely-related bi-iron complex, dibutadienyl iron carbonyl, $Bu_2Fe(CO)$.

Negative ion fragmentation of C_4H_6 isomeric homologs of $BuFe(CO)_3$ was examined by Blake in 1979[4,5]and Krusic in 1982[41]; its reactions with molecular hydrogen, in 1985[45]; cyclic voltammetry of $BuFe(CO)_3$ in solution was studied by Murr in 1985[49]. In 1987 Wang and Squires[63] examined gas phase positive and negative ion fragmentation patterns of 1,3 butadiene iron tricarbonyl, η^4-$BuFe(CO)_3$, and the reactivity of its negative ions with small molecules such as O_2, NO and CO_2, concluding that the η^4-C_4H_6 ligand would exchange with many incoming substituent groups such as n-$C_3H_5^-$, hydride, and CO ligands. Recently, iron has been shown to participate in some unusual bridging activity between oxygen, carbon and hydrogen atoms within aromatic molecules[4,5].

For these, and for other reasons, η^4-$BuFe(CO)_3$ was chosen for this study. Although cyclobutadiene ought to have been chosen as the aryl ligand corresponding to the other members of this series, it was decided to use the 1,3-butadiene analogue instead. Having less bond strain than does cyclobutadiene, ligated 1,3-butadiene was expected to produce simpler mass spectral fragmentation patterns, and to yield mechanistic data more consistent with those of the other metal systems examined. Ion-molecule kinetic behaviour of both positive and negative fragment ions of η^4-$BuFe(CO)_3$ has been examined in the present study.

II Results and Discussion

1 Positive Ion Chemistry

Using 25 eV electron ionisation on η^4-$BuFe(CO)_3$ at $6.0x10^{-8}$ torr nominal pressure, the following positive daughter ions were produced: Fe^+=21%; $FeCO^+$=3%; $BuFe^+$=27%; $BuFeCO^+$=9%; $BuFe(CO)_2^+$=12%; $BuFe(CO)_3^+$= 8%, these proportions being generally in accord with those observed by Wang and Squires in 1987[63]. (Wang-Squires: Fe^+ = 19%; $BuFe^+$=17%; $BuFeCO^+$=10%; $BuFe(CO)_2^+$=26%; $BuFe(CO)_3^+$=7% at 70 eV EI.) Figure 5.1 is a typical positive mass spectrum, showing the principal daughter cation fragments of $BuFe(CO)_3$, Table 5.1 lists mass data for a sample FT-ICR experiment.

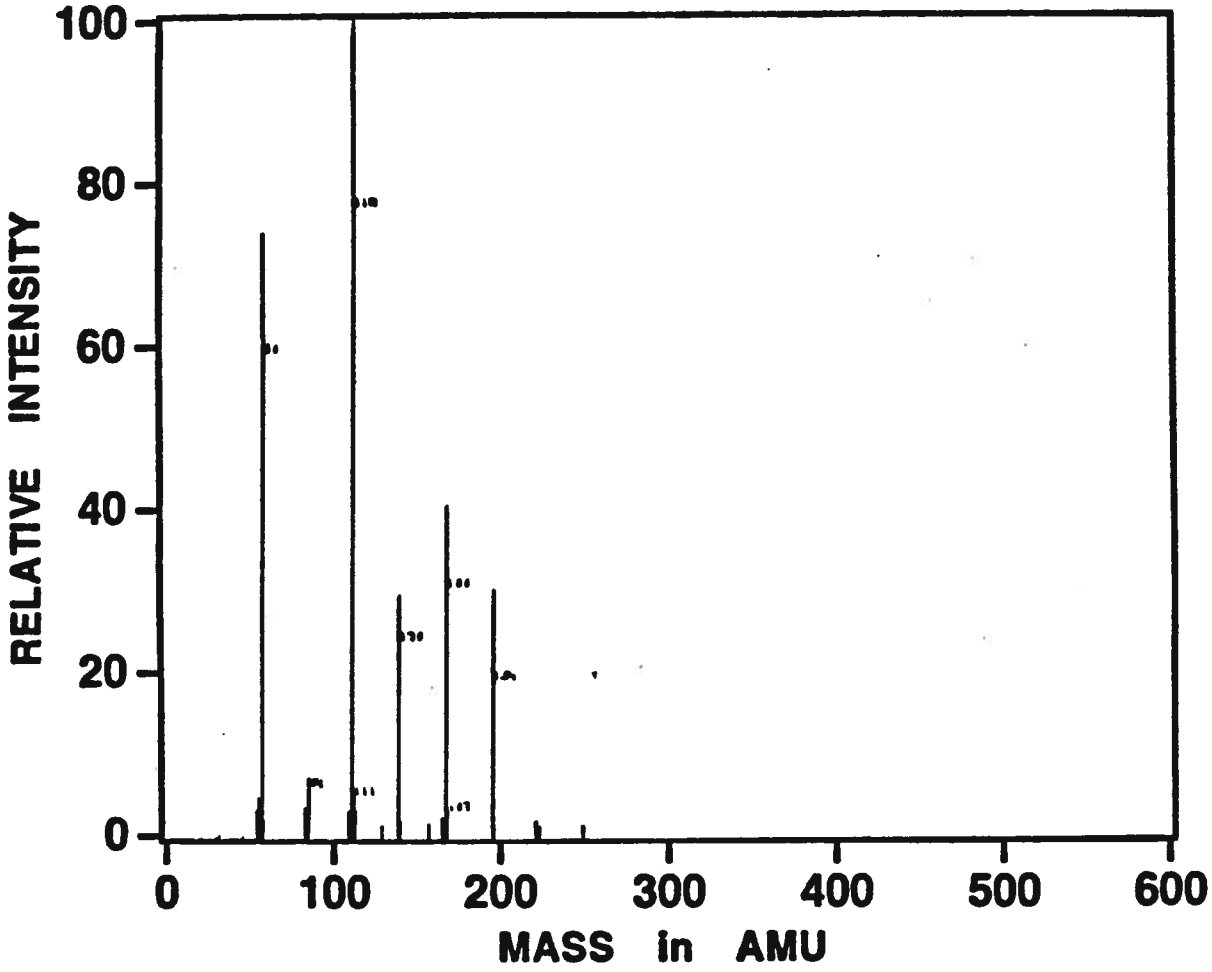

Figure 5.1. FT-ICR Positive Ion Mass Spectrum of $BuFe(CO)_3$; 0 msec.; 25 eV; $p = 6.0 \times 10^{-8}$ torr

TABLE 5.1

Sample Mass Table for $BuFe(CO)_3$ Cations (500 msec)

Formula	Nominal Mass[a]	Measured Mass[a]	Expected Mass[a]	Δ (ppm)	Rel. Int. (%)
^{54}Fe	54	53.9344	53.9391	47	7.4
^{56}Fe	56	55.9332	55.9344	12[b]	73.6
^{57}Fe	57	56.9348	56.9349	1	3.0
$Bu^{54}Fe$	108	107.9828		5.4	
$Bu^{56}Fe$	110	109.9678	109.9814	14	100
$Bu^{57}Fe$	111	110.9746		7.8	
$Bu^{54}FeCO$	136	135.9120		2.2	
$Bu^{56}FeCO$	138	137.9200	137.9763	56	35.5
$Bu^{57}FeCO$	139	138.9310		3.1	
$Bu^{54}Fe(CO)_2$	164	163.9683		4.1	
$Bu^{56}Fe(CO)_2$	166	165.9674	165.9712	4[b]	43.7
$Bu^{57}Fe(CO)_2$	167	166.9874		4.3	
$Bu^{54}Fe(CO)_3$	192	192.0401		3.0	
$Bu^{56}Fe(CO)_3$	194	194.0524	194.0551	3[b]	29.3
$Bu^{57}Fe(CO)_3$	195	195.0428		3.2	

[a] based throughout on ^{12}C only
[b] calibrant mass

In this system, each primary cation is reactive except for the parent molecular ion, $BuFe(CO)_3^+$. At reaction times of up to 25 seconds, all the following polynuclear cluster cation fragments, identified by their iron isotope distribution, are generated:

Symmetric clusters (where Bu=Fe)

$(BuFe)_2(CO)_{0,1,2,3}^+$

$(BuFe)_3(CO)_{1,2,3,4}^+$

Asymmetric (iron-rich) clusters (where Bu<Fe)

$BuFe_2(CO)_{2,3}^+$

$Bu_2Fe_3(CO)_{2,3}^+$

Typical temporal decay of reactive primary fragment ions (i.e., Fe^+, $FeCO^+$, $BuFe^+$, $BuFeCO^+$, and $BuFe(CO)_2^+$) and temporal persistence of $BuFe(CO)_3^+$ is illustrated in Figure 5.2. Figure 5.3 shows temporal growth and decay behaviour of some of the principal binuclear cationic clusters (i.e., $BuFe_2(CO)_{2,3}^+$, $(BuFe)_2(CO)_{0,1,2,3}^+$); and Figure 5.4 shows temporal growth and decay behaviour of the most abundant trinuclear cationic clusters (i.e., $Bu_2Fe_3(CO)_{2,3}^+$, $(BuFe)_3(CO)_{2,3}^+$). An example of a set of triple resonance spectra for the $BuFe^+$ ion, taken initially and later at 1000 msec is given in Figure 5.5(a,b), illustrating the products of this single ion.

Early temporal behaviour of $BuFe^+$ and its cation products is shown in Figure 5.6. Comparable temporal behaviour plots for another primary ion, Fe^+, and for a secondary ion, $(BuFe)_2CO^+$ are shown in Figures 5.7 and 5.8 respectively. These results show that a wide variety of binuclear and trinuclear clusters are generated. Reaction pathways revealed by multiple resonance for principal daughter cations of the $BuFe(CO)_3$ system are summarized in the following section.

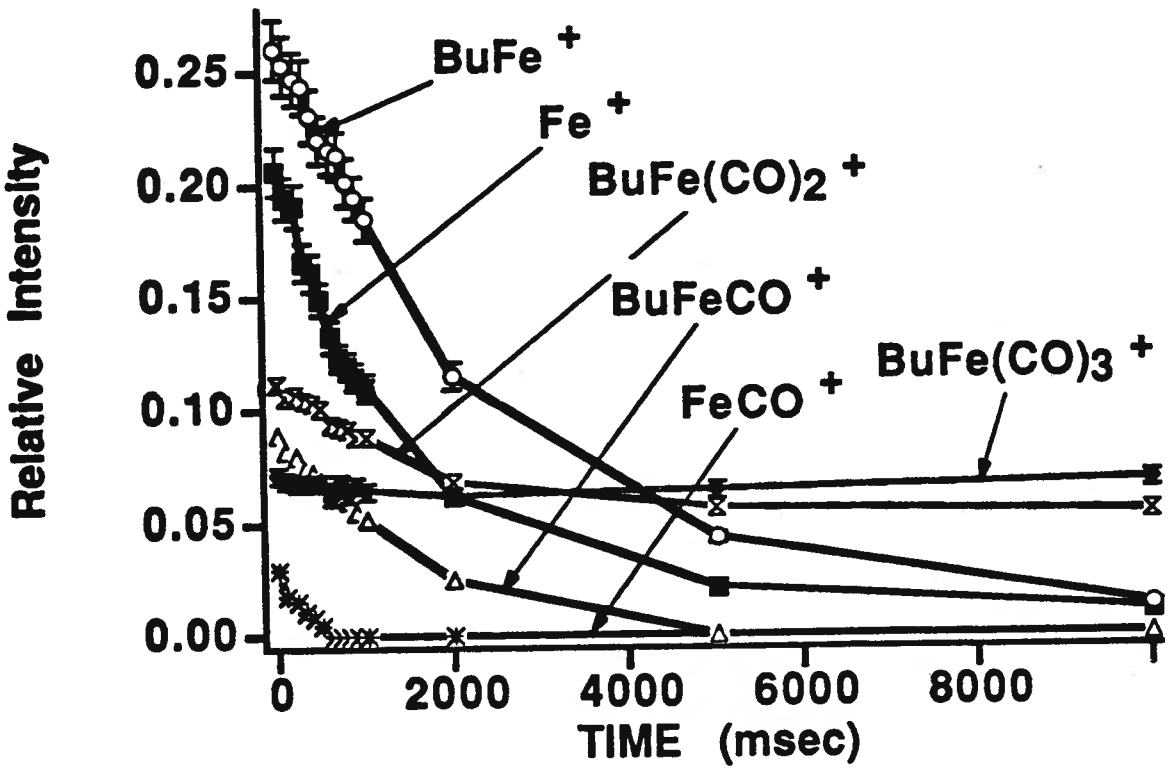

Figure 5.2. Temporal Behaviour of Primary Fragment Cations of $BuFe(CO)_3$

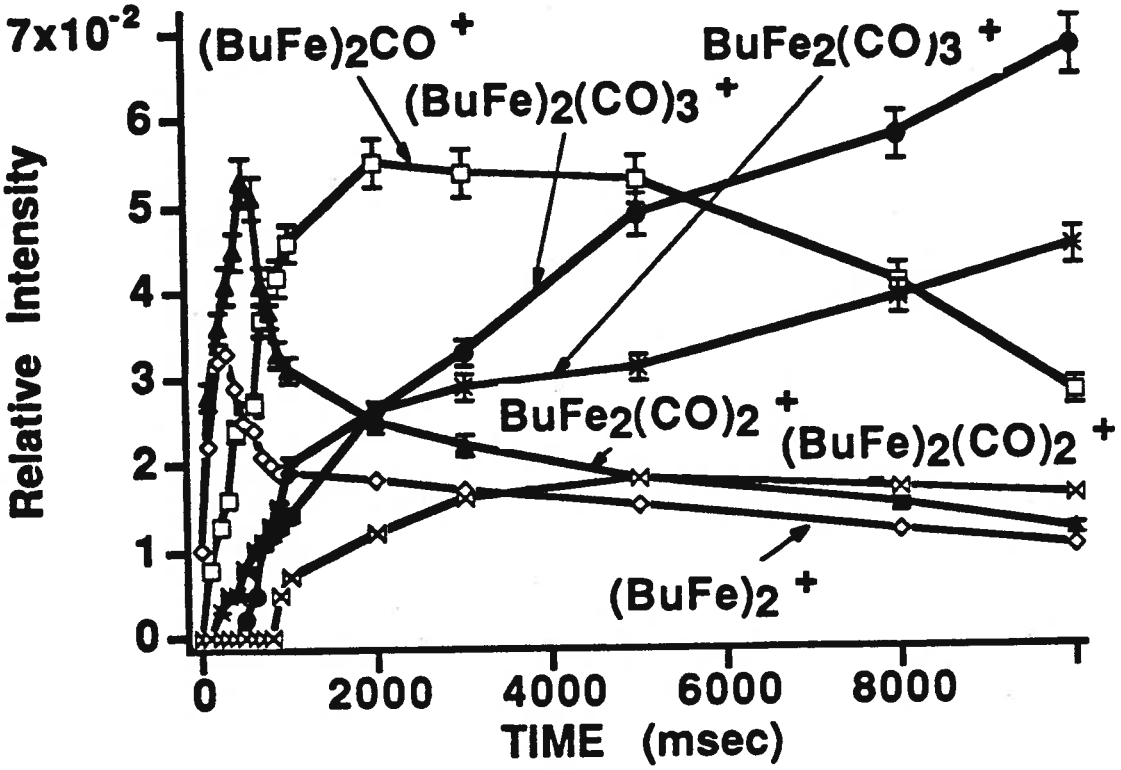

Figure 5.3. Temporal Behaviour of Binuclear Cluster Cations of $BuFe(CO)_3$

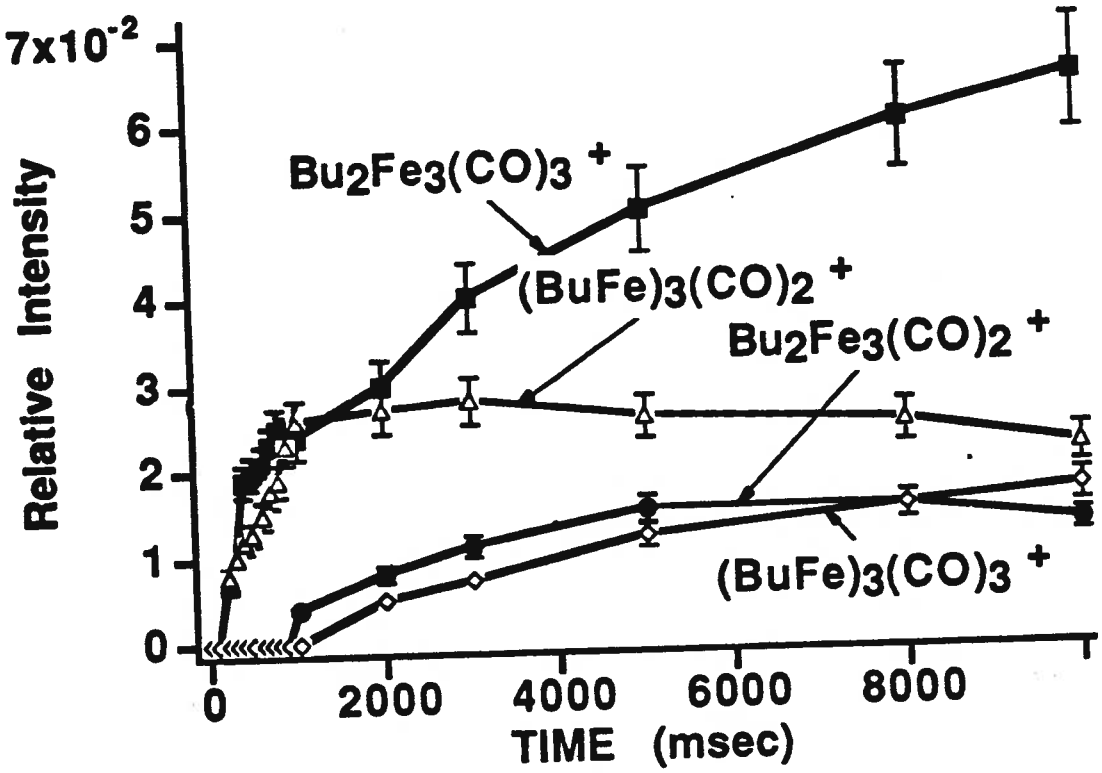

Figure 5.4. Temporal Behaviour of Trinuclear Cluster Cations of $BuFe(CO)_3$

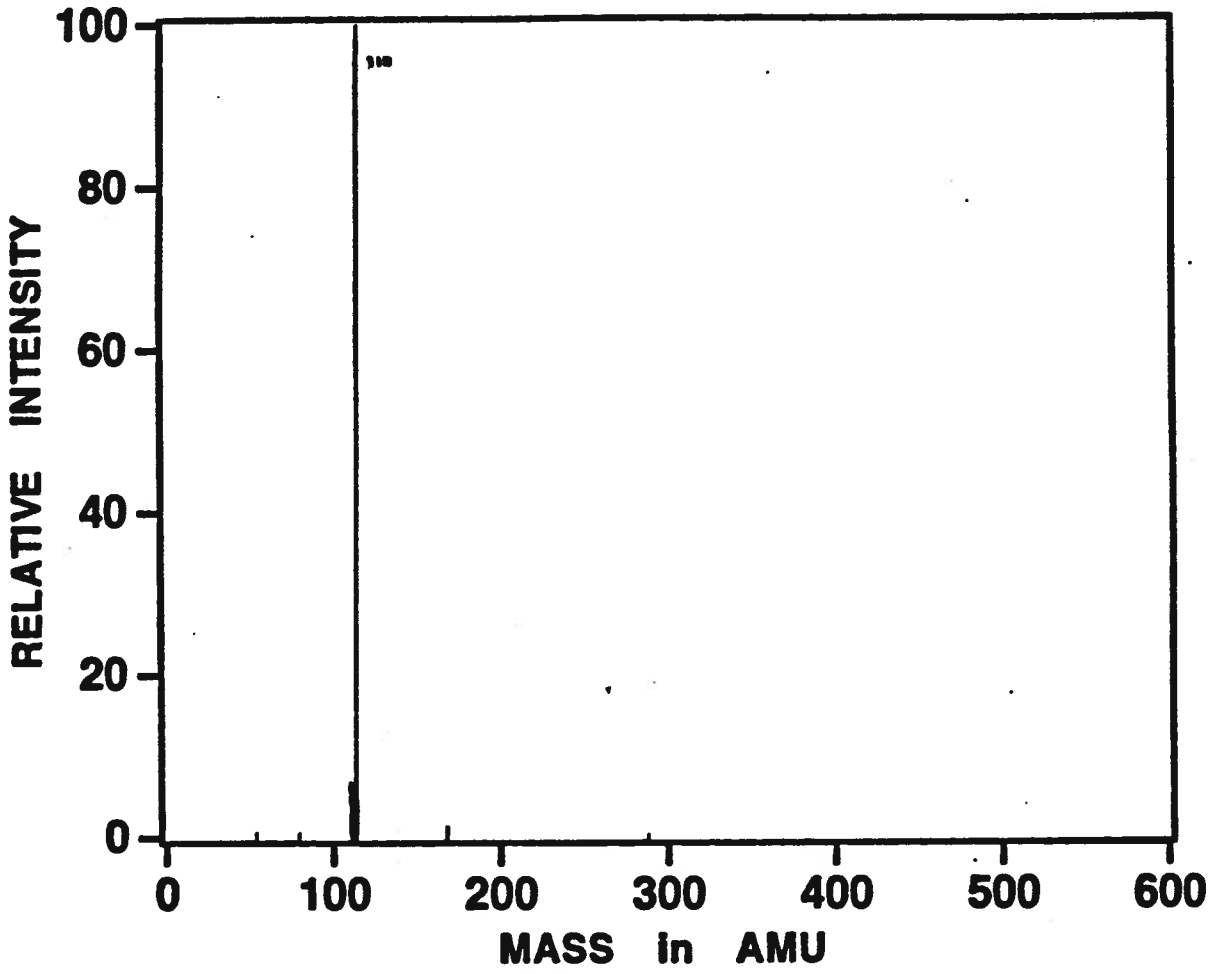

Figure 5.5(a). Multiple Resonance Mass Spectrum of $BuFe^+$; 0 msec.; p = 6.0×10^{-8} torr

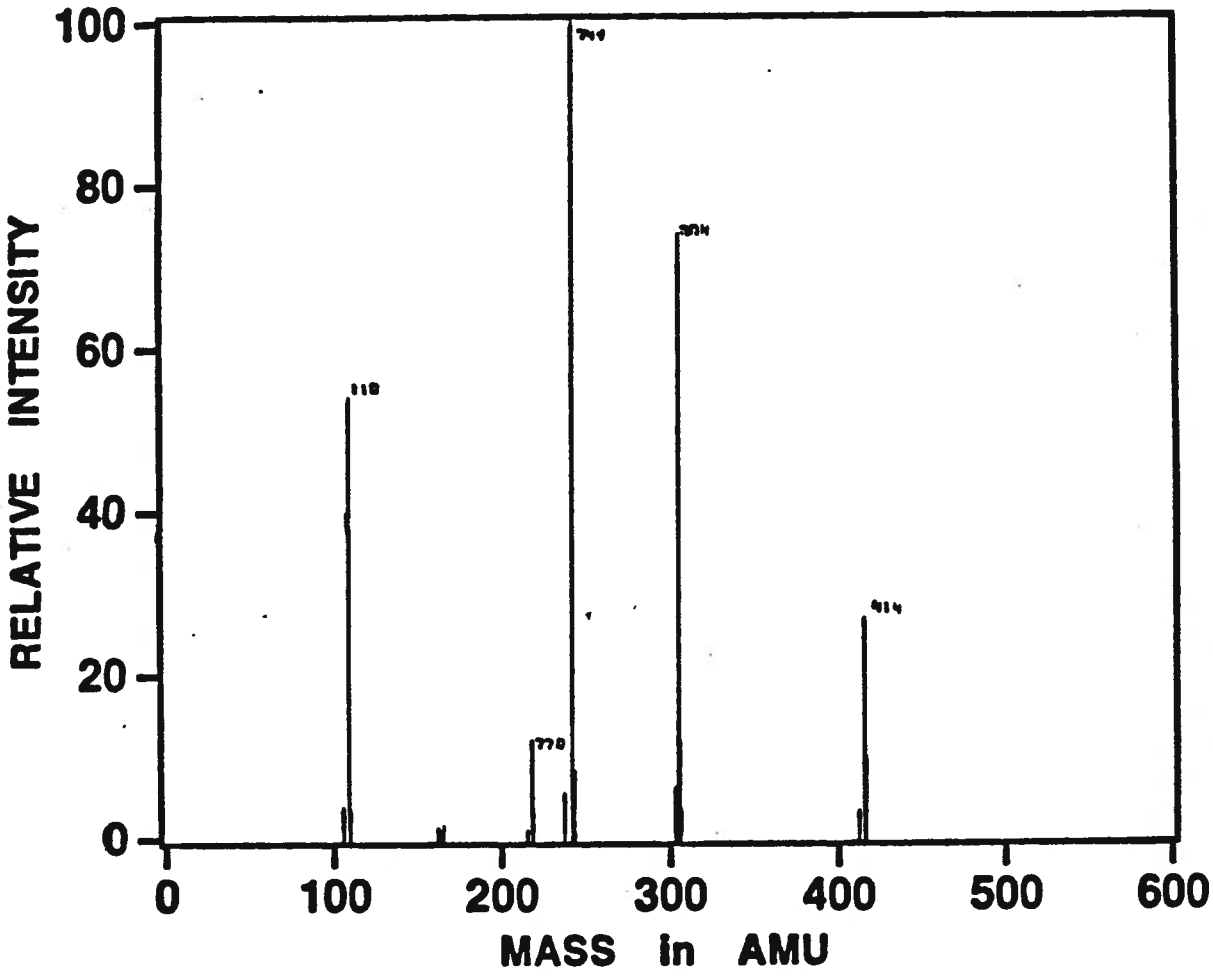

Figure 5.5(b). Multiple Resonance Mass Spectrum of $BuFe^+$ and Cation Products; 1000 msec.; p = 6.0×10^{-8} torr

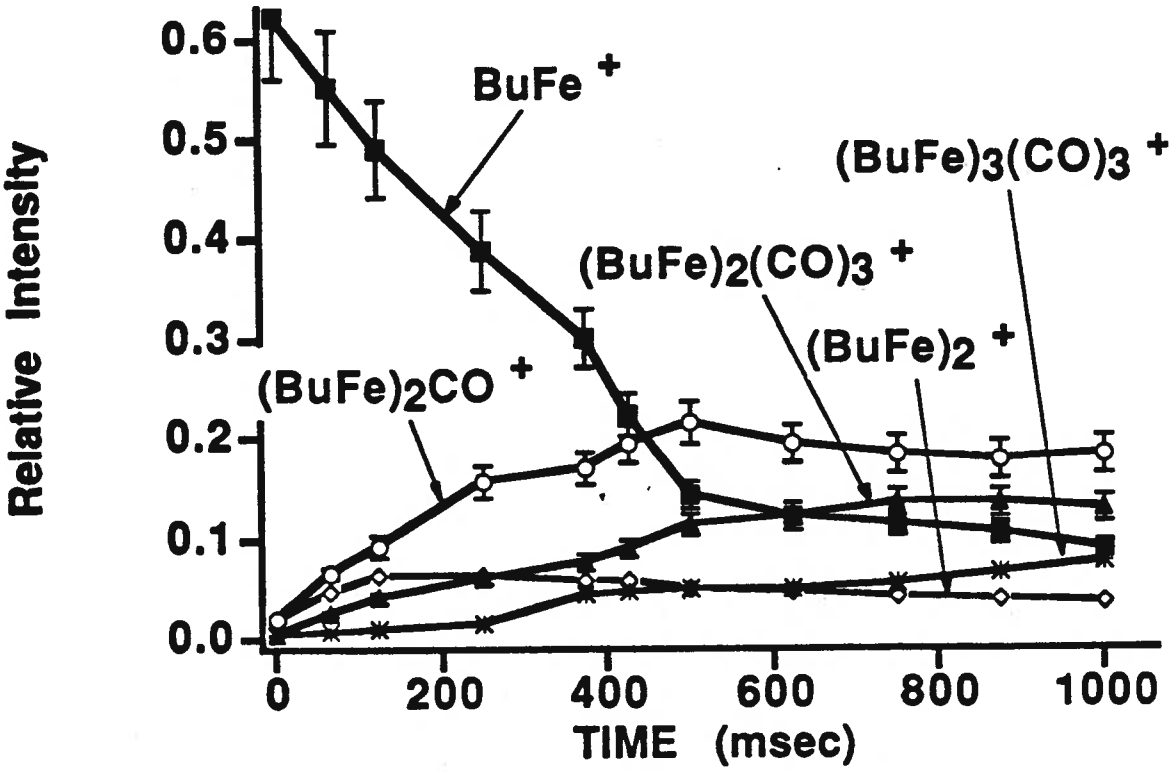

Figure 5.6. Temporal Behaviour of BuFe+ and Cation Products

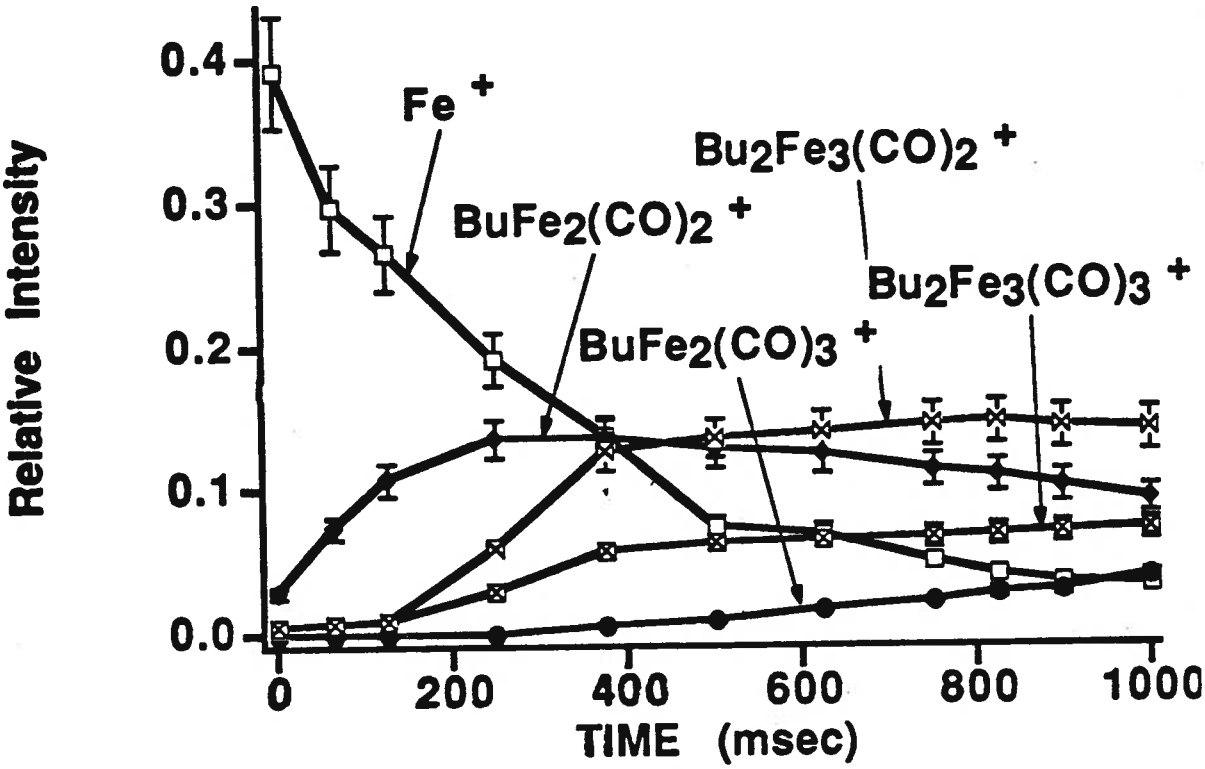

Figure 5.7. Temporal Behaviour of Fe^+ and Cation Products

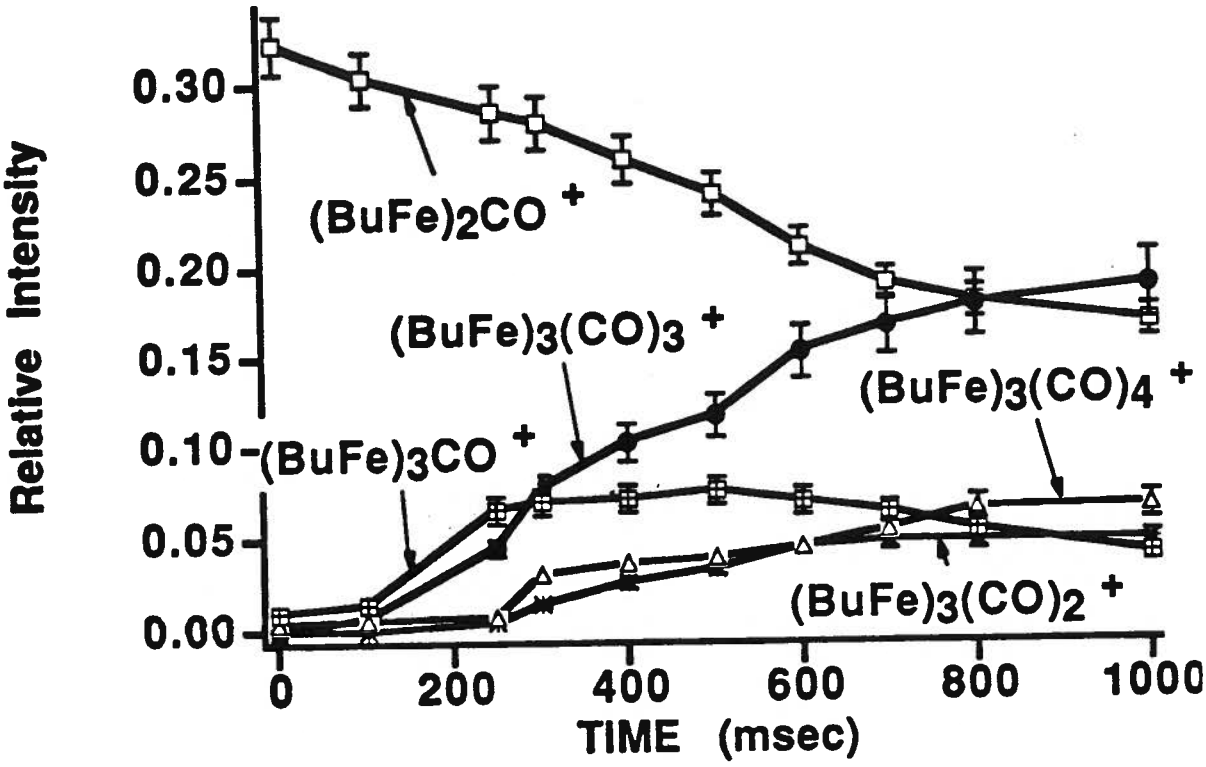

Figure 5.8. Temporal Behaviour of $(BuFe)_2CO^+$ and Cation Products

Decay rate constants obtained from first order rate plots for each iron cation which reacts with the parent neutral molecule $BuFe(CO)_3$ are listed in Table 5.2. The predominant reactive process undergone by most daughter cations is that of clustering with the parent neutral. Charge exchange with the parent neutral molecule, prominent in the vanadium, chromium and manganese systems, is evidently not exhibited by the daughter cations in this system. Because the iron cation reactive pathways involve clustering only, rate constants listed in Table 5.2 are identical to overall clustering rates. As was the case for the cations of $CpV(CO)_4$, $BzCr(CO)_3$ and $CpMn(CO)_3$, clustering rates of iron cations depend inversely upon carbonyl number and cluster size (Table 5.2).

TABLE 5.2

Disappearance Rates for Iron Cations Reacting with Neutral $BuFe(CO)_3$ Molecules

Ion	Rate Constant (k') (sec^{-1}) *	Rate Constant (k) ($x10^9$ molec.$^{-1}cm^3sec^{-1}$) #
Fe^+	0.417	1.49
$BuFe^+$	0.347	1.24
$BuFeCO^+$	0.326	1.16
$BuFe(CO)_2^+$	0.185	0.66
$BuFe(CO)_3^+$	0.010	0.04
$FeCO^+$	0.271	0.97
$(BuFe)_2^+$	0.140	0.50
$(BuFe)_2CO^+$	<0.01	<0.04

* Calculated from linear first-order rate plots; all data ± 10%

\# Calculated from experimental parameters:
pressure = $6.0x10^{-8}$ torr; temperature = 350°K; α = 18.3;
all data ± 30%

PRINCIPAL REACTIVE PATHWAYS IN THE $BuFe(CO)_3$ SYSTEM

Primary (EI) fragmentation of the neutral parent $BuFe(CO)_3$ molecule occurs as follows:

$$BuFe(CO)_3 + e^- \rightarrow BuFe(CO)_{0,1,2,3}^+ , \quad Fe^+ , \quad FeCO^+$$

Ion-Molecule Reactions **(Cation + $BuFe(CO)_3$ → products)**

Condensation reactions with simultaneous ejection of up to 4 CO ligands. Principal reaction paths for each fragment ion are as follows:

Primary fragment ions:

Asymmetric (Bu<Fe) cluster formation*

$$Fe^+ + BuFe(CO)_3 \rightarrow BuFe_2(CO)_{2,3}^+ + n\,CO$$

$$FeCO^+ + BuFe(CO)_3 \rightarrow BuFe_2(CO)_{2,3}^+ + n\,CO$$

Symmetric (Bu=Fe) cluster formation*

$$BuFe^+ + BuFe(CO)_3 \rightarrow (BuFe)_2(CO)_{(0^*),1,2,3}^+ + \text{"}$$

$$BuFeCO^+ + \text{"} \rightarrow (BuFe)_2(CO)_{(0^*),1,2,3}^+ + \text{"}$$

$$BuFe(CO)_2^+ + \text{"} \rightarrow (BuFe)_2(CO)_{2,3}^+ + \text{"}$$

The parent molecular ion, $BzCr(CO)_3^+$ was unreactive for 25 seconds.

Binuclear ionic cluster fragment condensations:

Asymmetric cluster formation*

$$BuFe_2(CO)_{2,3}^+ + BuFe(CO)_3 \rightarrow Bu_2Fe_3(CO)_{2,3}^+ + n\,CO$$

Symmetric cluster formation*

$$(BuFe)_2(CO)_{1,2,3}^+ + BuFe(CO)_3 \rightarrow (BuFe)_3(CO)_{(1^*),2,3,4}^+ + n\,CO$$

[*Note: Iron is tetraisotopic, having the following isotopic distribution: ^{54}Fe=5.90%; ^{56}Fe=91.52%; ^{57}Fe=2.25%; ^{58}Fe=0.33%. Mass ambiguity can arise from confusion of ^{56}Fe with 2 CO ligands (i.e., 2x28 amu=56 amu). Therefore, ion products were characterised only if they appeared in sufficiently large intensities to permit recognition of iron isotopic patterns.]

Except for the absence of electron transfer pathways, in most cases reactivity of ions in this iron system closely mirror those observed in the $CpV(CO)_4$, $BzCr(CO)_3$ and $CpMn(CO)_3$ systems, this $BuFe(CO)_3$ system most closely resembling that of chromium; with principal pathways involving condensation with the parent neutral $BuFe(CO)_3$ molecule, resulting in the generation of larger, multi-iron-containing clusters. Symmetric clusters (Bu=Fe, e.g. $(BuFe)_2(CO)_2^+$) resemble those observed in the chromium system, as well as asymmetric, "iron-rich" clusters (Bu<Fe, e.g., $BuFe_2(CO)_3^+$) formed by condensations of Fe^+ and $FeCO^+$, resemble those generated in both the chromium and manganese systems. Clustering rates appearing to dwindle with cluster size and ligand saturation, as observed in the three other systems examined. Both types of clusters retained their aryl : iron ratios during subsequent interactions, as was also observed in the CpV, BzCr and CpMn systems. As seen here as well as in the other complexes in this study, reactivity in general varies directly with formal electron deficiency.

The "iron-rich" clusters $BuFe_2(CO)_{2,3}^+$ and $Bu_2Fe_3(CO)_{2,3}^+$ may possess double- and triple-decker sandwich structures similar to those demonstrated to exist in ferrocene (Cp_2Fe) and $Cp_3Fe_2^+$ ion[38,46,58,64]. "Sandwich" structures containing alternating iron-butadiene-iron linkages are found in a few substituted ferrocene and ferrocene-like systems (e.g.[6]), but most multi-iron cluster complexes consist of multi-iron cores surrounded by

ligand shells, as exemplified by the multi-iron carbonyl complex, $Fe_3(CO)_{12}$. The marked similarity between reactions of $BuFe(CO)_3$ and those of the other transition metal systems studied here probably reflects closely-related composition of the clusters, as well as similar electronic structure within the first transition series (i.e., V, Cr, Mn, Fe and Co) complexes[1,2,59]. Structural uniformity (i.e. central multi-metal cluster core arrangements) within the present ion complexes may be inferred; on the other hand, the larger electron density of the iron atom core compared to those of vanadium, chromium or manganese may permit multi-sandwich chain formation.

Presumably, highly stable electron distribution within the iron-ligand core in any of these ions does not favour electron transfer pathways: in contrast with the other metal systems studied here, in the $BuFe(CO)_3$ system there is no apparent charge-exchange equilibration with the parent neutral molecule, which in the other systems results in eventual molecular ion domination of the cation population. Instead, clustering of monomeric $BuFe(CO)_3$ with its daughter ions produces successively larger, multi-iron clusters.

2. Negative Ion Chemistry

In accordance with observations of Wang and Squires, using 2.5 eV electron impact and 6.0×10^{-8} torr nominal pressure, just one anion, $BuFe(CO)_2^-$, dominates the negative ion mass spectrum of η^4-$BuFe(CO)_3$. (Wang[63], $BuFe(CO)_2^-$ =87%; in this study: $BuFe(CO)_2^-$ =74%.) This anion product was unreactive for 25 seconds. Figure 5.9 is a typical FT-ICR negative ion mass spectrum of $BuFe(CO)_3$. Not surprisingly, interaction such as adduct formation with N_2, CO or CO_2, by the 17-electron anion

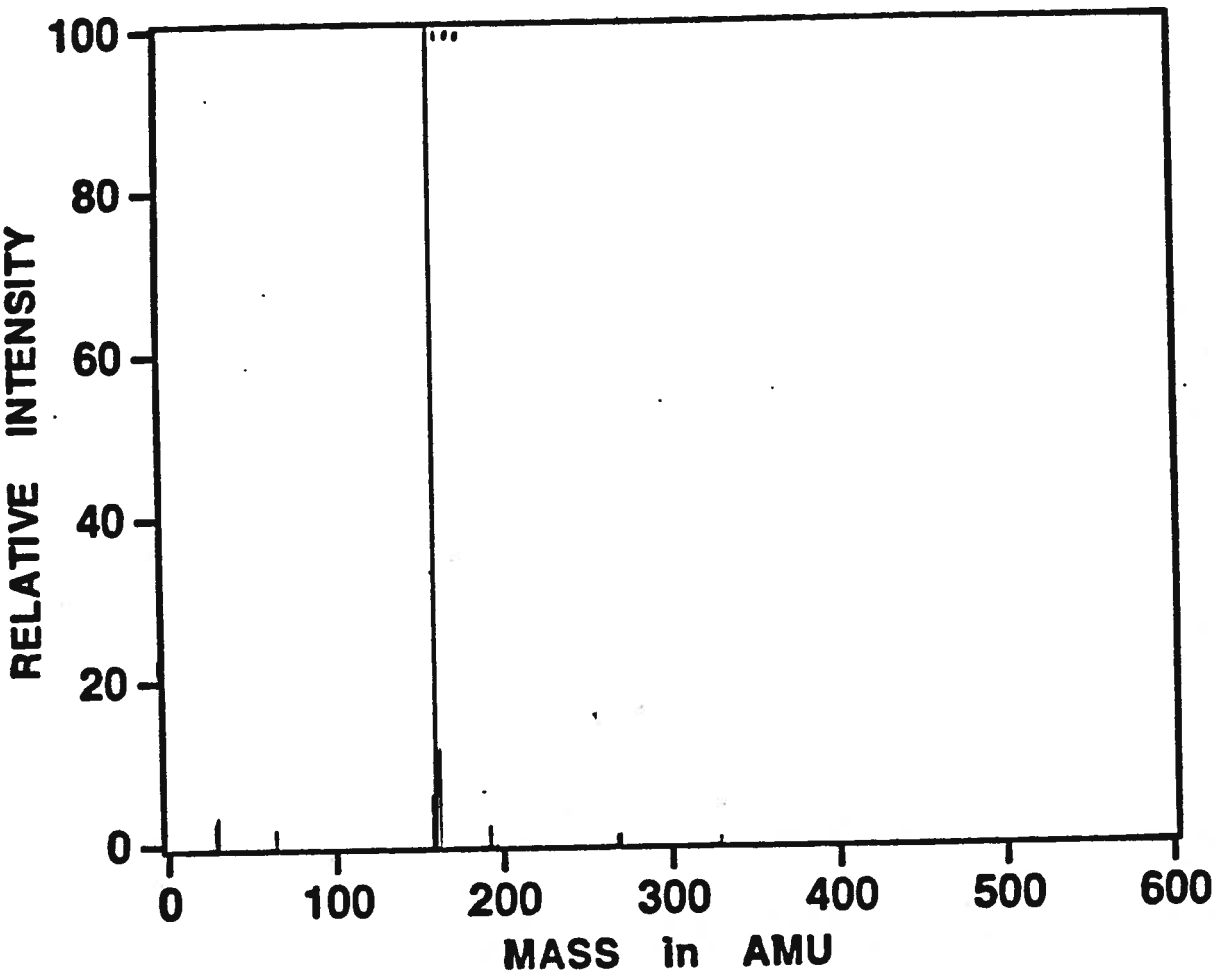

Figure 5.9. FT-ICR Negative Ion Mass Spectrum of $BuFe(CO)_3$; 0 msec.; 2.5 eV; p = 6.0×10^{-8} torr

$BuFe(CO)_2^-$ was not observed at reagent gas pressures of up to 10^{-6} torr. However, in an earlier study, $BuFe(CO)_2^-$ was observed to react with strong proton-donors such as CF_3CO_2H by accepting one proton per anion[45]. For this reason, self-protonation products were sought, but not observed here.

The negative ion-molecule chemistry of $BuFe(CO)_3$ strongly resembles that of $CpV(CO)_4$, $BzCr(CO)_3$, and $CpMn(CO)_3$, in that aryl-metal linkages in the anion products are retained, anion chemistry is simple, and only a few, unreactive anion species observed.

III Conclusions

GENERAL FEATURES OF THE $BuFe(CO)_3$ SYSTEM

1) Except for the molecular ion $BuFe(CO)_3^+$, all of the cations initially formed by electron impact on $BuFe(CO)_3$ are chemically reactive with parent neutral, whereas the single daughter anion $BuFe(CO)_2^-$ (17 electrons) is unreactive. Cation distribution followed a pattern similar to those of the other complexes studied here, i.e., electron loss, then successive decarbonylations, followed by olefin loss. All intermediate cations were present in the initial mass spectrum.

2) Electron transfer reactions, important in the vanadium, chromium and manganese systems, were not observed here. The bare metal cation Fe^+ reacted by condensation with a neutral molecule to produce asymmetric, iron-rich clusters. Parallel behaviour, in which metal-rich cores are generated by condensation of the bare metal cation with a neutral molecule, was seen in the analogous Cr^+ and Mn^+ systems studied here, and has been observed in many other similar studies[50,51].

3) The integrity of the Bu-Fe bond within cluster cores is usually sustained throughout successive reaction hierarchies, so that cation cluster cores of increasing size, such as $BuFe_2$, $(BuFe)_2$, and $(BuFe)_3$ appear in the mass spectra. Such clusters have been the subject of much speculation with regard to internal bonding and reactivity[37,54,67,69].

4) Clustering dwindles after the formation of tri-iron, $(BuFe)_3^+$ cores, at pressures presently used (10^{-6} - 10^{-9} torr); hence $(BuFe)_4$ or larger cation cluster fragments were not observed. Some or all of these cluster cations probably possess double or triple metal-metal bonds, as suggested earlier[67]. With increasing cluster size and concomitant coordination saturation of the iron core, the properties may approximate that of the bulk metal, resulting in stable metal centres which are unreactive with respect to further ligation[69].

5) Reaction decay rate constants for cations in this BuFe system, as seen in all the other analogous systems studied here, appear to be directly related to formal electron deficiency, as discussed in earlier reviews[54,55]. In Figure 5.10, pseudo-first order rate constants (for clustering pathways) are compared with formal electron deficiencies for each daughter cation in this system. As is the case for the fragment cations of vanadium, chromium and manganese, clustering rates vary with electron deficiency of the central metal iron atom in a fairly well-behaved manner. For this iron system, the steep slope between electron deficiencies of zero and two (Figure 5.10) suggests that nucleophilic reagent species with one or two-electron donor properties would react readily with such iron fragment ions, as postulated by Ridge in 1984[67].

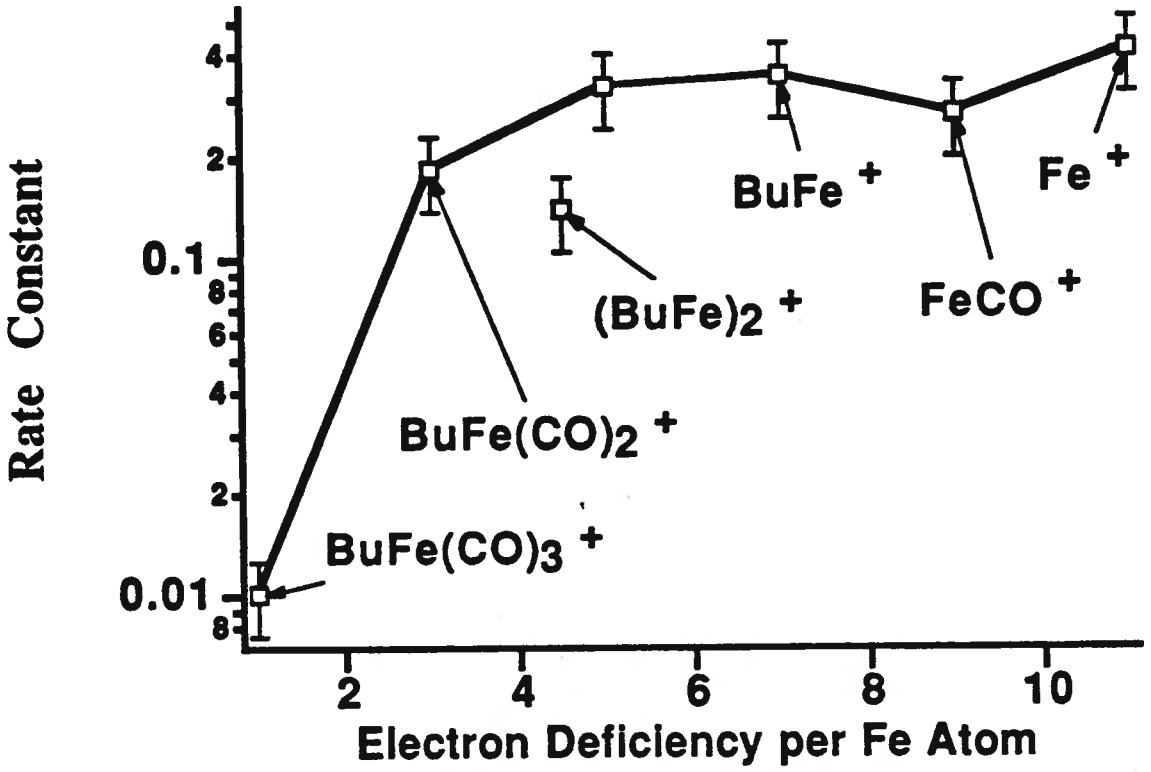

Figure 5.10. Relationship Between Reactivity and Electron Deficiency for Cations in the $BuFe(CO)_3$ System

6) Participation by excited state cations, as seen in the present vanadium, chromium and manganese systems, and in earlier studies[16,17,56] probably occurs in this iron system as well. Non-linear pseudo-first order (semi-log) decay rate behaviour of ions Fe^+ and $BuFe^+$, is shown in Figure 5.11. Initial rapid rates of decay of the two cations are followed by slower decay, as would be expected if both the initial excited state iron cations (which later become relaxed), as well as ground state iron cations, are disappearing. The smaller ions Fe^+ and $BuFe^+$ may absorb and retain excess energy from the ionisation process, and hence react more rapidly (or in more than one mode), than do their ground state counterparts. By extrapolation of the plots in Figure 5.11, excited state content for both the small ions can be estimated as follows: Fe^+, 52%; $BuFe^+$, 65%. Values for these and other excited state cations are collected in Table 7.5, Chapter 7.

The energy difference between ground and first excited state Fe^+ is only 0.25 eV[2,56], much less than that injected during the 25 eV ionisation procedure, hence much of the product Fe^+ and some of the other small fragment cations react via excited state pathways before collisional relaxation has time to occur.

7) A clastogram for appearance of $BuFe(CO)_3$ cations with ionising voltage is illustrated in Figure 5.12, following Figure 5.11. Successive losses of CO are followed by C_4H_6 loss from the $BuFe(CO)_3^+$ parent ion as energy is increased; behaviour was as expected from similar studies[9,51].

8) A study of addition chemistry of $BuFe(CO)_3$ was attempted using reactant gases dioxygen, nitrogen and hydrogen. Many addition products were observed, some with very closely-spaced masses. The complex iron isotopic pattern of bi-iron and tri-iron species made resolution of the products difficult; consequently identification of all ion products

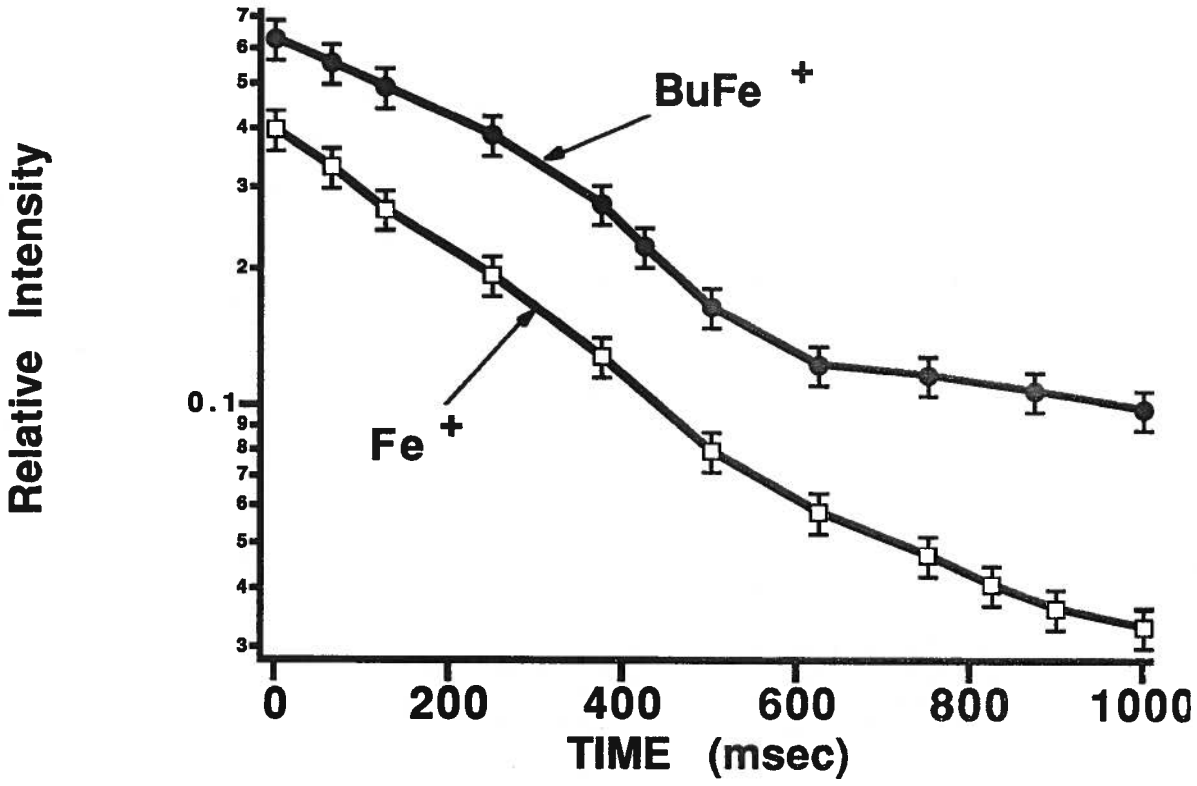

Figure 5.11. Deviations from Pseudo-First Order Decay Behaviour in the $BuFe(CO)_3$ System

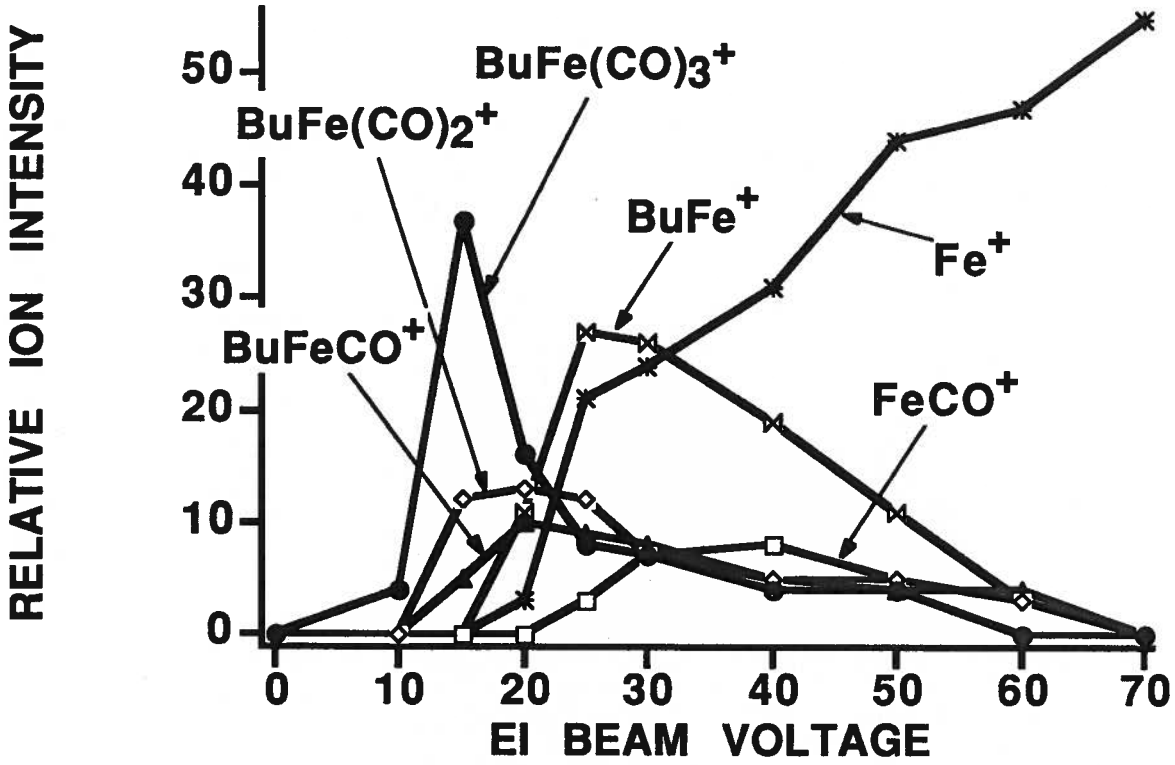

Figure 5.12. Clastogram for Cations of $BuFe(CO)_3$

was not successful. Nevertheless, the pattern of generation of multiple adducts containing one or two oxygen or hydrogen atoms seems to mirror that seen in the other metal systems. Further studies utilising higher pressures of reagent gases and iron isotope labelling will yield information regarding the addition chemistry of these iron clusters.

IV References

(1) Allison, J. *Prog. Inorg. Chem.* **1986**, *34*, 627.

(2) Armentrout, P. B. in *Gas Phase Inorganic Chemistry*; Russell, D. H.; Plenum Press, New York, **1989**; pp 1 - 42.

(3) Bjarnason, A.; Taylor, J. W. *Organomet.* **1990**, *9*, 1493.

(4) Blake, M. R.; Garnett, J. L.; Gregor, I. K. *J. Organomet. Chem.* **1979**, *178*, C37.

(5) Blake, M. R.; Garnett, J. L.; Gregor, I. K.; Wild, S. B. *J. Chem. Soc., Chem. Commun.* **1979**, 496.

(6) Burdett, J. K.; Canadell, E. *Organometallics* **1985**, *4*, 805.

(7) Byrd, G. D.; Burnier, R. C.; Freiser, B. S. *J. Am. Chem. Soc.* **1982**, *104*, 3565.

(8) Cassady, C. J.; Freiser, B. S. *J. Am. Chem. Soc.* **1984**, *106*, 6176.

(9) Chen, S.-P.; Comisarow, M. B. *Ann. Conf. ASMS All. Topics* **1989**, *37*, 323.

(10) Chen, H.; Lin, H.-Y.; Sohlberg, K.; Ridge, D. P. *Ann. Conf. ASMS All. Topics* **1991**, *39*, 1596.

(11) Connor, J. A.; Derrick, L. M. R.; Hall, M. B.; Hillier, I. H. *Mol. Phys.* **1974**, *28*, 1193.

(12) Corderman, R. R.; Beauchamp, J. L. *Inorg. Chem.* **1976**, *15*, 665.

(13) Davis, M. L.; Speed, C. S. *J. Organomet. Chem.* **1970**, *21*, 401.

(14) Dewar, M. J. S.; Worley, S. D. *J. Chem. Phys.* **1969**, *50*, 654.

(15) Elkind, J. L.; Armentrout, P. B. *J. Am. Chem. Soc.* **1986**, *108*, 2765.

(16) Elkind, J. L.; Armentrout, P. B. *J. Chem. Phys.* **1987**, *86*, 1868.

(17) Elkind, J. L.; Armentrout, P. B. *J. Phys. Chem.* **1987**, *91*, 2037.

(18) Faulk, J.; Dunbar, R. C. *Ann . Conf. ASMS All. Topics* **1987**, *35*, 920.

(19) Foster, M. S.; Beauchamp, J. L. *J. Am. Chem. Soc.* **1971**, *93*, 4924.

(20) Foster, M. S.; Beauchamp, J. L. *J. Am. Chem. Soc.* **1975**, *97*, 4808.

(21) Foster, M. S.; Beauchamp, J. L. *J. Am. Chem. Soc.* **1975**, *97*, 4814.

(22) Freas, R. B.; Ridge, D. P. *J. Am. Chem. Soc.* **1980**, *102*, 7129.

(23) Fredeen, D. J. A.; Russell, D. H. *J. Am. Chem. Soc.* **1985**, *107*, 3762.

(24) Hallam, B. F.; Pauson, P. L. *J. Chem. Soc.* **1956**, 3030.

(25) Hallam, B. F.; Pauson, P. L. *J. Chem. Soc.* **1958**, 642.

(26) Huang, Y.; Freiser, B. S. *J. Am. Chem. Soc.* **1989**, *111*, 2387.

(27) Huang, Y.; Freiser, B. S. *Inorg. Chem.* **1990**, *29*, 1102.

(28) Huang, Y.; Freiser, B. S. *J. Am. Chem. Soc.* **1990**, *112*, 5085.

(29) Huang, Y.; Freiser, B. S. *J. Am. Chem. Soc.* **1990**, *112*, 1682.

(30) Huang, Y.; Freiser, B. S. *Inorg. Chem.* **1990**, *29*, 2052.

(31) Jacobson, D. B.; Freiser, B. S. *J. Am. Chem. Soc.* **1983**, *105*, 5197.

(32) Jacobson, D. B.; Freiser, B. S. *J. Am. Chem. Soc.* **1983**, *105*, 7485.

(33) Jacobson, D. B.; Freiser, B. S. *J. Am. Chem. Soc.* **1984**, *106*, 3900.

(34) Jacobson, D. B.; Freiser, B. S. *J. Am. Chem. Soc.* **1984**, *106*, 3891.

(35) Jacobson, D. B.; Freiser, B. S. *J. Am. Chem. Soc.* **1984**, *106*, 4623.

(36) Jacobson, D. B.; Freiser, B. S. *J. Am. Chem. Soc.* **1985**, *107*, 1581.

(37) Jacobson, D. B.; Freiser, B. S. *J. Am. Chem. Soc.* **1986**, *108*, 27.

(38) Kealy, T. J.; Pauson, P. J. *Nature* **1951**, *168*, 1039.

(39) King, R. B. *Inorg. Chem.* **1966**, *5*, 2227.

(40) Krusic, P. J.; San Filippo Jr., J.; Hutchinson, B.; Hance, R. L.; Daniels, L. M. *J. Am. Chem. Soc.* **1981**, *103*, 2129.

(41) Krusic, P. J.; San Filippo Jr., J. *J. Am. Chem. Soc.* **1982**, *104*, 2645.

(42) Lauher, J. W.; Elian, M.; Summerville, R. H.; Hoffman, R. *J. Am. Chem. Soc.* **1976**, *98*, 3219.

(43) Lin, L.; Kutal, C. R.; Amster, I. J. *Ann. Conf. ASMS All. Topics* **1991**, *39*, 1616.

(44) Maddox, M. L.; Stafford, S. L.; Kaesz *Adv. Organomet. Chem.* **1965**, *3*, 1.

(45) McDonald, R. N.; Schell, P. L.; Chowdury, A. K. *J. Am. Chem. Soc.* **1985**, *107*, 5578.

(46) Miller, S. A.; Tebboth, J. A.; Tremaine, J. F. *J. Chem. Soc.* **1952**, 632.

(47) Mills, O. S.; Robinson, G. *Acta Crystallogr.* **1963**, *16*, 758.

(48) Mond, L.; Langer, C. *Trans. Chem. Soc.* **1891**, *59*, 1090.

(49) Murr, N. L.; Payne, J. D. *J. Chem. Soc. Chem. Commun.* **1985**, 162.

(50) Operti, L.; Vaglio, G. A.; Gord, J. R.; Freiser, B. S. *Organometallics* **1991**, *10*, 104.

(51) Parisod, G.; Comisarow, M. B. *Adv. Mass Spectrom.* **1980**, *8A*, 212.

(52) Reed, D. T.; Meckstroth, W. K.; Ridge, D. P. *J. Phys. Chem.* **1985**, *89*, 4578.

(53) Reihlen, H.; Gruhl, A.; Hessling, G. v.; Pfrengle, O. *Liebig's Annalen Der Chemie* **1930**, *482*, 161.

(54) Ridge, D. P.; Meckstroth, W. K. in *Gas Phase Inorganic Chemistry*; Russell, D. H.; Plenum Press, New York, **1989**; pp 93-113.

(55) Russell, D. H.; Fredeen, D. A.; Tecklenburg, R. E. in *Gas Phase Inorganic Chemistry*; Russell, D. H.; Plenum Press, New York, **1989**; pp 115-135.

(56) Russell, D. H. *Ann. Conf. ASMS All. Top.* **1989**, *38,* 1261.

(57) Sallans, L.; Lane, K. R.; Freiser, B. S. *J. Am. Chem. Soc.* **1989**, *111,* 865.

(58) Schumacher, E.; Taubenest, R. *Helv. Chim. Acta* **1964**, *47,* 1525.

(59) Skinner, H. A.; Connor, J. A. *Pure Appl. Chem.* **1985**, *57,* 79.

(60) Squires, R. R. *Chem. Rev.* **1987**, *87,* 623.

(61) Veltman, P. L. U. S. P. 2., 409,167 *Chem. Abs.* **1946**, *41,* 595.

(62) von Gustorf, E. K.; Buchkremer, J.; Pfaifer, Z.; Grevels, F.-W. *Angew. Chem. Int. Ed.* **1971**, *10,* 260.

(63) Wang, D.; Squires, R. R. *Organometallics* **1987**, *6,* 905.

(64) Wilkinson, G.; Rosenblum, M.; Whiting, M. L.; Woodward, R. B. *J. Am. Chem. Soc.* **1952**, *74,* 2125.

(65) Williams-Smith, D. L.; Wolf, L. R.; Skell, P. S. *J. Am. Chem. Soc.* **1972**, *94,* 4042.

(66) Worley, S. D. *J. Chem. Soc. Chem. Commun.* **1970**, 980.

(67) Wronka, J.; Ridge, D. P. *J. Am. Chem. Soc.* **1984**, *106,* 67.

(68) Young, D. A. T.; Holmes, J. R.; Kaesz, H. D. *J. Am. Chem. Soc.* **1969**, *91,* 6968.

(69) Zakin, M. R.; Cox, D. M.; Whetten, R. L.; Trevor, D. J.; Kaldor, A. *Chem. Phys. Lett.* **1987**, *135,* 223.

CHAPTER 6

Ion Molecule Chemistry of

Bicarbonyl (η^5 - Cyclopentadienyl) Cobalt

{ $CpCo(CO)_2$ }

I Introduction

Bicarbonyl (η^5-cyclopentadienyl) cobalt , $CpCo(CO)_2$, is a dark red reactive liquid at room temperature, melting at -22° C and boiling at 75° C (20 mm Hg); first synthesised by Fischer (1954) and Piper, Cotton and Wilkinson (1955), the complex is unstable at room temperature, especially in the presence of oxygen[8,37]. Its structure resembles that of a two-legged piano stool:

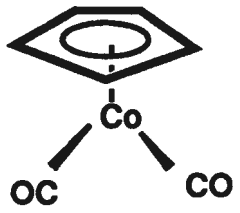

The properties of aryl cluster compounds containing cobalt have been of interest for some time: for example, King first prepared and characterised the trimetallic cluster $Cp_3Co_3(CO)_3$ in solution in 1966[24]; hydrides such as $(CpCoH)_4$ were prepared in solution by reduction of $(CpCoNO)_2$ in 1973[33]; solid state geometry of $(CpCoH)_4$ was determined in 1975 by Huttner[17]. Ligand substitution reactions of anions $Co(CO)_2(NO)^-$, $C_3H_5Co(CO)_2^-$, $C_3H_5Co(CO)_3^-$ and $CpCo(CO)_2^-$ in the gas phase were studied by McDonald and Schell in 1988[29]. More recently Mevs (1991) studied electron transfer chemistry of the $Cp_3Co_3(CO)_3$ cluster in solution[30].

Mass spectral studies on $CpCo(CO)_2$ were begun by Winters and Kiser in 1965[47], and later Müller (1970) examined positive ion mass spectral fragmentation

patterns of $CpCo(CO)_2$ and determined appearance potentials for several of its daughter product cations. Evidence for formation of bimetal clusters such as $Cp_2Co_2(CO)_3^+$ in the mass spectra of this system was noted[32]. In 1977, Corderman and Beauchamp studied the kinetic behaviour of the negative ion products of $CpCo(CO)_2$ using ICR methods[7]. They observed only two anions in the negative ion spectrum, $CpCoCO^-$ and $CpCo(CO)_2^-$, noting that the latter anion was kinetically unreactive, while the former ion, $CpCoCO^-$, rapidly clustered with the parent neutral to form unreactive $Cp_2Co_2(CO)_2^-$. Reactions with PF_3, NO, and small anions by carbonyl-ligand displacement, were also noted[6]. Bond lengths and angles in this cluster anion, $Cp_2Co_2(CO)_2^-$ were determined in 1977 by Shore[41] and reexamined in 1979 by Pinhas and Hoffman[36]. In 1981, Jones and Staley studied positive ion-molecule reactions of $CpCo(CO)_2$, noting that product ion Cp_2Co^+ (an 18 electron ion) was an important cluster product[23]. These results were complicated by the presence of excess cyclopentadiene in the reaction chamber.

Many recent studies on the reactivity of gaseous atomic cobalt and ligated cobalt ions have examined reactivity with respect to alkanes[5,18]; cycloalkanes[1,2,19,20,35]; alkenes[11]; dioxygen[12]; aldehydes and ketones[14]; ethers[28]; thiols[39]; butanes[45]. Reactivities of bare cobalt ions with respect to activation of C-H, C-C and other bonds, and bond strengths of Co-H, Co-C, Co-O and other linkages, have been quantified[3,11,42,43,44] and related to electronic structure and stability of the central metal core[3,27,34,42,43,44].

The present work extends the earlier gas phase positive and negative ion - molecule studies of $CpCo(CO)_2$ and its daughter ion fragments by examining long-time (25 second) kinetic behaviour of pure $CpCo(CO)_2$ and its daughter ions as well as some of its reactions with small molecules CO, CO_2 and N_2.

II Results and Discussion

1. Positive Ion Chemistry

Under 25 eV electron ionization and gauge pressure of 6.0×10^{-8} torr, the following fragment daughter cation distribution was observed for positive ions of $CpCo(CO)_2$: Co^+=4%, $CpCo^+$=31%, $CpCoCO^+$=7%, $CpCo(CO)_2^+$=13%, $CoCO^+$=4%, CO^+=24%. (These data compare with those of Winters and Kiser: Co^+=24%, $CpCo^+$=39%, $CpCoCO^+$=10%, $CpCo(CO)_2^+$=10% with 70 eV EI[47]; Jones and Staley: $CpCo^+$=15%, $CpCoCO^+$=14%, $CpCo(CO)_2^+$=39% with 12 eV EI[23]) An example of a FT-ICR mass spectrum exhibiting these positive ions immediately after generation is shown in Figure 6.1. Table 6.1 lists the mass data for a typical experiment.

Like the $CpV(CO)_4$ system (Chapter 2) but unlike the $BzCr(CO)_3$, $CpMn(CO)_3$ and $BuFe(CO)_3$ systems (Chapters 3, 4 and 5 respectively), all of the daughter fragments including the molecular ion, $CpCo(CO)_2^+$, in this $CpCo(CO)_2$ system are kinetically reactive. Typical temporal behaviour patterns of primary fragment ions Co^+, $CpCo^+$, $CpCoCO^+$ and $CpCo(CO)_2^+$, determined by single resonance techniques, are illustrated in Figure 6.2. At reaction times of up to 25 seconds, the following product cations are generated:

$CpCoCOH^+$; $CpCo(CO)_2H^+$; $CpCo(CO)_{3,4}^+$;

Cp_2Co^+ ; $(CpCo)_2(CO)_{2,3}^+$; $(CpCo)_2(CO)_3H^+$

Figure 6.3 shows formation and disappearance patterns of four of the most abundant of these secondary cationic clusters.

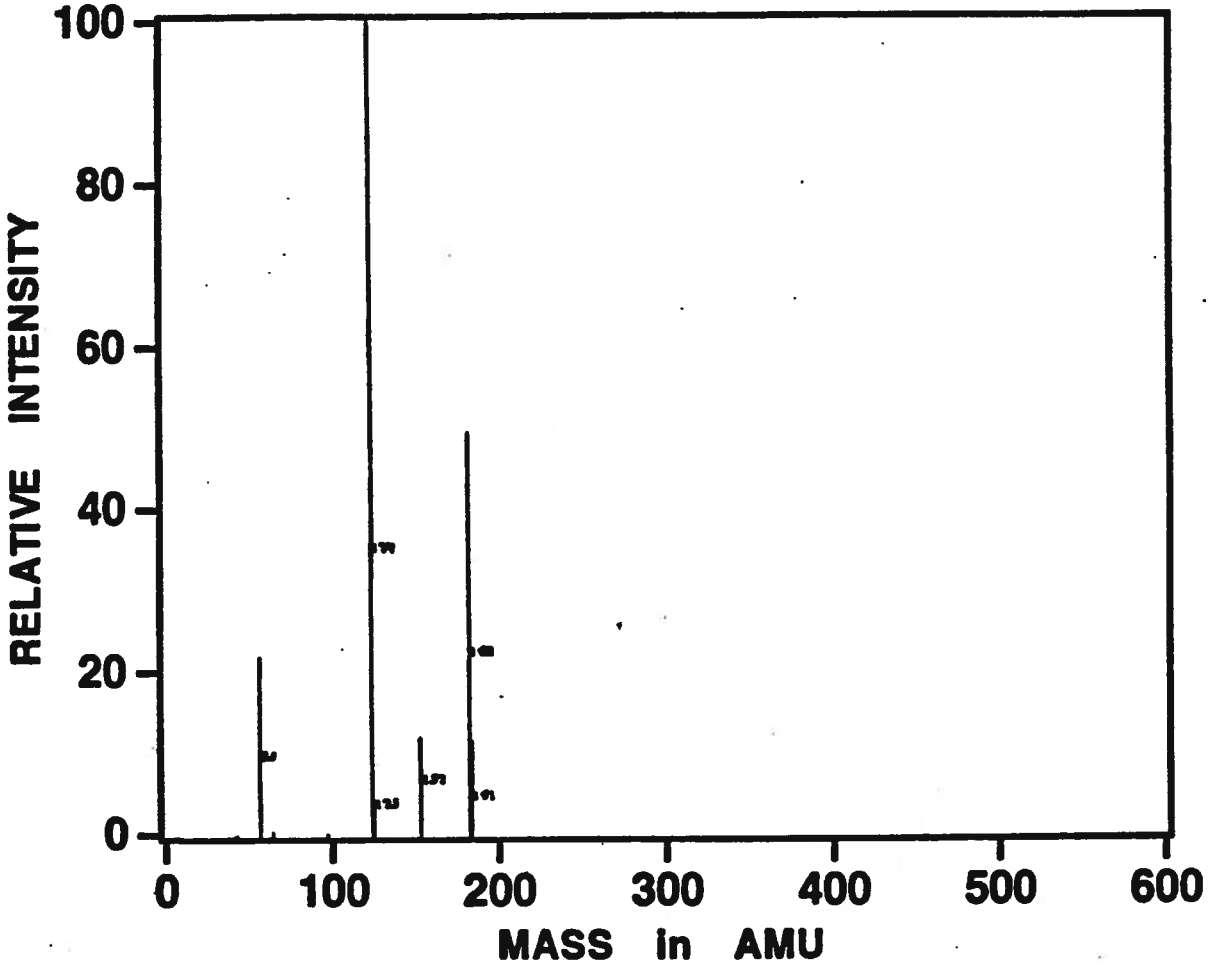

Figure 6.1. FT-ICR Positive Ion Mass Spectrum of $CpCo(CO)_2$; 0 msec.; 25 eV; $p = 6.0 \times 10^{-8}$ torr

TABLE 6.1

Sample Mass Table for $CpCo(CO)_2$ Cations (500 msec)

Formula	Measured Mass[a]	Expected Mass[a]	Δ (ppm)	Rel. Int. (%)
^{59}Co (100%)	58.9759	58.9327	43[b]	3.5
CpCo	123.9344	123.9718	37	13.0
CpCoCO	151.9765	151.9667	98	4.0
$CpCo(CO)_2$	179.9635	179.9617	2[b]	65.6
$CpCo(CO)_3$	207.9513	207.9566	5	2.5
CpCoCOH	152.9975	152.9746	23	2.9
$CpCo(CO)_2H$	180.9381	180.9695	31	39.7
Cp_2Co	189.0010	189.0109	10[b]	100.0
$(CpCo)_2(CO)_2$	----	303.9340	----	----
$(CpCo)_2(CO)_3$	331.7840	331.9289	145	3.1

[a] in daltons

[b] calibrant mass

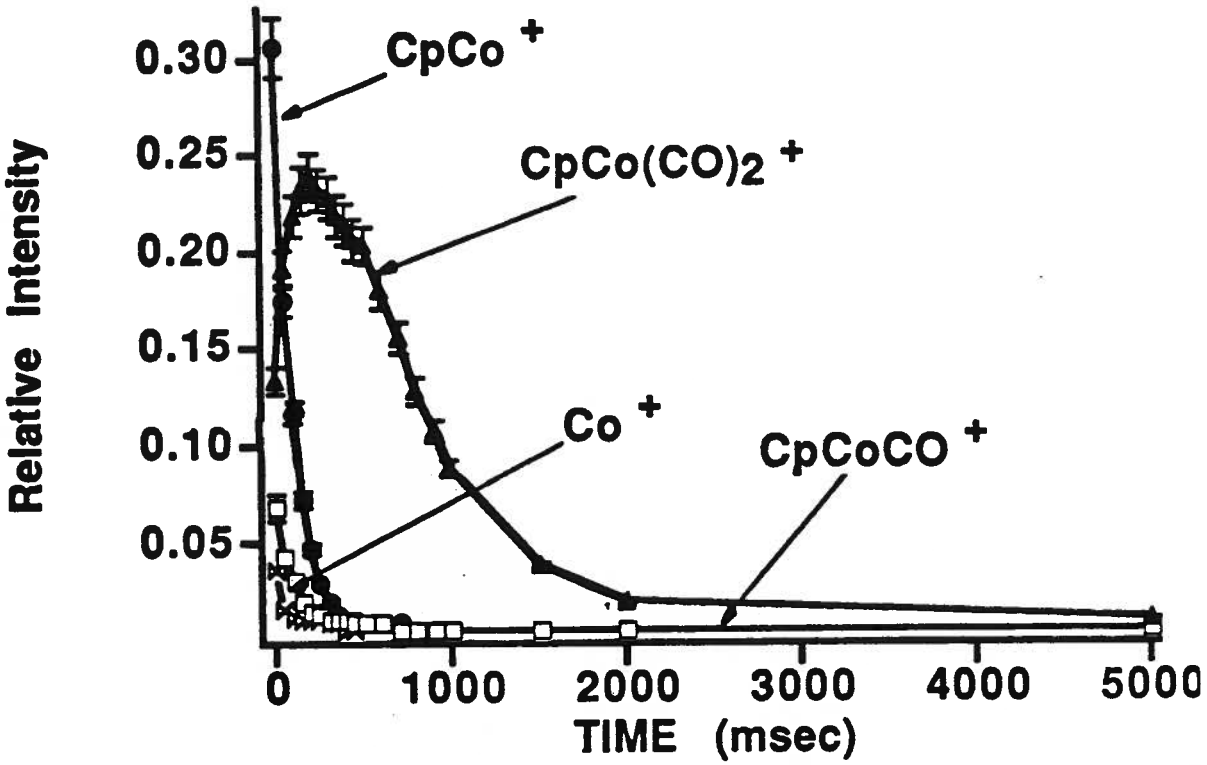

Figure 6.2. Temporal Behaviour of Primary Fragment Cations of $CpCo(CO)_2$

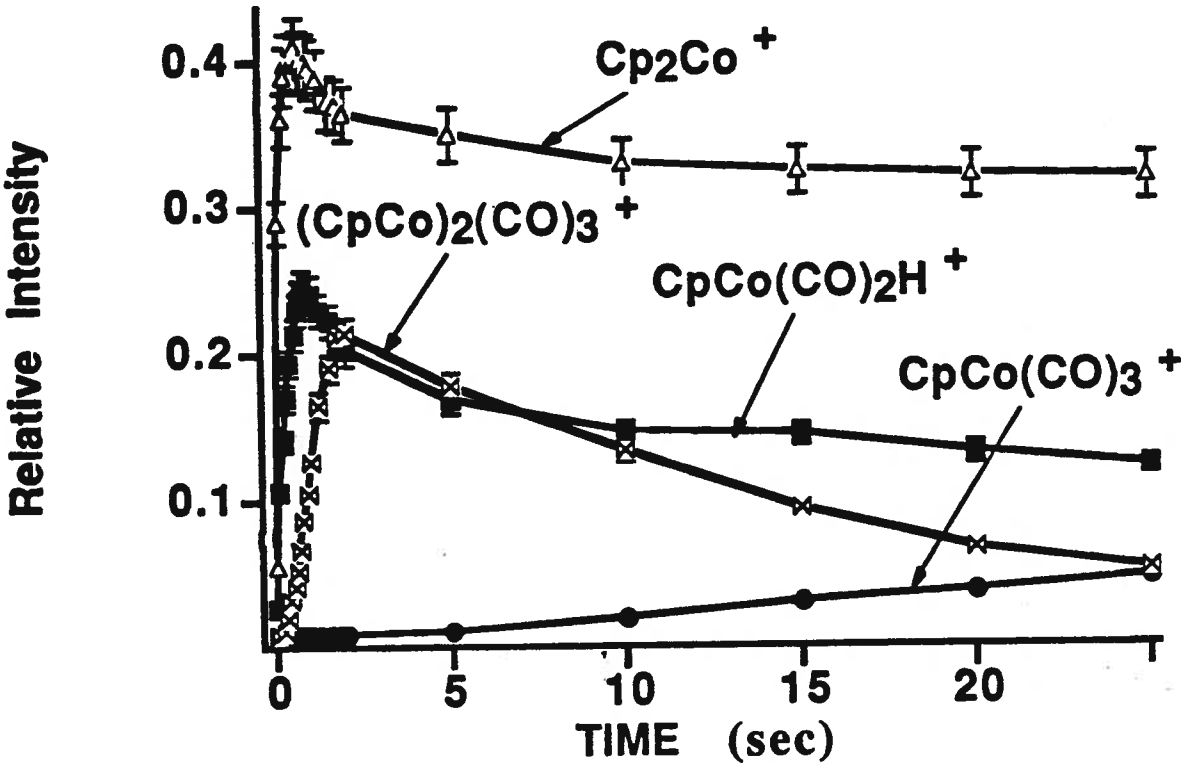

Figure 6.3. Temporal Behaviour of Secondary Cluster Cations of $CpCo(CO)_2$

Application of FT-ICR multiple resonance permitted identification of reaction products from each daughter ion by successive isolation of each ion followed by product monitoring. Figure 6.4(a,b) displays two multiple resonance spectra of the Co^+ ion, initially and at 500 msec, after its ion products had formed. Figure 6.5 illustrates the resultant temporal behaviour of Co^+ and its cation products. Comparable temporal behaviour of the $CpCo^+$ ion and its cation products is illustrated in Figure 6.6; for the ion $CpCoCO^+$, in Figure 6.7; and for the molecular ion $CpCo(CO)_2^+$, in Figure 6.8. Pseudo-first order rate constants for the disappearance of reactive cobalt cations reacting with the parent neutral molecule $CpCo(CO)_2$ are listed in Table 6.2. Principal reactive pathways of these ions are summarized in the following sections.

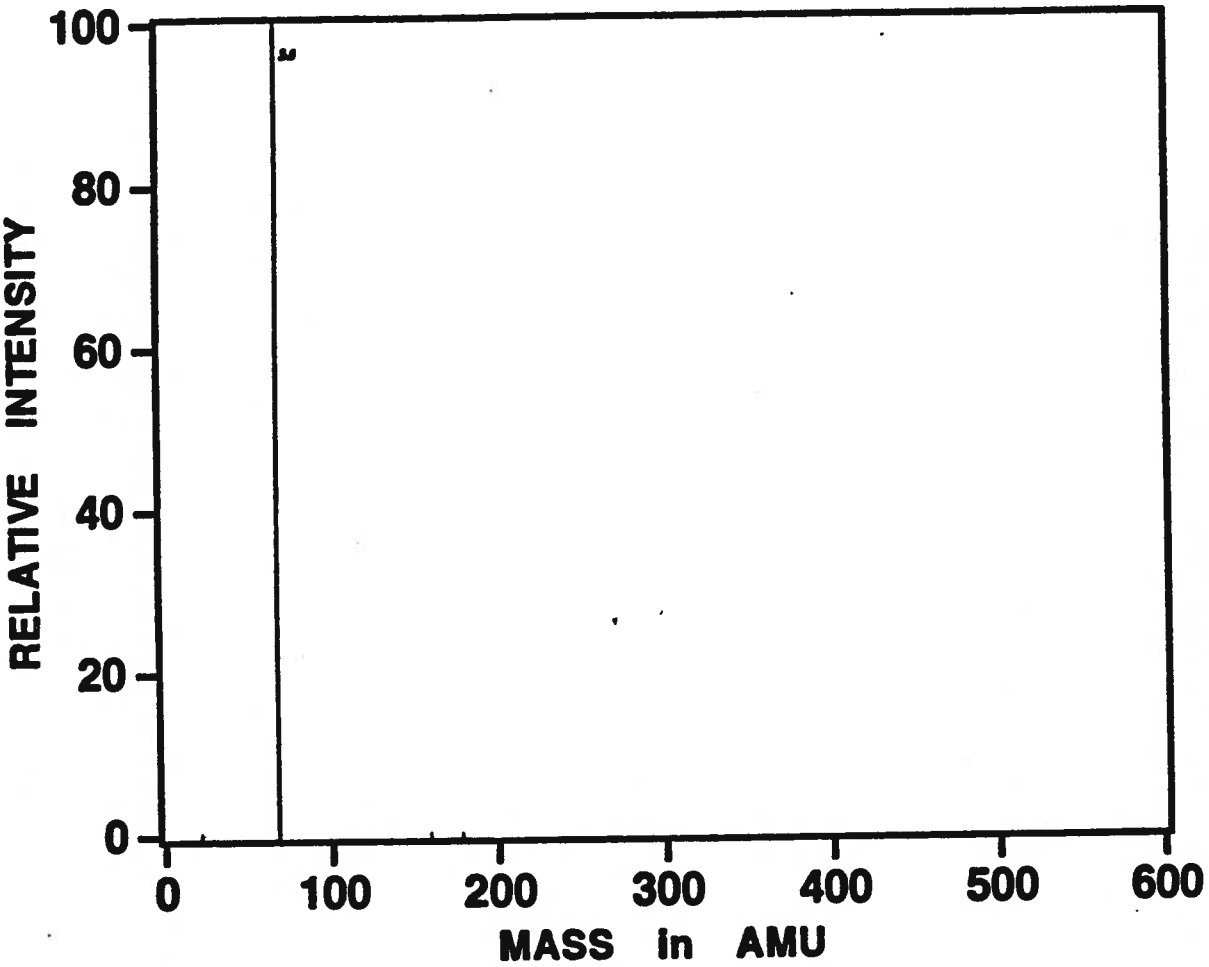

Figure 6.4(a). Multiple Resonance Mass Spectrum of Co^+; 0 msec.; p = 6.0×10^{-8} torr

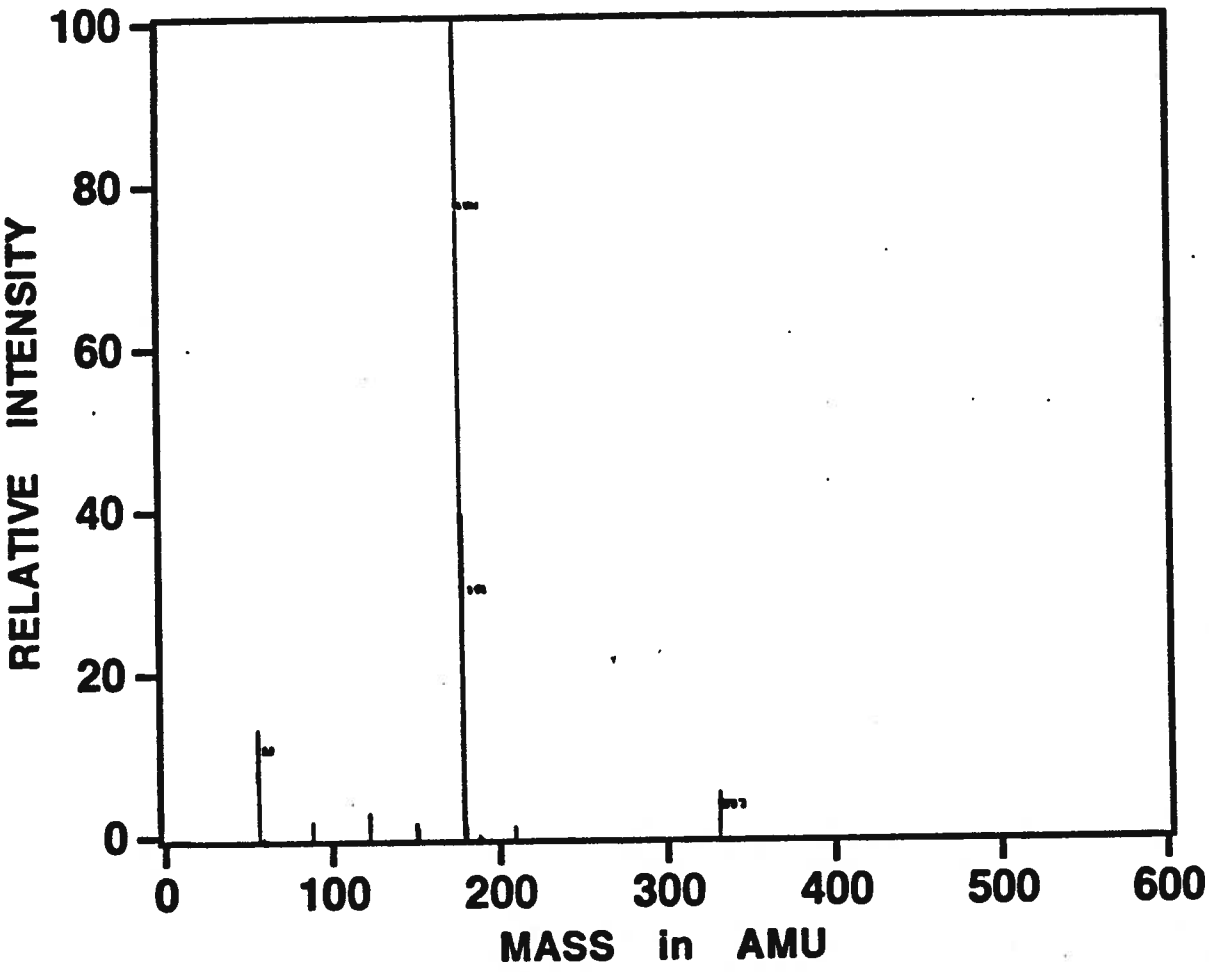

Figure 6.4(b). Multiple Resonance Mass Spectrum of Co^+ and Cation Products; 500 msec.; p = 6.0×10^{-8} torr

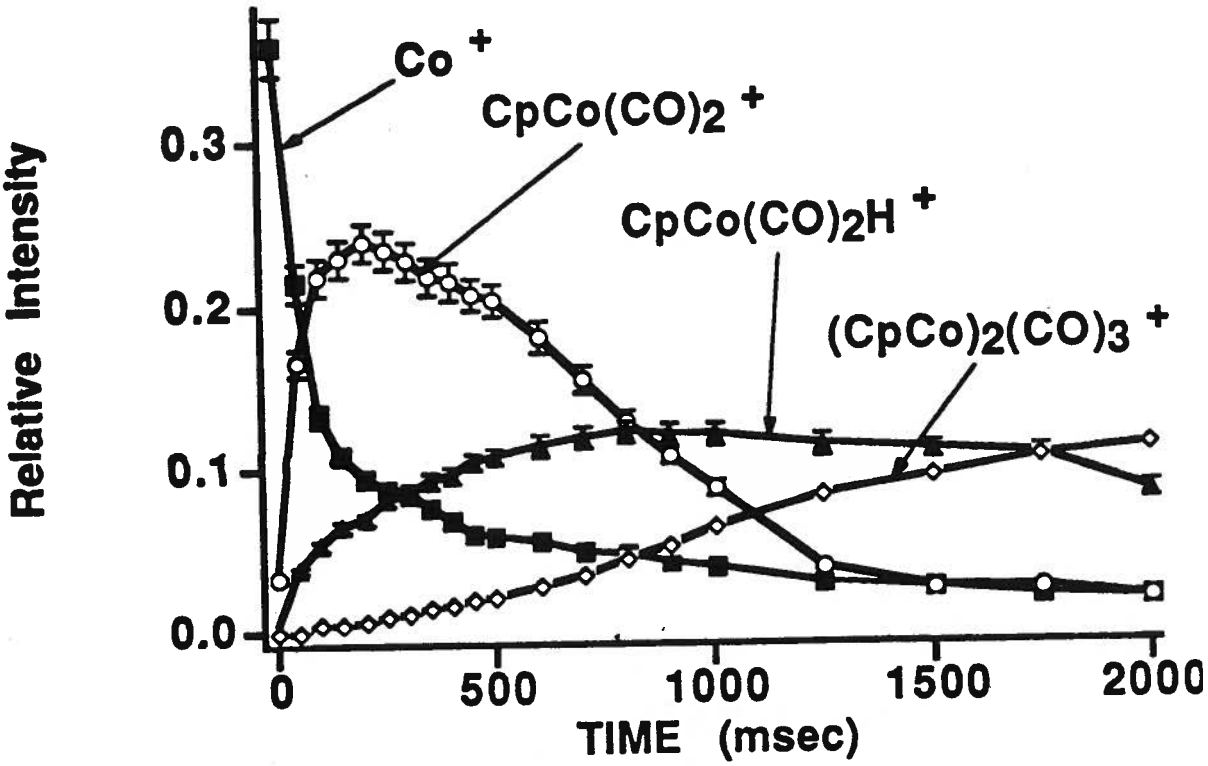

Figure 6.5. Temporal Behaviour of Co^+ and Cation Products

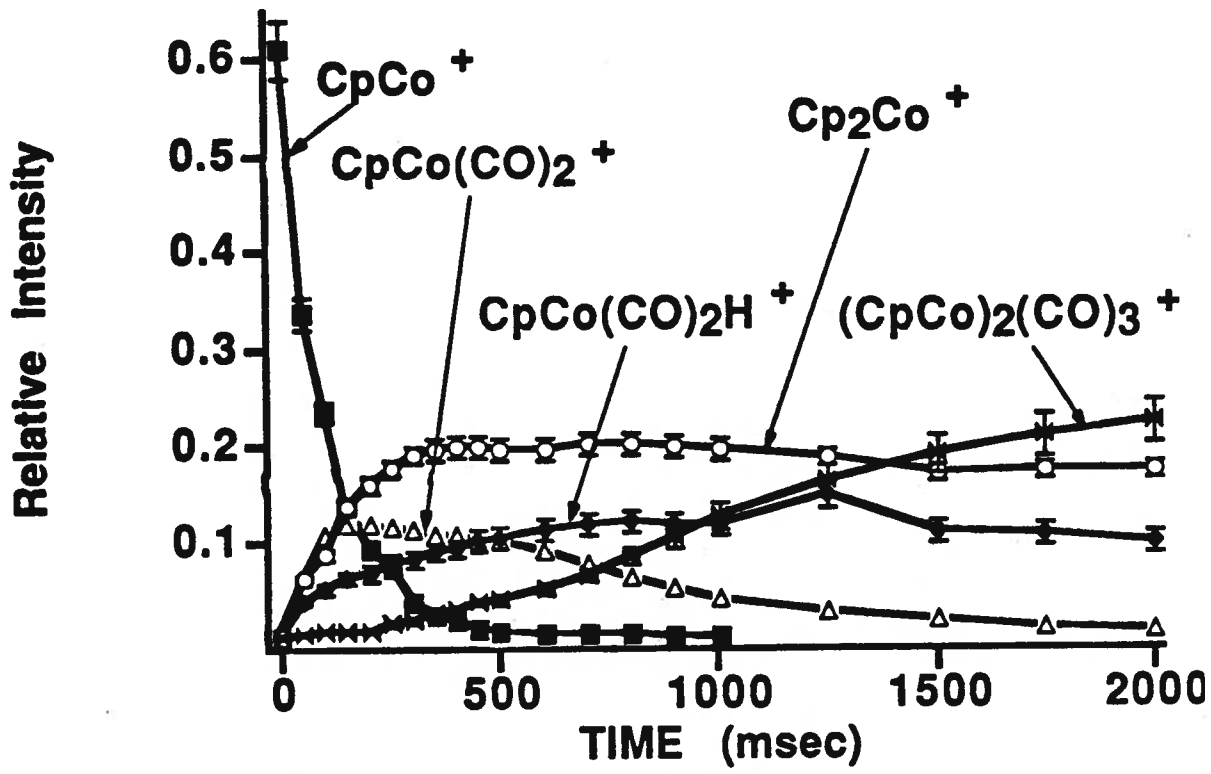

Figure 6.6. Temporal Behaviour of $CpCo^+$ and Cation Products

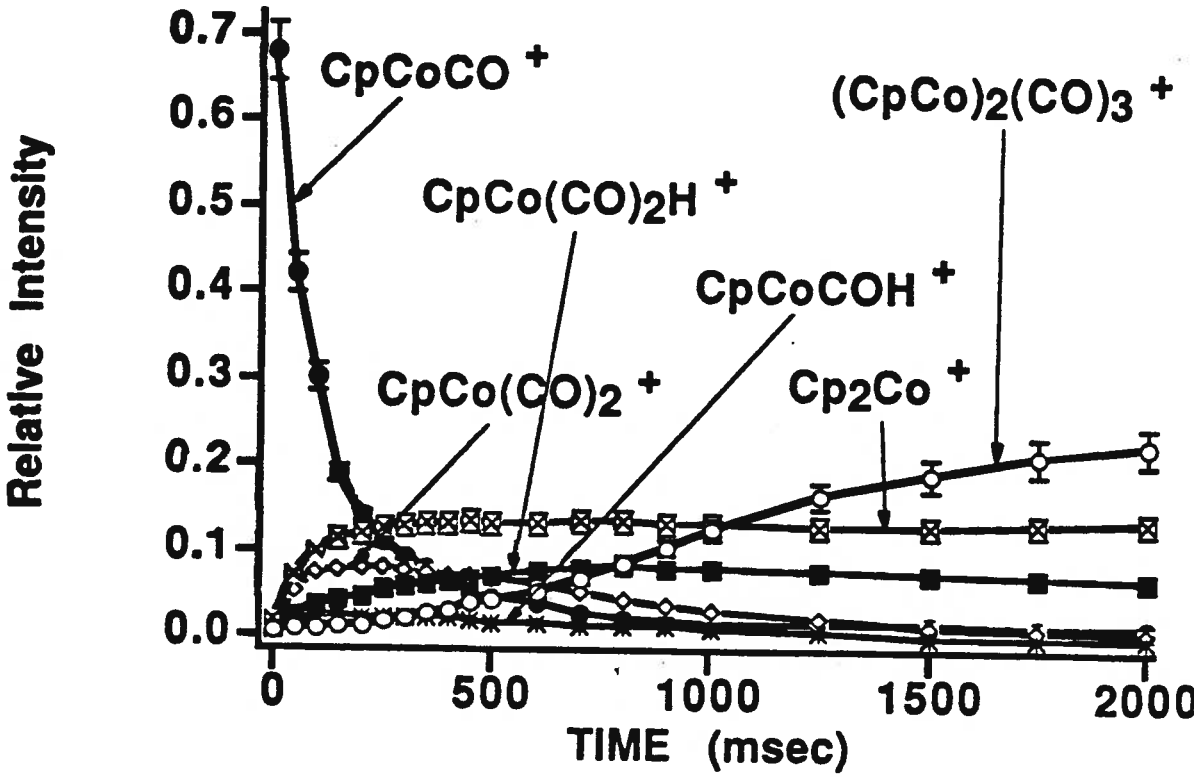

Figure 6.7. Temporal Behaviour of CpCoCO+ and Cation Products

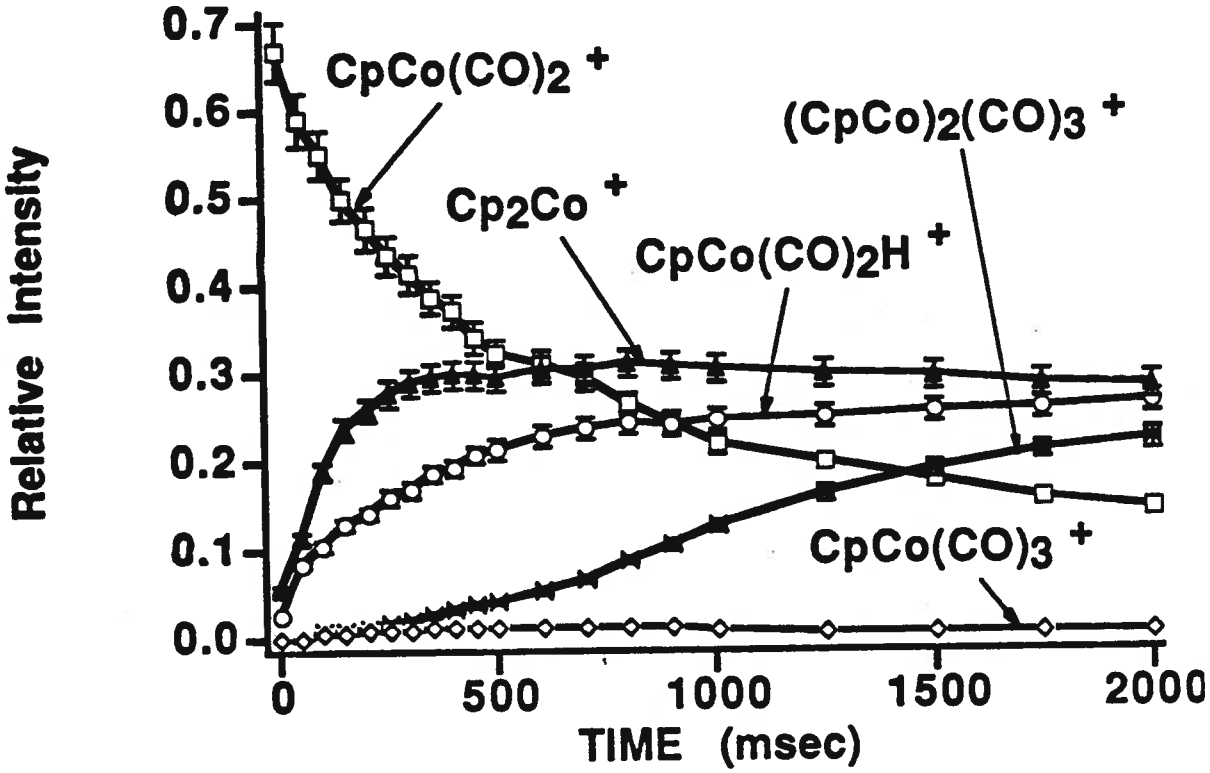

Figure 6.8. Temporal Behaviour of $CpCo(CO)_2^+$ and Cation Products

TABLE 6.2

Disappearance Rates for Cobalt Cations Reacting with Neutral $CpCo(CO)_2$ Molecules

Ion	Rate Constant (k') (sec^{-1}) *	Rate Constant (k) ($x10^9$ molec.$^{-1}cm^3sec^{-1}$) #
Co^+	0.589	1.93
$CpCo^+$	0.384	1.26
$CpCoCO^+$	0.211	0.69
$CpCoCOH^+$	0.251	0.82
$CpCo(CO)_2^+$	0.207	0.68
$CpCo(CO)_2H^+$	0.127	0.42
Cp_2Co^+	0.01	0.03
$(CpCo)_2(CO)_3^+$	<0.01	<0.03

* Calculated from linear first-order rate plots; all data ± 10%

\# Calculated from experimental parameters:
pressure = $6.0x10^{-8}$ torr; temperature = 350°K; α = 16.72;
all data ± 30%

PRINCIPAL REACTIVE PATHWAYS IN THE $CpCo(CO)_2$ CATION SYSTEM

1.Primary (EI) fragmentation of the neutral parent $CpCo(CO)_2$ molecule occurs as follows:

$CpCo(CO)_2 + e^- \rightarrow CpCo(CO)_{0,1,2}^+$, Co^+ (and minor $CoCO^+$ and $C_3H_3Co^+$)

2.Ion-Molecule Reactions (Cation + $CpCo(CO)_2$ → products)

Class 1. Electron transfer from neutral parent molecule to ion-molecule product cation:

$Co^+ + CpCo(CO)_2 \rightarrow CpCo(CO)_2^+ + \cdots$

$CpCo(CO)_{0,1}^+ + \text{"} \rightarrow \text{"} + \ldots$

Relative rates of electron transfer for these three processes are given in Table 6.3. Electron transfer from neutral $CpCo(CO)_2$ molecules to daughter cations in this system parallels exactly those processes seen in the vanadium (i.e., Chapter 2), chromium (Chapter 3), manganese (Chapter 4) and iron (Chapter 5) systems: again reflecting the fact that electron affinities of the cobalt daughter fragment cations exceed the ionization potential of the neutral molecule. As in the five other transition metal systems, ions with large formal electron-deficient cobalt atom cores should react relatively rapidly, for example, Co^+ (with 8 electrons) predictably reacts approximately three times as fast as $CpCoCO^+$ (15 electrons). Relative rates of electron transfer are listed in Table 6.3.

TABLE 6.3

Relative Electron Transfer Rates for Cobalt Cations Reacting with Neutral $CpCo(CO)_2$ Molecules

Ion	Rate Constant (k) ($\times 10^9$ molec.$^{-1}$cm^{3}sec^{-1}) *	Relative Rate #
Co^+	1.93	100
$CpCo^+$	0.656	34
$CpCoCO^+$	0.262	14

* Calculated from total decay rate constant of reacting cation; all data ± 30%

Relative to Co^+ rate taken as 100; all data ± 10%

Class 2. Ion-molecule reactions with transfer of various ligands from neutral molecule to ion, or condensation. Principal reactions of each fragment ion are as follows:

Primary fragment ion reactions:

$CpCo(CO)_{0,1,2}^+ + CpCo(CO)_2 \rightarrow Cp_2Co^+ +$ neutral fragments

$CpCoCO^+ +$ " $\rightarrow CpCoCOH^+ +$ "

$CpCo(CO)_2^+ +$ " $\rightarrow CpCo(CO)_2H^+ +$ "

$CpCo(CO)_2^+ +$ " $\rightarrow CpCo(CO)_{3,4}^+ +$ "

The preceding reactions involve transfer of Cp, H or CO ligands from neutral molecule to reactive cation.

Secondary ion condensations:

$CpCo(CO)_{1,2}H^+ + CpCo(CO)_2 \rightarrow (CpCo)_2(CO)_{2,3}^+ +$ "

These preceding reactions involve simultaneous condensation of the cation with a neutral molecule, and ejection of hydrogen and carbonyl ligands.

Condensation with the parent neutral molecule and generation of multi-metal core clusters has been a prominent feature in each of the vanadium, chromium, manganese and iron aryl transition-metal carbonyl systems as well (Chapters 2-5). However, in this cobalt system, condensation proceeds via the hydrogenated intermediates $CpCo(CO)_{1,2}H^+$ and terminates with bicobalt clusters; further condensations and generation of cluster ions containing Co_3 or Co_4 cores are not observed. In this $CpCo(CO)_2$ system, condensation must compete with formation of electronically stable (18 electron), kinetically unreactive Cp_2Co^+ by Cp ligand transfer from neutral molecule to reactive cations.

The cluster cations, Cp_2Co^+ and $Cp_2Co_2(CO)_{2,3}^+$ are unreactive for 25 seconds. In contrast with the work of Jones and Staley[23], (where cyclopentadiene was present in the reaction chamber, producing complicating cyclopentadienyl dimer ions and Cp adduct ions in the mass spectra), cyclopentadiene dimers and their cluster products were not observed in the present mass spectra. In this study the predominant clustering channels

proceed solely via the hydrogenated intermediates, i.e., $CpCo(CO)_{1,2}H^+$. Since all of the final cation products possess very low coordination unsaturation (i.e., Cp_2Co^+ possesses 18 electrons per central cobalt atom; $CpCo(CO)_2H^+$, 18 electrons; $Cp_2Co_2(CO)_{2,3}^+$, 16.5 and 17.5 electrons per central metal respectively, assuming singly-bonded cobalt in the bimetal clusters) further condensations are apparently kinetically unfavorable and indeed are not seen here.

As observed earlier in other systems, as well as in the V, Cr, Mn, and Fe systems studied here, ion-molecule reactivity rates in the Co system depend strongly upon electron deficiency of the central metal atom. This generalisation is especially true in the cobalt system. Figure 6.9 illustrates this: pseudo-first order rate constants for disappearance of each reactant cation are plotted against electron deficiency per cobalt atom and show a well-behaved relationship, with a steep slope at electron deficiencies between zero and one. In contrast with the four other metal systems studied here, clustering reactions in the Co system appear to be of minor importance compared to ligand (H, Cp or CO) or electron transfer from the parent neutral molecule. The dominant reaction channels in this cobalt system are those in which 18-electron configuration is approached or achieved, as for example, via the single ligand transfer reactions shown above.

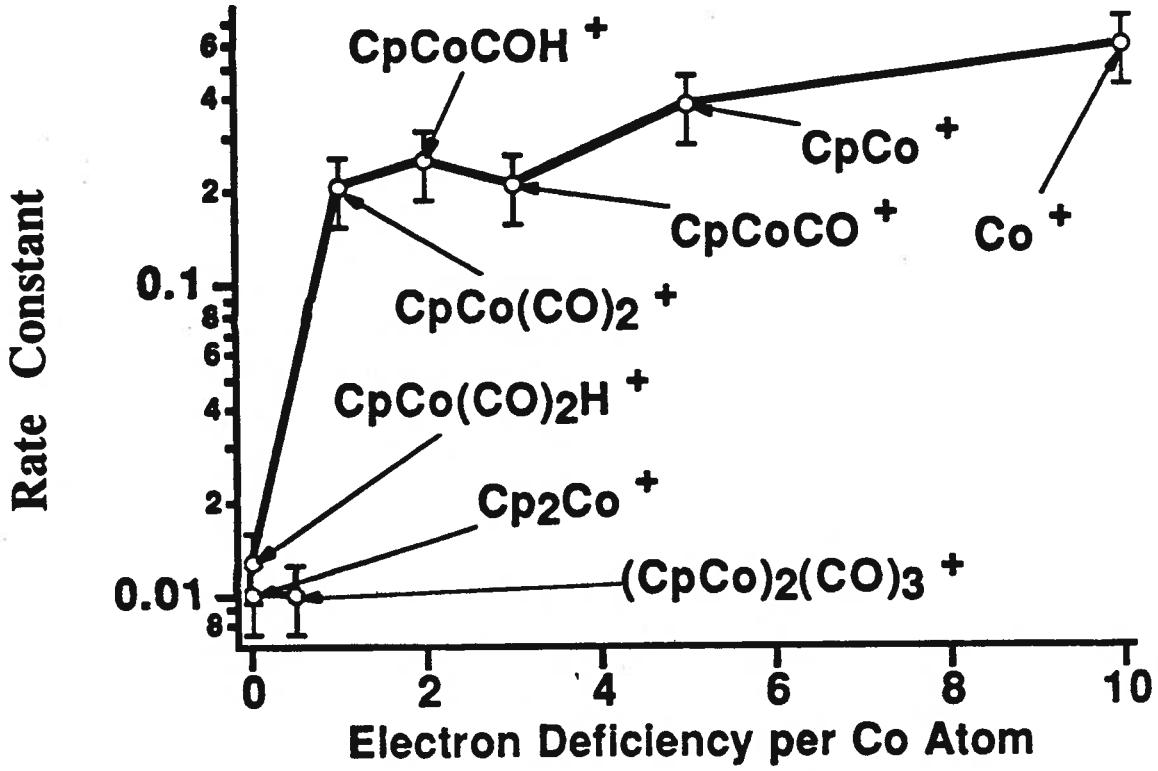

Figure 6.9. Relationship Between Reactivity and Electron Deficiency for Cations in the $CpCo(CO)_2$ System

2. Reactions with Gases N_2, CO, and CO_2

At pressures of $6x10^{-7}$ torr, all three reagent gases underwent electron ionisation, followed by hydrogen species exchange with neutral $CpCo(CO)_2$ molecules, as follows:

1. Nitrogen Reactions*

$N_2^+ + CpCo(CO)_2 \rightarrow N_2H^+ + ..$ (H atom transfer)

$N_2H^+ +$ " $\rightarrow CpCo(CO)_{1,2}H^+ + ..$(Proton transfer)

Temporal behaviour of N_2^+ and its principal products is shown in Figure 6.10.

(* pseudo-first kinetic order in N_2^+ and N_2H^+)

2. Carbon Monoxide Reactions*

$CO^+ + CpCo(CO)_2 \rightarrow COH^+ + ..$ (H atom transfer)

$COH^+ +$ " $\rightarrow CpCo(CO)_{1,2}H^+ + ..$(Proton transfer)

Temporal behaviour of CO^+ and its principal products is shown in Figure 6.11.

(* pseudo-first kinetic order in CO_2^+ and COH^+)

3. Carbon Dioxide Reactions*

$CO_2^+ + CpCo(CO)_2 \rightarrow CO_2H^+ + ..$ (H atom transfer)

$CO_2H^+ +$ " $\rightarrow CpCo(CO)_{1,2}H^+ + .$ (Proton transfer)

Temporal behaviour of CO_2^+ and its principal products is shown in Figure 6.12.

(* pseudo-first kinetic order in CO_2^+ and CO_2H^+)

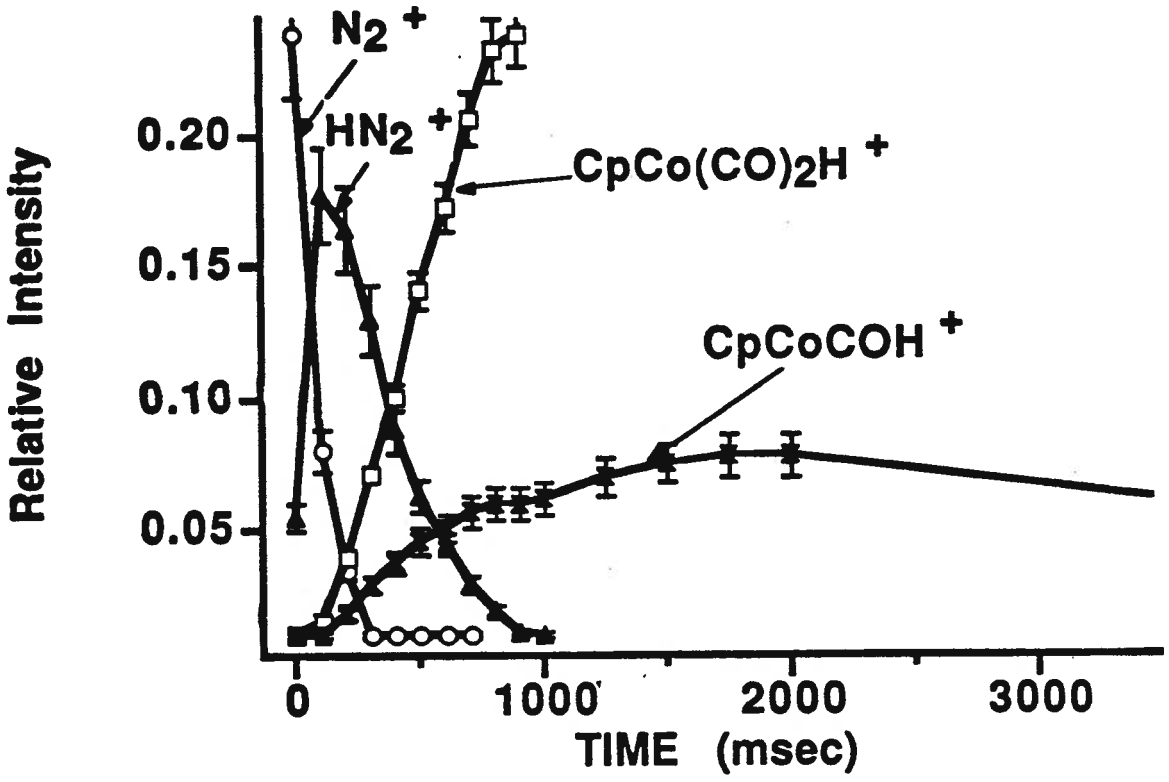

Figure 6.10. Temporal Behaviour of N_2^+ and Cation Products: p (N_2) = 6.0×10^{-7} torr; p($CpCo(CO)_2$) = 6.0×10^{-8} torr

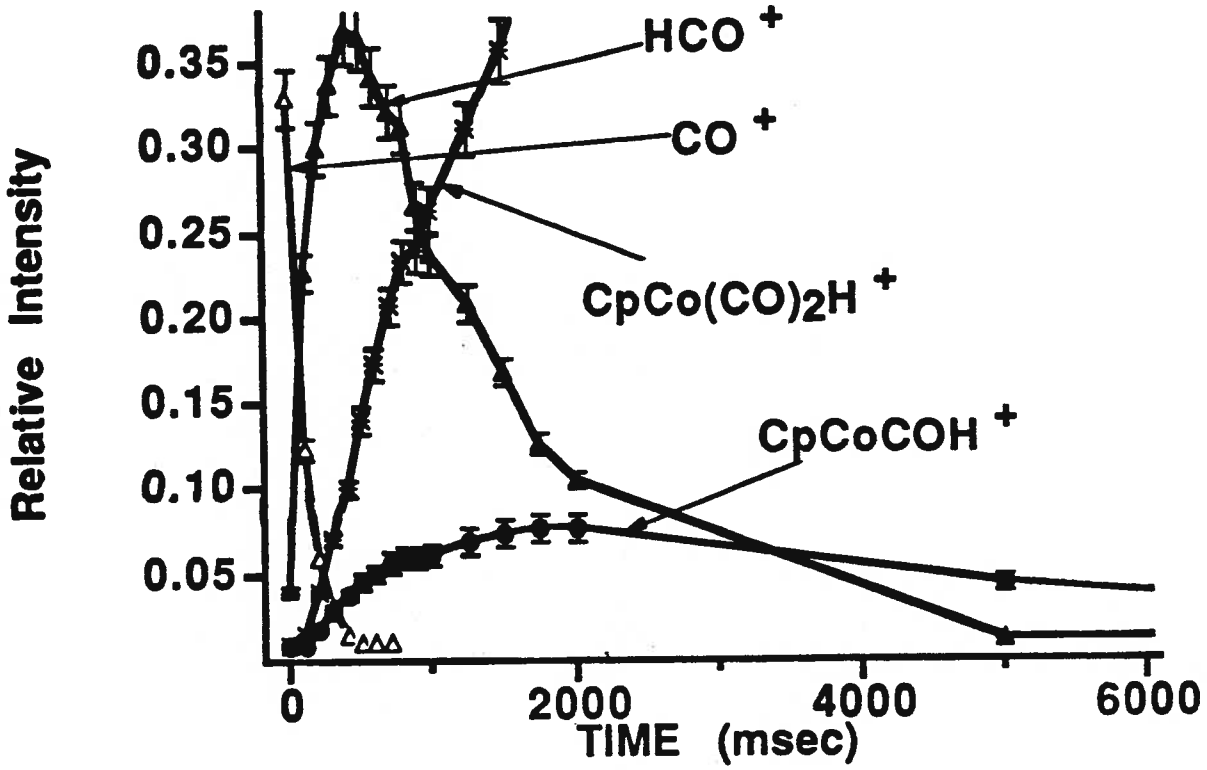

Figure 6.11. Temporal Behaviour of CO^+ and Cation Products: $p(CO) = 6.0 \times 10^{-7}$ torr; $p(CpCo(CO)_2) = 6.0 \times 10^{-8}$ torr

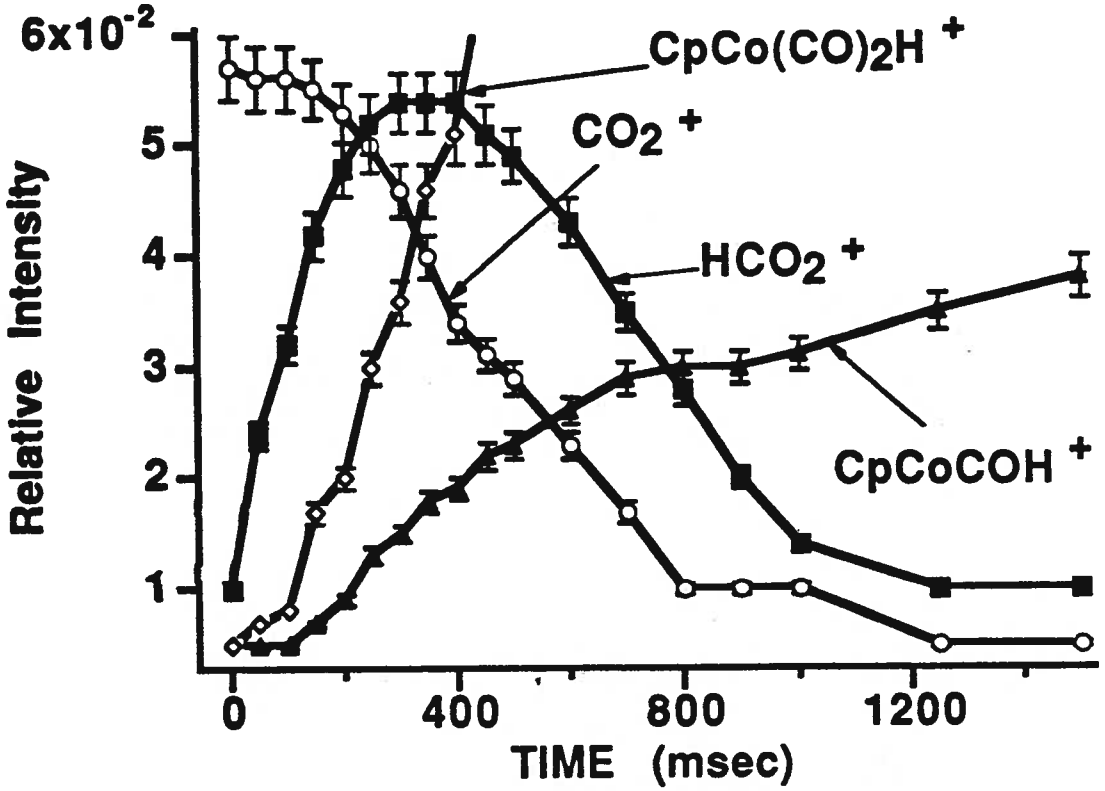

Figure 6.12. Temporal Behaviour of CO_2^+ and Cation Products: $p(CO_2) = 6.0 \times 10^{-7}$ torr; $p(CpCo(CO)_2) = 6.0 \times 10^{-8}$ torr

In each of the preceding three reactant ion sequences, transfer of a hydrogen atom from a neutral molecule to a reagent gas cation is followed by proton transfer to a second neutral molecule. Values for pseudo-first order rate constants (k') obtained from linear semilog plots from data such as in Figures 6.10 - 12 are listed in Table 6.4, along with second order rate constants (k"). These latter quantities were estimated from ambient pressure of neutral $CpCo(CO)_2$, assuming that concentration of the latter reactant ($CpCo(CO)_2$) remains always in large excess of the ion reactant (i.e., N_2^+, CO^+, etc.) formed from electron ionisation of N_2, CO or CO_2.

Calculated values of second order rate constants listed in Table 6.4 are close to the upper (theoretical collision) limit for bimolecular ion-molecule reactions in the gas phase (10^{-9} molecule^{-1}cm^{3}sec^{-1})[16], and are comparable with rates measured earlier for other small cation-molecule interactions(10^{-11} - 10^{-9} molecule^{-1}cm^{3}sec^{-1})[4,43,46]. In each sequence of reactions, the predominant final cation product is $CpCo(CO)_2H^+$ (18 electrons); again, the abundance of this product ion reflects its inherent electronic stability in the gas phase. The first reaction in each sequence involves abstraction of a hydrogen atom from the Cp ligand of $CpCo(CO)_2$. The second reaction involves proton transfer from the newly-hydrogenated reagent gas cation (N_2H^+, COH^+ or CO_2H^+) to the cobalt center in another neutral molecule, generating the final product cation, $CpCo(CO)_{1,2}H^+$. The existence of proton transfer from N_2H^+, COH^+ and CO_2H^+ permits an approximation of the proton affinity of CpCoCO and $CpCo(CO)_2$ moieties: since proton affinities of N_2, CO_2 and CO are 117.4, 128.6, and 141.4 kcal/mole respectively[15], proton affinities of the two cobalt species must therefore be at least 140 kcal/mole. On the other hand, hydrogen atom affinities of N_2^+, CO^+ and CO_2^+ must be larger than that of $CpCo(CO)_2$ in order for intermediates N_2H^+, COH^+ and CO_2H^+ to be detected and quantified.

TABLE 6.4

Relative Rates of Reaction of $CpCo(CO)_2$ with Some Small Molecules

Reactant Ion	k' (sec^{-1})	k" ($molec.^{-1}cm^3sec^{-1}$)*
N_2^+	10.4	3.4×10^{-8}
HN_2^+	3.74	1.2×10^{-8}
CO^+	6.98	2.3×10^{-8}
HCO^+	7.65	2.5×10^{-8}
CO_2^+	2.11	6.9×10^{-9}
HCO_2^+	2.17	7.1×10^{-9}

* Estimated from ambient $CpCo(CO)_2$ pressure = 6.0×10^{-8} torr
Temperature 300°K; pressure of reactant gas = 6.0×10^{-7} torr
all data ± 30%

2. Negative Ion Chemistry

Under 2.5 eV electron impact and at 6.0×10^{-8} torr gauge pressure, only the negative ions $CpCoCO^-$ (17 electrons) and parent anion $CpCo(CO)_2^-$ (19 electrons) were generated as follows: $CpCoCO^-$ = 49%; $CpCo(CO)_2^-$ = 41%. This distribution is consistent with measurements made by Beauchamp using 70 eV EI[7]: $CpCoCO^-$ = 16%; $CpCo(CO)_2^-$ = 84%. Further reaction of $CpCoCO^-$ with the parent neutral produced only one anion cluster, $Cp_2Co_2(CO)_2^-$ (17.5 electrons per metal). Both parent anion, $CpCo(CO)_2^-$ and cluster anion, $Cp_2Co_2(CO)_2^-$ were unreactive for 25 seconds. An example of a FT-ICR negative ion mass spectrum of $CpCo(CO)_2$, measured at 500 msec, is shown in Figure 6.13; and the temporal behaviour of these anions is illustrated in Figure 6.14 on the following page.

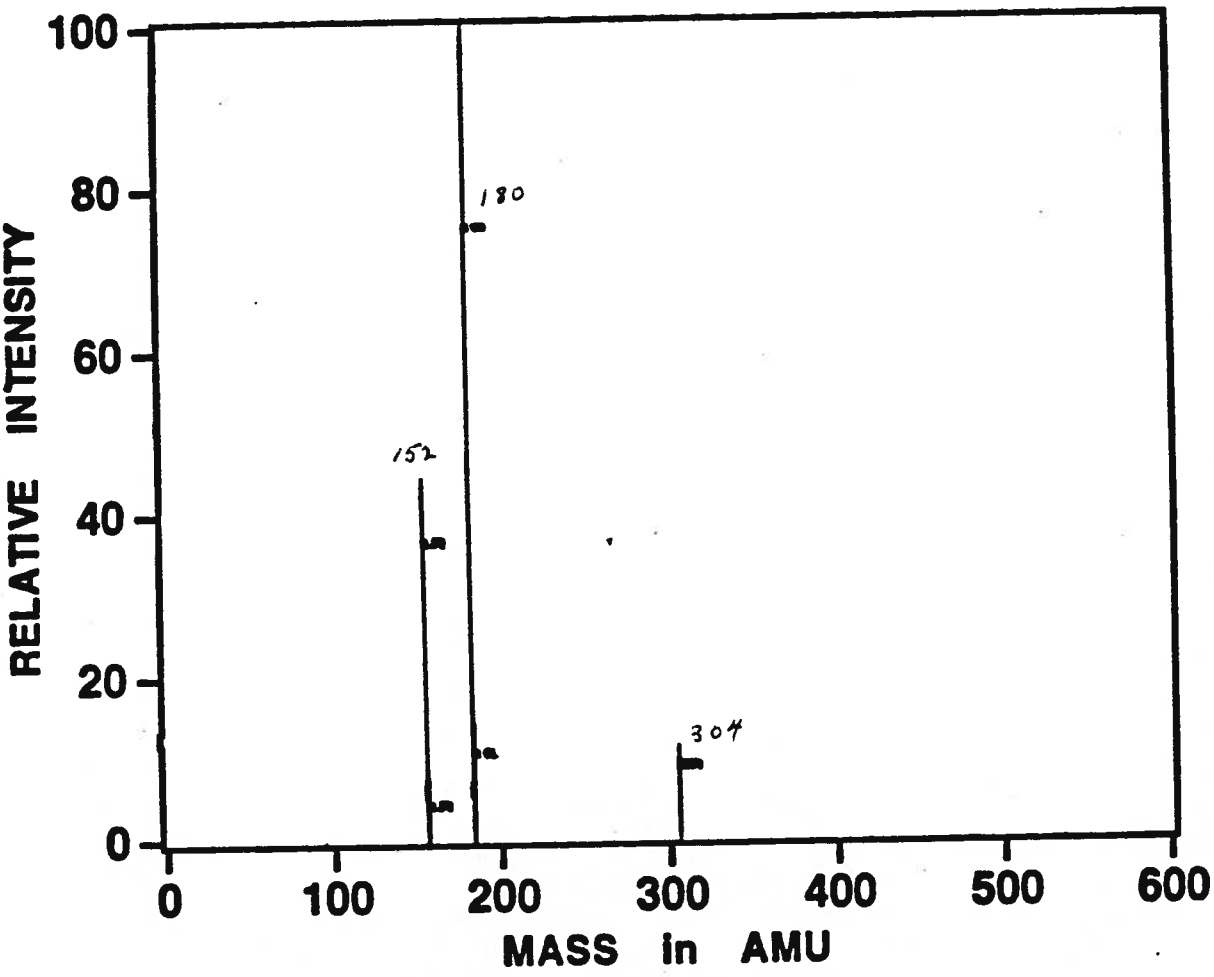

Figure 6.13. FT-ICR Negative Ion Mass Spectrum of $CpCo(CO)_2$; 500 msec.; 2.5 eV; $p = 6.0 \times 10^{-8}$ torr

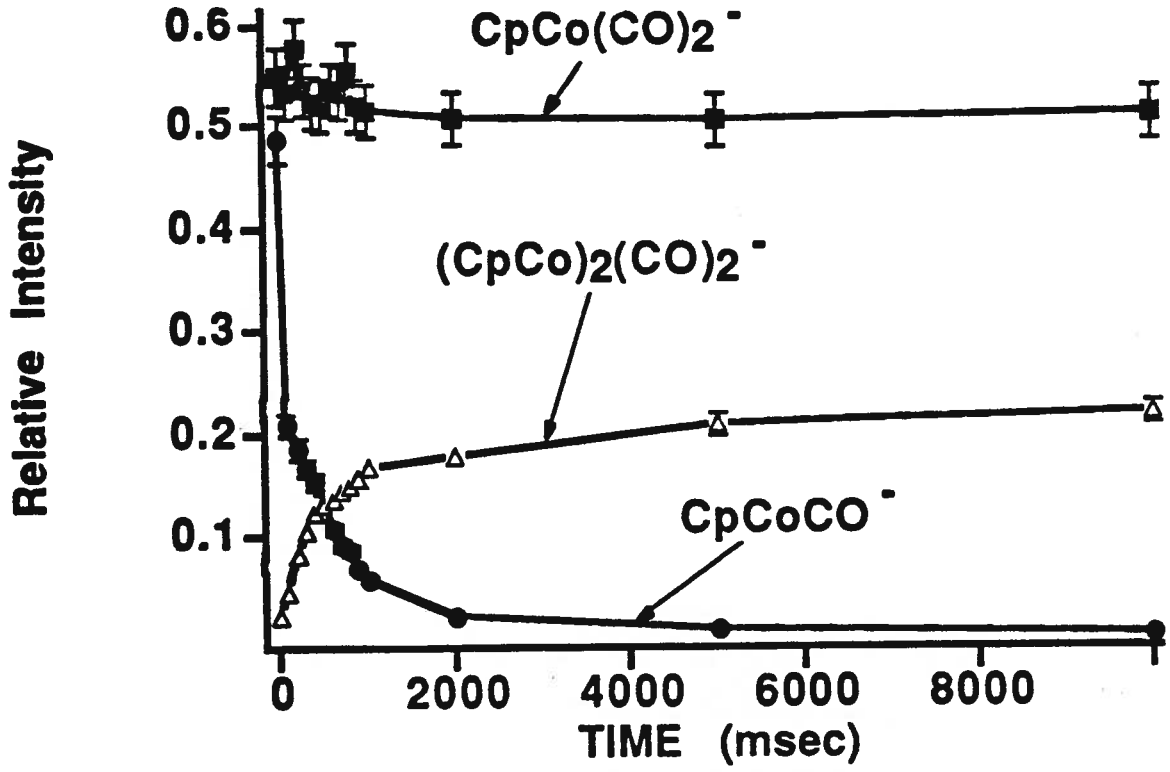

Figure 6.14. Temporal Behaviour of Primary Fragment Anions of $CpCo(CO)_2$

The only observable reaction of the anion daughter fragments in this system is that of condensation of $CpCoCO^-$ with its parent neutral molecule:

$$CpCoCO^- + CpCo(CO)_2 \rightarrow Cp_2Co_2(CO)_2^- + CO$$

Like positive ions in this $CpCo(CO)_2$ system, as well as all of the negative ions studied in the vanadium, chromium, manganese and iron systems, a tendency toward possession of an 18-electron metal core configuration appears to govern the negative ion chemistry of $CpCo(CO)_2$. The Co-Co bond within the binuclear cluster $Cp_2Co_2(CO)_2^-$ is known to be unusually short for a single bond, thus increasing the electron density of each cobalt atom to nearly 18 electrons, resulting in notable stability[36,41].

4. Reactions with Gases N_2, CO, and CO_2

At reagent pressures of 10^{-7} torr, charge exchange, adduct formation or further anion condensation reactions were not observed in the presence of N_2, CO, or CO_2 reagent gases. Although the $Cp_2Co_2(CO)_2^-$ cluster is notably unreactive, the lack of observed reactivity may also be kinetic, a result of low anion concentration and low reagent gas pressures.

III Conclusions

GENERAL FEATURES OF THE $CpCo(CO)_2$ SYSTEM

1) All of the daughter cations initially formed by electron impact on $CpCo(CO)_2$ are chemically reactive with the parent neutral molecule, whereas only one daughter anion, $CpCoCO^-$, is reactive. In general the abundance distribution of these ions after formation

by electron impact is in agreement with appearance potentials in the literature[38]. Sequential elimination of one or two carbonyl ligands requires approximately 2.5 eV each; while rupture of the much stronger CpCo linkage requires at least 7 eV; therefore the most prominent ions in the mass spectrum using low energy electron ionisation (25 eV) are expected to be the parent ion $CpCo(CO)_2^+$, completely and partially decarbonylated ions; i. e., $CpCo^+$ and $CpCoCO^+$, as well as the bare Co^+ cation.

2) All of the daughter cations, Co^+, $CpCo^+$, and $CpCoCO^+$ undergo electron transfer with the parent neutral molecule, producing $CpCo(CO)_2^+$. Relative rates of these processes were listed in Table 6.3. The bare metal cation Co^+ reacts principally by electron transfer, like V^+ in the $CpV(CO)_4$ system.

3) Three cations, $CpCo^+$, $CpCoCO^+$ and $CpCo(CO)_2^+$ apparently can abstract one Cp ligand from a neutral molecule, rupturing the Cp-Co linkage and generating Cp_2Co^+. This latter cation, an extremely stable 18 electron species, becomes one of the predominant products in later mass spectra, whereas in the other four metal systems, formation of $aryl_2metal^+$ (i.e., Cp_2Mn^+, Bz_2Cr^+, etc.) was of minor importance. Electronic saturation of the central metal cobalt atom, and consequent high kinetic stability of Cp_2Co^+ probably accounts for this.

In all other ion-molecule pathways the Cp-Co linkage is maintained throughout ligand exchange and condensation regimes; i.e., in formation of $CpCo(CO)_2H^+$ and $(CpCo)_2(CO)_{2,3}^+$.

4) Clustering terminates with the formation of bicobalt, $(CpCo)_2^+$ cores at experimental pressures (10^{-6} - 10^{-9} torr); cation cluster fragments containing more than two cobalt atoms were not observed. Cluster termination in this system may be a consequence of ligand crowding around the central cobalt core, electronic saturation of the ion-molecule clusters already formed, or else low neutral molecule pressures dictated by the experimental procedure. Clustering channels compete with the formation of Cp_2Co^+ and clustering routes are constrained by prerequisite formation of the precursor, $CpCo(CO)_2H^+$.

5) The hydrogenated cations $CpCoCOH^+$ (16 electron) and $CpCo(CO)_2H^+$ (18-electron) are important precursors to cluster formation in this cobalt system. Such hydrogenated cations are only of minor importance in the other four systems. This may be simply a reflection of the importance of coordination saturation (i.e. 18-electron configuration) in all species of the later transition elements such as cobalt, nickel and copper. Several other hydrogenated transition metal clusters in solution or as solids are known; for example: $Cr(CO)_3H$[25,26]; $(CpCoH)_4$[33]; $CrCpH(CO)_3$, $TcCp_2H$[9,10]; and $MoCp_2H_2$[13], but gas phase ion-molecule studies of their cluster chemistry have not yet been undertaken.

6) Evidence for participation by excited state daughter ion fragments in this cobalt system, such as was found in the other four systems, was observed only for the bare metal cation, Co^+. For the other reactive cations, pseudo-first order semi-log plots are reasonably linear, unlike the results obtained for the vanadium, chromium and manganese systems. Figure 6.15 on the following page shows a non-linear kinetic semi-log plot for ion Co^+. Similar plots for the larger ions, $CpCo^+$, $CpCoCO^+$, and $CpCo(CO)_2^+$ are reasonably linear, indicating ground state configurations only.

An approximation of 67% population of excited state Co^+ ions was obtained from the extrapolated slope in Figure 6.15. The first excited state (^5F, $4s^1$ configuration) of Co^+ is only 0.43 eV above the ground state (^3F, $4s^0$ configuration) energy[3] so that after ionisation with 25 eV electrons, large numbers of excited Co^+ ions should be present before relaxation can occur. (This is similar to the V^+ case, where the energy difference between the lowest two states is 0.33 eV; and to the Mn^+ case; 1.17 eV[3]). These conclusions are in contrast with those of other authors, wherein reactivity differences between cobalt carbonyl ions such as $Co_4(CO)_4^+$ (which is non-reactive with respect to cyclohexane) and $Co_4(CO)_5^+$ (which is reactive) were attributed to the existence of low-level empty coordination sites on cobalt in the latter ion, rather than to excited state cobalt

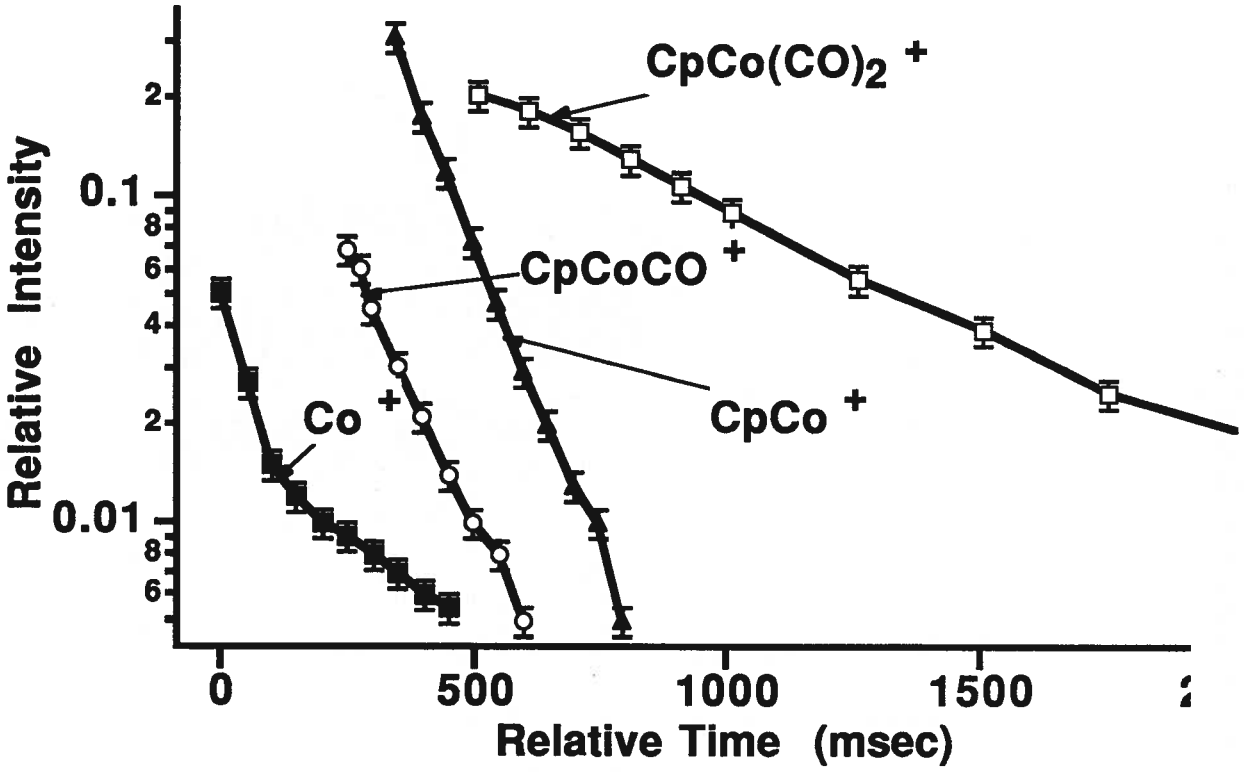

Figure 6.15. Pseudo-First Order Decay Behaviour of Some Cations in the $CpCo(CO)_2$ System

ion reactants[35].

7) Reactions with several addition reagents (e.g., N_2, CO, and CO_2) eventually generated adducts containing one atom of hydrogen, i.e., $CpCo(CO)_2H^+$, typifying the tendency of later transition metals to form complexes with low coordination number. No product cations containing more than one extra, new ligand were observed in this cobalt system.

8) A clastogram showing the appearance of fragment cations of $CpCo(CO)_2$ with electron ionising energies is illustrated in Figure 6.16. Predictably, larger cations predominate at lower energies whereas smaller cation fragments appear at higher energies.

9) Each of the bicobalt cluster ions, $(CpCo)_2(CO)_{2,3}^+$ and $(CpCo)_2(CO)_2^-$ probably consist of central cobalt-cobalt cores surrounded by single Cp and CO ligands, or by bridging CO ligands, like multi-cobalt central core compounds synthesized earlier, such as $Cp_3Co_3(CO)_3$ (King[24]);

$Cp_2Co_2(PPh_2)_2$ (Coleman and Dahl[6]); and $Cp_4Co_4H_4$ (Müller and Dörner[33]). The notable stability of all these condensed phase species, as in the ions $Cp_2Co_2(CO)_2^-$ and $(CpCo)_2(CO)_{2,3}^+$ probably arises from short cobalt-cobalt bond lengths, as well as ligand arrangements[30,36,41].

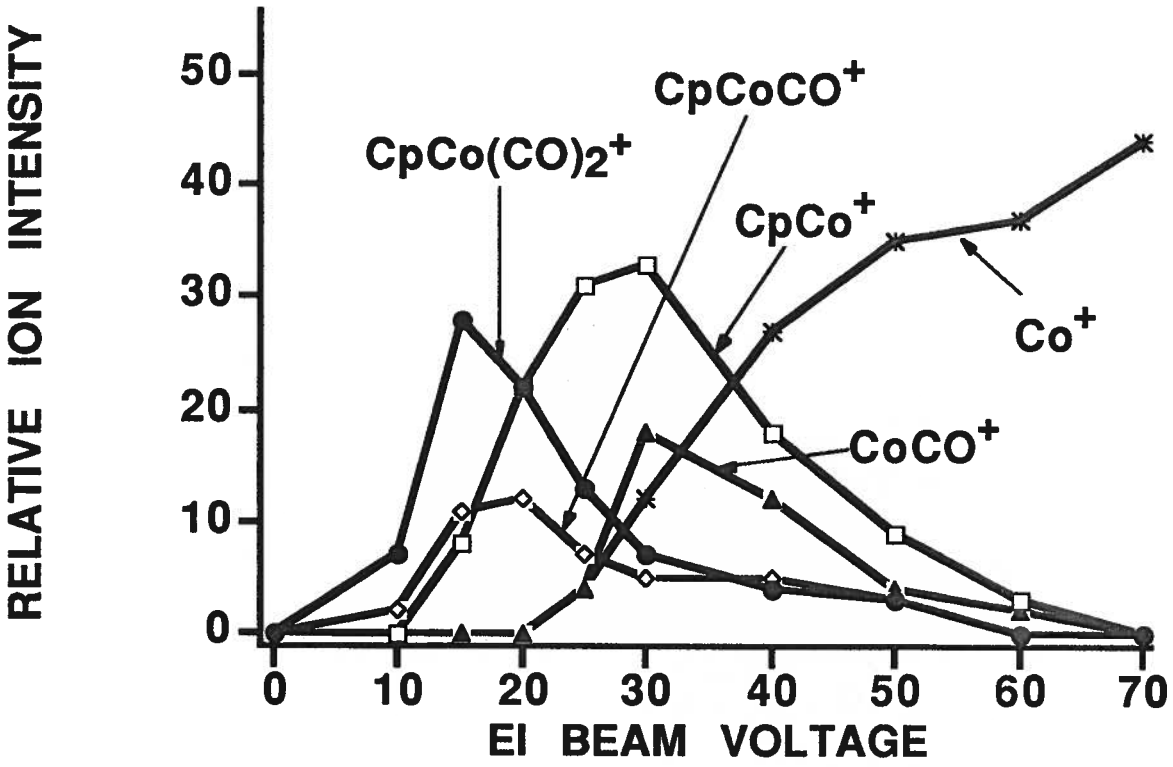

Figure 6.16 Clastogram for Cations of $CpCo(CO)_2$

IV References

(1) Armentrout, P. B.; Halle, L. F.; Beauchamp, J. L. *J. Am. Chem. Soc.* **1981**, *103*, 6624.

(2) Armentrout, P. B.; Beauchamp, J. L. *J. Am. Chem. Soc.* **1981**, *103*, 6628.

(3) Armentrout, P. B. in *Gas Phase Inorganic Chemistry*; Russell, D. H.; Plenum Press, New York, **1989**; pp 1 - 42.

(4) Bricker, D. L.; Russell, D. H. *J. Am. Chem. Soc.* **1987**, *109*, 3910.

(5) Chen, H.; Lin, H.-Y.; Sohlberg, K.; Ridge, D. P. *Ann. Conf. ASMS All. Topics* **1991**, *39*, 1596.

(6) Coleman, J. M.; Dahl, L. F. *J. Am. Chem. Soc.* **1967**, *89*, 542.

(7) Corderman, R. R.; Beauchamp, J. L. *Inorg. Chem.* **1977**, *16*, 3135.

(8) Fischer, E. O.; Jira, R. *Z. Naturforsch.* **1954**, *9B*, 618.

(9) Fischer, E. O.; Hafner, W.; Stahl, H. O. *Inorg. Synth.* **1963**, *7*, 136.

(10) Fischer, E. O.; Schmidt, M. W. *Chem. Ber.* **1969**, *102*, 1954.

(11) Freas, R. B.; Ridge, D. P. *J. Am. Chem. Soc.* **1984**, *106*, 825.

(12) Gord, J. R.; Freiser, B. S. *J. Am. Chem. Soc.* **1989**, *111*, 3754.

(13) Green, M. L. H.; McCleverty, J. A.; Pratt, L.; Wilkinson, G. *J. Chem. Soc.* **1961**, 4854.

(14) Halle, L. F.; Crowe, W. E.; Armentrout, P. B.; Beauchamp, J. L. *Organometallics* **1984**, *3*, 1694.

(15) Harrison, A. G. *Chemical Ionization Mass Spectrometry*; CRC Press: Boca Raton, Florida, **1983**.

(16) Henchman, M. in *Ion-Molecule Reactions*; Franklin, J. L.; Plenum Press, New York, **1972**; pp 101 - 259.

(17) Huttner, G.; Lorenz, H. *Chem. Ber.* **1975**, *108*, 973.

(18) Jacobson, D. B.; Freiser, B. S. *J. Am. Chem. Soc.* **1983**, *105*, 5197.

(19) Jacobson, D. B.; Freiser, B. S. *J. Am. Chem. Soc.* **1984**, *106*, 3900.

(20) Jacobson, D. B.; Freiser, B. S. *J. Am. Chem. Soc.* **1984**, *106*, 3891.

(21) Jacobson, D. B.; Freiser, B. S. *J. Am. Chem. Soc.* **1985**, *107*, 1581.

(22) Jacobson, D. B.; Freiser, B. S. *J. Am. Chem. Soc.* **1986**, *108*, 27.

(23) Jones, R. W.; Staley, R. H. *Int. J. Mass Spectrom. Ion Phys.* **1981**, *39*, 35.

(24) King, R. B. *Inorg. Chem.* **1966**, *5*, 2227.

(25) Lane, K. R.; Squires, R. R. *J. Am. Chem. Soc.* **1985**, *107*, 6403.

(26) Lane, K. R.; Sallans, L.; Squires, R. R. *Organometallics* **1985**, *4*, 408.

(27) Lichtenberger, D. L.; Calabro, D. C.; Kellogg, G. E. *Organometallics* **1984**, *3*, 1623.

(28) Lin, L.; Kutal, C. R.; Amster, I. J. *Ann. Conf. ASMS. All. Topics* **1991**, *39*, 1616.

(29) McDonald, R. N.; Schell, P. L. *Organometallics* **1988**, *7*, 1806.

(30) Mevs, J. M.; Gennett, T.; Geiger, W. E. *Organometallics* **1991**, *10*, 1229.

(31) Mingos, D. M. P.; May, A. S. in *The Chemistry of Metal Cluster Complexes*; Shriver, D. F.; Kaesz, H. D. Adams, R. D.; VCH Publishers, Inc., New York, **1990**; pp 11 - 119.

(32) Müller, J.; Fenderl, K. *Chem. Ber.* **1970**, *103*, 3141.

(33) Müller, J.; Dorner, H. *Angew. Chem., Int. Ed. Engl.* **1973**, *12*, 843.

(34) Oriedo, J. V.; H., R. D. *Ann. Conf. ASMS. All. Topics* **1991**, *39*, 1610.

(35) Pan, Y. H.; Sohlberg, K.; Ridge, D. P. *J. Am. Chem. Soc.* **1991**, *113*, 2406.

(36) Pinhas, A. R.; Hoffman, R. *Inorg. Chem.* **1979**, *18*, 654.

(37) Piper, T. S.; Cotton, F. A.; Wilkinson, G. *J. Inorg. Nucl. Chem.* **1955**, *1*, 165.

(38) Rosenstock, H. M.; Draxl, K.; Steiner, B. W.; Herron, J. T. *Energetics of Gaseous Ions*; American Chemical Society and American Institute of Physics: Washington, D. C., **1977**.

(39) Sallans, L.; Lane, K. R.; Freiser, B. S. *J. Am. Chem. Soc.* **1989**, *111*, 865.

(40) Schilling, J. B.; Goddard III, W. A.; Beauchamp, J. L. *J. Am. Chem. Soc.* **1986**, *108*, 582.

(41) Shore, N. E.; Ilenda, C. S.; Bergmann, R. G. *J. Am. Chem. Soc.* **1977**, *98*, 256.

(42) Simoes, J. A. M.; Beauchamp, J. L. *Chem. Revs.* **1990**, *90*, 629.

(43) Skinner, H. A.; Connor, J. A. *Pure and Applied Chemistry* **1985**, *57*, 79.

(44) Squires, R. R. *J. Am. Chem. Soc.* **1985**, *107*, 4385.

(45) Tsarbopoulos, A.; Allison, J. *Organometallics* **1984**, *3*, 86.

(46) VanOrden, S. L.; Pope, R. M.; Buckner, S. W. *Organometallics* **1991**, *10*, 1089.

(47) Winters, R. E.; Kiser, R. W. *J. Organomet. Chem.* **1965**, *4*, 190.

CHAPTER 7

GENERAL DISCUSSION

AND

CONCLUSIONS

I. General Periodic Trends

First row transition metals consist of those elements with progressively-filled 3d and 4s outer electronic orbitals, from element 21, Scandium on the left side of the series to element 30, Zinc on the right. In general, ionisation energy increases and atomic radius decreases across the period because of the increasing effective nuclear charge exerted on electrons by the atomic nucleus. Coordination number tends to lessen from left to right, as size and therefore space about the metal centre diminishes, and also as outer orbitals become increasingly filled. Consequently, although fewer, metal-ligand bonds generally tend to be stronger in late transition metal complexes (of Ni, Cu and Zn) than in earlier ones (of Sc, Ti andV)[45].

Although transition metal cations are smaller than the corresponding atom because the electronic orbitals are more constrained by the nuclear charges than they are in atoms, anions tend to be larger than their corresponding atom. Moreover, metals on the left hand side of the transition series tend to exhibit a greater variety of cationic oxidation states than do those on the right, owing to their less populated electronic levels as well as weaker effective nuclear charge.

Certain electronic arrangements in transition metal atoms or ions are stabilised by possession of half-full or full electronic orbital configurations. For example, ground state Cr^+ ($3d^5\ 4s^0$) is regarded as being less reactive than neighbouring ground state analogues, Fe^+ ($3d^6\ 4s^1$) or V^+ ($3d^4$)[16,18,40,45,48].

Gas phase metal ion thermochemical data from mass spectrometry were scarce until the development of ion beam[3,13,21,60] and laser techniques[26,32] over the past ten years. These techniques have demonstrated that general trends for gas phase ions across the first transition period are not easily predictable. For example, measured electron affinity (EA) of gaseous metal atoms increases from vanadium (12 kcal/mol) to chromium (15 kcal/mol); then drops markedly for manganese (<0 kcal/mol), thereupon increasing steadily to copper

(28 kcal/mol). Ionisation potentials increase unevenly from scandium (152 kcal/mol) to iron (182 kcal/mol), then decrease to nickel (175 kcal/mol)[24,39].

According to Armentrout and others, strengths of gas phase transition metal cation-ligand bonds (such as M^+-H; M^+-CH_3; M^+-O) increase slightly from vanadium to manganese or iron, then decrease with atomic number to copper (e.g., for Cr^+-H, D=33 kcal/mol; for Fe^+-H, D=50 kcal/mol; for Ni^+-H, D=40 kcal/mol[3,4]).

Squires and Sallans have shown that metal-hydrogen bond strengths (M-H) decrease unevenly from scandium (48 kcal/mol) to iron (30 kcal/mol), then increase to copper (60 kcal/mol), whereas acidities of metal hydrides remain relatively constant across the period (341±5 kcal/mol), because of the compensation of electron affinity values with metal-hydrogen bond strengths[54,60]. Metal-oxygen linkages tend to be especially strong: Cr^+-O, 77 kcal/mol; Fe^+-O, 68 kcal/mol.

Metal-aryl bonds (M-Cp; M-benzene) have been shown thermochemically to be uniformly rather strong (e.g., D=88 kcal/mol for Cp-vanadium; 71 kcal/mol for Cp-iron); whereas metal-CO bonds are uniformly moderately weak (e.g., D=37 kcal/mol for vanadium; 25 kcal/mol for chromium; 33 kcal/mol for cobalt)[17,59,68]. First row transition metal bond strength data from studies of Armentrout, Connor, Freiser and Squires are summarised in Table 7.1[3,4,17,26,54,59,60,61,68] on the following page.

TABLE 7.1

Energy Parameters for the First Transition Metal Series*

Metal	Sc	Ti	V	Cr	Mn	Fe	Co	Ni	Cu	Zn
EA[a]	4.4	1.8	12.1	15.4	<0	3.8	15.3	26.7	28.3	<0
IP[b]	151	157	155	156	171	181	181	176	178	216
ΔE[c]	0.31	0.10	0.33	1.52	1.17	0.25	0.43	1.08	2.81	--
M-Cp	--	--	87.6	67.6	50.7	70.7	63.8	58.8	--	--
M-CO	--	--	37	25	24	28.1	32.5	35.1	--	--
M-Bz	--	--	68.1	39.0	--	--	--	--	--	--
M-M	38	30	57	36	10	24	40	61	47	--
M-H	47.5	38	37.9	41.2	<32	29.6	42.2	60	60	20.5
$M\text{-}H^+$	--	--	47.3	27.7	47.5	47.3	44	--	--	--
$M^+\text{-}H$	56.2	54.2	48.2	32.5	48.4	49.8	46.6	39.5	22.1	60
$M^+\text{-}CH_3$	59	58	50	30	51	58	51	47	30	71
$M^+\text{-}O$	--	--	--	77	57	68	65	45	--	--

[a] electron affinity; [b] ionisation potential of the gaseous ion;

[c] energy difference between ground and first excited state of univalent metal cation.

* Values from references 3, 4, 17, 26, 54, 59, 60, 61

All values expressed as kcal/mole at 298 ^oK

II. Kinetic Results

1. General Trends

The present mass spectral measurements on aryl-transition metal-carbonyl complexes generally **reflect the trends seen in earlier studies**; especially with respect to initial fragmentation patterns. Ion-molecule interactions also exhibit patterns which are not inconsistent with the preceding thermodynamic data: for instance; **aryl ligands were persistently unreactive** throughout ion-molecule reactive pathways; **CO ligands are moderately mobile**; and **new bonds were readily generated** through additive or substitutive pathways, either by abstraction of ligands from the neutral molecule, or else by hydrogen, oxygen or other substituent insertion by reactive small molecular gases. Final ion products typically tended to retain aryl-metal stoichiometry, maintain low carbonyl content, and **general reactivity varied with electron deficiency of the central metal**; i.e., in all five aryl transition-metal systems, the chemical behaviour of ions varied approximately with electronic density about the central metal.

In all five systems, since cations are more electron deficient than corresponding anions; **cation-molecule chemistry was rich**, with reactant ions undergoing multiple, simultaneous interactive pathways. Except for the five molecular ions, all cations reacted in one of two modes: either by accepting an electron from the neutral molecule (charge transfer); or by condensing with a neutral molecule to produce successively larger cluster ions (clustering).

In contrast with cation-molecule chemistry, in all five systems **anion-molecule chemistry was limited** to relatively simple clustering or ligand exchange, whence only one or two unreactive anion products were generated. This aryl-metal-carbonyl anion

chemistry contrasts with that of metal-carbonyl anion systems, in which multiple, interacting pathways have been observed[1,25,36,46,65,66].

Reaction rate constants were evaluated by conventional procedures[27] outlined in the Appendix, by assuming that concentrations of the parent neutral molecule are always much larger than that of any reacting ion generated either during the electron ionisation or by subsequent ion-molecule interactions in the FTICRMS reaction cell. Pseudo-first order rate constants were obtained from linear slopes of the semilog rate plots for each reactive cation. Values of these rate constants (ln k') were plotted against electron deficiency in Figures 2.18, 3.11, 4.11, 5.10 and 6.9, each one illustrating a monotonic trend of reactivity as a function of electron deficiency or coordination unsaturation for the suite of cations generated in each system.

Second order rate constants for the bimolecular ion-molecule reactions were estimated by assuming that initial concentrations are zero for all other cations except the ion of interest: a condition occurring directly after multiple resonance ejection of all ions except the reactant cation in question. The proportion of any ion product present in a product mixture at several subsequent time periods was used to obtain its rate of formation. Second order rate constants were computed using neutral reactant gas concentrations estimated by methods of Bartmess[6,7] and Chen[15] using molecular polarisibility values as determined by Aroney and Le Févre.

Tables of calculated **second order rate constants** (k_A, k_B, etc.) and **relative rate constants** ($100k'_B / k'_A$; $100k'_C / k'_A$; etc.) are listed for reactions of vanadium cations in Table 2.2 - 5 in Chapter 2; for chromium cations, Table 3.2 in Chapter 3; for manganese cations, Table 4.2 in Chapter 4; for iron cations, Table 5.2 in Chapter 5; and for cobalt cations, Table 6.2 in Chapter 6. **A summary of second order reaction rate constants** for cations in the five metal systems is presented in the tables on the following pages. Table 7.2 lists absolute decay rates for monometallic cations, their rates

TABLE 7.2

Comparative Rates for Transition Metal Ions (Monometallic)

1. Cation decay rates ($x10^9$ molec.$^{-1}$cm^{3}sec^{-1})*

Metal	M^+	ArM^+	$ArMCO^+$	$ArM(CO)_2^+$	$ArM(CO)_3^+$	$ArM(CO)_4^+$
V	2.61	1.65	0.98	0.52	0.12	0.043[e]
Cr	2.33	1.54	1.23	0.93	<0.05	----
Mn	2.02	1.49	0.80	0.70	0.18[e]	----
Fe	1.49	1.24	1.16	0.66	<0.05	----
Co	1.93	1.26	0.69	0.68	----	

2. Electron transfer rates ($x10^9$ molec.$^{-1}$cm^{3}sec^{-1})*

Metal	M^+	ArM^+	$ArMCO^+$	$ArM(CO)_2^+$	$ArM(CO)_3^+$	$ArM(CO)_4^+$
V	2.61	0.541	0.372	0.238	0.06	----
Cr	1.44	0.848	0.761	0.597	----	
Mn	1.35	0.753	0.361	0.224	----	
Fe	<0.05	<0.05	<0.05	<0.05	----	
Co	1.93	0.656	0.262	----		

3. Cation clustering rates ($x10^9$ molec.$^{-1}$cm^{3}sec^{-1})*

Metal	M^+	ArM^+	$ArMCO^+$	$ArM(CO)_2^+$	$ArM(CO)_3^+$	$ArM(CO)_4^+$
V	< 0.02	1.02	0.355	0.199	0.028	0.017[e]
Cr	0.885	0.691	0.465	0.337	<0.05	
Mn	0.669	0.741	0.441	0.471	<0.05	
Fe	1.49	1.24	1.16	0.66	<0.05	
Co	<0.05	0.60	0.36	0.41	----	

*All data ± 30% ; M = metal ; Ar = aryl group; [e] = excited state only

TABLE 7.3

Comparative Rates for Transition Metal Ions (Bimetallic)

1. Cation decay rates ($x10^9$ molec.$^{-1}$cm^{3}sec^{-1})*

Metal	$(ArM)_2^+$	$(")_2CO^+$	$(")_2(CO)_2^+$	$(")_2(CO)_3^+$	$(")_2(CO)_4^+$
V	1.12	0.91	0.44	0.17	<0.02
Cr	<0.02	<0.02	0.24	0.13	----
Mn	0.36	0.30	0.23	0.17	----
Fe	0.50	<0.04	<0.04	<0.04	----
Co	----	----	----	<0.03	----

2. Electron transfer rates ($x10^9$ molec.$^{-1}$cm^{3}sec^{-1})*

Metal	$(ArM)_2^+$	$(")_2CO^+$	$(")_2(CO)_2^+$	$(")_2(CO)_3^+$	$(")_2(CO)_4^+$
V	0.368	0.273	0.134	0.02	<0.02
Cr	----	----	0.119	0.041	----
Mn	0.076	0.061	0.034	0.072	----
Fe	<0.05	<0.05	<0.05	<0.05	----
Co	----	----	----	----	

3. Cation clustering rates ($x10^9$ molec.$^{-1}$cm^{3}sec^{-1})*

Metal	$(ArM)_2^+$	$(")_2CO^+$	$(")_2(CO)_2^+$	$(")_2(CO)_3^+$	$(")_2(CO)_4^+$
V	0.290	0.411	0.208	0.100	<0.02
Cr	<0.02	<0.02	0.115	0.091	----
Mn	0.281	0.243	0.190	0.152	<0.05
Fe	0.50	<0.04	<0.04	<0.04	----
Co	----	----	----	<0.03	----

*All data ± 30% ; M = metal ; Ar = aryl group

TABLE 7.4

Comparative Rates for Transition Metal Ions (Trimetallic)

1. Cation decay rates ($x10^9$ molec.$^{-1}$cm^{3}sec^{-1})*

Metal	$(ArM)_3^+$	$(")_3CO^+$	$(")_3(CO)_2^+$	$(")_3(CO)_3^+$	$(")_3(CO)_4^+$
V	----	----	<0.02	0.18	0.32
Cr	----	----	0.10	0.11	----
Mn	----	<0.04	0.07	0.04	----
Fe	----	----	----	----	----
Co	----	----	----	<0.03	----

2. Electron transfer rates ($x10^9$ molec.$^{-1}$cm^{3}sec^{-1})*

Metal	$(ArM)_3^+$	$(")_3CO^+$	$(")_3(CO)_2^+$	$(")_3(CO)_3^+$	$(")_3(CO)_4^+$
V	----	----	----	0.043	<0.02
Cr	----	----	----	----	----
Mn	----	<0.04	0.065	<0.04	----
Fe	----	----	----	----	----
Co	----	----	----	----	

3. Cation clustering rates ($x10^9$ molec.$^{-1}$cm^{3}sec^{-1})*

Metal	$(ArM)_3^+$	$(")_3CO^+$	$(")_3(CO)_2^+$	$(")_3(CO)_3^+$	$(")_3(CO)_4^+$
V	-----	-----	<0.02	0.065	0.26
Cr	-----	-----	<0.02	<0.02	----
Mn	-----	<0.04	<0.04	<0.04	----
Fe	0.50	<0.04	<0.04	<0.04	----
Co	----	----	----	----	----

*All data ± 30% ; M = metal ; Ar = aryl group

of electron transfer, and condensation (clustering) rates; Table 7.3 lists these parameters for bimetallic cluster cations; and Table 7.4, for trimetallic cations.

In the preceding Tables 7.2-7.4, values for pseudo-first order rate constants are accurate to ±10%; however uncertainty in molecular polarisibilities may produce ±30% uncertainty in absolute second order rate constant values.

2. Decay Rates

A comparison of absolute second order decay rate constants of monometallic cations in all five systems is given in the upper section in Table 7.2. In general, **decay rates for reacting cations declines with coordination saturation.** Table 7.2 also shows that for metals with similar coordination, decay rate constants have the same order of magnitude. For example, for the five bare metal cations, decay rate constants vary from 1.5×10^{-9} and 2.6×10^{-9} (molec.$^{-1}$ cm^3 sec^{-1}).

Rate constants for the decay of bimetallic reactant cations are listed in Table 7.3. These rate constants are about one order of magnitude smaller than those of their monometallic counterparts, although just as for the monometallic ions, the general pattern of rate constant attenuation with increasing coordination follows the same trends as for monometallic ions. Table 7.4, presenting all data obtained for trimetallic cations, is included here for completeness, and although incomplete, demonstrates the same trends as shown by mono- and bimetallic cations. These rate constants (10^{-9} - 10^{-10} molec.$^{-1}$cm^{3}sec^{-1}) are of similar magnitude to those determined for other organometallic gas phase systems [14,22,25,34,35,50-2,64]. Most of the second order rate constants reported here are close to predicted Langevin collision rates for unpolarised reactants (10^{-9} molec.$^{-1}$cm^{3}sec^{-1}) indicating that the present processes are probably highly efficient with respect to collisional frequency, and also are strongly accelerated by the polarisability of each neutral molecule as it reacts with cation or anion species[23,30,41,42,50,55,56,64].

3. Electron Transfer Reactions

Electron transfer reactions dominated the chemistry of all cations in the vanadium system, were important in the chromium and manganese systems, were of minor importance or absent in the iron and cobalt systems, as summarised in Tables 7.2-7.4. Table 7.2 lists electron transfer rates for monometallic cations; Table 7.3, for bimetallic cations; and Table 7.4, for trimetallic cations.

Absolute rates of electron transfer for reactive metal ions of equal coordination were of very similar magnitude. For example: for monometallic ion CpV^+, $k = 0.54x10^{-9}$molec.$^{-1}$cm^{3}sec^{-1}, and for $CpCo^+$, $k = 0.66x10^{-9}$molec.$^{-1}$cm^{3}sec^{-1}; for bimetallic ions $(CpV)_2(CO)_2^+$, $k = 0.13x10^{-9}$ molec.$^{-1}$cm^{3}sec^{-1} and for $(BzCr)_2(CO)_2^+$, $k = 0.12x10^{-9}$molec.$^{-1}$cm^{3}sec^{-1}; for trimetallic ions $(CpV)_3(CO)_3^+$, $k = .043x10^{-9}$ molec.$^{-1}$cm^{3}sec^{-1} and for $(CpMn)_3(CO)_2^+$, $k = .065x10^{-9}$molec.$^{-1}$cm^{3}sec^{-1}. For any one metal, rates diminish as coordination increases in each table from right to left (corresponding to periodic table position of the central metal), and as cluster size increases from monometallic ion fragment to bi- and trimetallic cluster.

These trends of **diminishing reactivity apparently reflect the relative electron deficiency of the central transition metal core of each cation** compared with that of its neutral molecule. On the other hand, the tendency of reactive cations across the vanadium-cobalt transition series to undergo charge transfer depends upon the electron-donating property of the aryl ligand as well. For example, 17-electron molecular cations (e.g., $CpV(CO)_4^+$, $BzCr(CO)_3^+$, $CpMn(CO)_3^+$) are important end-products in the rarified gas phase environment within the ICR mass spectrometer, because even though solvating molecules are not present to stabilise them, these cations may be coordination-saturated by partial electron donation from their aryl ligand (and carbonyl ligands) to the metal centre.

Only in the iron system were iron cation fragments inactive with respect to electron transfer from the neutral molecule. In this system, reacting cations preferentially condensed with the neutral molecule instead. Possibly, electron donation from the less-aromatic, η^4-butadienyl ligand to the central iron atom of the molecular cation is not pronounced enough to favour preferential formation and subsequent electronic stabilisation of a 17-electron $BuFe(CO)_3^+$. The principal reactive mode in this iron system is condensation with the parent neutral molecule, with formation of larger clusters, rather than ligand addition or electron exchange with the neutral molecule.

All bare metal cations except Fe^+ reacted by electron transfer; and also, all except V^+ and Co^+ formed asymmetric, metal-rich clusters by condensing with a neutral molecule. Similar reactive patterns in which bare metal cations either condense or absorb electrons have been seen in related systems[14,34,51,52].

4. Condensation (Clustering) Reactions

As is apparent in Tables 7.2-7.4, **cluster formation rates did not vary greatly with central metal present, but diminished with cluster size.** For instance, for monometallic cations $ArMCO^+$, rates vary from 0.36-1.2($x10^{-9}$molec.$^{-1}cm^3sec^{-1}$); for bimetallic cations $(ArM)_2(CO)_2^+$, rates vary from <0.04-0.21($x10^{-9}$molec.$^{-1}cm^3sec^{-1}$); and for trimetallic cations $(ArM)_3(CO)_3^+$, rates vary from <0.02-0.07($x10^{-9}$molec.$^{-1}cm^3sec^{-1}$). No cluster containing more than four aryl-metal units was observed in large quantity. This rate diminution may be due to spatial constraint and ligand saturation in the multi-metal core clusters[33,44,63].

Some cluster ions such as $(CpV)_3(CO)_3^+$, Bz_2Cr^+ and $(CpMn)_3(CO)_2^+$ were relatively long-lived in the gas phase, owing either to electronic stability (e.g., Cp_2Co^+, Bz_2Cr^+), or possibly to multiple metal-metal bonding within the central core, or ligand restructuring and repositioning. Carbonyl ligand saturation around the core may act as a

shield against further reactivity. Such modes of cluster stabilisation, and ligand restructuring in order to increase stability have been examined closely by many authors [2,11,12,19,25,31,37,38,43,65,68].

In all final cluster ion products **carbonyl coordination number remained relatively low** (i.e., 0-6 carbonyls; and typically only 2-4 CO ligands per cluster), indicating that the metal atoms are concentrated in the central cores of the clusters with limited space for carbonyl ligation. Metal-carbonyl linkages, always in the forefront in organometallic studies[11,12,25,36,46,47,62] play an important role in the present studies because of their action as coordination shields about the central metal cores. Tables 7.2-7.4 show rates of clustering for all cations in the five systems.

In all five metal systems, strong, multi-haptic **aryl-to-metal linkages were maintained throughout most of the reaction sequences.** Appearance potentials for EI rupture of these linkages are large: they vary from approximately 12 eV (benzene-chromium) to 20 eV (Cp-vanadium)[24,39]. On the other hand, as seen in all systems the **carbonyl linkage was easily broken** (appearance energies predictably range from 0.5 to 2 eV per metal-CO link[24,39]) both during ionisation as well as during subsequent interactions. Freed from spatial constraint caused by the presence of many carbonyl ligands, reactive centres of aryl-metal cation fragments are able to approach the neutral molecule easily: close approach of a reactant cation to the reactive core of a neutral molecule can favour subsequent electron transfer or formation of a new metal-metal bond, generating a larger cluster product.

The relation between transition metal-carbonyl linking, metal-hydrogen linking and reduction of oxycarbon molecules such as CO is of fundamental importance in understanding the catalytic action of these transition metal centers, which can simultaneously bind and later release both CO and hydrogen. Essential components of reduction catalysts, these metal centres operate both homogeneously as gaseous molecular clusters, as well as heterogeneously, embedded upon solid surfaces.

Many of the reactive ionic species in all five transition metal systems examined here retained, as well as released CO ligands during ion-molecule interactions. Furthermore most, and probably all underwent hydrogen ligation, in which new metal-hydrogen links were generated. Under higher pressures and temperatures, this same activity mimics the heterogeneous catalytic behaviour of cobalt or nickel in Fischer-Tropsch or Raney type catalysis on supported solid surfaces, or in bulk[28,38,47,62,67].

5. Ligand Exchange Reactions

Detailed examination of cation chemistry revealed that for all five metal systems, **many cations underwent ligand exchanges with neutral molecules.** In the **vanadium cation system** alone, **most cations underwent carbonyl transfer reactions.** In the **vanadium, manganese and cobalt** systems, **transfer of hydrogen** from neutral to cation occurred. **Addition reaction pathways were seen in most systems**: reactions with small molecular gases such as CH_4, N_2, H_2 and CO_2 resulted in new, addition product formation. Parallel adduct formation by reactive ions has been studied previously in many systems[1,9,10,20,30,46,61]. Together with electron transfer and cluster formation, generation of hydride addition products such as cations $CpCo(CO)_{1,2}H^+$, $CpV(CO)_4H^+$, etc., is one of the most prominent features of cation-molecule interaction in these metal systems.

Metal-hydride ions are produced here by one of two apparent mechanisms; firstly, by **donation of a proton** from a more acidic cation to one of lesser acidity. An example of this is in the cobalt system, where a protonated nitrogen molecule-cation (N_2H^+) donates a proton to a neutral $CpCo(CO)_2$ molecule, i.e.;

$$N_2H^+ + CpCo(CO)_2 \rightarrow CpCo(CO)_2H^+ + N_2$$

The second mechanism for generation of kinetically stable (i.e., long-lived) hydride ions is **hydrogen atom transfer** (which is equivalent to combined proton and electron

transfer), in which the final product cation becomes stabilised by the addition of the extra electron donated by the hydrogen ligand.

An example of this type of reaction, in the cobalt system, is the formation of $CpCo(CO)_2H^+$ end product from the reactant molecular cation, $CpCo(CO)_2^+$, i.e.;

$$CpCo(CO)_2^+ + CpCo(CO)_2 \rightarrow CpCo(CO)_2H^+ + \text{neutral fragments}$$

6. Excited State Reactions

Evidence for **reactive pathways involving excited state ions was observed in all five of the metal systems** studied. For example, most of the bare metal cations, as well as the $CpV(CO)_4^+$ molecular ion itself, apparently reacted with the neutral molecule before collisional relaxation had occurred. Several other studies, in which ionisation is effected by high energy electrons, have shown the existence of kinetic participation by excited state reactant ions[4,49,53].

All five bare metal cations exhibited non-linear disappearance rates, showing that for each reacting ion at least two species may be participating, most likely a ground state species and at least one excited state species. These relationships were shown in Figures 2.19, 3.12, 4.12, 5.11 and 6.15. As well, in most of the five systems the simple aryl-metal$^+$ cation (CpV^+, $BzCr^+$, etc.) as well as certain other larger cations showed nonlinear kinetic behavior.

Participation by excited state cations occurred in all five metal systems, producing non-linear semi-log kinetic plots which were extrapolated to zero time in order to obtain initial proportions of excited and non-excited state ion concentrations. A list of initial ion abundances in their excited and ground states is shown in Table 7.5 on the following page. Smaller ions in each metal system evidently were more readily excited, while apparently, larger fragment ions remained essentially in ground states during monitored time periods.

Table 7.5

Initial Abundances - Excited State Ions

ION	% excited state*	% ground state*
V^+	45	55
CpV^+	81	19
$CpV(CO)_4^+$	30	70
Cr^+	63	38
$BzCr^+$	42	58
$BzCrCO^+$	45	55
Mn^+	77	23
$CpMn^+$	83	17
$CpMn(CO)_3^+$	48	52
Fe^+	52	48
$BuFe^+$	65	35
Co^+	67	33

*Data calculated from intercepts of semilog rate plots

*Most values ± 25%

Excitation of cation fragments was not unexpected, considering the high energies (at least 25 eV) injected during the electron ionisation process. In the low pressure regimes required experimentally (10^{-6}-10^{-9} torr), collisional relaxation of reactant species does not always have time to occur before ion-molecule interactions have begun. Residual energy may be retained by these and by even larger ions for many milliseconds. Even the molecular ion in both the vanadium and manganese systems also apparently underwent initial excited state reactions, which later subsided.

Excitation may be translational, vibrational-rotational or electronic, although in the case of bare metal ions, only translational or electronic excitation can occur. Because of higher kinetic energies (from translational excitation) or differing electronic configurations (from electronic excitation), excited state bare metal ions would be expected to react more rapidly, or in different modes than their ground state counterparts. Earlier studies have shown both of these behaviour patterns[4,21,15,49,53]. In the present study, only in those cases where both ground state and excited state ions are reactive can evidence of different rates be measured (and consequently, different species distinguished).

In Table 7.5, initial proportions of excited state ions are large, varying from 30% to 83% of total ion populations. In most systems, the smaller ions showed larger proportions of excited states, as in the chromium system where Cr^{+*} = 63%, $BzCr^{+*}$ = 42% and $BzCrCO^{+*}$ = 45%. Since relaxation can occur by vibrations, collisions or ejection of energetic fragments, the larger ions with greater number of vibrational modes and large size should predictably be more rapidly relaxed. Lifetimes of these excited state ions are of the order of milliseconds, this evidence supporting the view that possibly these ions are excited vibrationally or translationally rather than electronically.

III General Conclusions

In summary, **rates of reaction of cations are directly related to electron deficiency of the central metal atoms,** rather than which specific metal is present in the metallic core of the ion. In general, cluster ions having electron counts much less than 18 per metal were highly reactive; and those ions whose electron deficiencies were less than 2 electrons per metal atom were relatively unreactive, reflecting their lack of reactive site accessibility, both electronic and spatial. This behaviour, noted earlier by Ridge[51] and Russell[52], is a prominent feature of the present five systems. The apparently well-behaved relationship between rate constants and electron deficiency of reactant ions is obvious from Figures 2.18, 3.11, 4.11, 5.10 and 6.9. Each of the five plots shows low reactivity of ions with formal 17- or 18-electron per metal counts, as for example, in $CpV(CO)_4^+$, (17 electrons); Bz_2Cr^+ (17 e); $(CpMn)_3(CO)_3^+$, (18 e); $BuFe(CO)_3^+$, (17 e); and $CpCo(CO)_2H^+$ (18 e). Conversely, ions with large electron deficiencies such as CpV^+ (9 e); $CpMnCO^+$ (13 e); $BzCr(CO)_2^+$ (15 e) disappeared rapidly.

All the above five plots show steep slopes for electron deficiencies above two, indicating that reactivity sharply increases when one or two-electron sites are vulnerable to attack by an incoming reactant species: since there is a vacant coordination site for reaction on the surface of the active ion. For vanadium and manganese ions the steep part of the deficiency curve is spread over 0-5 electron deficiency, pointing to a less rigid electronic requirement for incoming reactants.

For chromium and iron ions, ions with electron deficiencies of 1 to 3 show pronounced increase in reactivity, reflecting that 1-, or 2-electron reagents may interact strongly with these ions. For cobalt ions, the increase appears at the one electron deficiency point; exhibiting the strong tendency for cobalt to engage in one-electron interactions. The presence of low-lying vacant or partially-vacant coordination sites for formation of adduct transition states appears to be the governing criterion for all interaction within this

analogous series of complexes. Because the cobalt ions have valence shells which are almost full, (as well as a larger nuclear charge) they are more selective with respect to multi-metal clustering.

Addition of small molecules to ions of the five complexes followed the same "electron deficient" behaviour trend discussed in the preceding paragraph. In all systems, **all five molecular ions are observed to accept readily one hydrogen atom** (in effect, accepting an electron plus a proton), thus **becoming 18-electron species, the hydrogenated molecular cation,** MH^+. Formation of similar hydride species has been observed previously in many systems[3,22,30,35,36,67]; and is especially prominent in the present cobalt system, where $CpCo(CO)_2H^+$ dominates the mass spectra.

Hydrogenated species (e.g., $CpMn(CO)_3H_{1,2}^+$) were also seen in the $CpMn(CO)_3$ system, in which mono- and dihydrogen adducts were generated by reaction with molecular H_2, as was shown in Figure 4.13. Hydrogenation provides greater electronic saturation, and consequently greater gas phase stability for these ions. Again, catalytic hydrogenation or dehydrogenation by a transition metal depends upon its ability to bind and later release hydrogen under specific conditions[4,28,29,60,67]. The pervasiveness of metal-hydrogen cluster fragments in these five systems accentuates the reactivity of hydrogen species with these metals.

Certain **highly-stable species,** formed by abstraction of a ligand from the neutral molecule, **are dominant products** in the mass spectra of all five systems: examples are: cations Cp_2Co^+, Bz_2Cr^+, and $CpMn_2(CO)_2^+$; and anions $Cr(CO)_4^-$, and $Cr(CO)_5^-$. The abundances of these ions emphasise the high stability of the Cp-to-metal, Bz-to-chromium or Cr-to-oxygen linkages. Most of these ions are well known in the literature, having been synthesised in solution and solid phases; a few which have been observed here; i.e., $(CpV)_2(CO)_3^+$, $CpCo(CO)_2H^+$, may be sufficiently stable to be prepared in solution.

Interactions between ligated metal cations and molecular or ionic species of the reagent gases were observed in all systems. Addition reactions were limited kinetically by the low concentrations mandated in FT-ICR, so that in order to examine further addition chemistry, higher reagent gas pressures will be required. In proof, many adduct cations of vanadium were observed in the high pressure DCI experiments using NH_3 and CH_4 chemical ionisation reagent gases, which were not detected at low pressures.

Some FT-ICR-MS evidence of adducts containing N_2, N atoms, O_2, O atoms and H_2 were observed in the vanadium, chromium, manganese and iron systems, but because of very low abundances, or difficulty in interpretation of extremely complex isotopic patterns, could not be quantified. Further study of these and other adducts involving secondary ionisation or secondary resonance ejection techniques will enable a more definitive analysis of their chemistry.

In the cobalt system, ion-molecule interactions involving small reactive cations N_2^+, CO^+, CO_2^+, N_2H^+, COH^+, and CO_2H^+ with neutral $CpCo(CO)_2$ molecules were quantifiable. The overall result of these interactions amounts to abstraction of a hydrogen atom by the small cation from the Cp ligand of one neutral, followed by proton donation to the central cobalt atom of another neutral, creating the extremely unreactive, 18-electron ion, $CpCo(CO)_2H^+$. Similar hydrogen-metal stabilising linkages in some gas phase chromium and iron cation clusters have been proposed by Kan[35] to explain the anomalously large abundance of certain ions.

Proportions of excited state cations are large (Table 7.5), for the smaller fragments generated by EI in all five systems. Excited state cations reacted faster than their nonexcited state counterparts in all cases. The excited molecular ions $CpV(CO)_4^+$ and $CpMn(CO)_3^+$ were reactive, whereas after relaxation (by means of reaction or simply through collisional de-excitation), their nonexcited forms were not, presumably because of stable, 17-electron configurations.

No addition reactions were apparent in the anion systems of any metal selected for this study. This may be solely a result of kinetic factors: i.e., low anion concentrations characteristically produced by EI, and low pressure regimes dictated in FT-ICR procedures. The only exception was seen in the chromium system, where CrO_3^- and CrO_4^- both accepted an additional CO from neutral $BzCr(CO)_3$ molecules. As well, because anions possess greater inherent electron saturation than do their cation counterparts, they are less active kinetically.

IV Further Research Projects

More detailed investigations into ion-molecule interactions of these transition metal compounds should include a quantitive examination of interactions with specific adducts including a study of the kinetics of their formation, using a variety of small molecules such as ammonia, water, oxygen and chlorine, including measurements of absolute reactivity rates. A combination of electron-, proton- and hydrogen atom- (= electron + proton) transfer kinetic studies may enable correlation of the three processes.

Some of the new, fairly unreactive cluster cations found in the five metal systems studied here may be sufficiently stable for isolation in solution; examples are $(CpV)_2(CO)_3^+$; $(CpMn)_3(CO)_3^+$; $(BzCr)_3(CO)_3^+$; and $Bu_2Fe_3(CO)_3^+$.

Other closely-related systems should be examined; for instance, complexes with unstable, or less stable arene ligands than are Cp and benzene, perhaps yielding new evidence of internal restructuring and ligand repositioning for enhancement of stability; complexes of scandium and titanium ('electron-poor' transition metals), and nickel and copper ('electron-rich' transition metals) in the first transition series; homologous complexes of the second and third transition metal series (i.e., Nb, Mo, Ru, Rh); and finally, homologous complexes of the present five metals containing NO, O_2 and N_2 ligands rather than carbonyl ligands only.

Catalytic activity of the vanadium-cobalt series of transition metals has been a subject of enormous interest over many years[1,3,22,26,29,36,54,57,58]. Ability to cleave C-H and C-C bonds varies across the first transition row of transition metals: for example, both V^+ and Cr^+ cleave C-C bonds in ethane to produce methane and MCH_2^+; whereas Fe^+, Co^+ and Ni^+ preferentially cleave C-H in ethane to produce H_2 and $MC_2H_4^+$, reflecting a fundamental mechanistic difference in operation between early and late transition metals[3]. Other reaction products have been demonstrated to vary with transition metal precursors in a similar way[9,10,21]. Greater insight into these and other differing pathways may become accessible with laser excitation and isotopic labelling studies of the metal intermediates in such systems.

Utilising Marcus' theory, electron transfer rates in solution can be predicted from isotope charge exchange reaction rates[41,42,50]. Parallel gas phase rates for the present five systems and similar ones could be determined by FT-ICR without the complication of solvent interference; and rate constants for electron transfer from any neutral molecule to ion would hence be measurable both directly and indirectly. Some self-exchange kinetic studies on metallocene complexes have been performed earlier by Richardson and Eyler[50]. A comparison of large numbers of such data may enable collision efficiency studies in the gas phase, as well as enlarging and extending scales of proton affinities and ionisation potentials for organometallic molecules.

A careful comparison of excited and ground state ion-molecule chemistry over very short time-scales would allow better discrimination between mechanisms of reactivity of ions in excited and ground energy states.

Instrumentally, implementation of a larger magnetic field will permit easier discrimination between closely-spaced, heavier ion masses, such as mono- and di-hydrogenated adducts of multi-nuclear clusters, permitting characterisation of new ion products. Narrow-band ionisation energy (laser) sources will permit determination of bond dissociation parameters.

Thermostatted temperature regulation of the entire ion source assembly, within a temperature range compatible with the instrument, would enable experimental determination of thermodynamic parameters (activation energies, entropies, etc.) of the various reactive pathways. A comparison of such values with those in solution would be of theoretical, as well as of practical interest for synthetic and catalytic studies.

Tandem methods, with appropriate computer programming instrumentation designed to identify and isolate specific secondary ions, followed by laser ionisation of the secondary (or tertiary) ion beam and detection of subsequent products, will enable more precise determination of the fates and the stereochemistries of the larger cluster ions produced in these systems.

Lastly, collisional relaxation techniques[53] employing dual-cell ion chambers, or use of high pressure inert gases will lessen complications caused by the presence of reacting ions in excited states.

V References

(1) Allison, J. *Prog. Inorg. Chem.* **1986**, *34*, 627.

(2) Aradi, A. A.; Fehlner, T. P. *Adv. Organomet. Chem.* **1990**, *30*, 189.

(3) Armentrout, P. B.; Halle, L. F.; Beauchamp, J. L. *J. Am. Chem. Soc.* **1981**, *103*, 6501.

(4) Armentrout, P. B. in *Gas Phase Inorganic Chemistry*; Russell, D. H.; Plenum Press, New York, **1989**; pp 1 - 42.

(5) Aroney, M. J.; Cooper, M. K.; Pierens, R. K.; Pratten, S. J. *J. Organomet. Chem.* **1985**, *295*, 333; Aroney, M. J.; Clarkson, R. M.; Klepetko, R. J.; Masters, A. F.; Pierens, R. K. *J. Organomet. Chem.* **1990**, *393*, 371.

(6) Bartmess, J. E.; McIver, R. T., Jr. in *Gas Phase Ion Chemistry, vol. 2;* Bowers, M. T.; Academic Press, New York, **1979**; pp 87-121.

(7) Bartmess, J. E.; Georgiadis, R. M. *Vacuum* **1983**, *33*, 149.

(8) Beran, J. A.; Kevan, L. *J. Phys. Chem.* **1973**, *73*, 3866.

(9) Bjarnason, A. *Organomet.* **1991**, *10*, 1244.

(10) Bjarnason, A. *Anal. Chem.* **1991**, *61*, 1889.

(11) Bottomley, F.; Grein, F. *Inorg. Chem.* **1982**, *21*, 4170.

(12) Bottomley, F.; Sutin, L. *Adv. Organomet. Chem.* **1988**, *28*, 339.

(13) Brodbelt-Lustig, J.; van Koppen, P.; Bowers, M.; Dearden, J.; Beauchamp, J. *Ann. Conf. ASMS All. Top.* **1989**, *37*, 830.

(14) Chen, S.-P.; Comisarow, M. B. *Ann. Conf. ASMS All. Top.* **1989**, *37*, 323.

(15) Chen, S.-P. *Ph. D. Dissertation* **1992**.

(16) Collman, J. P.; Hegedus, L. S.; Norton, J. R.; Finke, R. G. *Principles and Applications of Transition Metal Chemistry*; University Science Books: Mill Valley, California, **1987**.

(17) Connor, J. A. *Top. Curr. Chem.* **1977**, *71*, 71.

(18) Cotton, F. A.; Wilkinson, G. *Advanced Inorganic Chemistry*; John Wiley and Sons: New York, **1980**.

(19) Cotton, F. A.; Walton, R. A. *Struct. Bond.* **1985**, *62*, 1.

(20) Crabtree, R. H. *Chem. Rev.* **1985**, *85*, 245.

(21) Elkind, J. L.; Armentrout, P. B. *Inorg. Chem.* **1986**, *25*, 1078; Elkind, J. L.; Armentrout, P. B. *J. Chem. Phys.* **1987**, *86*, 1868.

(22) Eller, K.; Schwarz, H. *Chem. Rev.* **1991**, *91*, 1121.

(23) Eyler, J. R.; Richardson, D. E. *J. Am. Chem. Soc.* **1985**, *107*, 6130.

(24) Franklin, J. L.; Dillard, J. G.; Rosenstock, H. M.; Herron, J. T.; Draxl, K.; Field, F. H. *Ionization Potentials, Appearance Potentials and Heats of Formation of Gaseous Positive Ions*; American Chemical Society, American Institute of Physics: Washington, D. C., **1969**.

(25) Fredeen, D. J. A.; Russell, D. H. *J. Am. Chem. Soc.* **1985**, *107*, 3762.

(26) Freiser, B. S. in *Bonding Energetics in Organometallic Compounds*, Marks, T.; American Chemical Society, Washington, D. C., **1990**; pp 55-69.

(27) Frost, A. A.; Pearson, R. G. *Kinetics and Mechanism*; John Wiley and Sons, Inc.: New York, **1953**.

(28) Geusic, M. E.; Morse, M. D.; Smalley, R. E. *J. Chem. Phys.* **1985**, *82*, 590.

(29) Halpern, J. *Inorg. Chim. Acta* **1985**, *100*, 41.

(30) Harrison, A. G. *Chemical Ionization*; Wiley - Interscience: New York, **1984**.

(31) Hoffman, R. *Science* **1981**, *211*, 995.

(32) Jacobson, D. B.; Freiser, B. S. *J. Am. Chem. Soc.* **1985**, *107*, 5870.

(33) Kaldor, A.; Cox, D. M.; Trevor, D. J.; Zakin, M. R. *Metal Clusters*; Trager, F. zu Putlitz, G.; Springer: Berlin, **1986**.

(34) Kan, Z.; Comisarow, M. *Ann. Conf. ASMS All. Top.* **1991**, *39*, 461.

(35) Kan, Z. *private communication* **1992**.

(36) Lane, K. R.; Sallans, L.; Squires, R. R. *Organometallics* **1985**, *4*, 408.

(37) Lauher, J. W. *J. Am. Chem. Soc.* **1978**, *100*, 5305.

(38) Lauher, J. W. *J. Am. Chem. Soc.* **1979**, *101*, 2604.

(39) Levin, R. D.; Lias, S. G. *Ionization Potential and Appearance Potential Measurements*; NSRDS-NBS; U. S. Department of Commerce: Washington, D. C., **1982**.

(40) Lukehart, C. M. *Fundamental Transition Metal Organometallic Chemistry*; Geoffroy, G. L.; Brooks/Cole Publishing Company: Monterey, California, **1985**.

(41) Marcus, R. A. *J. Phys. Chem.* **1963**, *67*, 853.

(42) Marcus, R. A. *Ann. Rev. Phys. Chem.* **1966**, *15*, 155.

(43) Mingos, D. M. P.; May, A. S. in *Structural and Bonding Aspects of Metal Cluster Chemistry*; Shriver, D. F.; Kaesz, H. D. Adams, R. D.; VCH Publishers, New York, **1990**; pp 11 - 119.

(44) Mingos, D. M. P.; Slee, T.; Zhenyang, L. *Chem. Revs.* **1990**, *90*, 383.

(45) Owen, S. M.; Brooker, A. T. *A Guide to Modern Inorganic Chemistry*; John Wiley and Sons: New York, **1991**.

(46) Pan, Y. H.; Ridge, D. P. *J. Am. Chem. Soc.* **1989**, *111*, 1150.

(47) Pearson, R. G. *Inorg. Chem.* **1984**, *23*, 4675.

(48) Pruchnik, F. P. *Organometallic Chemistry of the Transition Elements*; Fackler Jr., J. P.; Plenum Press: New York, **1990**.

(49) Reents, J., W. D. ; Strobel, F.; Freas, R. B.; Wronka, J.; Ridge, D. P. *J. Phys. Chem.* **1985**, *89*, 5666.

(50) Richardson, D. E.; Christ, C. S.; Sharpe, P.; Eyler, J. R. *J. Am. Chem. Soc.* **1987**, *109*, 3894; Richardson, D. E. *J. Phys. Chem.* **1986**, *90*, 3697.

(51) Ridge, D. P.; Meckstroth, W. K. in *Gas Phase Inorganic Chemistry*; Russell, D. H.; Plenum Press, New York, **1989**; pp 93-113.

(52) Russell, D. H.; Fredeen, D. A.; Tecklenburg, R. E. in *Gas Phase Inorganic Chemistry*; Russell, D. H.; Plenum Press, New York, **1989**; pp 115-135.

(53) Russell, D. H. *Ann. Conf. ASMS All. Top.* **1990**, *38*, 1261.

(54) Sallans, L.; Lane, K. R.; Squires, R. R.; Freiser, B. S. *J. Am. Chem. Soc.* **1987**, *107*, 4379.

(55) Schildcrout, S. *J. Chem. Phys.* **1969**, *51*, 4055.

(56) Schildcrout, S. M. *J. Am. Chem. Soc.* **1973**, *95*, 3864.

(57) Schultz, R. H.; Elkind, J. L.; Armentrout, P. B. *J. Am. Chem. Soc.* **1988**, *110*, 411.

(58) Simoes, J. A. M.; Beauchamp, J. L. *Chem. Revs.* **1990**, *90*, 629.

(59) Skinner, H. A.; Connor, J. A. *Pure Appl. Chem.* **1985**, *57*, 79.

(60) Squires, R. R. *J. Am. Chem. Soc.* **1985**, *107*, 4385.

(61) Squires, R. R.; Lane, K. R. in *Gas Phase Inorganic Chemistry*, Russell, D. H.; Plenum Press, New York, **1989**; pp 43-91.

(62) Sung, S.-S.; Hoffman, R. *J. Am. Chem. Soc.* **1985**, *107*, 578.

(63) Teo, B. K.; Longoni, G.; Chung, F. R. K. *Inorg. Chem.* **1984**, *23*, 1257.

(64) VanOrden, S. L.; Pope, S. M.; Buckner, S. W. *Organometallics*, **1991**, *10*, 1089.

(65) Wronka, J.; Ridge, D. P. *J. Am. Chem. Soc.* **1984**, *106*, 67.

(66) Wronka, J.; Forbes, R. A.; Laukien, F. H. *Int. J. Mass Spectrom. Ion Proc.* **1988**, *83*, 23.

(67) Zakin, M. R.; Cox, D. M.; Whetten, R. L.; Trevor, D. J.; Kaldor, A. *Chem. Phys. Lett.* **1987**, *135*, 223.

(68) Ziegler, T.; Tschinke, V. in *Periodic Trends in the Bond Energies of Transition Metal Complexes*; Marks, T.; American Chemical Society, Washington, D. C., **1990**; pp 279-292.

Appendices

Appendix I

Kinetic Development

For all five systems **reaction rate constants** were evaluated by assuming that concentrations of the parent neutral molecule, [M], were always much larger than that of any reacting ion, $[I^+]$, generated either during the electron ionisation or by subsequent ion-molecule interactions. In any sequence of ion-molecule reactions involving ion I^+ and neutral molecule M;

$$I^+ + M \Rightarrow A^+ + X \qquad \text{(Rate constant } k_A\text{)}$$
$$I^+ + M \Rightarrow B^+ + Y \qquad \text{(} \quad " \quad k_B\text{)}$$
$$I^+ + M \Rightarrow C^+ + Z \qquad \text{(} \quad " \quad k_C\text{)}$$

where $k_{A,B,C}$ are second-order rate constants for the reactions, A^+, B^+, C^+ are product ions and X, Y, Z are uncharged products. Accordingly, the decay rate of I^+ will be

$$-d[I^+]/dt = k_A [I^+][M] + k_B [I^+][M] + k_C [I^+][M]$$
$$= (k_A + k_B + k_C)[I+][M]$$
$$= k [I^+][M] \quad \text{where } k = \text{the overall second order rate constant for}$$

decay of ion I^+.

1. Evaluation of Pseudo-First Order Rate Constants (k')

If the concentration of neutral molecules, $[M] >> \Sigma [I^+]$, the sum of all the ion fragments generated by electron ionisation, which is assumed to be valid in FT-ICR-MS; then [M] will remain relatively constant with time.

Therefore let

$$k_A[M] = k'_A ; \; k_B[M] = k'_B ; \text{ and } k_C[M] = k'_C$$

where k'_A, k'_B, k'_C are pseudo-first order rate constants in the preceding equation, and let

$$(k'_A + k'_B + k'_C) = k'$$

where **k' is the total pseudo-first order rate constant** for disappearance of $[I^+]$.

Then $-d[I^+]/dt = (k_A' + k_B' + k_C')[I^+] = (k')[I^+]$

Integrating, $-d[I^+]/dt = (k')[I^+]$ yields a pseudo-first order relationship,

$$[I^+] = [I^+]_o \, e^{-k't}$$

where $[I^+]_o$ is the initial concentration of ion $[I^+]$. A linear plot results when ln $[I^+]$ is plotted against time. Hence monitoring the disappearance of $[I^+]$ permits a graphical evaluation of k', the total first-order rate constant, from the slope.

Estimated **values of ln k'** were used in the plots of **electron deficiency versus reaction rate constants (k'), in Figures 2.18, 3.11, 4.11, 5.10 and 6.9.**

2. Evaluation of Second Order Rate Constants (k)

Recall that for the production of ion A^+,

$I^+ + M \Rightarrow A^+ + X$ (with rate constant k_A)

Then for ion product A^+,

$$d[A^+]/dt = k_A [I^+][M] = k'_A [I^+] = k'_A [I^+]_o \, e^{-k't}$$

Integrating this equation for ion product A^+ ; and integrating parallel equations for ion products B^+ and C^+ :

$$[A^+] = [A^+]_o + (k'_A [I^+]_o / k')(1 - e^{-k't})$$

$$[B^+] = [B^+]_o + (k'_B [I^+]_o / k')(1 - e^{-k't})$$

$$[C^+] = [C^+]_o + (k'_C [I^+]_o / k')(1 - e^{-k't})$$

If initial concentrations $[A^+]_o = [B^+]_o = [C^+]_o = 0$, a condition which occurs directly after multiple resonance ejection of all ions except I^+; then these three equations simplify to become

$$[A^+] / [B^+] / [C^+] = k'_A / k'_B / k'_C$$

Thus, **an individual pseudo-first order rate constant** (k'_A, k'_B, etc.) for the appearance of a product ion (A^+, B^+, etc.) **will be proportional to its relative concentration** in a mixture of appearing products. The proportion of any ion product A^+, B^+, etc. present in a product mixture at any time can be used to estimate its rate of formation from the decay rate of the reactant ion, I^+. Concentration values for each product were measured at several times on at least three separate temporal plots, then averaged in order to calculate final k' values for each ion product.

3. Evaluation of Neutral Reactant Gas Pressures, [M]

Second order rate constants k_A, k_B, etc., were calculated from k'_A, k'_B, etc., using [M] values calculated from experimental temperature and pressures using the following procedure. Since $k'_A = k_A [M]$, then in order to calculate second order rate constants, the relationship between the molecular neutral concentration [M], which is directly proportional to the true pressure P(true) and the nominal pressure read from the pressure gauge, is required. This is because each gaseous compound affects a pressure gauge differently. According to methods devised by Bartmess et. al., the true pressure, P(true), exerted by a sample gas inside an ion chamber can be estimated from the molecular polarisability (α) of the neutral sample gas present in the chamber using the following relationship:

$$P(true) = P(gauge) / R \qquad \text{where } R = (0.36\alpha + 0.30)$$

Values of R for each organometallic reactant system were approximated by using known or estimated values for the molecular polarisibility α, and the calculated true pressure for the five complexes listed in Table A.1 on the following page. Because of the large molecular polarisability of $CpV(CO)_4$, neutral pressures in the vanadium system are affected most: nominal (gauge) pressure in the vanadium system must actually be diminished by a factor of 8.35. Polarisibility effects in the other four metal systems apparently decrease with increasing atomic number of the metal.

Since the molecular polarisibility α is a three-dimensional property rather than a linear one, the values given for true pressures in Table A.1, as determined from nominal ion gauge readings are approximate. Consequently, values of k are accurate to within 25-30% only.

Table A. 1

Molecular Polarisabilities and Pressures

Compound	Molecular Polarisablity (α) [a] $(Å)^3$	Gauge Pressure (torr)	True Pressure [b] (torr)
$CpV(CO)_4$	22.36	$6.0x10^{-8}$	$7.19x10^{-9}$
$BzCr(CO)_3$	21.25	"	$7.55x10^{-9}$
$CpMn(CO)_3$	19.53	"	$8.19x10^{-9}$
$BuFe(CO)_3$	18.3[c]	"	$8.7\ x10^{-9}$
$CpCo(CO)_2$	16.72	"	$9.49x10^{-9}$

[a] Relative ion gauge sensitivities calculated by method of Bartmess (Bartmess, J. E.; Georgiadis, R. M. *Vacuum* 1983, *33*, 149.) with Chen modification (Chen, S.-P., Ph. D. Dissertation; 1992.)

[b] True pressures estimated from known literature values for α (*Handbook of Chemistry and Physics*, 72nd ed., CRC; Boca Raton, 1991-1992, pp. 194-210.) and using extension of Aroney's approximation for α of ferrocene. (Aroney, M.; Le Fèvre, R. J. W.; Somasundaram, K. M. *J. Chem. Soc.* 1960, 1812.)

[c] Data for butadiene iron tricarbonyl estimated by method of Aroney (Aroney, M. J.; Cooper, M. K.; Pierens, R. K.; Pratten, S. J.; *J. Organomet. Chem.* 1985, *295*, 333.)

Approximate absolute second order rate constants (k_A, k_B, etc.) were calculated using P(true) values to obtain concentrations (molecules cm^{-3}) of the neutral molecule [M] for each system at experimental pressures.

For each reacting ion, sets of relative values of product ions $[A^+]$, $[B^+]$, $[C^+]$, etc., were determined at several specific times. Setting k'_A at some arbitrary value, say k'_A = 100, then k'_B , k'_C, etc., were assigned values relative to k'_A for each time period. These rate constants were averaged for each product ion. Tables of calculated **second order rate constants** (k_A, k_B, etc.) and **relative rate constants** ($100k'_B / k'_A$; $100k'_C / k'_A$; etc.) are listed for all reactive cations as follows: Vanadium cations in Table 2.2 - 5 in Chapter 2; for Chromium cations, Table 3.2 in Chapter 3; for Manganese cations, Table 4.2 in Chapter 4; for Iron cations, Table 5.2 in Chapter 5; and for Cobalt cations, Table 6.2 in Chapter 6. As well, most of these data are summarised in Tables 7.2 - 4 in Chapter 7.

Appendix II

Figure A.1. Schematic Diagram of FT - ICR Reaction Cell*

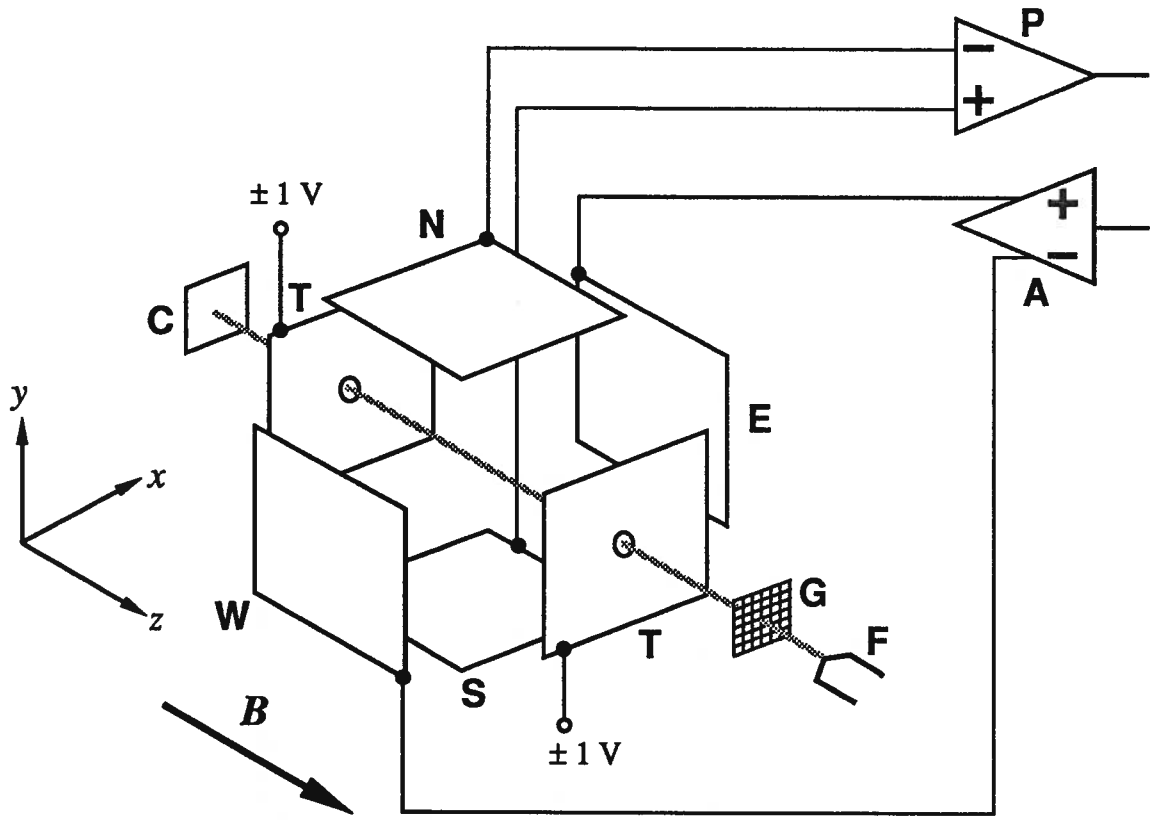

FT - ICR Cubic Reaction Cell* for FT-ICR Studies:

The cell is composed of six square metal plates. The two **T**'s are trapping plates to which is applied a direct current voltage, typically + 1 V for trapping positive ions and – 1 V for negative ions; **N** and **S** are receiver plates for detection of the ion cyclotron motion; **E** and **W** are transmitter plates for rf excitation for ion excitation and ejection; **F** is a thermionic filament for electron ionisation; **G** is a grid for shielding the cell and contents from the strong ionisation voltage; **C** is an electron collector for attracting and monitoring the electron current; **P** is the preamplifier for ion detection; **A** is a transmitter amplifier for the rf field.; **B** is the magnetic field applied across the cubic cell.

* Adapted from Chen, S.-P.; Ph.D. Dissertation, 1992.

Figure A.2. FT - ICR Mass Spectrometer Instrumentation*

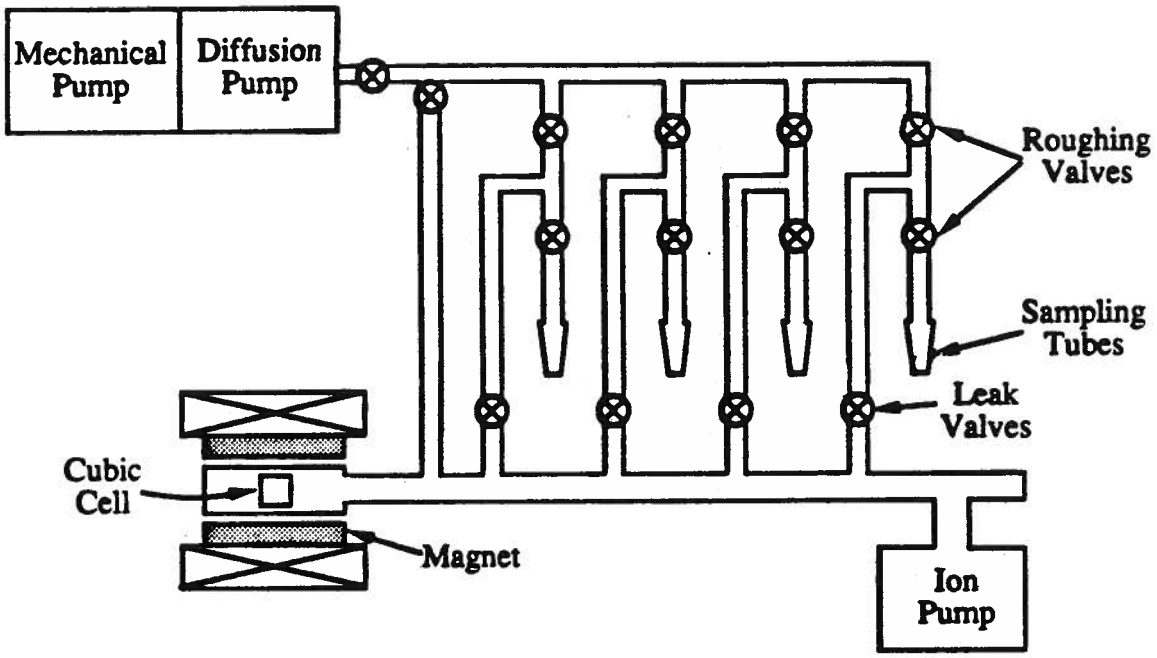

Schematic Diagram of the Vacuum System of an FT-ICR Mass Spectrometer*

A sample contained in a sampling tube is introduced by means of a roughing valve, then passes through a leak valve into the high vacuum chamber containing the cubic reaction cell. The entire system is evacuated by means of the diffusion and mechanical pumps. Sample pressure is maintained at low, constant dynamic pressure by continuous ion pumping.

* Adapted from Chen, S.-P.; Ph.D. Dissertation, 1992.